THE UNIVERSITY OF MICHIGAN
7260-1-T

Technical Report ECOM-01263-4

Broadband Antenna Techniques Study

1 January Through 15 April 1966
Report No. 4
June 1966

Contract No. DA-28-043 AMC-01263(E)
DA Project No. 5A0-21101A902-01-08

Prepared by

J. E. Ferris, J. A. M. Lyon, G. G. Rassweiler,
D. L. Smith, P-R. Wu, W. E Zimmerman

The University of Michigan
Department of Electrical Engineering
Radiation Laboratory
Ann Arbor, Michigan 48104

For

United States Army Electronics Command, Fort Monmouth, N. J.

ABSTRACT

Work on the design, fabrication and testing of three broadband antennas is described. The antenna types are: 1) high-gain constant beamwidth, 2) omnidirectional, and 3) loaded conical helix.

During this reporting period, an experimental study has been conducted to determine techniques by which a parabolic reflector may be broadbanded such that a constant beamwidth secondary major lobe can be achieved. Three reflector surfaces have been considered which are: 1) a solid reflector, 2) a doily structure, and 3) a wire grid structure. The results of this study have suggested that the doily configuration best satisfies the requirements of the technical guidelines of the contract. Although the present doily structure exhibits a constant beamwidth (beamwidth variation of less than 2:1) for a frequency band of 8.3:1, the results suggest that a 10:1 frequency band could be achieved. From this study, it has been found that the holes placed in the reflector should be distributed in a random fashion, so as to be non-symmetrically located. Typical pattern data for the doily reflector is presented along with tabulated data for the wire grid and solid structure. To satisfy the requirements of the contract, a doily reflector and necessary supporting structure have been packaged with the ridged horn for shipment to the Fort Monmouth facilities for further evaluation.

A bird cage antenna has been designed, fabricated and tested to satisfy the requirements of the broadband omnidirectional antenna task of the technical guidelines. Both VSWR and pattern data have been obtained for this antenna and are presented as a part of this report. The antenna exhibits good omnidirectional patterns across the frequency range of 100 - 1000 MHz and the VSWR characteristics are less than 3:1 for the same frequency range. In addition to the data presented for the bird cage antenna, a discussion of trap antenna concepts is included along with additional results of the coupling study that is being carried on to better understand the coupling characteristics of the manipole antenna.

One of the primary objectives of this research activity has been the design of a conical helix antenna covering the frequency range from 50 MHz to 1.1 GHz, with a 2:1 size reduction over conventional unloaded designs. A design has been produced and a prototype based upon this design has been built; this design and a description of the prototype are included in this report. Data on the experimental test of this prototype including a comparison with specifications are also included.

Although the weight of the prototype is considerably in excess of that specified, some size reduction has been accomplished. The electrical characteristics involving radiation pattern measurements have been satisfactorily ascertained except for the extreme low end of the frequency range where radiation pattern measurements are subject to a considerable experimental error. This last difficulty is not a shortcoming of the prototype, but rather the usual difficulty in radiation pattern work at the frequencies involved.

TABLE OF CONTENTS

FOREWORD

This report was prepared by The University of Michigan Radiation Laboratory of the Department of Electrical Engineering under United States Army Electronics Command Contract No. DA 28-043 AMC-01263(E). The contract was initiated under United States Army Project No. 5A0-21101-A902-01-08, "Broadband Antenna Techniques Study." The work was administered under the direction of the Electronics Warfare Laboratory, Supporting Developments Technical Area at Fort Monmouth, New Jersey. Mr. Anthony DiGiacomo is the Project Manager and Mr. George Haber is the Contract Monitor.

The material reported herein represents the results of the preliminary investigation into techniques applicable to the design and development of broadband antennas.

The authors wish to acknowledge the contributions of Professor C. T. Tai for his work on the omnidirectional antenna, and to J. Burch, P. Eng. T. Lewis, A. Loudon, K. Jagdmann and U. E. Gilreath for their contributions in obtaining much of the data presented in this report.

LIST OF ILLUSTRATIONS

I
INTRODUCTION

This contract is divided into three tasks: 1) broadband constant beamwidth high-gain antenna, 2) omnidirectional broadband antenna, and 3) broadband loaded conical helix.

Under Task 1, a high-gain antenna is to be developed that covers the frequency range 1 - 10 GHz. The beamwidth is to vary less than 2:1 such that a relatively constant gain of 20 db above an isotropic source is achieved with a VSWR less than 3:1 with respect to a 50 ohm load. The investigation is to include a theoretical and experimental study of broadband, constant beamwidth, high-gain antennas. Electronic switching, electromechanical or mechanical motion to effect the constant beamwidth characteristics of the antenna are not to be considered. As a result, the constant beamwidth characteristics must be achieved employing antenna beam shaping techniques.

Under Task 2, a broadband omnidirectional antenna of the monopole or dipole configuration is to be developed which will be operational over the frequency range of 100 MHz to 1 GHz having a VSWR of less than 3:1 with respect to a 50 ohm load. It is desired that the configuration be as thin as possible and its overall length comparable to that of a half-wave dipole at the low end of the frequency band (100 MHz). The maximum diameter of the configuration is to be less than 20 inches.

The objective of Task 3 was to design a circularly polarized antenna for operation in the frequency region from 50 MHz to 1.1 GHz with a 2:1 reduction in size and having a maximum weight of 20 lbs. In order to accomplish the reduction in size, use was made of L-2 loading consisting of Flexible Hi-K6 material supplied by Emerson-Cuming. The final prototype antenna is classed as a loaded conical helix. Rather than a circular cone, a square based pyramidal helix was formed. Details on the electrical performance, including the VSWR, gain, and beamwidths

over the specified range of frequency are included in this report. An Anzac broadband hybrid is used to couple this antenna to a 50 ohm coaxial line. The design of the prototype antenna was based upon a series of experiments involving loaded and unloaded helical and log conical antennas. These underlying experiments were important in establishing the active region of a loaded conical helix with a given type of loading at a specific frequency. Results on the underlying experiments are also included in this report.

II
BROADBAND HIGH GAIN CONSTANT BEAMWIDTH ANTENNA

A broadband high gain antenna is being developed to satisfy the following requirements: 1) it is to operate in the frequency range of 1:10 GHz, 2) it is to have a constant gain of approximately 20 db above an isotropic source, 3) half-power beamwidth variation is to be less than 2:1, 4) the VSWR is to be less than 3:1 with respect to 50 ohms, and 5) the antenna is to be capable of receiving any component of linear polarization.

During the period covered by this report, an experimental study has been conducted to determine the electrical characteristics of several secondary reflector surfaces. The reflector surfaces considered during this reporting period were: 1) a solid asymmetrical parabolic reflector, 2) a solid asymmetrical parabolic reflector with non-uniformly spaced holes of random diameters, and 3) a wire grid structure mounted on a fiberglass supporting structure.

2.1 Primary Feed

The electrical characteristics of the primary feed (ridged horn) were presented in the Third Quarterly Report (Ferris, et al 1965) and will not be discussed further at this time. During the study of the secondary reflector, it was learned that it would be desirable for the horn to have a longer throat and a larger aperture. The longer throat is required to minimize phase errors inherent in the aperture field distribution because of the curving of the ridges in the aperture region and the larger aperture would help to more adequately illuminate the reflector. Some consideration should be given to the desirability of including a corrugated surface in the interior of the horn to minimize side lobes in the E-plane (Peters, et al 1965).

The power handling capabilities of this horn have been estimated from an expression derived by Hopfer (1955) and found to be 2.08 kilowatts in the center of

the ridge, assuming breakdown occurs at the center of the ridges. However, since the ridges have sharp corners, the power handling capability will be reduced. Hopfer has also developed an expression for the edge effects and using this expression the power handling capacity of the horn is 80 watts.

2.2 Asymmetrical Reflector

Each of the reflecting surfaces consdiered during this reporting period was fabricated from fiberglass using the mold described in the Second Quarterly Report (Ferris, et al 1965). Therefore, each has the same F/D ratio and idential parabolic surfaces. All pattern data has been collected following the coordinate system of Fig. 2-1. All gain measurements were made employing the substitution technique, i. e. the pattern maximum of the constant beamwidth antenna was compared to the pattern maximum of a standard gain horn antenna.

2.2.1 Solid reflector

The data for the solid reflector is summarized in Table II-1 and presented graphically in Figs. 2-2 through 2-4. This data differs slightly from that reported in the Third Quarterly because of the narrower half power beamwidths observed at 10 GHz. Upon checking, it was found that the broader patterns were due to the use of a supporting wood structure that extended into the aperture region of the reflector. The present data has been obtained having the reflector supported from the back. To confirm the effects of the wood structure in the aperture, pattern data have been retaken employing the earlier configuration.

A major portion of the experimental study has been confined to obtaining data for the $\theta = 90^{o}$ plane and rotating the antenna in the ϕ plane. Beam steering for this plane has been negligible. Data recorded in the $\phi = 0^{o}$ plane have been recorded at several frequencies in the 1 - 10 GHz band to determine the pattern characteristics in this plane. The above data was collected with the antenna

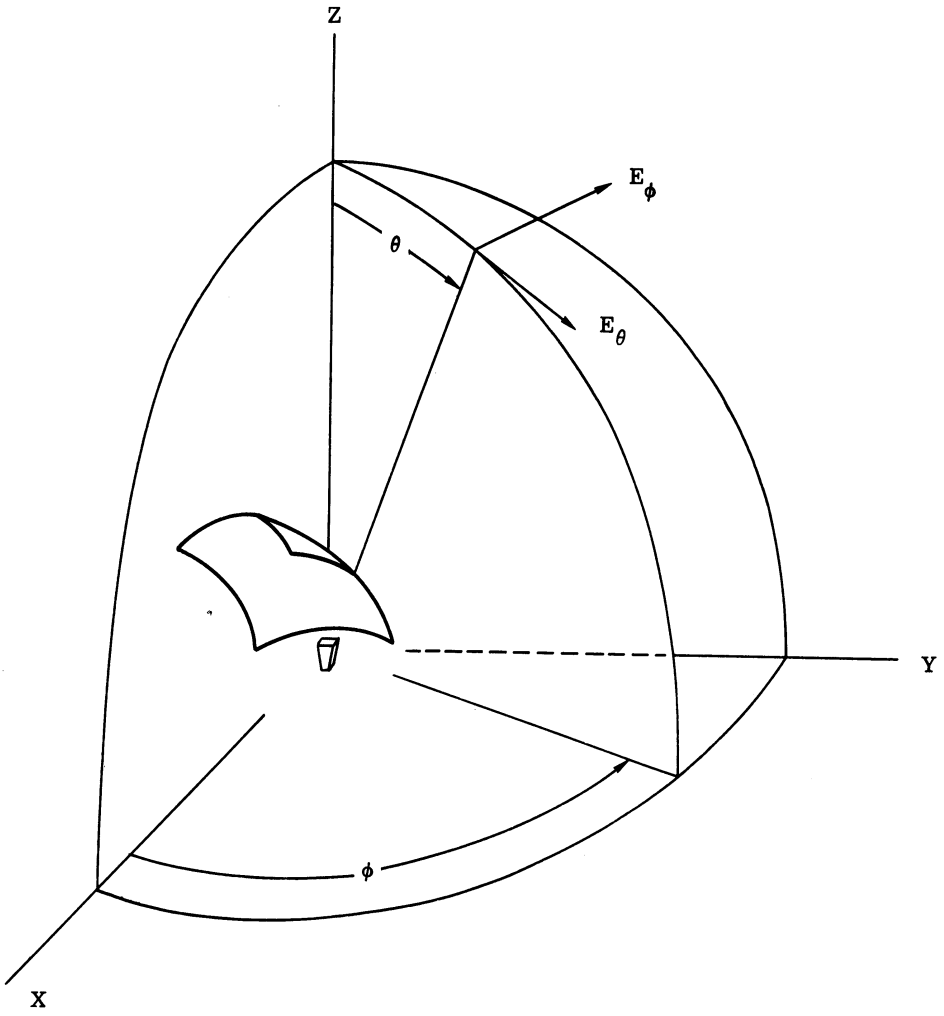

FIG. 2-1: ASYMMETRICAL PARABOLIC REFLECTOR SPHERICAL COORDINATE SYSTEM

TABLE II-1

PARABOLA No. 3 (SILVER PAINT)

f	3 db B.W.	S L L	Gain of Reflector
1.0	17.0	21	18.1
1.5	11.0	25	22.3
2.0	8.0	28.4	25.4
2.2	8.0	>23	—
2.5	7.0	>24	26.7
3.0	7.0	>29	27.8
3.5	5.5	>29	28.3
4.0	5.5	>29	28.9
5.3	5.0	~33	27.8
5.9	4.5	24	25.8
6.95	4.5	15.7	30.3
8.2	5.0	26	26.6
9.12	5.0	31.6	27.9
10.0	4.0	33.0	29.7

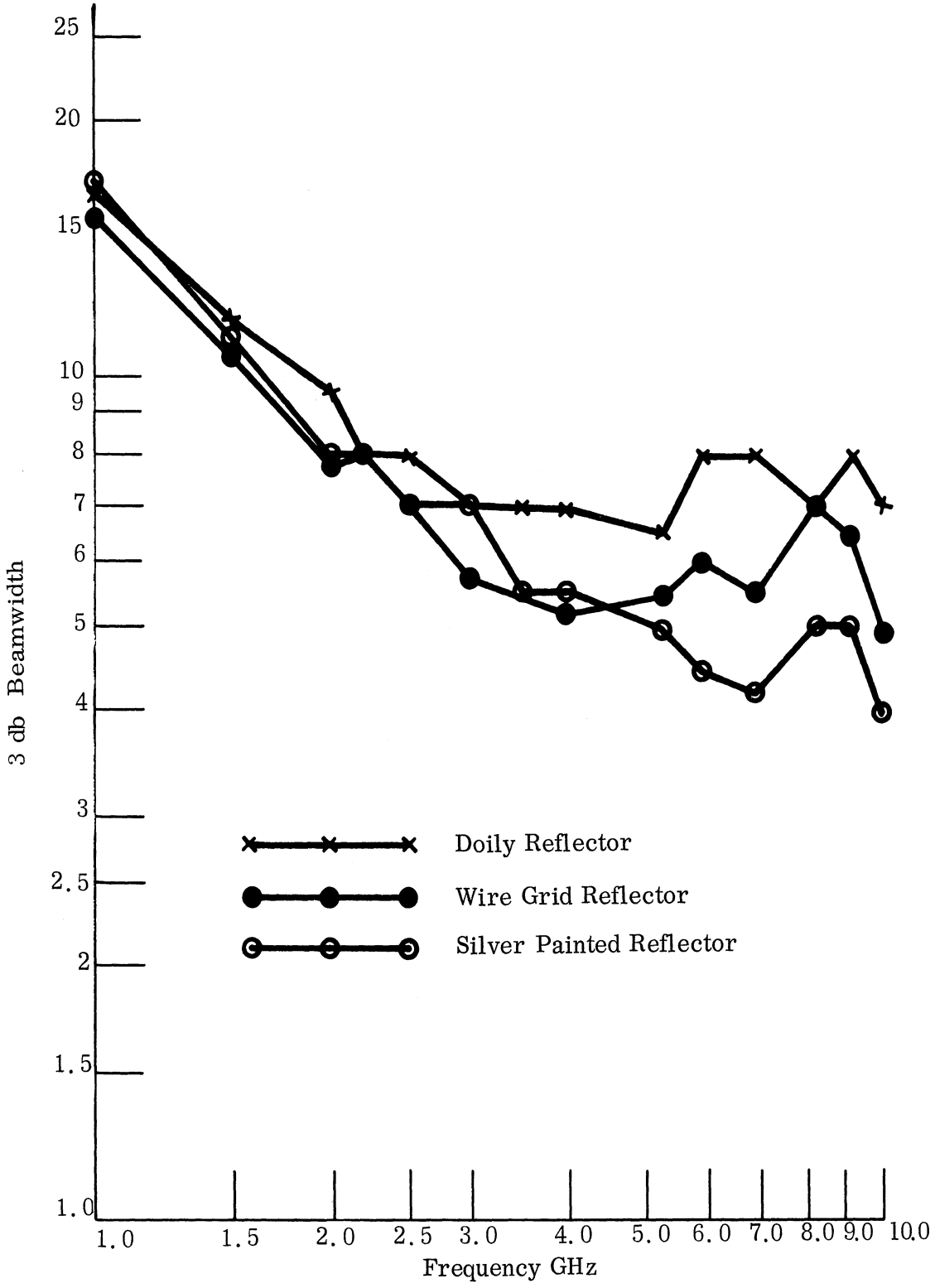

FIG. 2-2: 3 db H-PLANE BEAMWIDTH VS. FREQUENCY ($\theta = 90^{o}$)

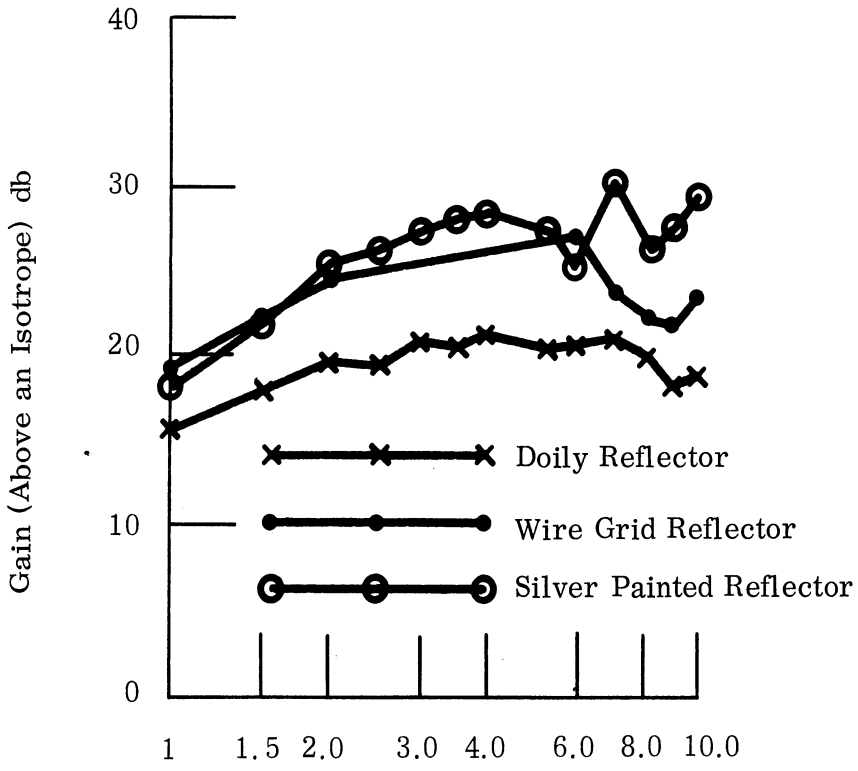

FIG. 2-3: H-PLANE GAIN REFERRED TO AN ISOTROPE ($\theta = 90^{o}$)

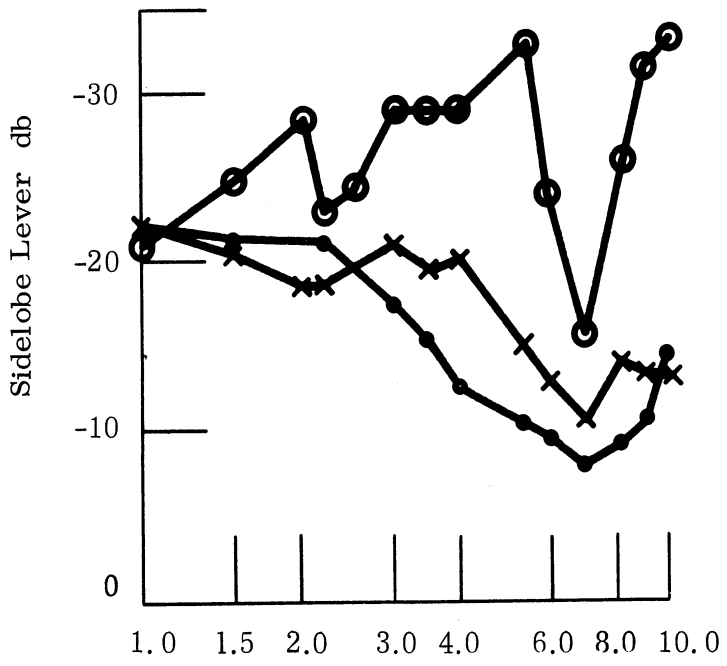

FIG. 2-4: H-PLANE SIDE LOBE LEVEL VS. FREQUENCY ($\theta = 90^{o}$)

polarized in the $E(\theta)$ direction. A small amount of data has been collected for $E(\phi)$ polarization to determine the polarization characteristics of the reflector. In general the patterns for $E\phi$ and $E\theta$ polarization were of a poorer quality in ϕ variable and θ variable planes respectively. The cause for this deterioration in both cases was assumed to be due to the high side lobes of the ridged horn in the E-plane.

To ensure that the reflector was properly oriented with respect to the focal point, a special test fixture was designed and employed when attaching the reflector to the test stand. To aid in the use of the test fixture, markers were laid out on the surfaces of the reflector mold. The marker locations were determined analytically and were accurately known with respect to the focal point of the reflector. In this way, it was possible to position the reflector so that phase errors at the aperture of the reflector were minimized.

In general the data collected from the solid parabolic reflector exhibited a constant beamwidth over a frequency range of 5:1 with a variation of less than 2:1. The cause for the limited bandwidth was felt to be due to the relatively broad beamwidths of the primary feed as noted in the Third Quarterly Report. To minimize the effects of these broad beams and the high side lobes associated with the E-plane at the higher frequencies, some form of frequency sensitivity loading was necessary in the secondary reflector. Two techniques considered were the use of holes and a wire grid structure.

2.2.2 Doily reflector

The second asymmetrically fed parabolic reflector after being fabricated and coated with a silver conductive paint was perforated with many holes. The purpose of these holes was to cause the effective aperture of the secondary reflector to vary in proportion to the wavelength such that a broader beam could be achieved at the higher frequencies and also to minimize the effects of the side lobes of the feed.

The design criteria for the constant beamwidth reflector has been to determine the physical parameter of the reflector to produce half power beamwidths in the neighborhood of 18^{o} at all frequencies from 1 - 1- GHz. Table II-2 lists the effective solid reflector sizes to achieve this design goal at several discrete frequencies in the above band. To effect a reflector surface whose area varies with frequency, six rings of holes were symmetrically located about the central portion of the reflector. The holes varied in diameter from 1 to 5 inches with the smaller holes being located near the central portion of the reflector and the larger holes at the outer edge. The smaller holes were placed in the center as this area is to be sensitive at the highest frequency of interest. For the lower frequencies and the outer areas of the reflector, the holes were made larger for a larger effective solid surface with the arrangement indicated in Table II-2.

TABLE II-2

CALCULATION OF PRIMARY REFLECTOR SURFACE AND HOLE SIZE FOR DOILY ($f_o/f \simeq 1.4$)

Freq. (GHz)	Reflector Diameter for 18^{o} 3db Beamwidth	λ_o	a = radius of hole $= \frac{\lambda_o}{3.41}$
10.0	5.0"	1.2"	No Holes
7.0	7.25"	1.7"	0.50"
5.0	10.0"	2.4"	0.70"
3.57	14.0"	3.3"	0.97"
2.55	20.0"	4.6"	1.35"
1.82	27.5"	6.5"	1.90"
1.3	38.0"	9.0"	2.64"

Initial patterns of the reflector with the holes symmetrically located about the center were not acceptable. For example, at the higher frequencies, the main beam had a null at the pattern maximum and many high side lobes. Later it was noted that the symmetrically located holes were separated by a number of symmetrically located rings of solid reflector. These rings were assumed to function as electrically large loops having uninterrupted currents flowing around them. The pattern characteristics of electrically large loops exhibit a lobing structure similar to that noted surrounding the main lobe region of the secondary reflector. Therefore, it was concluded that to reduce the side lobes, it would be necessary to break up the currents flowing around the electrically large loops. To do this, additional holes of various sizes were placed in the reflector in a non-symmetrical manner. Additional holes were placed in the reflector and as the number was increased, the patterns gradually improved such that the main lobe broadened and the side lobe level was reduced. Data for the final configuration (Fig. 2-5) is shown in Table II-3 and Figs. 2-2 through 2-4. Because of the lacy appearance of the final reflector configuration the title "doily" reflector was selected for the antenna.

During this portion of the experimental study, the antenna was positioned as shown in the coordinate system of Fig. 2-1 and pattern data collected for the following set of conditions: $\theta = 90^{o}$, ϕ variable and $E\theta$ polarization. In the latter portion of the study some changes were made as will be noted later in the report. Typical patterns are shown in Figs. 2-6 - 2-15.

The doily exhibits approximately an 8.3:1 (3.06 octives) bandwidth over which the beamwidth variation is less than 2:1, i.e. it has a 13 1/2 degree half power beamwidth at 1.2 GHz and a 7 degree half power beamwidth at 10 GHz. Note that it came with 200 MHz of having a 10:1 bandwidth. The gain of the antenna was measured at several frequencies within the 10:1 (3.33 octives) band and results are shown in Table II-3.

TABLE II-3

PARABOLA No. 1 (WITH HOLES)

f	3 db B. W.	S L L	Gain
1.0	16.5	22.0	15.5
1.5	11.5	20.4	18.0
2.0	9.5	18.8	19.8
2.2	8.0	18.6	—
2.5	8.0	—	19.5
3.0	7.0	21.0	21.0
3.5	7.0	19.4	20.7
4.0	7.0	20.0	21.5
5.3	6.5	15.0	20.6
5.9	8.0	13.0	20.9
6.95	8.0	10.5	21.3
8.2	7.0	14.1	20.1
9.12	8.0	13.4	18.5
10.0	7.0	13.2	19.1

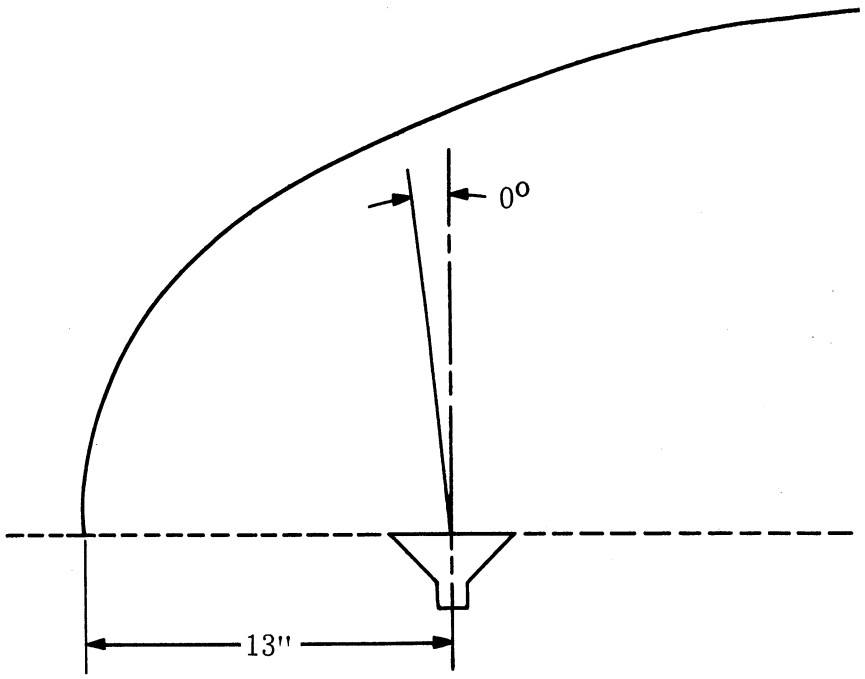

FIG. 2-5A: FINAL CONFIGURATION OF DOILY ANTENNA

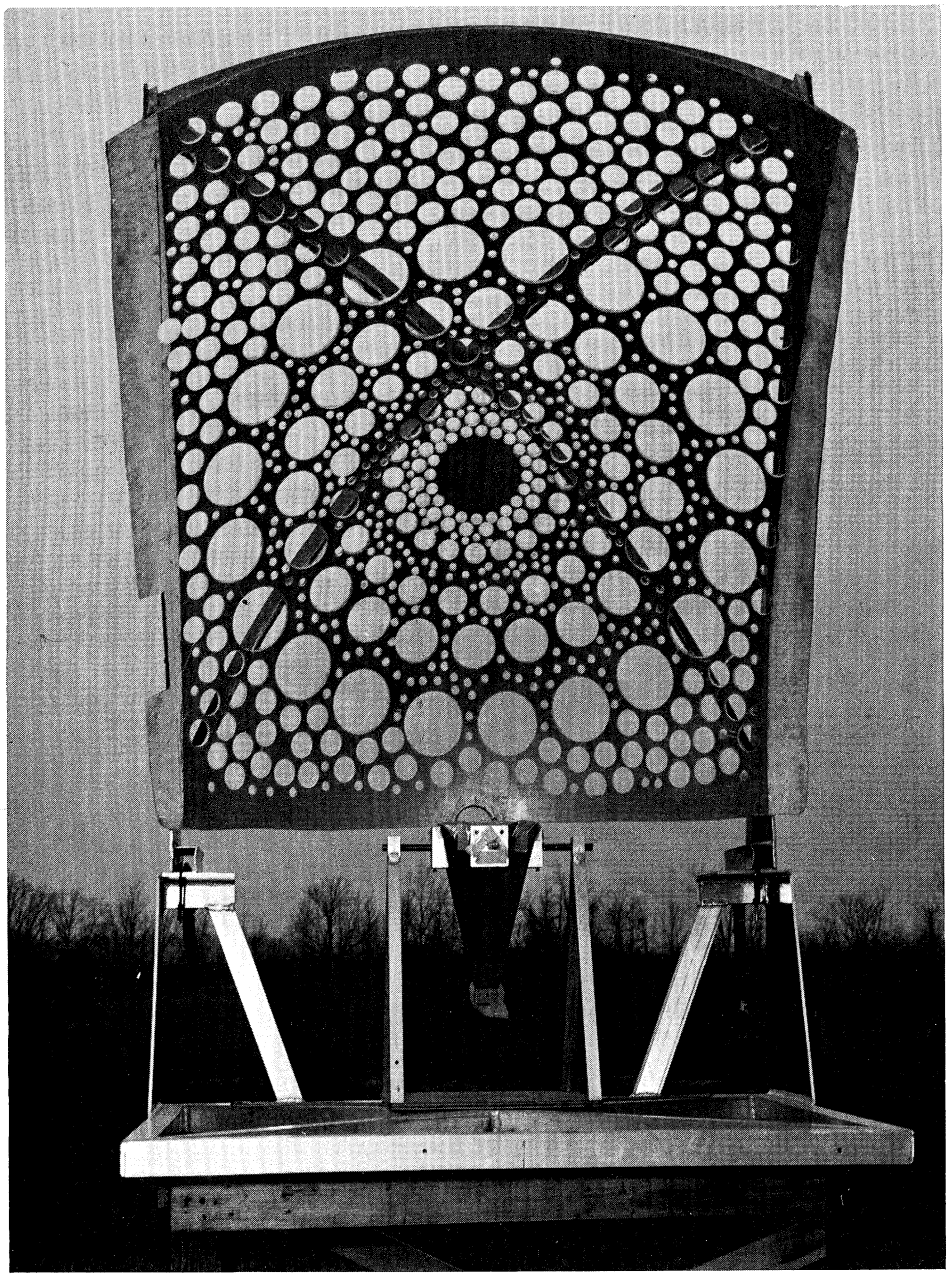

FIG. 2-5B: FINAL CONFIGURATION OF DOILY ANTENNA

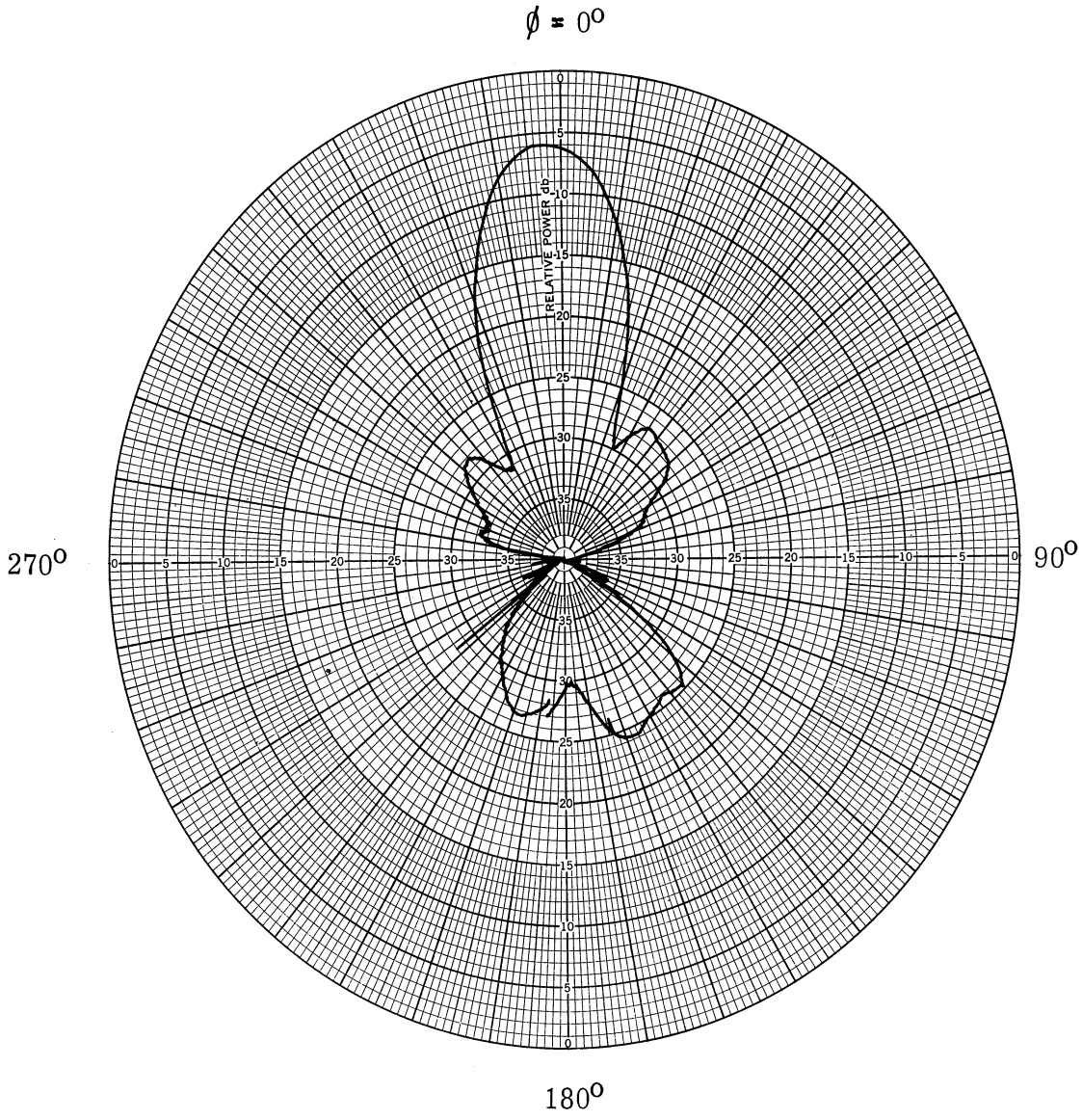

FIG. 2-6: H-PLANE POLARIZATION OF DOILY REFLECTOR AT 1.0 GHz.

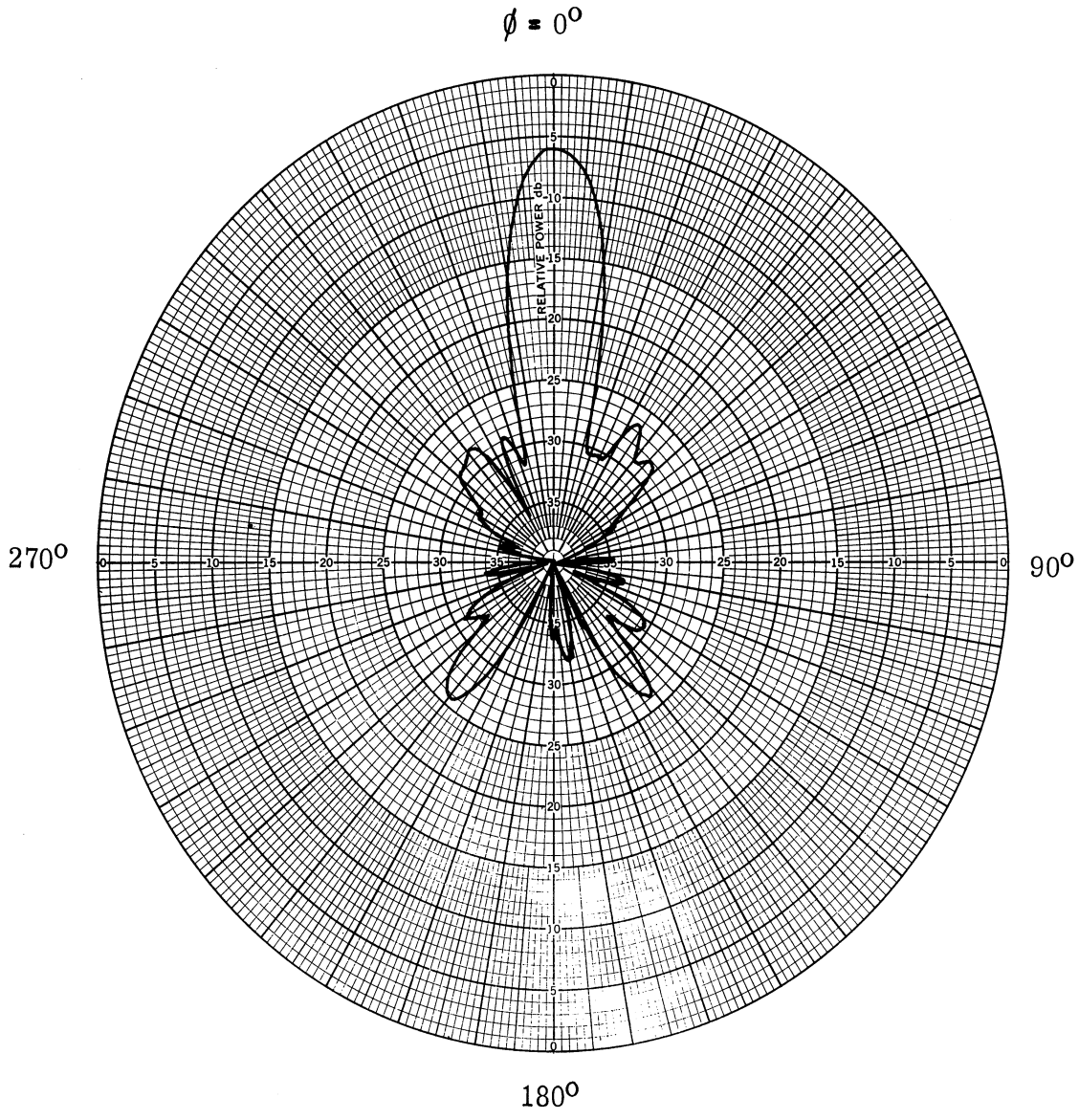

FIG. 2-7: H-PLANE POLARIZATION FOR DOILY REFLECTOR AT 1.5 GHz

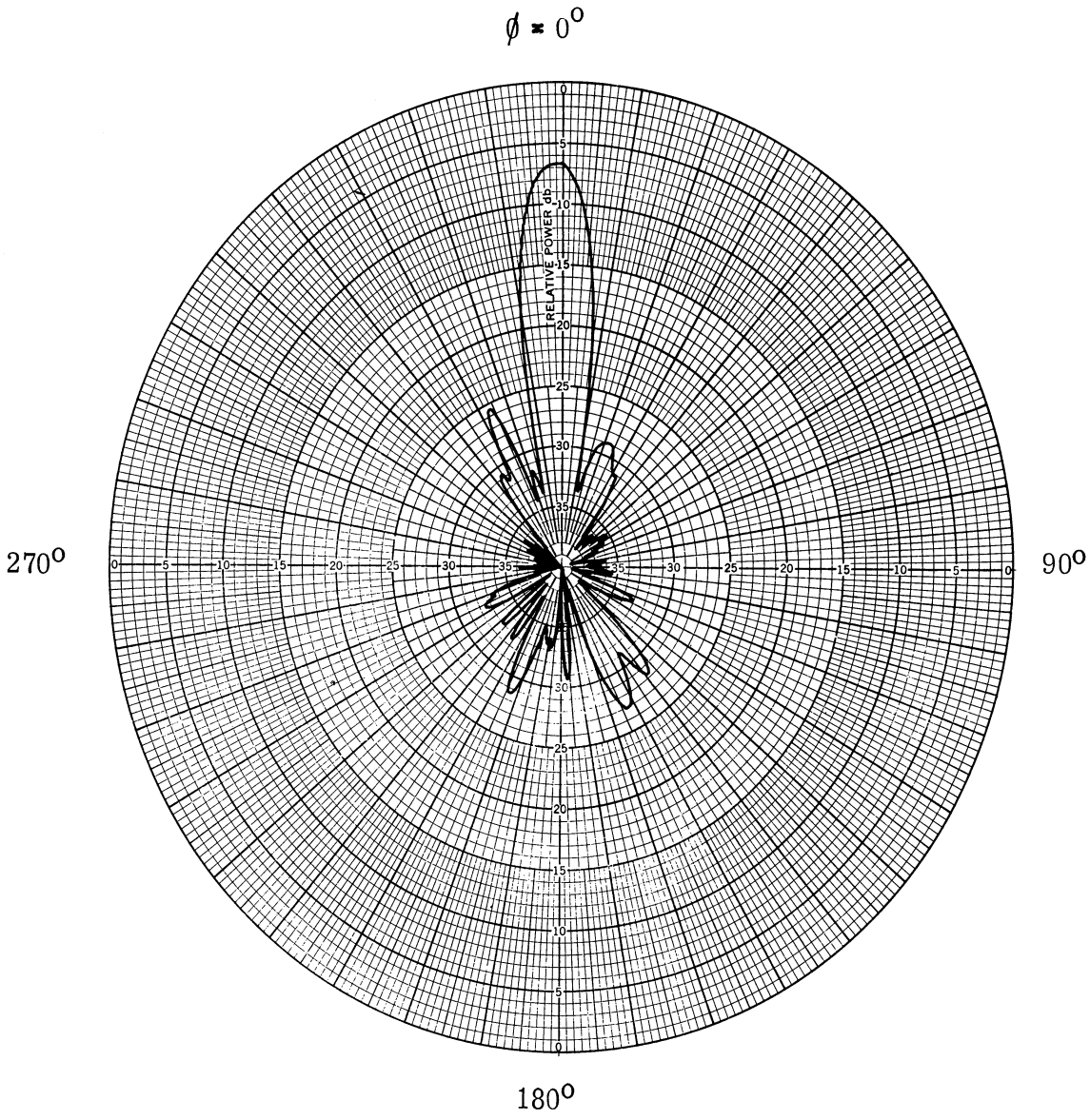

FIG. 2-8: H-PLANE POLARIZATION FOR DOILY REFLECTOR AT 2.0 GHz

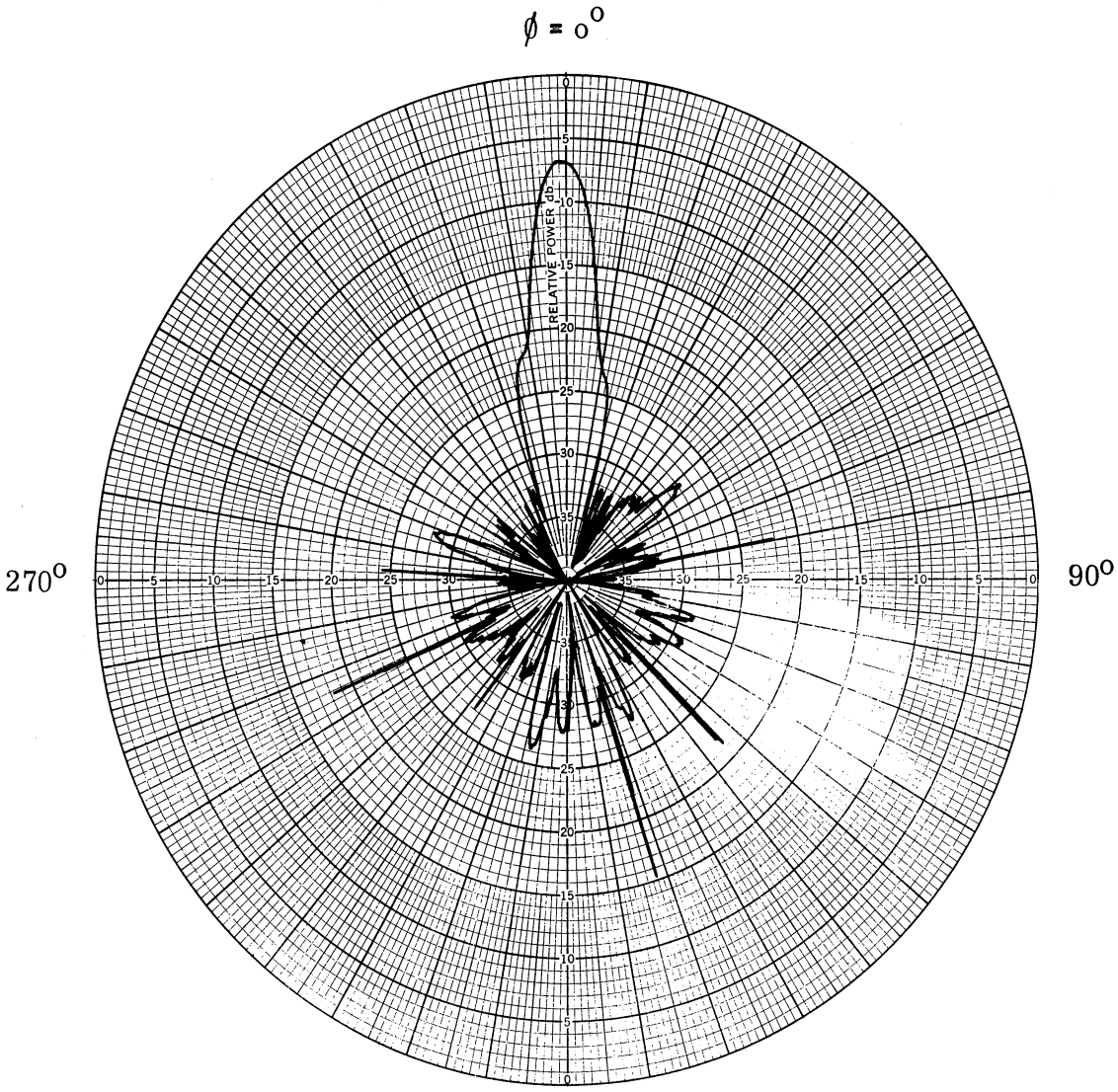

FIG. 2.9: H-PLANE POLARIZATION OF DOILY REFLECTOR AT 2.5 GHz

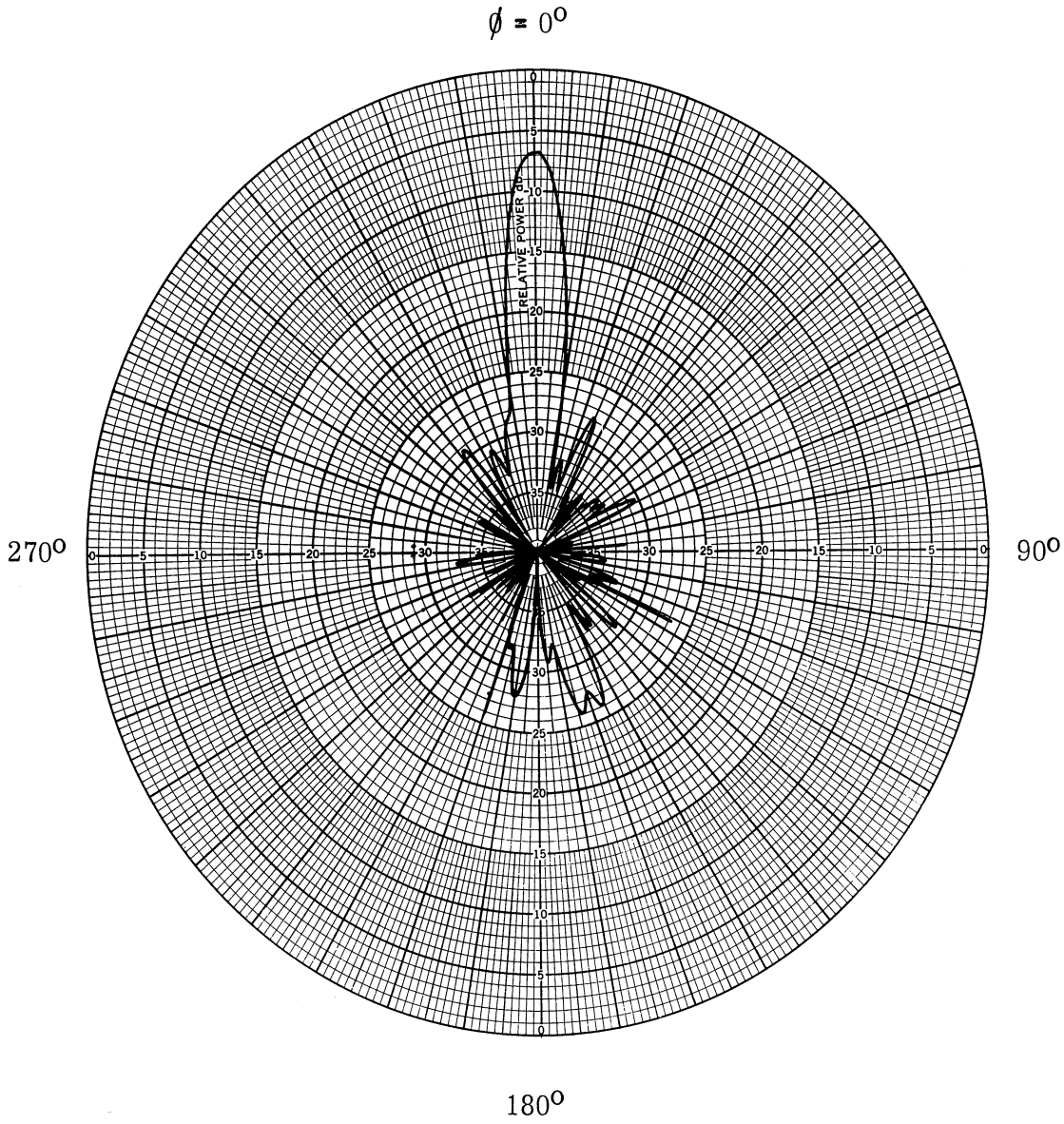

FIG. 2-10: H-PLANE POLARIZATION FOR DOILY REFLECTOR AT 3.0 GHz

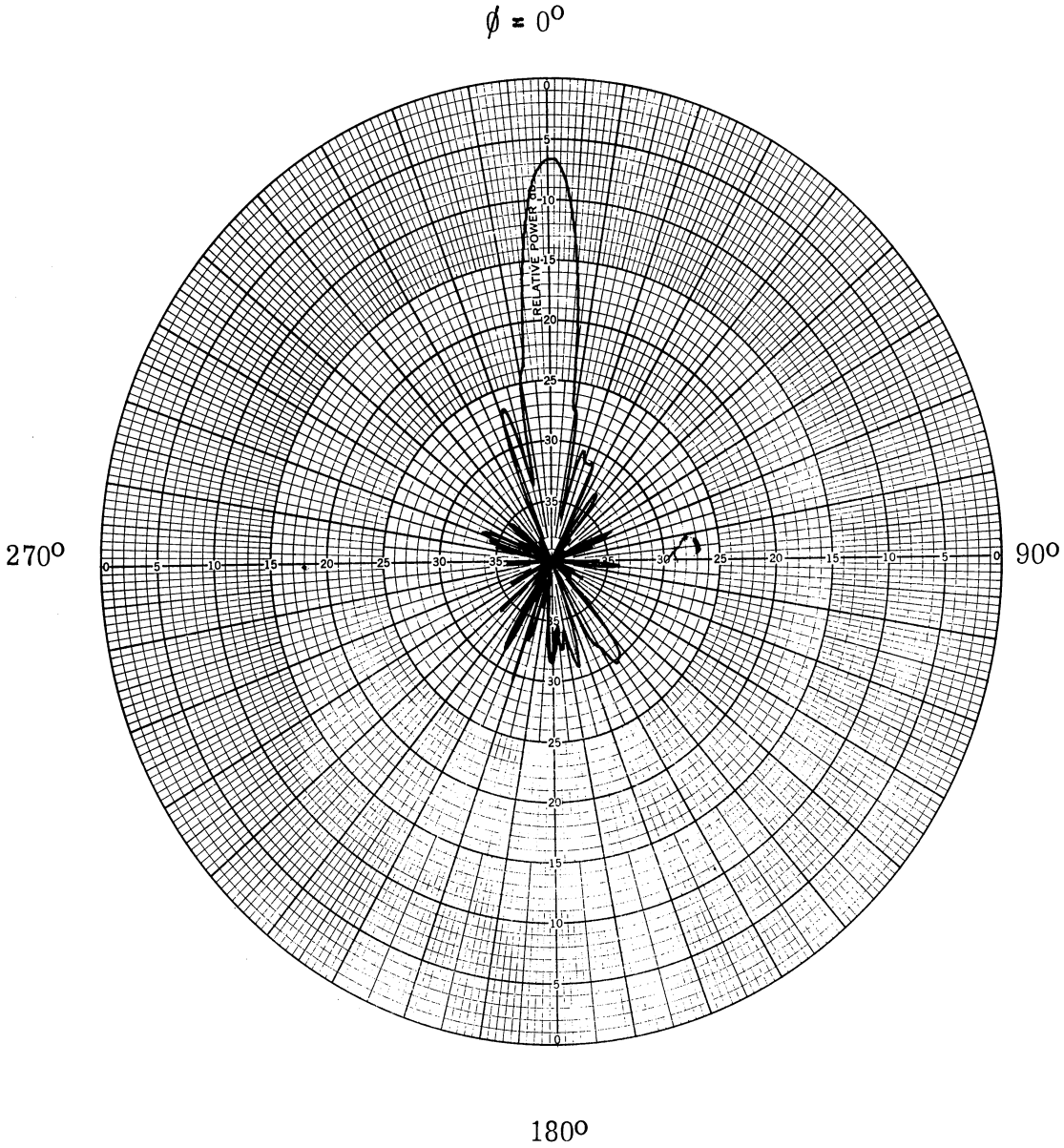

FIG. 2-11: H-PLANE POLARIZATION FOR DOILY REFLECTOR AT 4 GHz

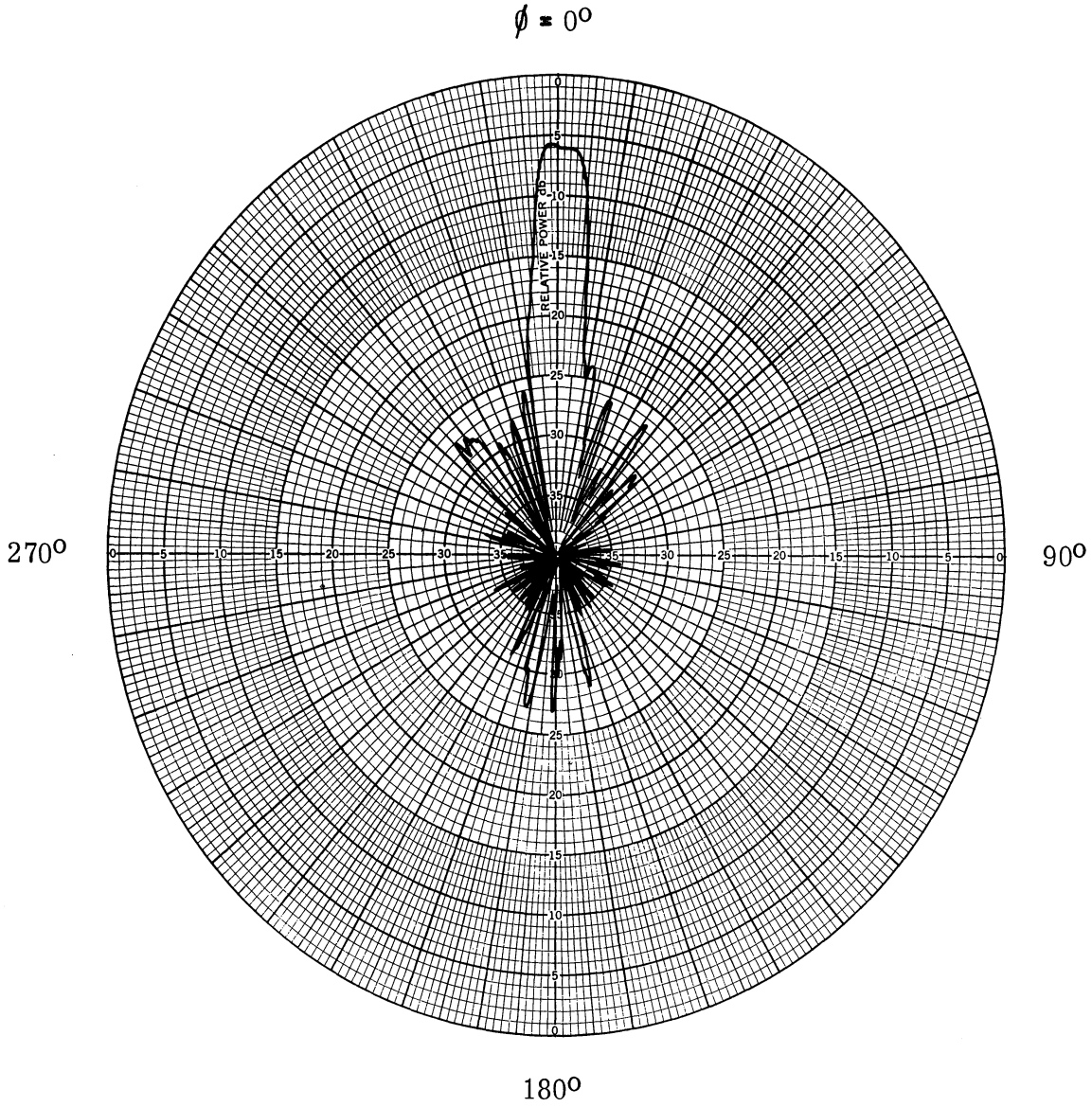

FIG. 2-12: H-PLANE POLARIZATION FOR DOILY REFLECTOR AT 5.3 GHz

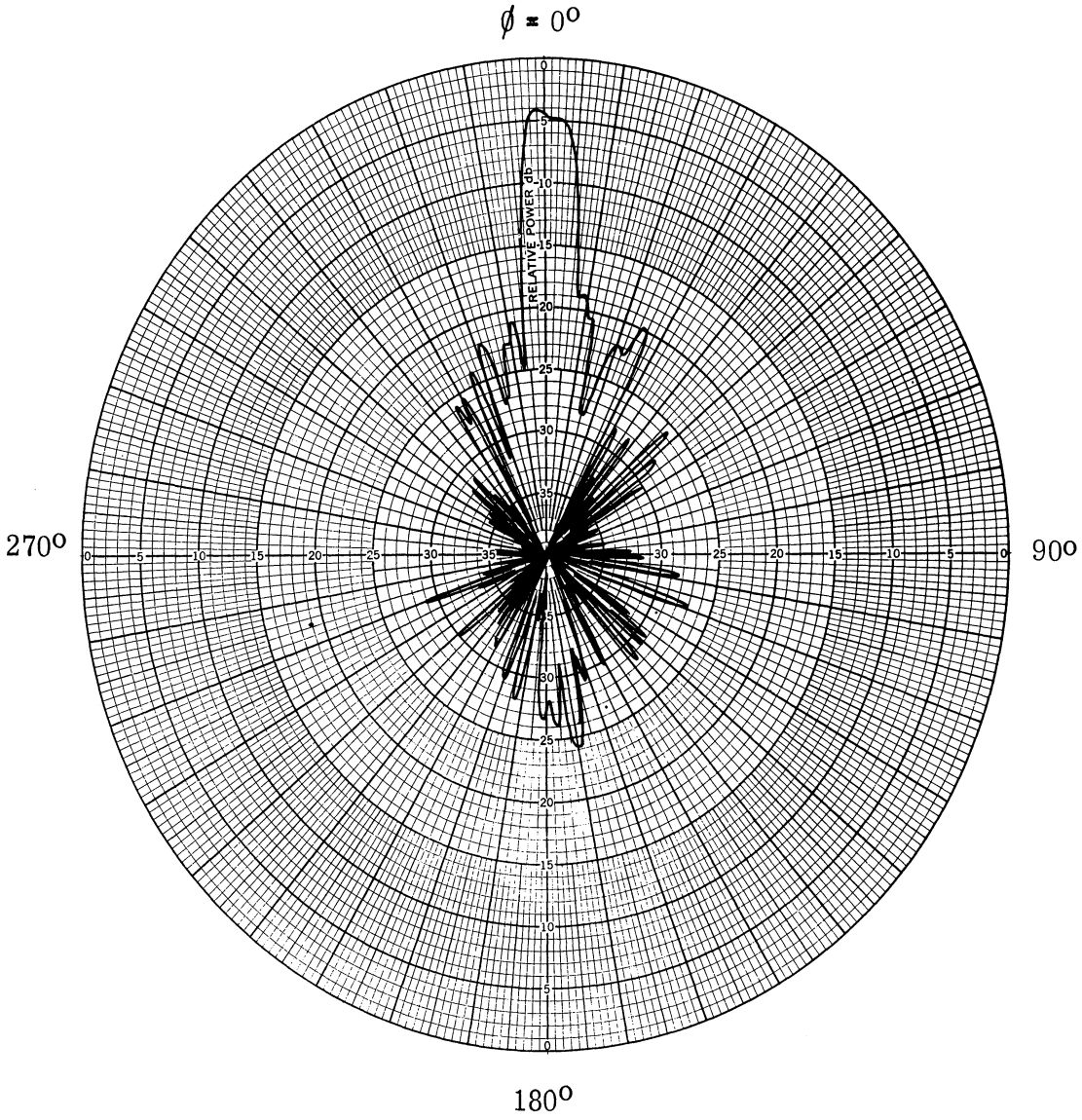

FIG. 2-13: H-PLANE POLARIZATION FOR DOILY REFLECTOR AT 8.2 GHz

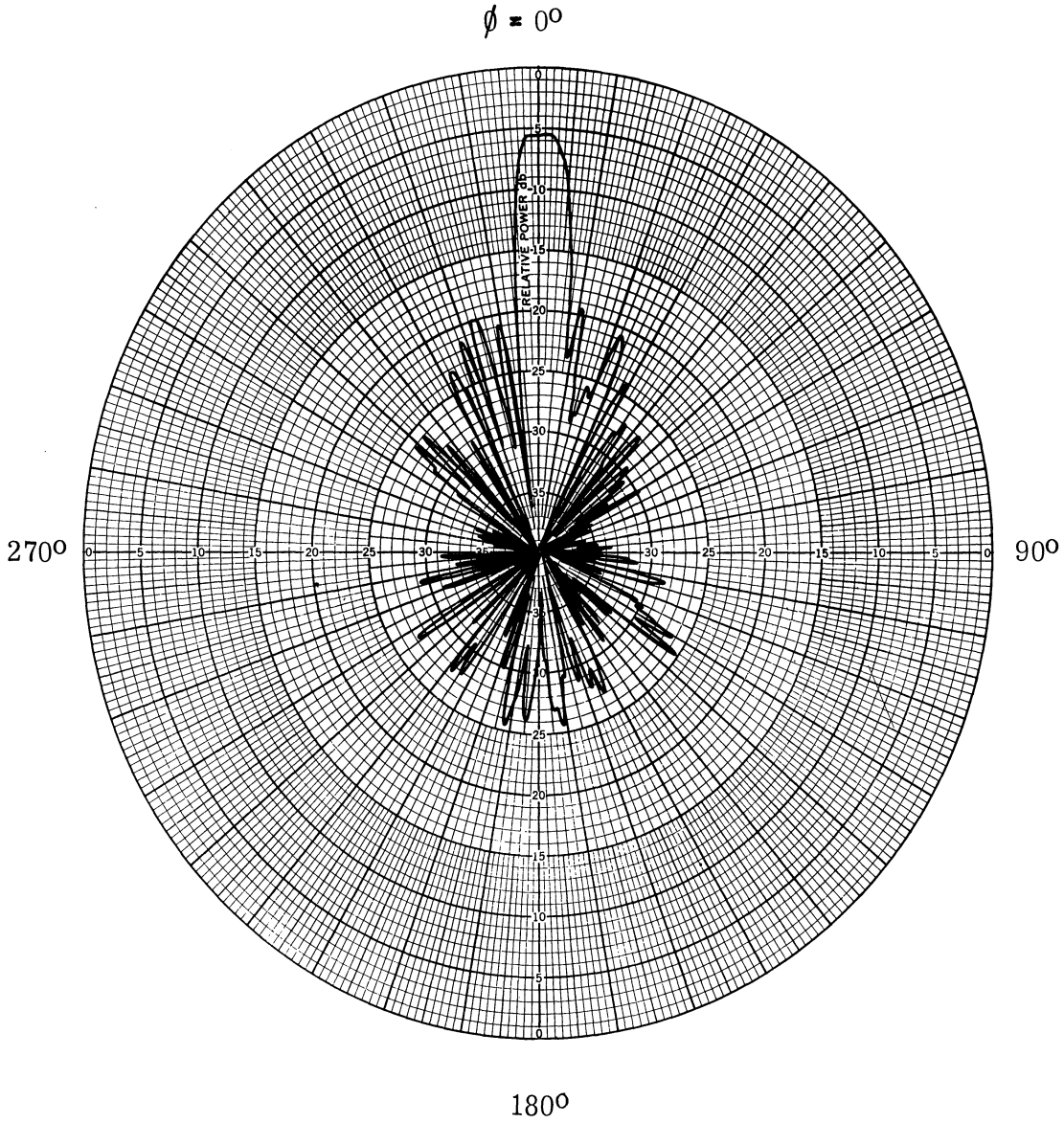

FIG. 2-14: H-PLANE POLARIZATION FOR DOILY REFLECTOR AT 9.12 GHz

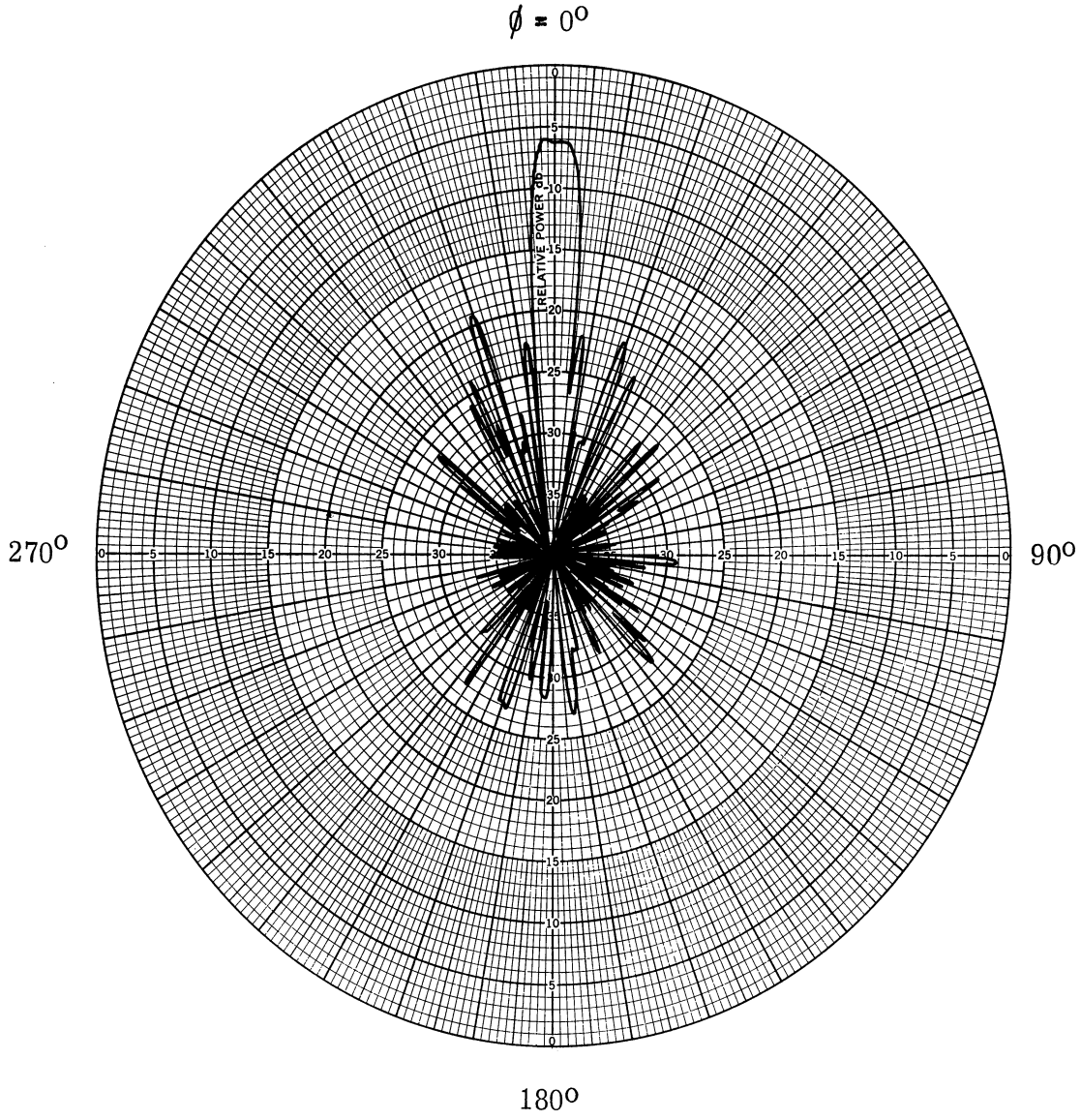

FIG. 2-15: H-PLANE POLARIZATION FOR DOILY REFLECTOR AT 10.0 GHz

As may be expected because of the holes, the efficiency of the reflector is reduced at the lower frequencies. However, this is not felt to be a severe limitation since the objective has been to effect a constant beamwidth design over a 10:1 frequency band. It was also observed that the side and back lobes were slightly higher than the 15 db design goal.

With the doily antenna in its final configuration and positioned as shown in Fig. 2-1 patterns were recorded at 10 GHz for the following conditions: 1) $\theta = 90^{o}$, ϕ variable and Eϕ polarization, 2) $\phi = 0^{o}$, θ variable and Eθ polarization, and 3) $\phi = 0^{o}$, θ variable and Eϕ polarization. In general the data for the antenna employing Eθ and Eϕ polarization in the θ variable and ϕ variable planes respectively was found to exhibit lower side lobes than observed for patterns of the solid reflector. This further confirmed the hypothesis that placing holes in the reflector would minimize contributors from the side lobes of the primary feed to the far field of the secondary reflector. Typical patterns for these conditions are shown in Figs. 2-16 and 2-17. The side lobes noted at $\theta = 0^{o}$ of Fig. 2-17 are caused by radiation through the holes of the secondary reflector. A preliminary study to determine the possibility of reducing these side lobes through the use of absorbing material was conducted. The results of this study showed that the side lobes could be reduced, however, an insufficient amount of data has been obtained to warrant placing absorber on reflector at this time.

Data was obtained only for a frequency of 10 GHz since a previous study with a solid reflector showed that it was most sensitive to physical changes at this frequency.

Results of the present study have demonstrated the feasibility of developing a linearly polarized antenna to function over a 10:1 frequency band having a beamwidth variation of less than 2:1. However, some reservations are held as to the possibility

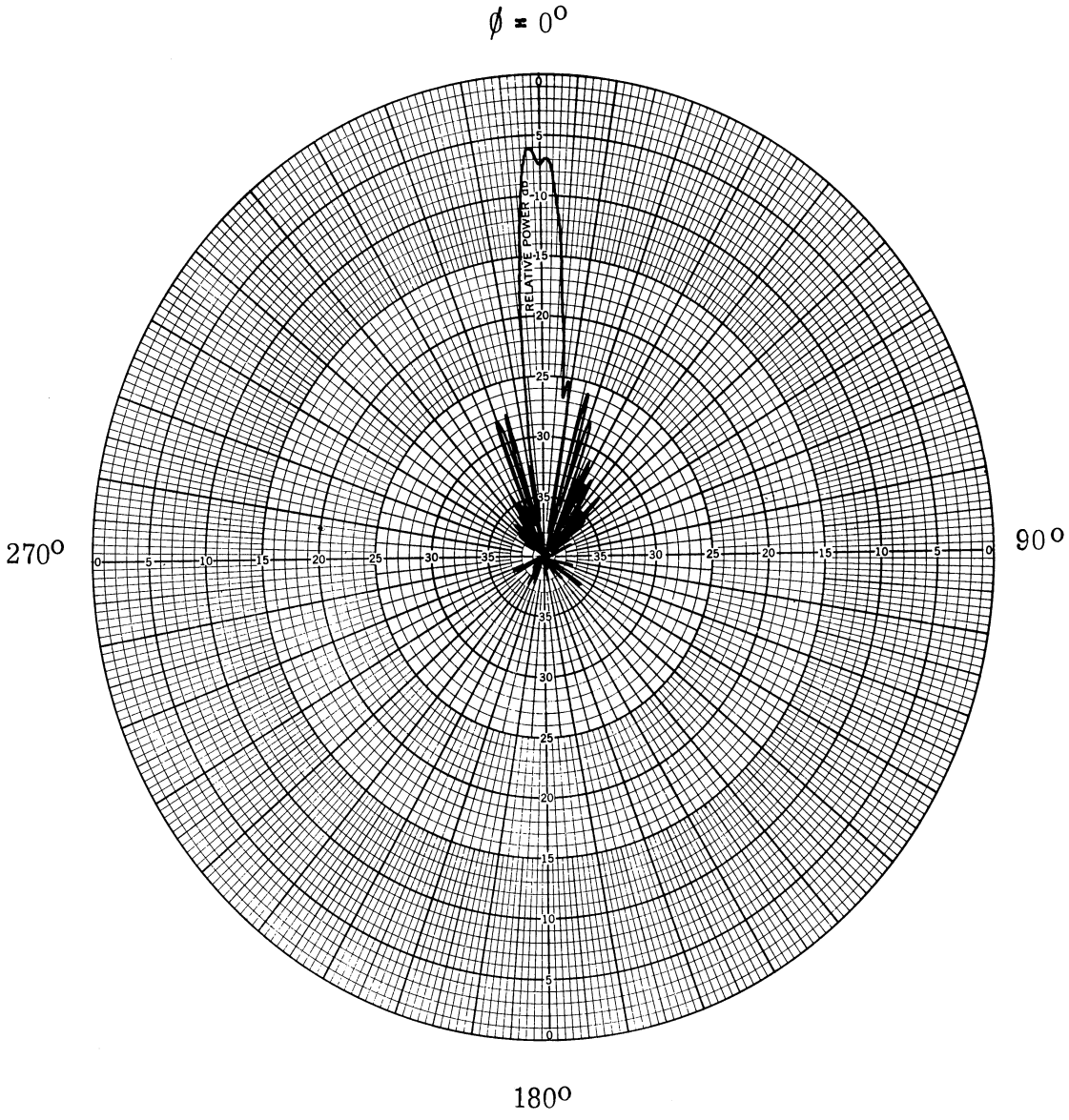

FIG. 2-16: DOILY REFLECTOR ($\theta = 90^{o}$ ϕ VARIABLE, Eϕ), F = 10.0 GHz

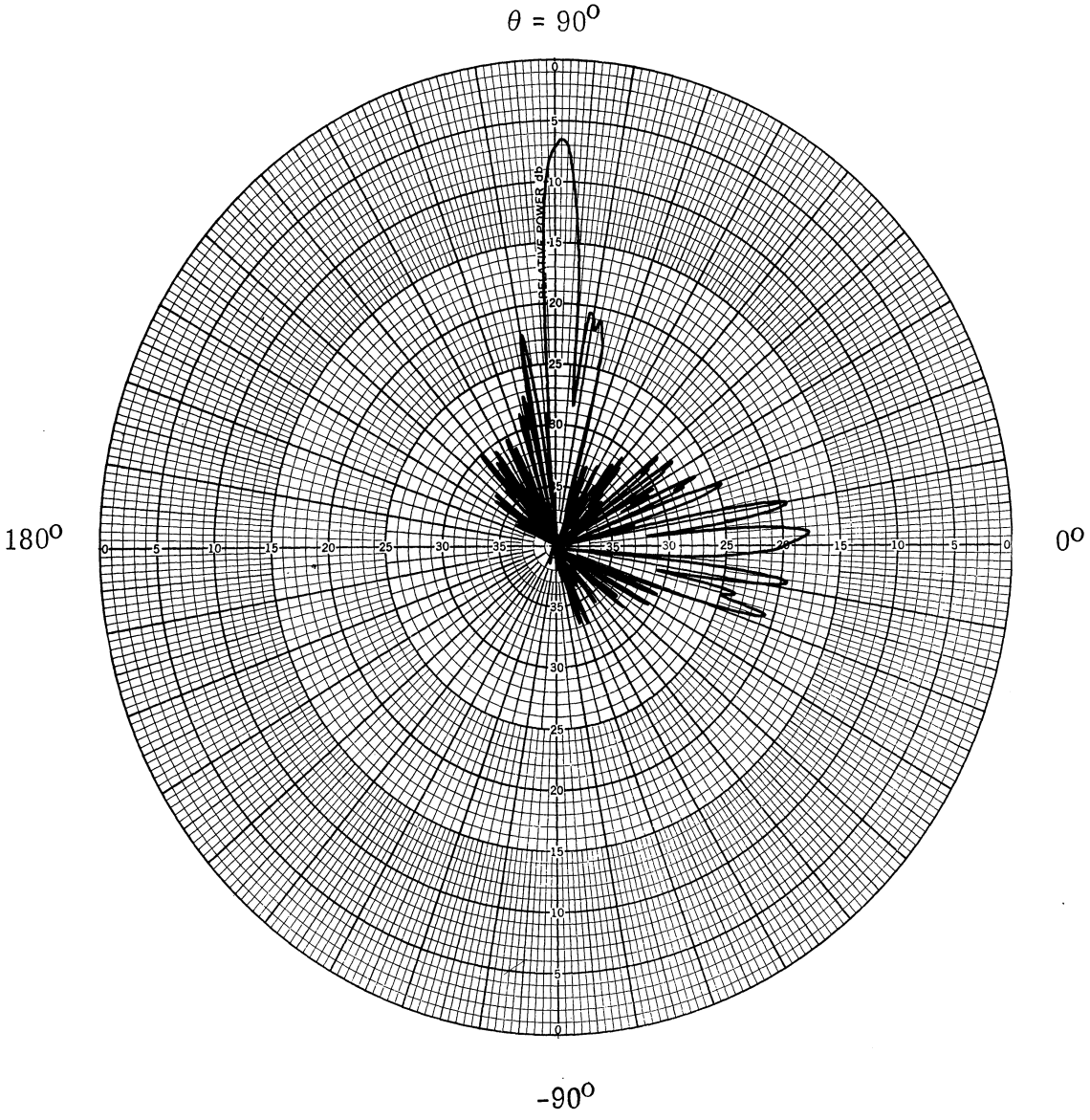

FIG. 2-17: DOILY REFLECTOR ($\phi = 0^{o}$, θ VARIABLE, Eθ), F = 10.0 GHz

of developing a circularly polarized constant beamwidth antenna, because of the constant beamwidth characteristics associated with conventional circularly polarized feed configurations, e.g. planar and log conical spirals.

2.2.3 Wire grid reflector

The wire grid reflector is shown in Fig. 2-18. The wire grid was attached to a fiberglass surface having the desired contour. The wire used for the structure is a No. 22 bus wire and was uniformly spaced 0.6 inches on the parabolic surface. The central portion of the fiberglass was silver painted to provide an area approximately 5 inches by 15 inches. The philosophy in the design of this reflector was that the central portion would be the only active portion at the higher frequencies (10 GHz) and the wire grid would function as a frequency sensitive surface. The grid surface was to be transparent at 10 GHz and as the frequency was decreased the surface would tend to have an increasing reflection coefficient. The reflection characteristics of the structure was expected to vary similar to that shown in the theoretical curve of Fig. 2-19. (Ref. Ferris, et al '65b). Pattern data recorded for the grid structure were discouraging since they were similar to those collected for the solid reflector noted in the above section. It was conjectured at this point that the fiberglass backing material (1/8 inch thick) had a high reflection coefficient such that it was contributing significantly to the far field radiation pattern. To further confirm this, patterns were obtained from a fiberglass parabolic contour (not metallized) and the data obtained substantiated the above assumption. Because of the reflection properties of the fiberglass structure, it was felt that further experimentation of the wire grid structure should be discontinued in favor of further evaluating the doily reflector. Data obtained with the wire grid reflector has been tabulated and the results are shown in Table II-4 and Figs. 2-2 - 2-4.

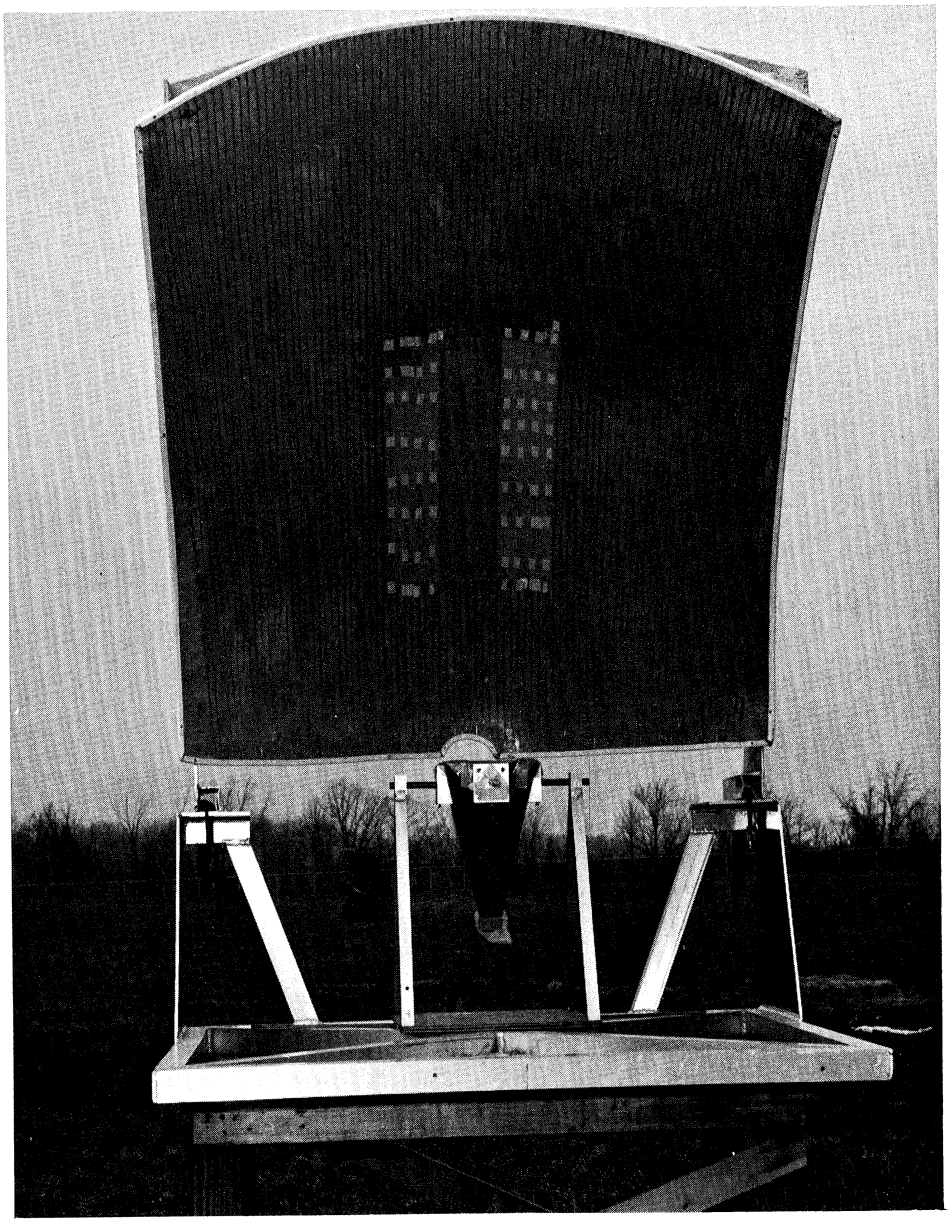

FIG. 2-18: WIRE GRID REFLECTOR

TABLE II-4

PARABOLA No. 2 (WIRE GRID)

f	3 db B.W.	S L L	Gain
1.0	15.5	22.1	19.3
1.5	10.5	21.4	22.5
2.0	7.8	19.0	24.8
2.2	8.0	21.4	—
2.5	7.0	19.9	—
3.0	5.8	17.8	—
3.5	5.5	15.4	—
4.0	5.3	12.6	—
5.3	5.5	10.5	—
5.9	6.0	9.8	27.3
6.95	5.5	8.0	24.0
8.2	7.0	9.2	22.4
9.12	6.5	10.4	22.0
10.0	5.0	14.7	23.6

III
BROADBAND OMNIDIRECTIONAL ANTENNA

Design goals for the omnidirectional antenna are: 1) a 10:1 frequency band (100-1000MHz), 2) gain is to be 1.5 db above an isotropic source over the above frequency range, 3) VSWR is to be less than 3:1 with respect to a 50 ohm load for the above frequency range, and 4) the maximum diameter of the antenna is not to exceed 20 inches. During this reporting period, a major portion of the effort has been spent on the design, fabrication and testing of the deliverable omnidirectional antenna. A small effort obtaining experimental data for the trap antennas and mutual coupling study has been continued. Patterns for the omnidirectional antennas were obtained with the antenna positioned in the coordinate system as shown in Fig. 3-1.

3.1 Double Cone Antenna

A larger version of the double cone (bird cage) antenna reported in the Third Quarterly has been fabricated and tested over the frequency range of 100-1000 MHz. The VSWR exhibited by this antenna is less than 3:1 over the above frequency range (see Fig. 3-2). It is to be noted that the impedance characteristics of the antenna were sensitive to the presence of personnel in the 100-250 MHz frequency range. The cause for this sensitive nature of the antenna is felt to be due to currents flowing on the feed line to the antenna. The presence of the currents flowing on the lead-in are due to the electrically small size of the ground plane (conic section having a 90^{o} included angle and a maximum base diameter of 20 inches) employed with the bird cage element. While making the impedance measurements the antenna was located on a platform six feet above the ground such that the operator could set directly beneath the antenna (in the null of the far-field radiation pattern) to make impedance measurements. In this way the operator was not in the high intensity region of the

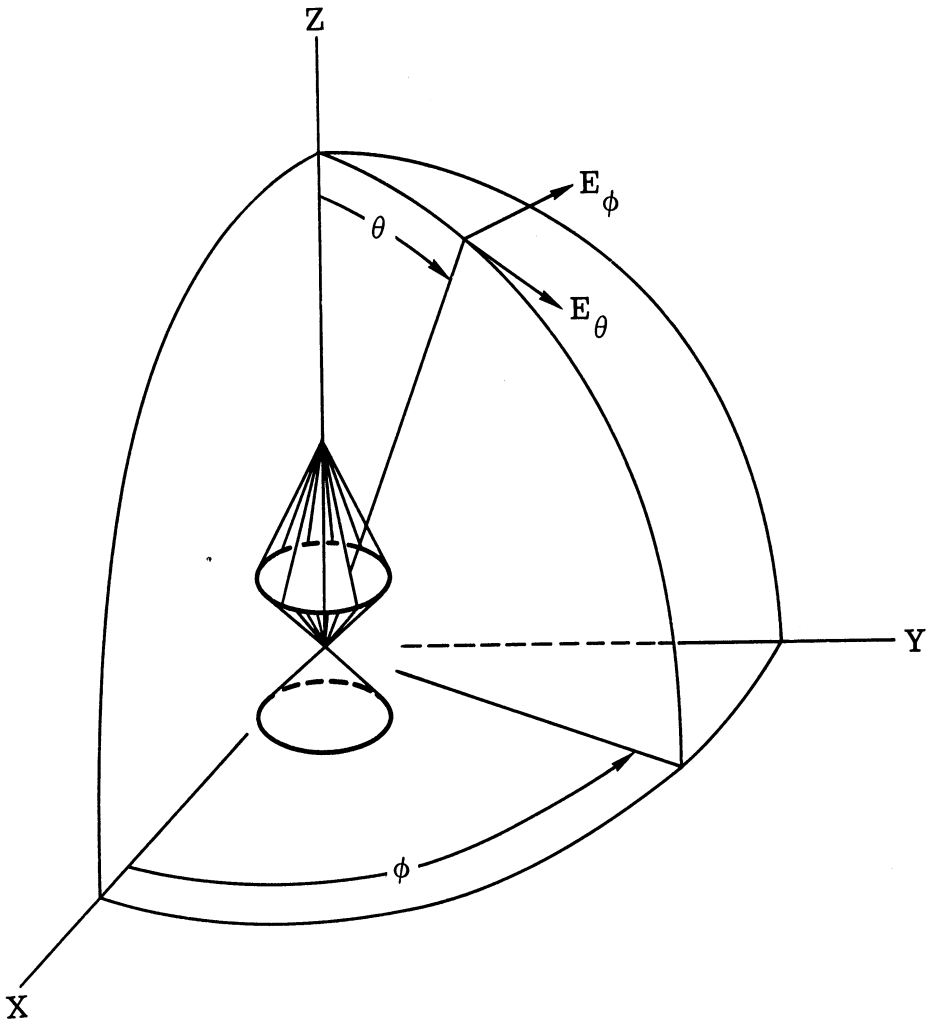

FIG. 3-1: COORDINATE SYSTEM FOR BIRD CAGE ANTENNA

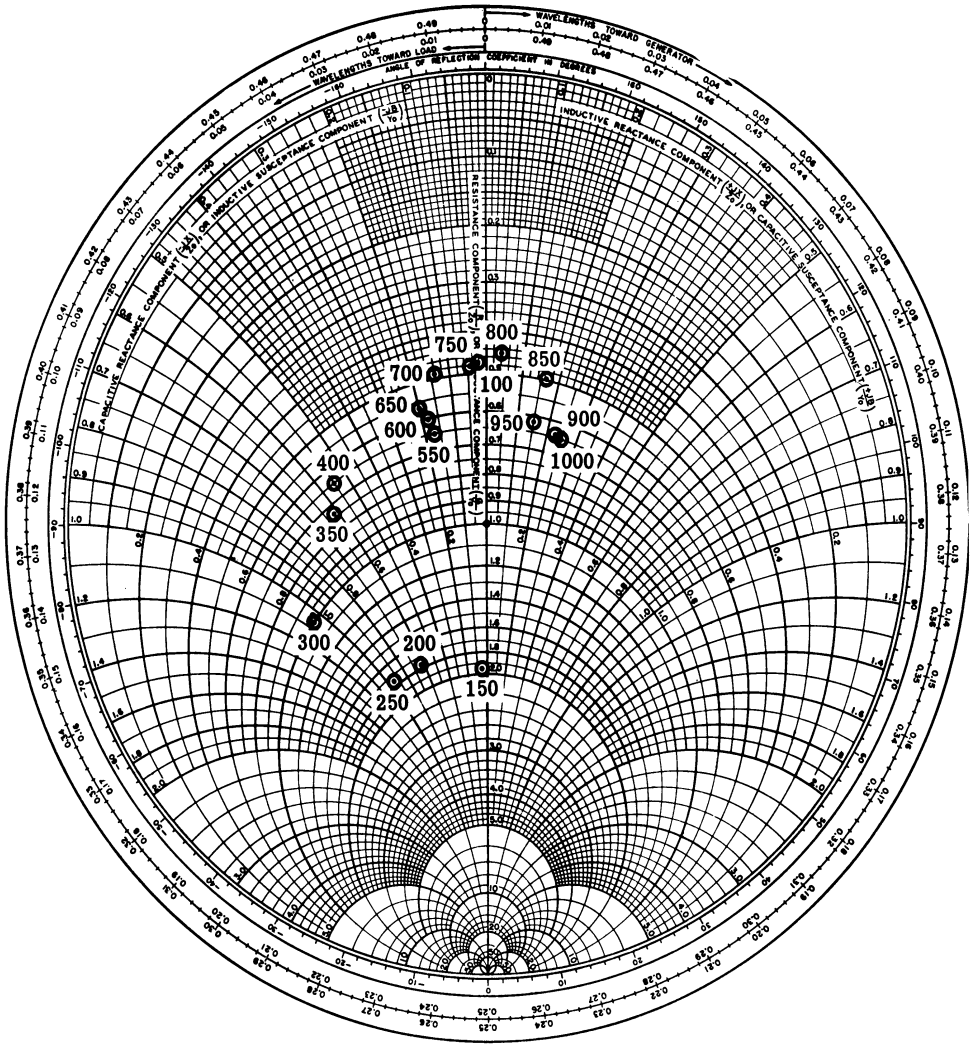

FIG. 3-2: IMPEDANCE OF BIRD CAGE ANTENNA (f = 100-1000 MHz)

antenna and variations noted, while making impedance measurements, were assumed to be caused by induced currents on the feed line to the antenna.

Because of the currents flowing on the lead-in the patterns of the antenna in the 100-250 MHz frequency range were sensitive to the positioning of the feed cable. It is felt that if the antenna is measured in the presence of vehicles or other metalic obstructions, the patterns will be further distorted. To avoid these errors care was taken, when recording patterns, to orient the lead-in normal to the incident field illuminating the antenna. Typical patterns for the bird cage are shown in Figs. 3-3 through 3-12. These patterns generally exhibit good coverage in the $\theta = 90^{o}$ plane. Patterns 3-13 through 3-18 illustrate the omnidirectivity characteristics of the antenna in the frequency range of 500-1000 MHz. H-plane patterns in the 100-400 MHz range were not recorded because of the limitations of the antenna range configuration employed. There is no question however, but that these patterns would show good omnidirectivity.

The noise in the omnidirectional patterns is due to electrical interference from the near by airport. To obtain patterns in the 100-400 MHz range, a special antenna range was employed. This is a ground reflection range that is arranged so that both direct and reflected energy (from the earth) illuminating the test antenna add in phase at the test antenna. A further discussion of this range configuration is available in an article by Cohn and Maltese (1961). Because of the physical parameters of the University of Michigan range only horizontal polarization measurements can be made.

Presently there is no good theoretical explanation of the electrical characteristics of the bird cage antenna. However, the following hypothesis has been suggested. In the low frequency range (100-500 MHz) the antenna functions as a fat monopole with radiation from the full length of the bird cage element which is fed against the small conic ground plane. Because the conic ground plane is small,

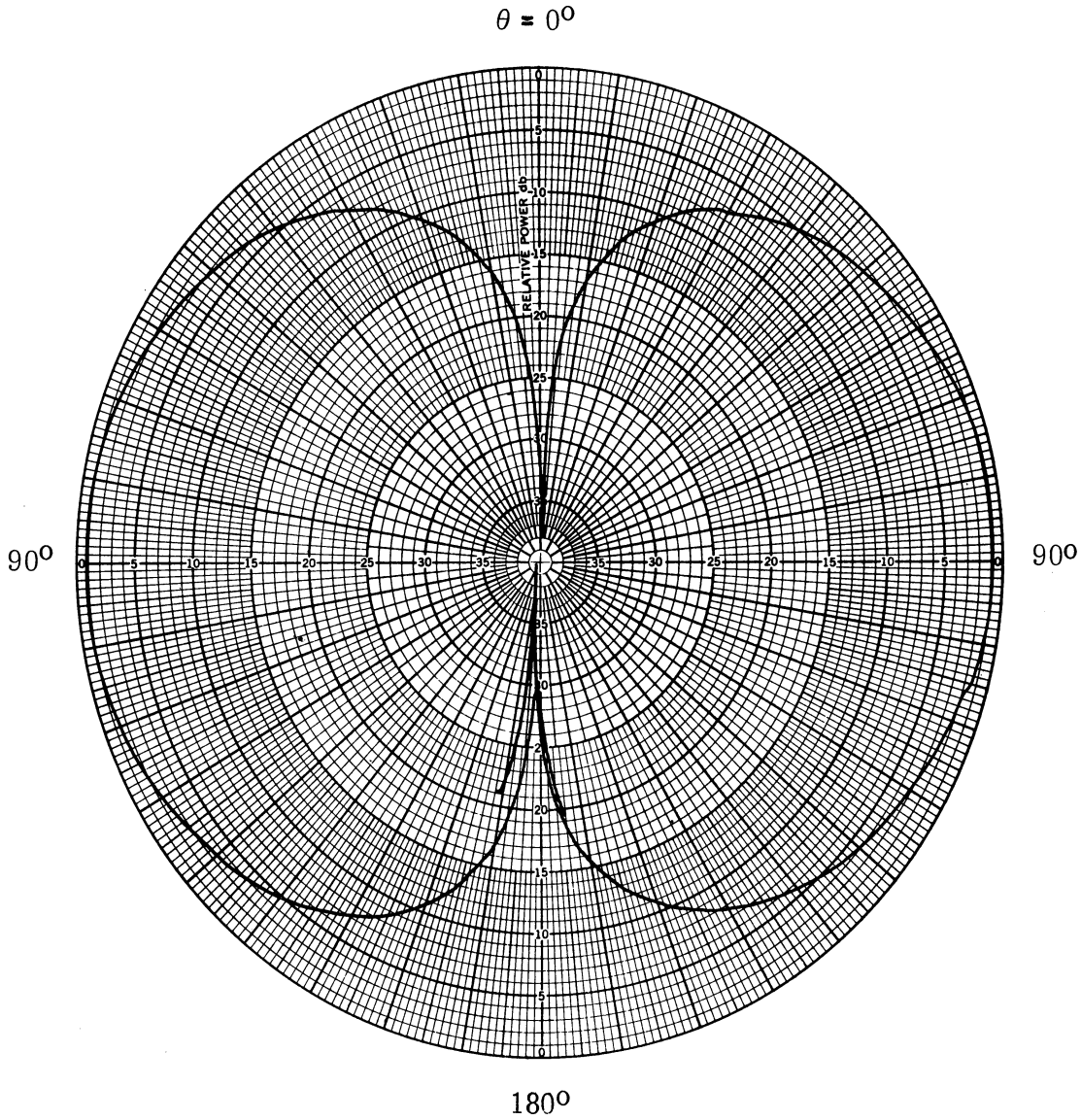

FIG. 3-3: E-PLANE POLARIZATION OF BIRD CAGE ANTENNA AT 100 MHz

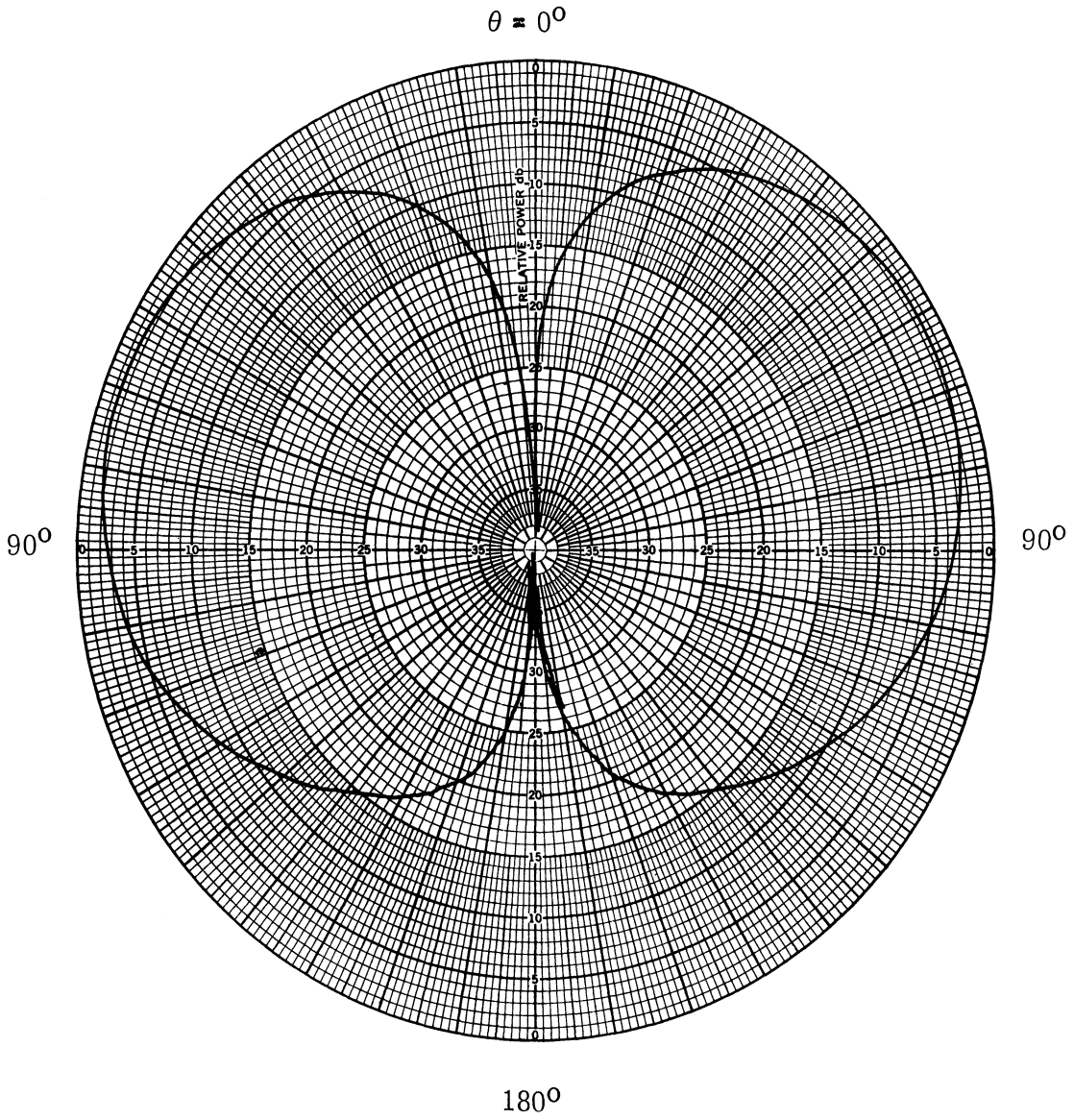

FIG. 3-4: E-PLANE POLARIZATION OF BIRD CAGE ANTENNA AT 200 MHz

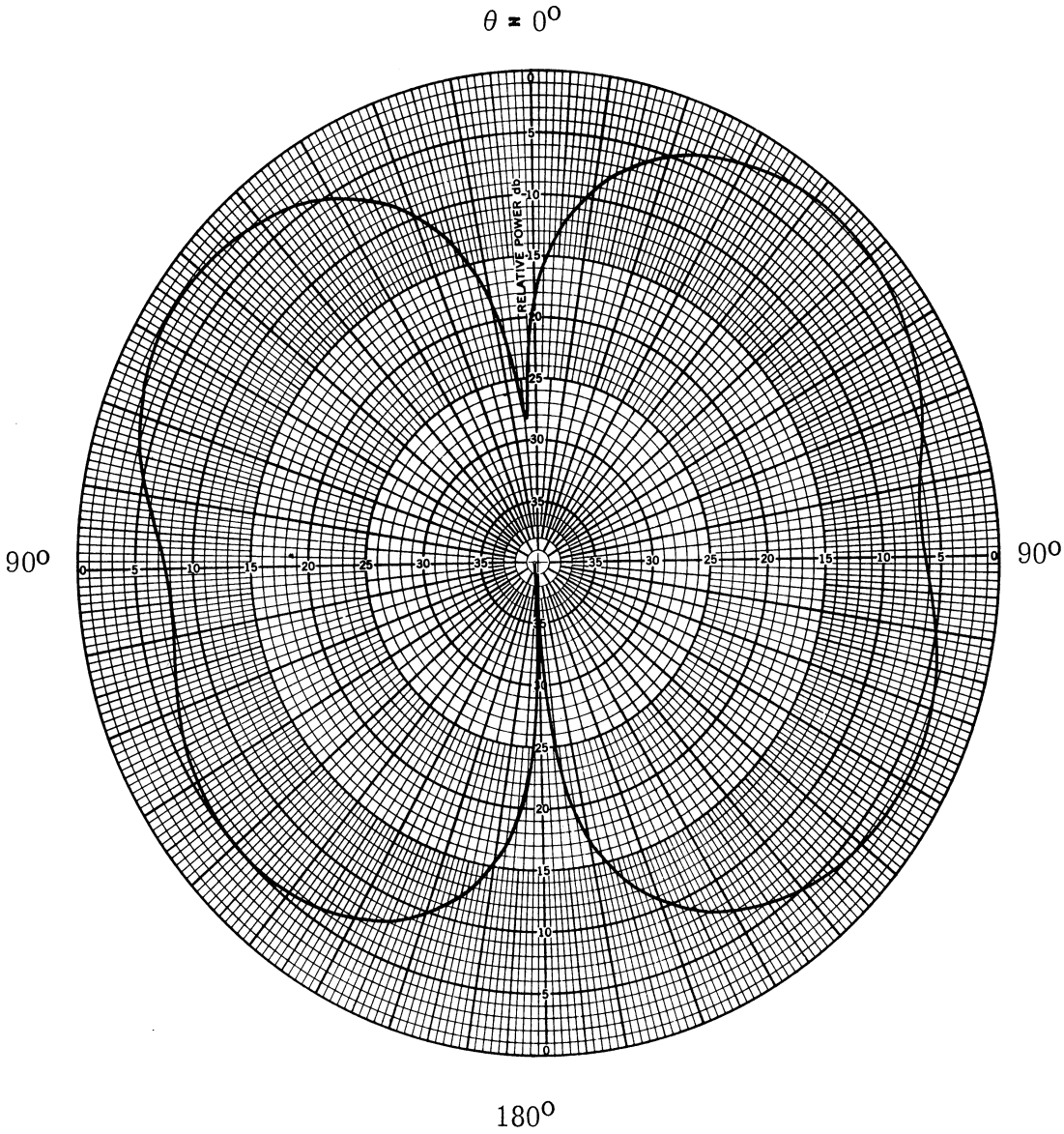

FIG. 3-5: E-PLANE POLARIZATION FOR BIRD CAGE ANTENNA AT 300 MHz

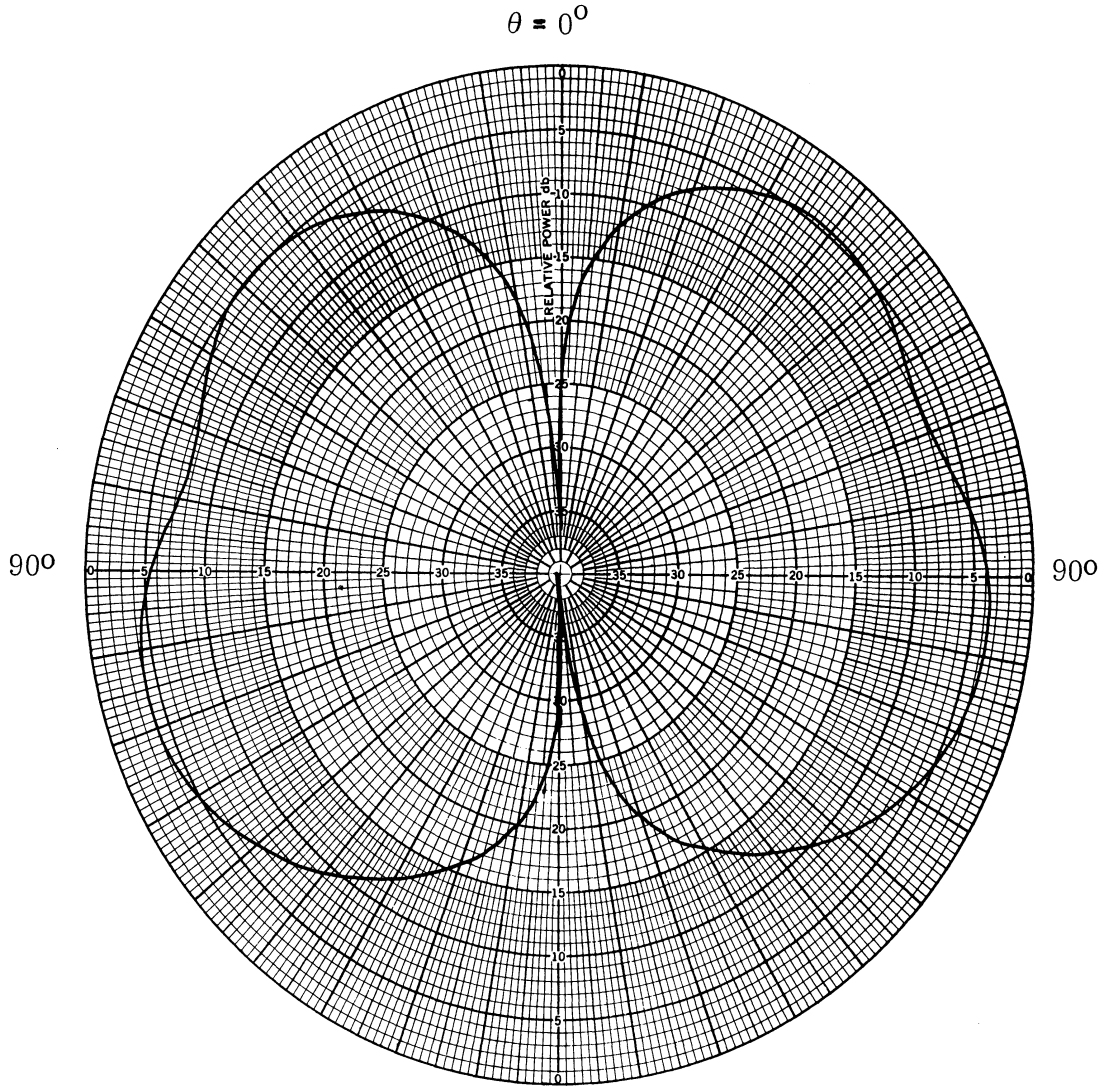

FIG. 3-6: E-PLANE POLARIZATION FOR BIRD CAGE ANTENNA AT 400 MHz

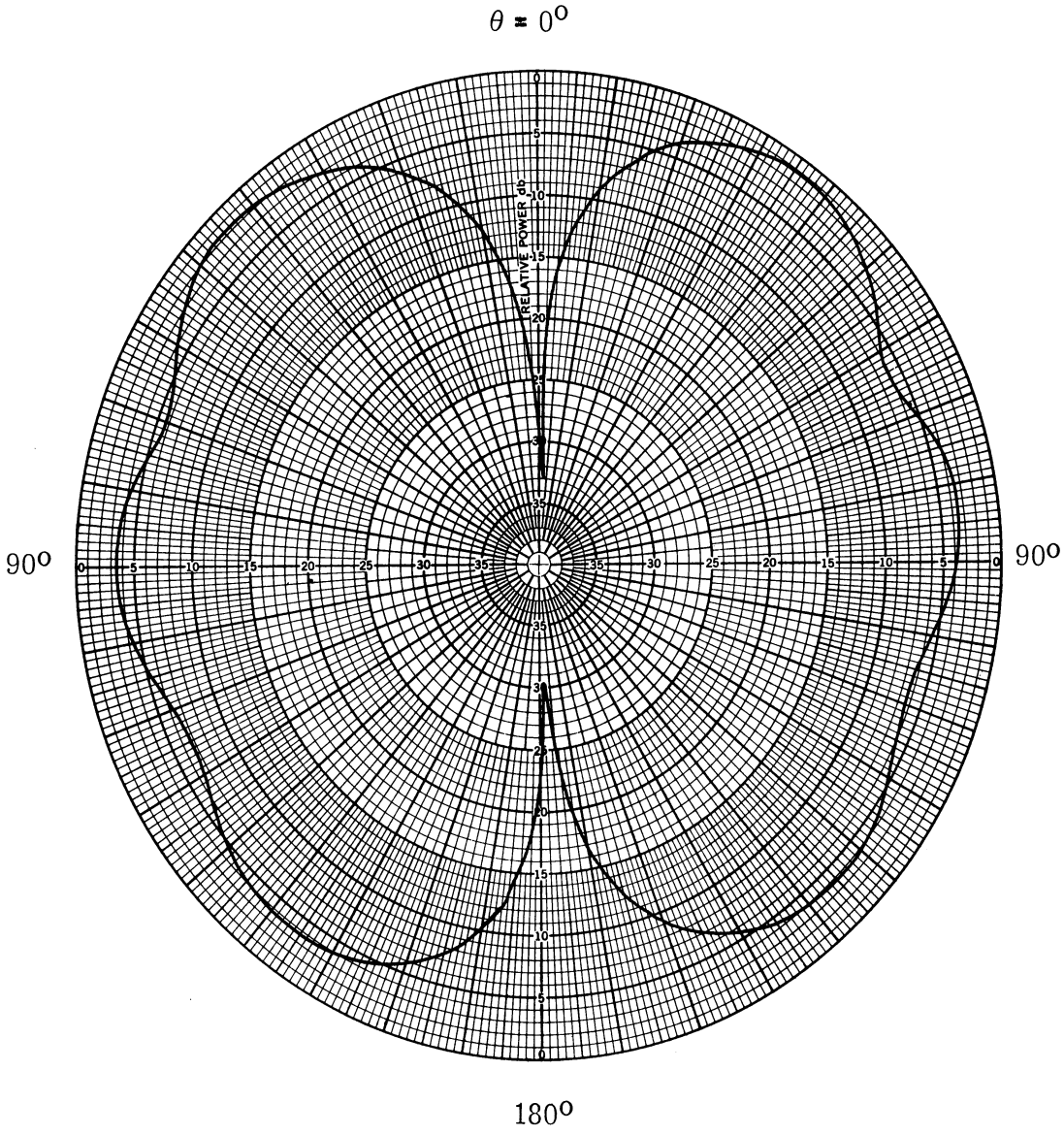

FIG. 3-7: E-PLANE POLARIZATION FOR BIRD CAGE ANTENNA AT 500 MHz

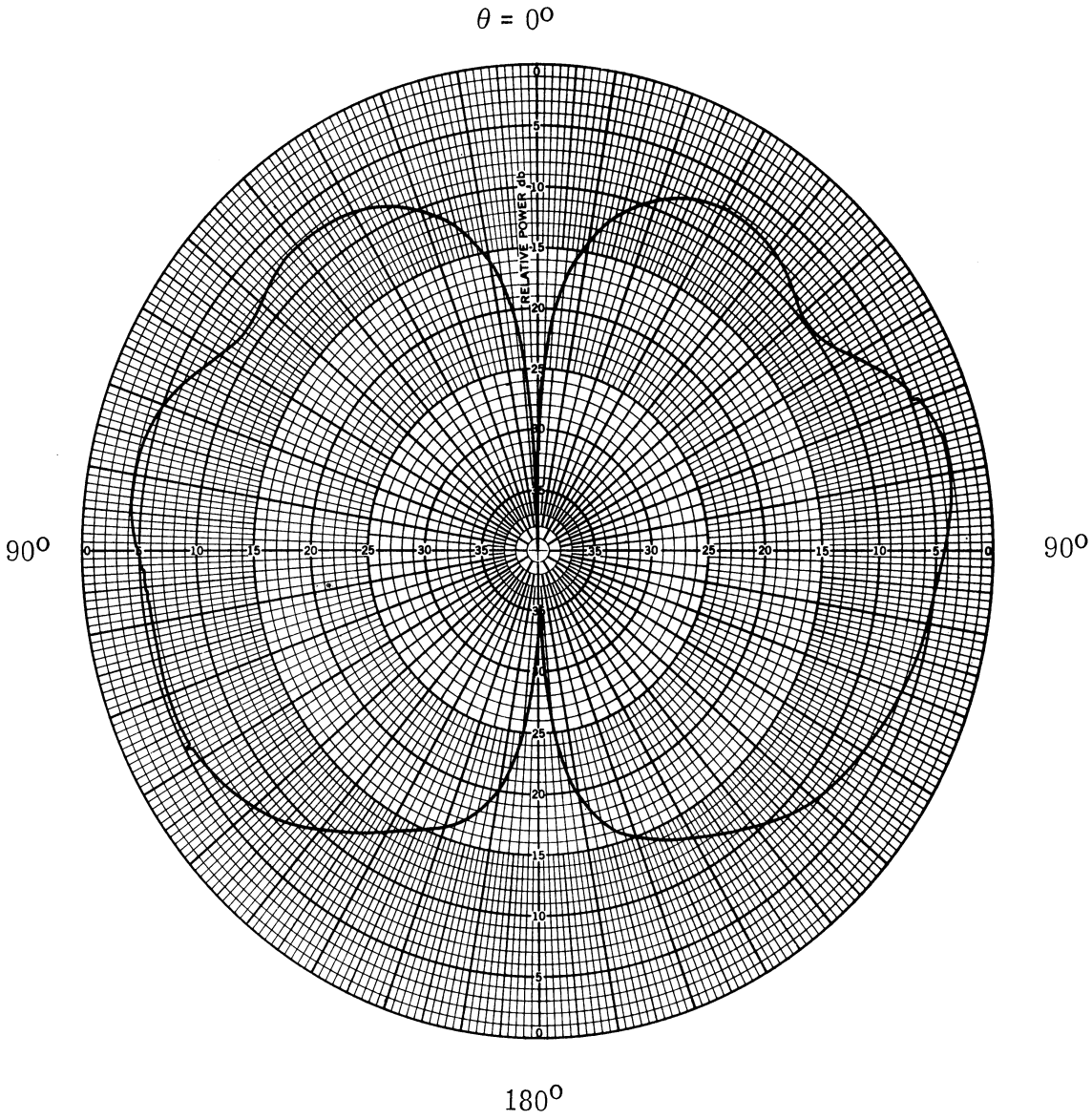

FIG. 3-8: E-PLANE POLARIZATION FOR BIRD CAGE ANTENNA AT 600 MHz

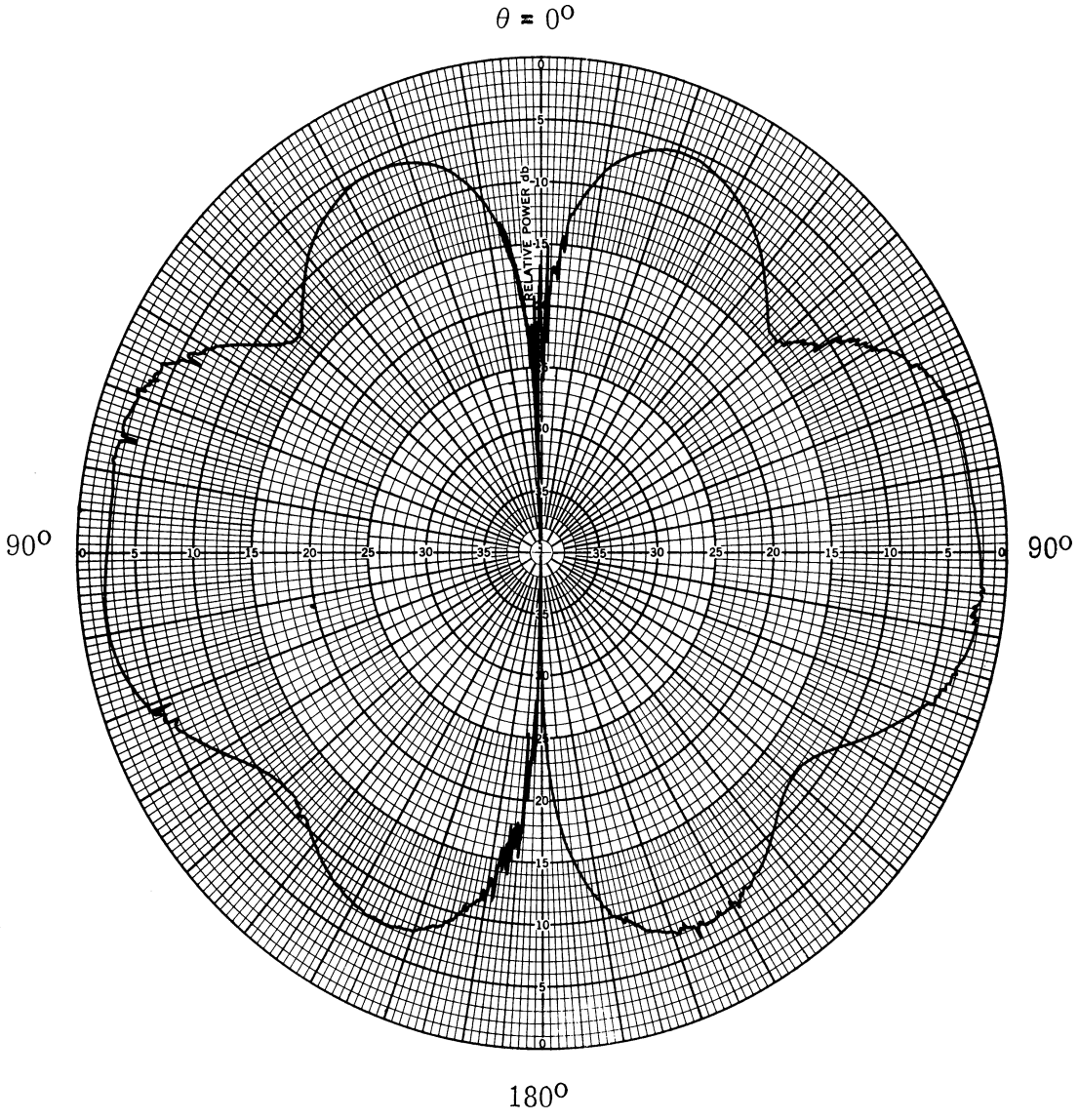

FIG. 3-9: E-PLANE POLARIZATION FOR BIRD CAGE ANTENNA AT 700 MHz

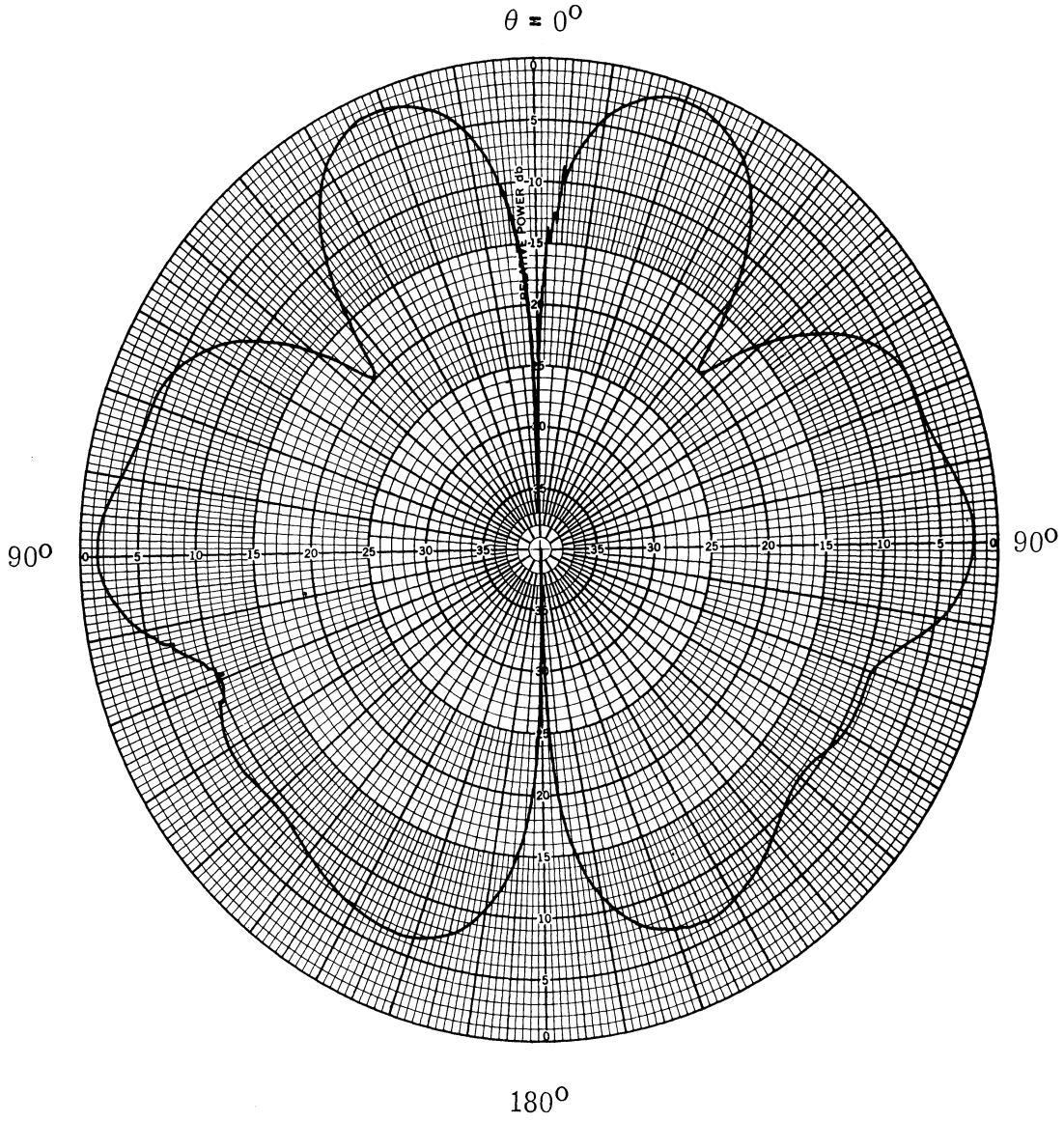

FIG. 3-10: E-PLANE POLARIZATION FOR BIRD CAGE ANTENNA AT 800 MHz

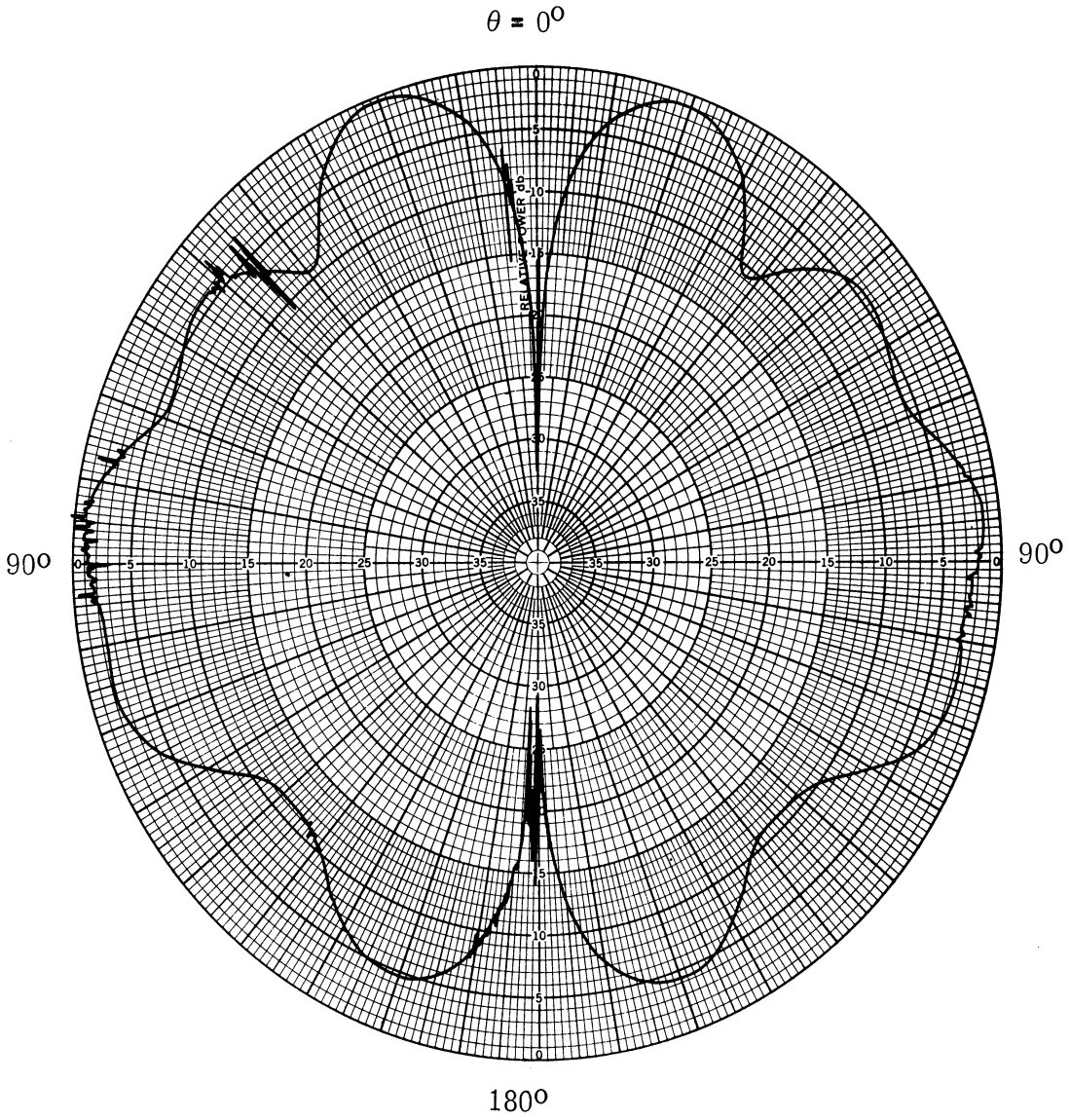

FIG. 3-11: E-PLANE POLARIZATION FOR BIRD CAGE ANTENNA AT 900 MHz

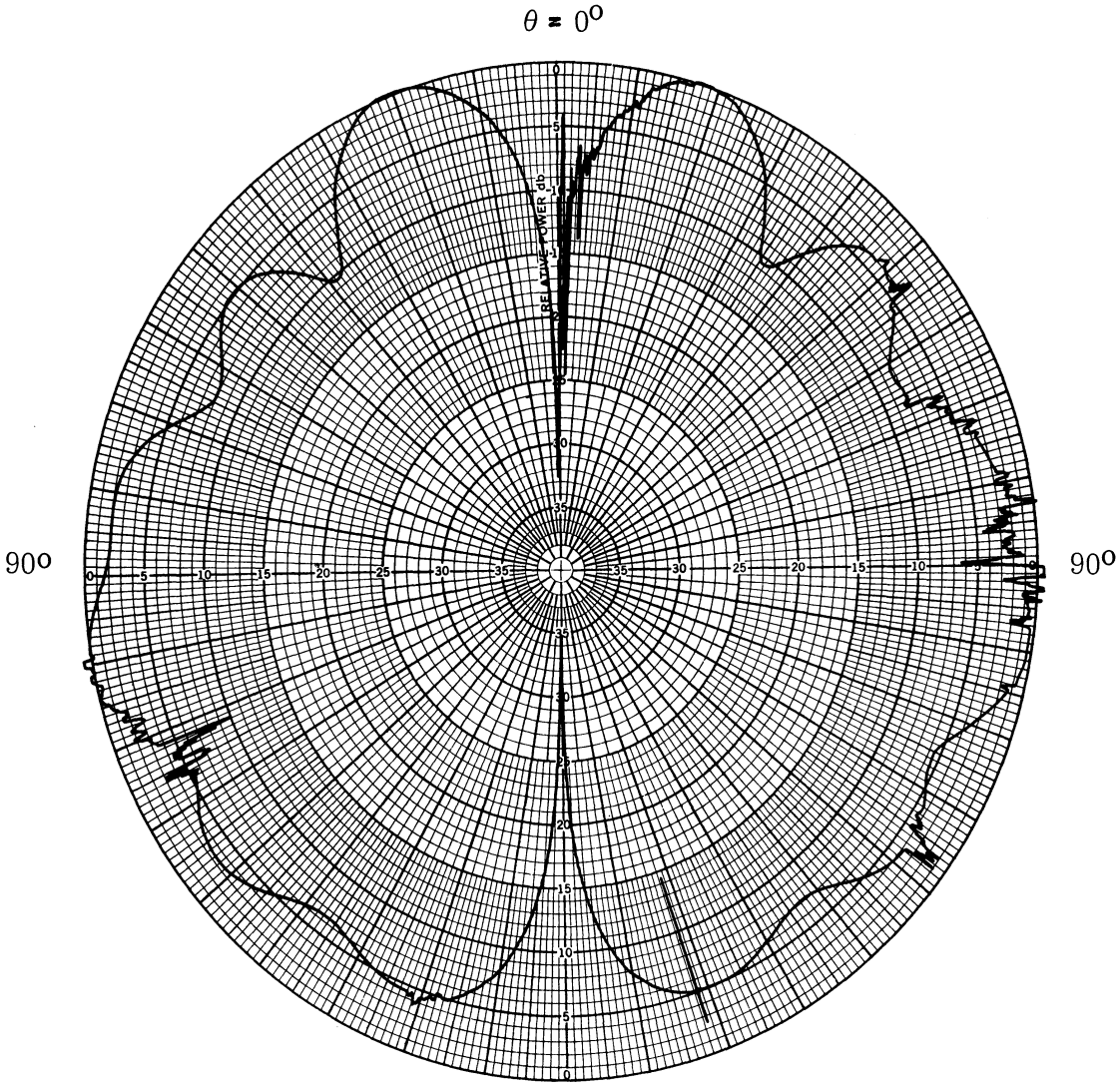

FIG. 3-12: E-PLANE POLARIZATION FOR BIRD CAGE ANTENNA AT 1000 MHz

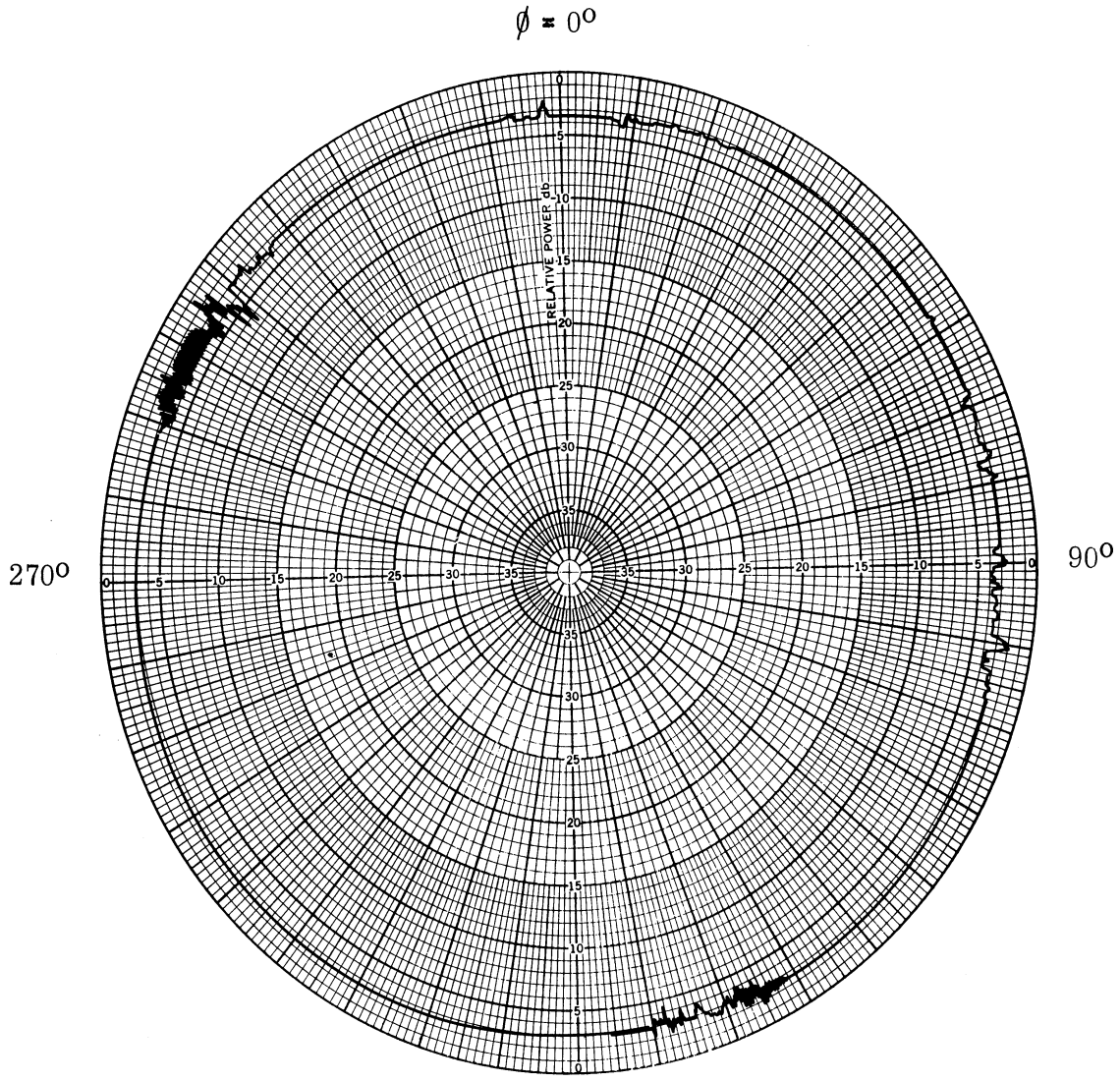

FIG. 3-13: H-PLANE POLARIZATION FOR BIRD CAGE ANTENNA AT 500 MHz

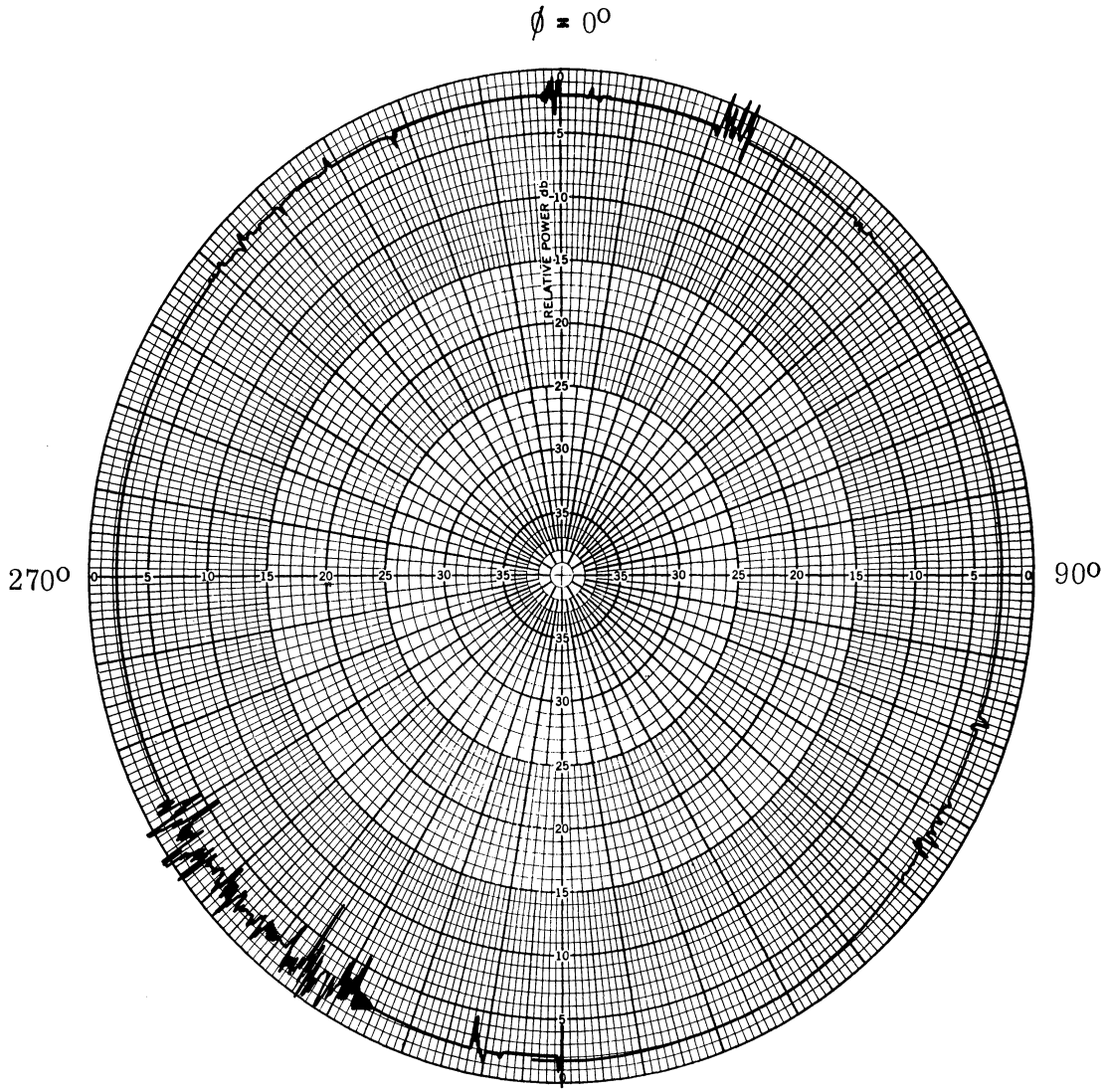

FIG. 3-14: H-PLANE POLARIZATION FOR BIRD CAGE ANTENNA AT 600 MHz

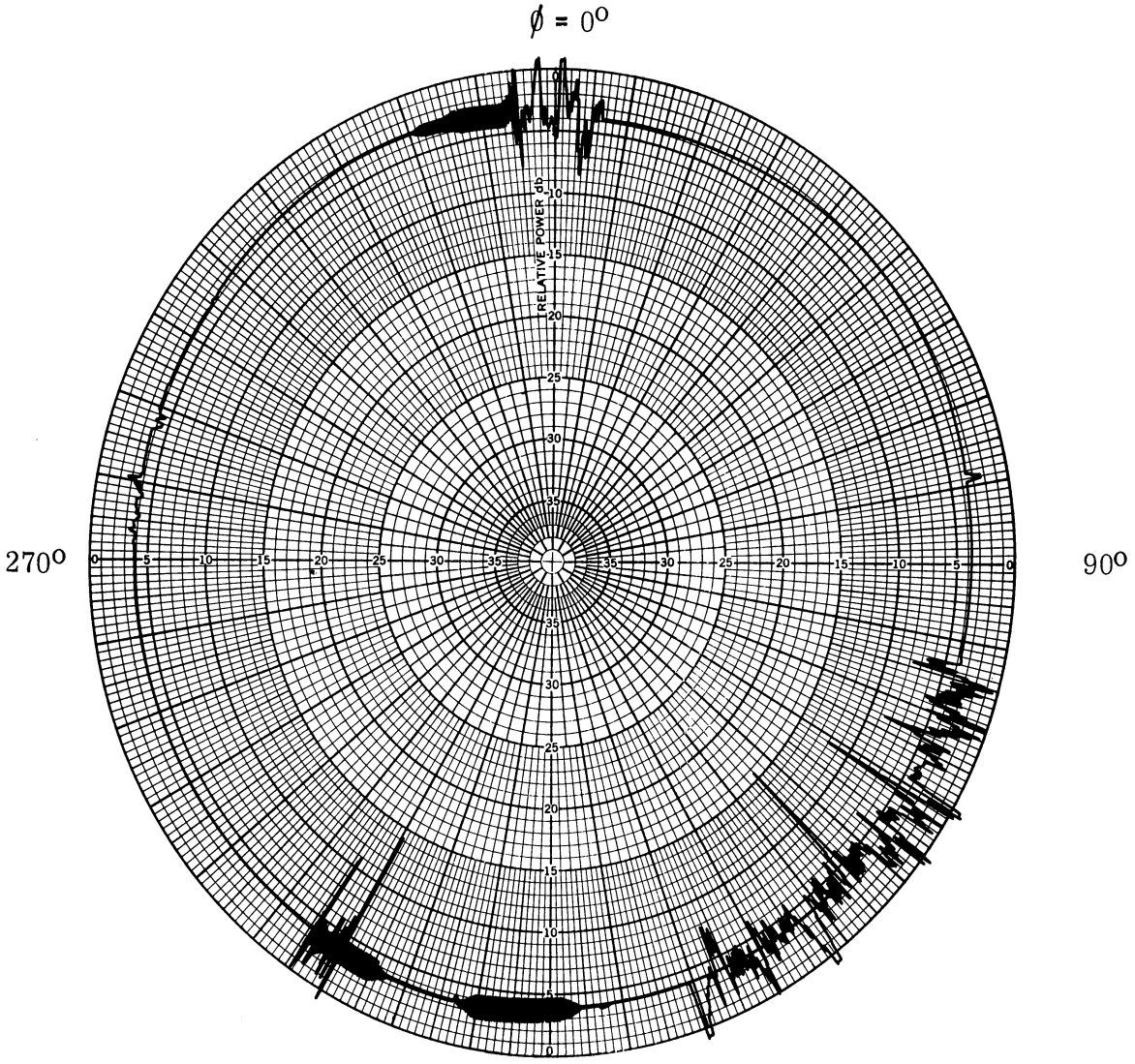

FIG. 3-15: H-PLANE POLARIZATION OF BIRD CAGE ANTENNA AT 700 MHz

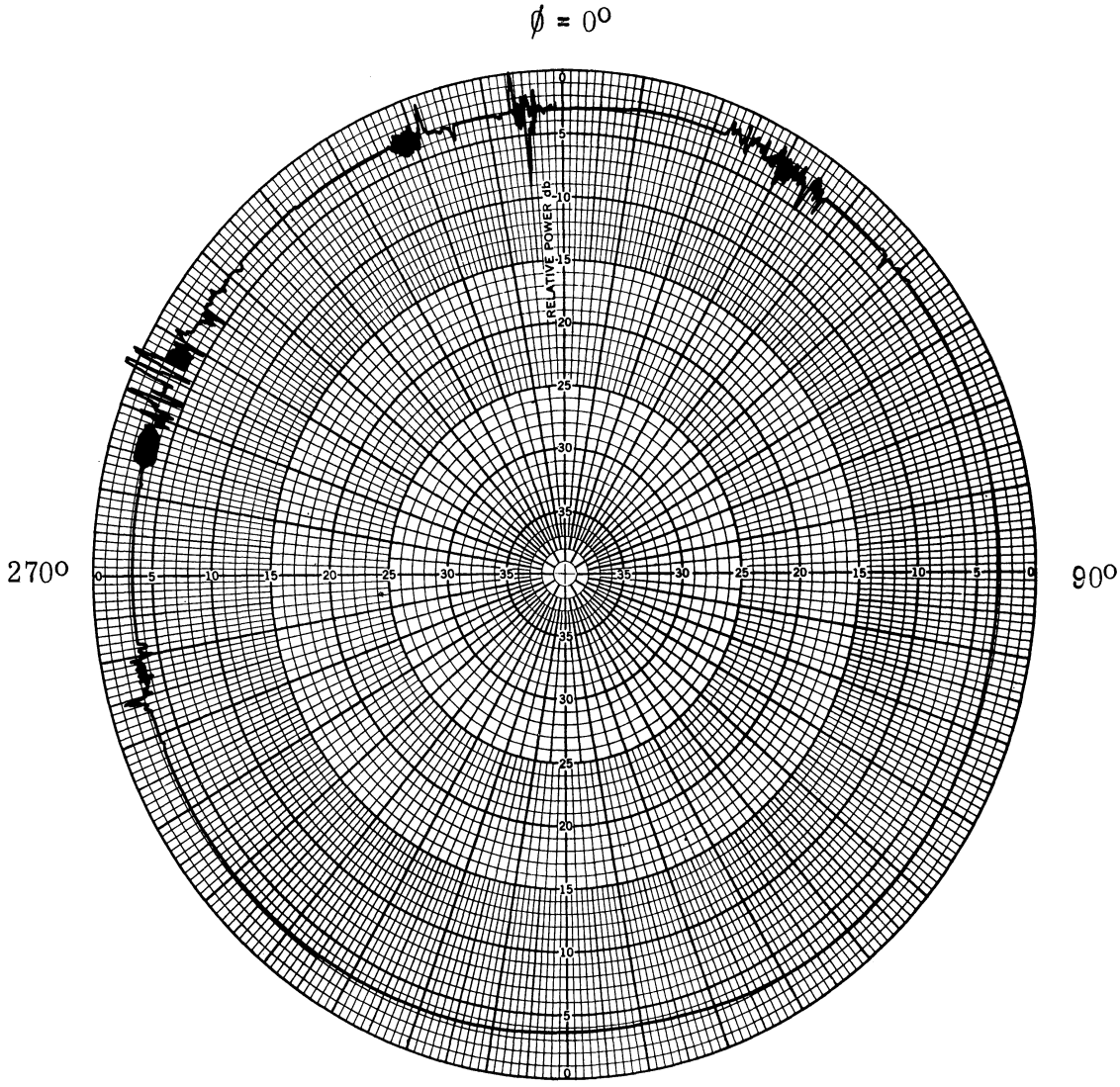

FIG. 3-16: H-PLANE POLARIZATION FOR BIRD CAGE ANTENNA AT 800 MHz

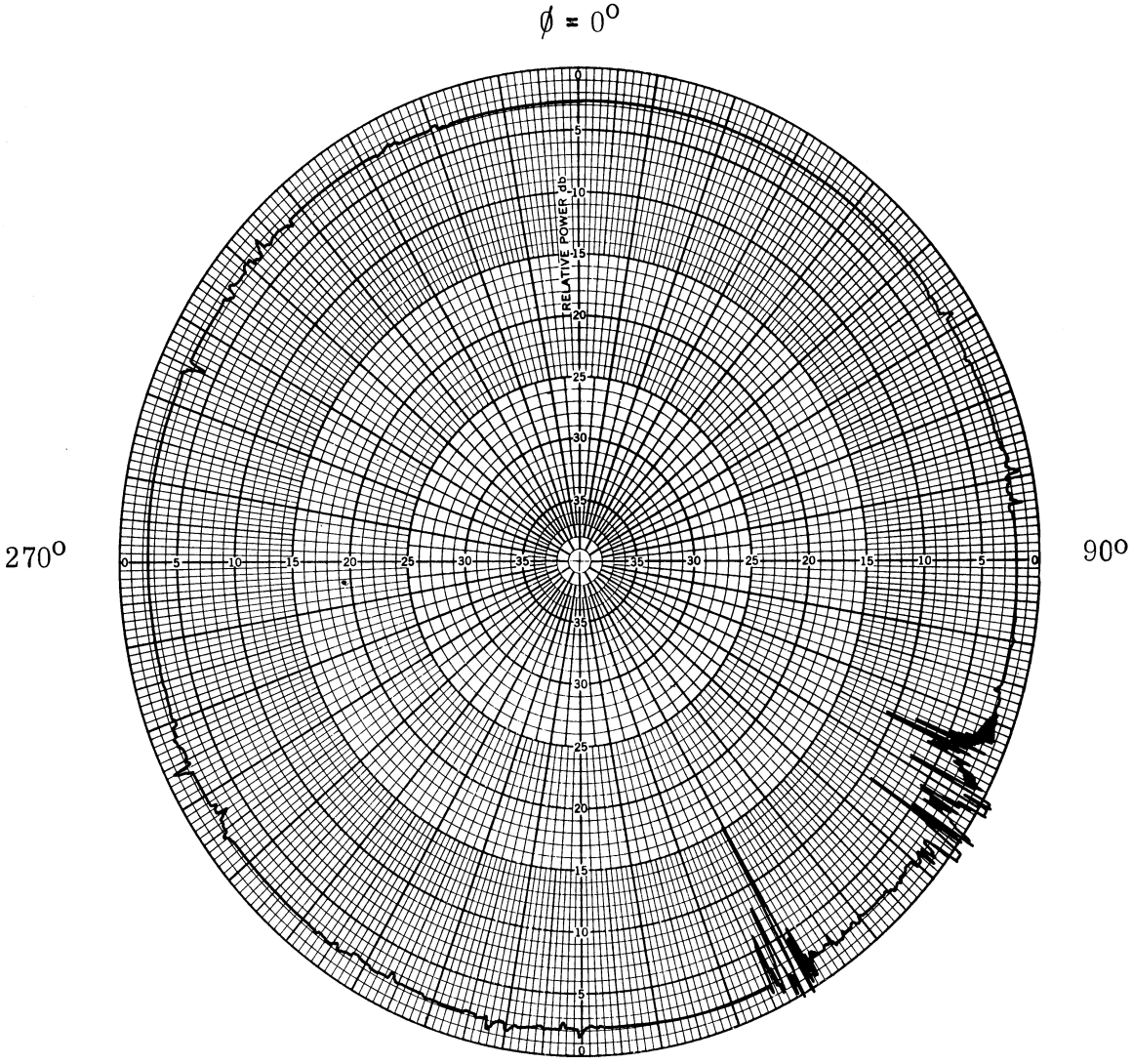

FIG. 3-17: H-PLANE POLARIZATION FOR BIRD CAGE ANTENNA AT 900 MHz

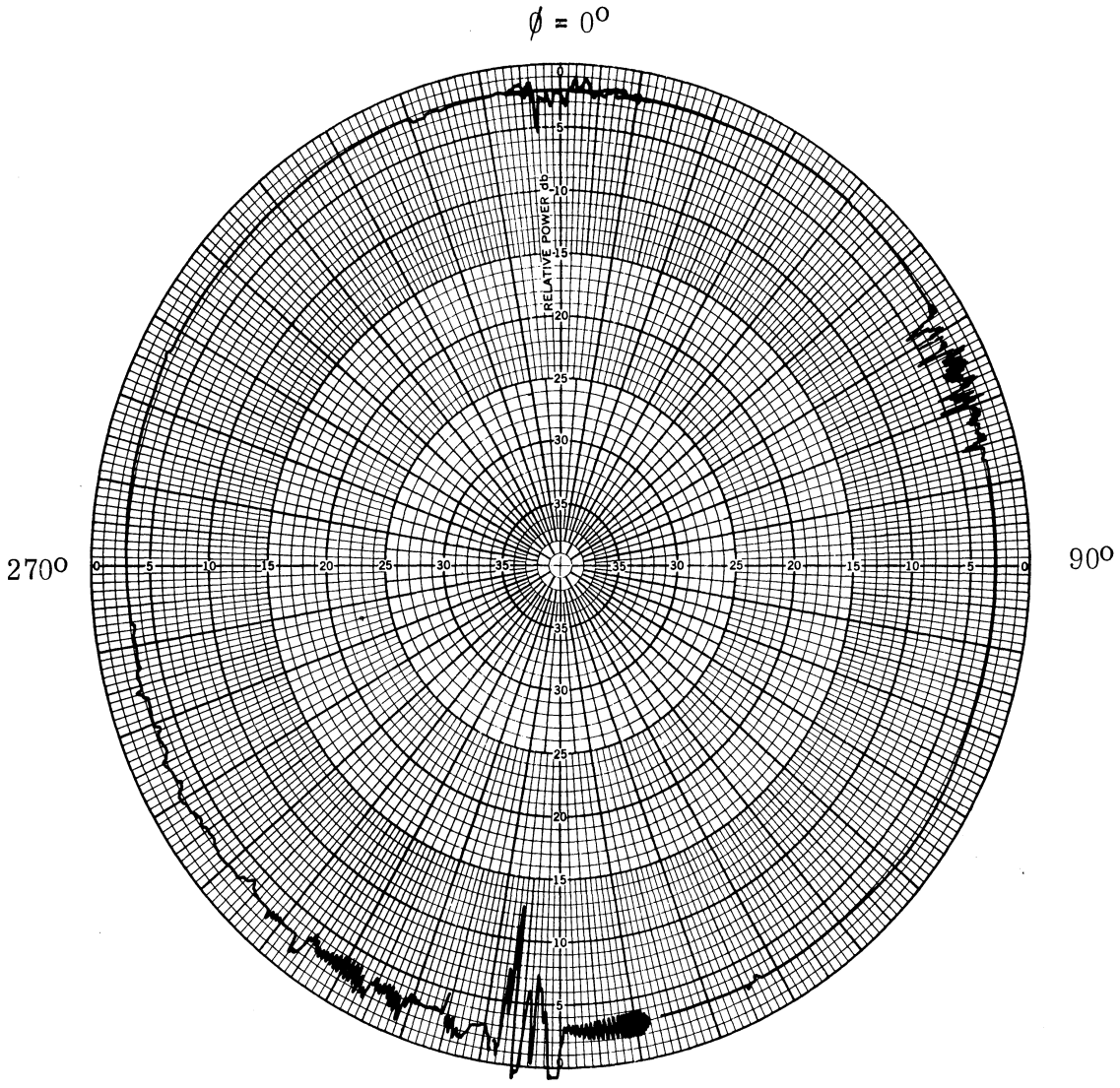

FIG. 3-18: H-PLANE POLARIZATION FOR BIRD CAGE ANTENNA AT 1000 MHz

unwanted currents are induced on the transmission line feeding the antenna. These unwanted currents are most appreciable in the 100-250 MHz range and can possibly be minimized through the use of a larger ground plane. At frequencies above 500 MHz, the region between the lower half of the bird cage and the conic ground plane tends to be most active and here the antenna functions in a biconical fashion.

To ensure maximum radiation in the $\theta = 90^{o}$ plane several ground plane configurations were investigated and reported in the Third Quarterly (Ferris et al, 1965). From that study, it was concluded that the 90^{o} conic ground plane would provide optimum impedance and pattern characteristics.

The mechanical configuration of the basic bird cage was felt to be inadequate for field use, therefore, additional support was added for mechanically strength. The added support consisted of a block of polyfoam contoured to fit snugly around the antenna. The antenna and its foam support structure are shown in Fig. 3-19. The complete antenna including the 45^{o} conical ground plane and encasing material occupy a cylindrical space 38 1/2" tall by 24" in diameter. The pattern and impedance data shown previously were obtained with the antenna encased in the polyfoam block as shown in the above figure.

3.2 Trap Antennas

A model of a new trap antenna configuration is shown in Fig. 3-20. Because of the limited time available during this interim, only impedance data has been collected for this antenna.

The basic element is a broadband fat monopole designed to operate from 500-1000 MHz. Since the monopole is 3" in diameter and approximately 3" tall, it should operate well over a 2:1 frequency range. To optimize impedance data from the element a conic section was employed at the base of the element whose included angle was 90^{o}. The fat monopole has a hollow center such that axially symmetric tubes may be added as shown in Fig. 3-21.

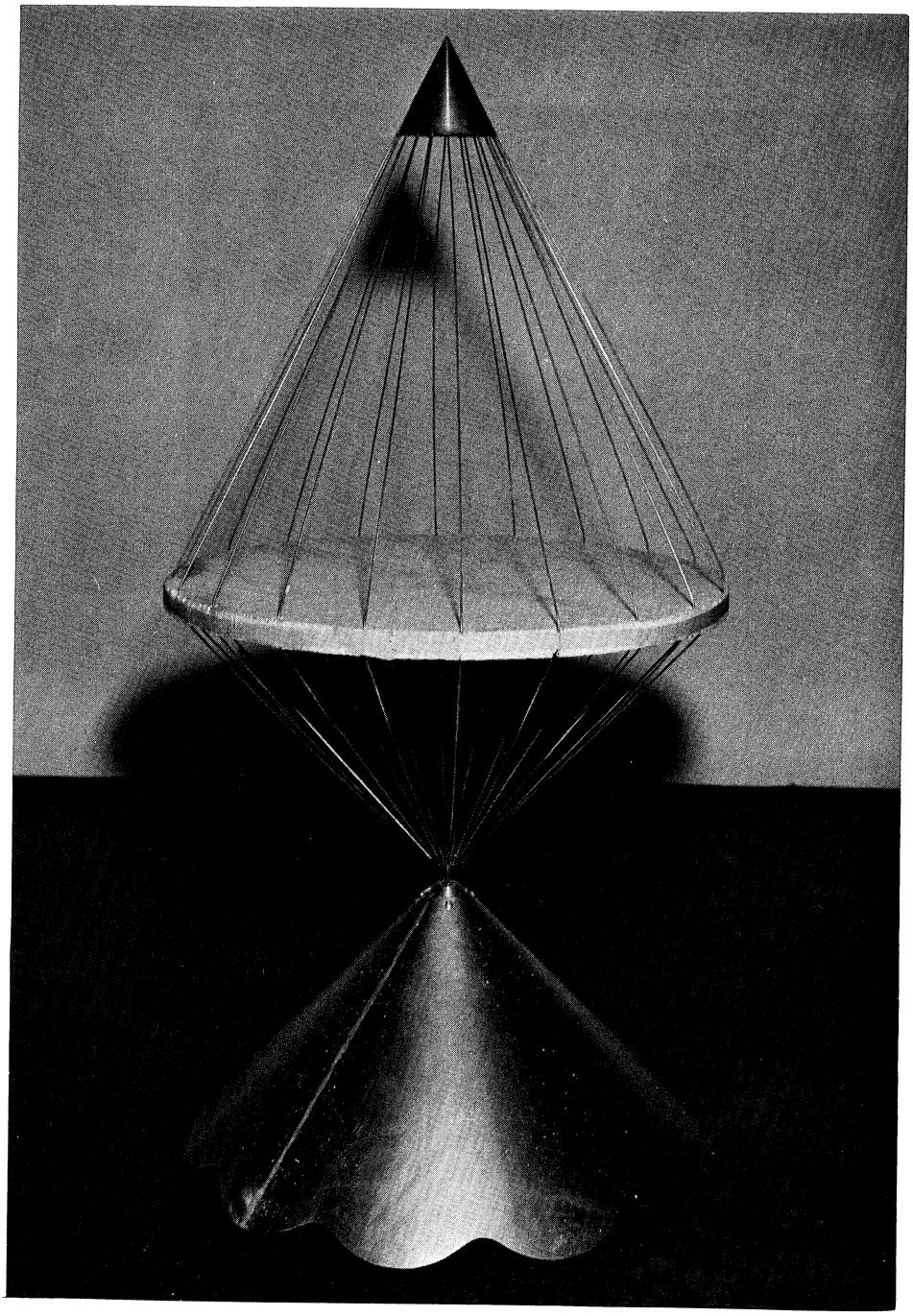

FIG. 3-19A: BIRD CAGE ANTENNA AND CONICAL GROUND PLANE

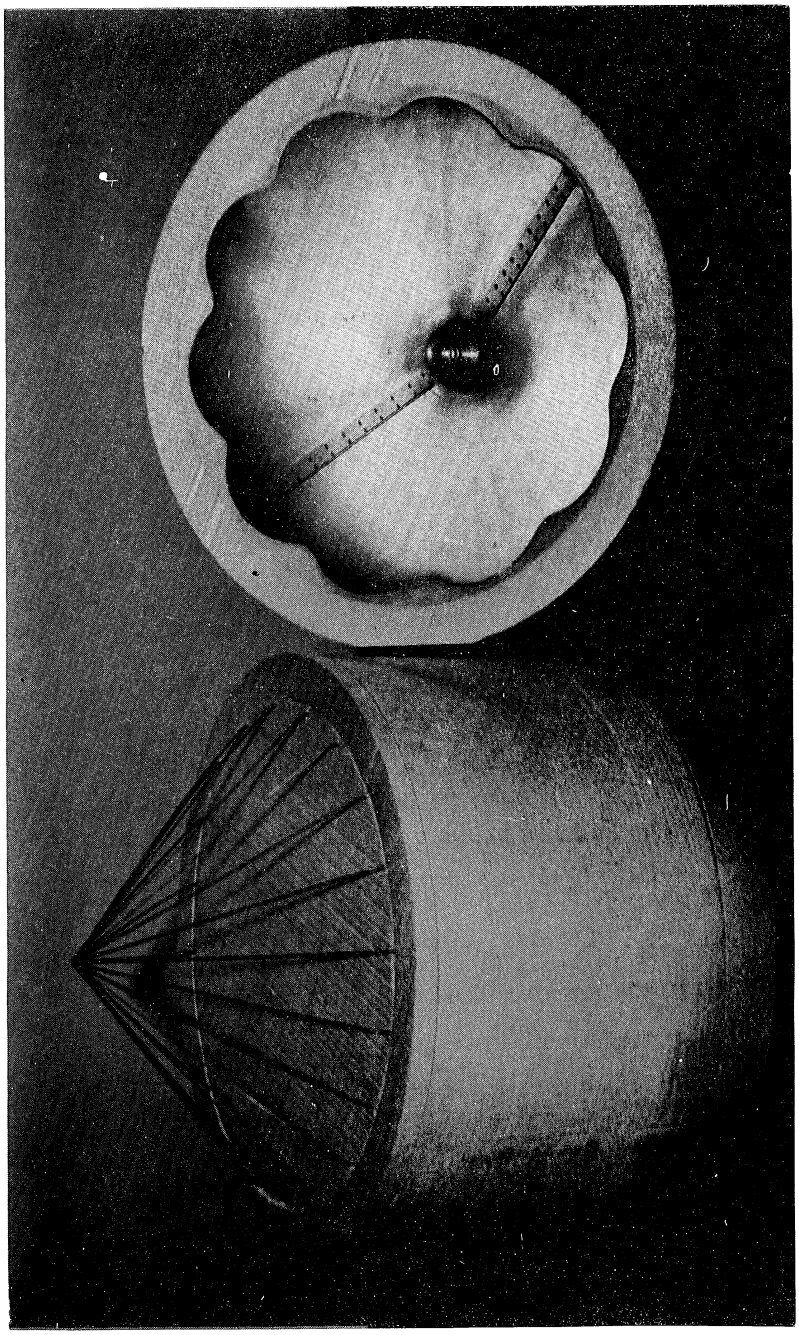

FIG. 3-19B: BIRD CAGE AND GROUND PLANE SHOWING PLACEMENT IN SUPPORT STRUCTURE

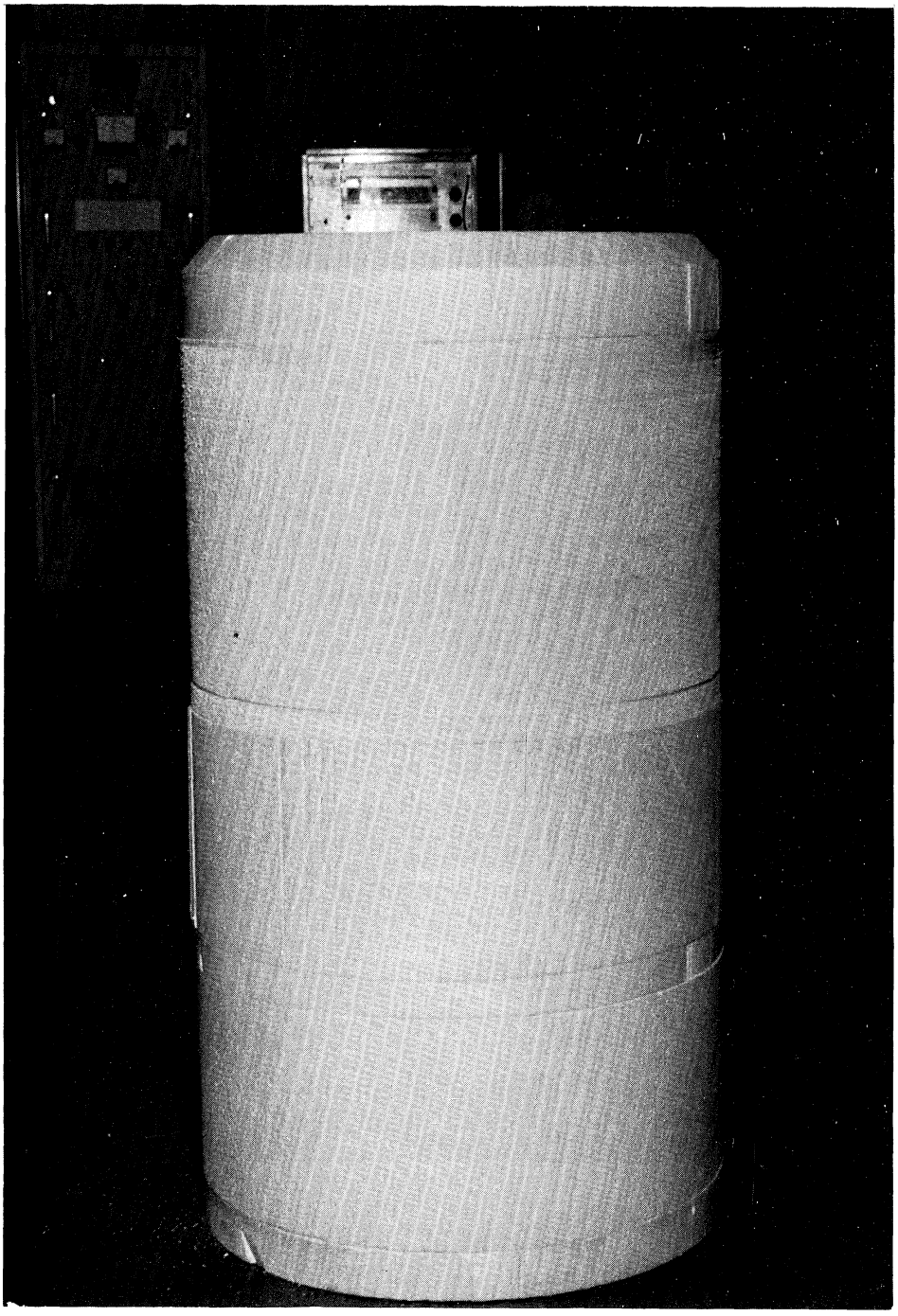

FIG. 3-19C: BIRD CAGE AND GROUND PLANE IN SUPPORT STRUCTURE

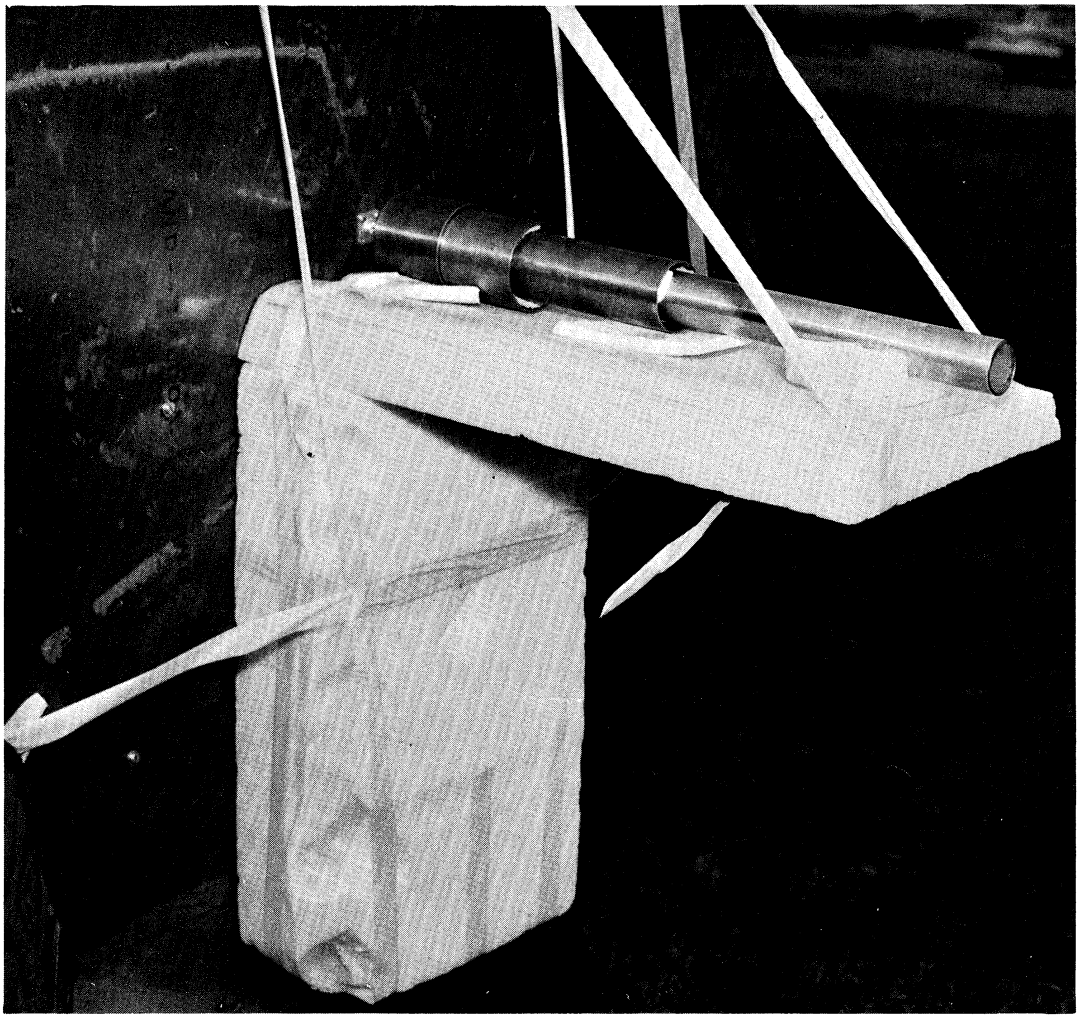

FIG. 3-20: SLEEVE TRAP MONOPOLE

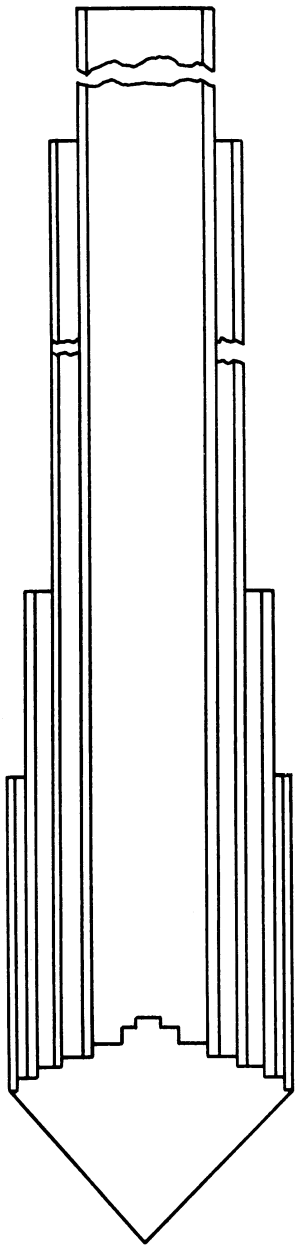

FIG. 3-21: CUT-AWAY VIEW OF SLEEVE TRAP MONOPOLE

The VSWR of the fat monopole less the axially symmetric tubes was measured over the frequency range of 500-1000 MHz and was less than 3:1. To this basic element three additional elements were added, one at a time. Their lengths varied such that they were $\lambda/4$ long at 500, 200 and 125 MHz. Employing the basic element and the 500 MHz tube, a VSWR of less than 3:1 for a 4:1 frequency band was observed. To this combination a third element (being $\lambda/4$ long at 200 MHz) was added but the bandwidth was reduced due to the high VSWR at approximately 400 MHz. This was assumed to be caused by the third element ($\lambda/4$ at 200 MHz) since it was approximately $\lambda/2$ long at 400 MHz. To minimize the effects of the third element, a fourth element ($\lambda/4$ long at 125 MHz) was added. With the four elements the VSWR was again less than 3:1 for a 4:1 frequency band; typical data are shown in Fig. 3-22. To determine the maximum usuable frequency range (impedance characteristic) the VSWR characteristic of the four element configuration was measured from 50 - 2000 MHz and the results are shown in Fig. 3-23. It is interesting to note that from 250 - 2100 MHz, the antenna exhibits a VSWR of less than 3:1. However, this data is incomplete and will require further study as the 3rd and 4th element did not significantly improve the VSWR at the lower frequencies. Pattern data has been recorded in the frequency of 100-500 MHz with axial symmetric tubes mounted over a circular (4 foot diameter) ground plane and these are shown in Figs. 3-24 — 3-28. Due to a shortage of standard 40 db pattern paper these patterns appear on 50 db paper. All data is collected on the 40 log db setting on the recorder.

3.3 Mutual Coupling Study

The mutual coupling study was initiated in an effort to solve resonance problems associated with the manipole antenna. The resonances which have been discussed in previous Quarterly Reports showed up as high VSWR's in the low end of the

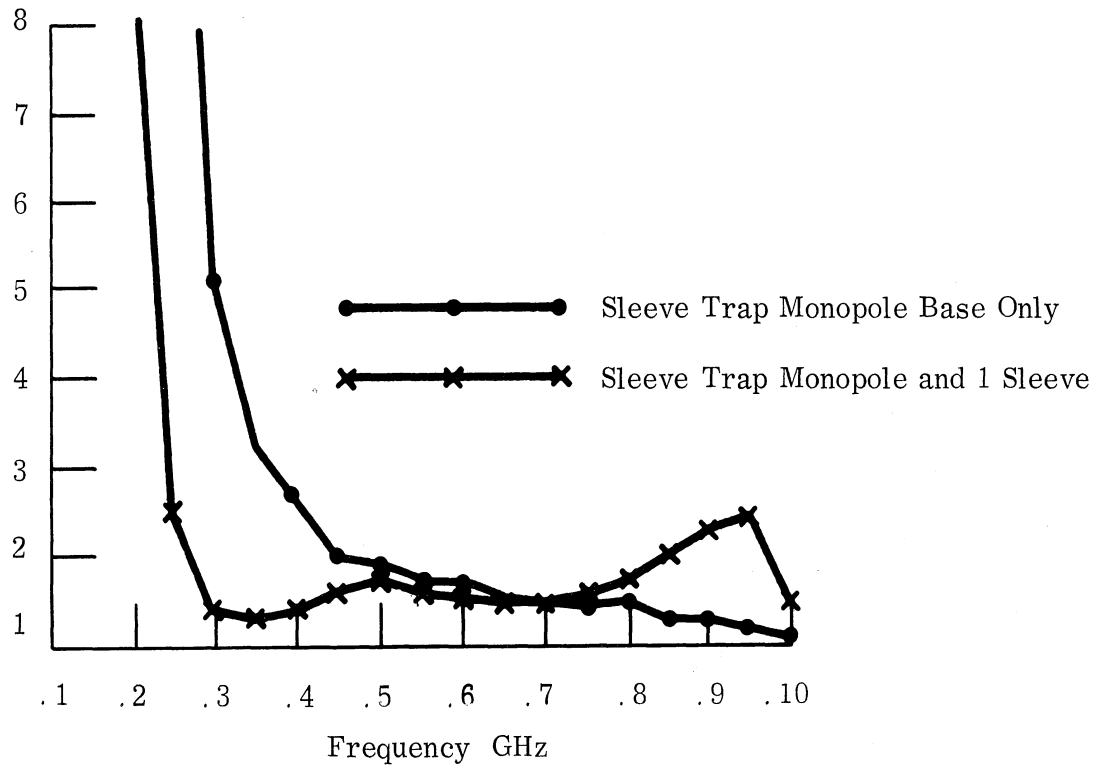

FIG. 3-22A: VSWR OF SLEEVE TRAP ANTENNA AS A FUNCTION OF ELEMENTS

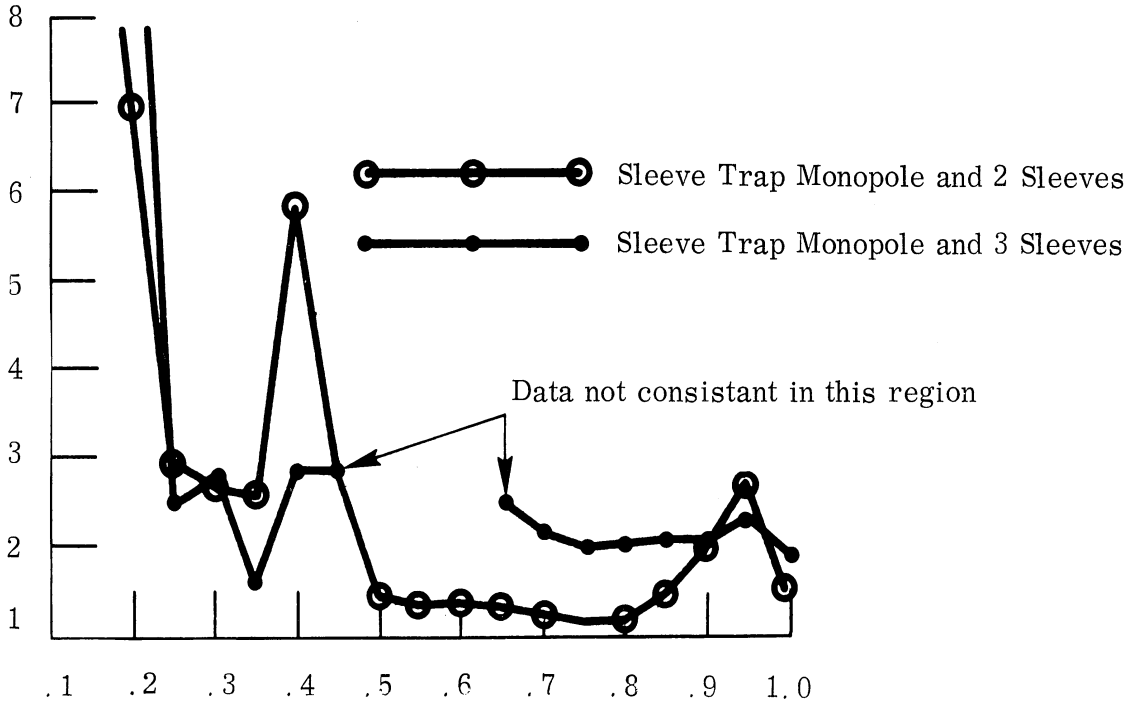

FIG. 3-22B: VSWR OF SLEEVE TRAP ANTENNA AS A FUNCTION OF ELEMENTS

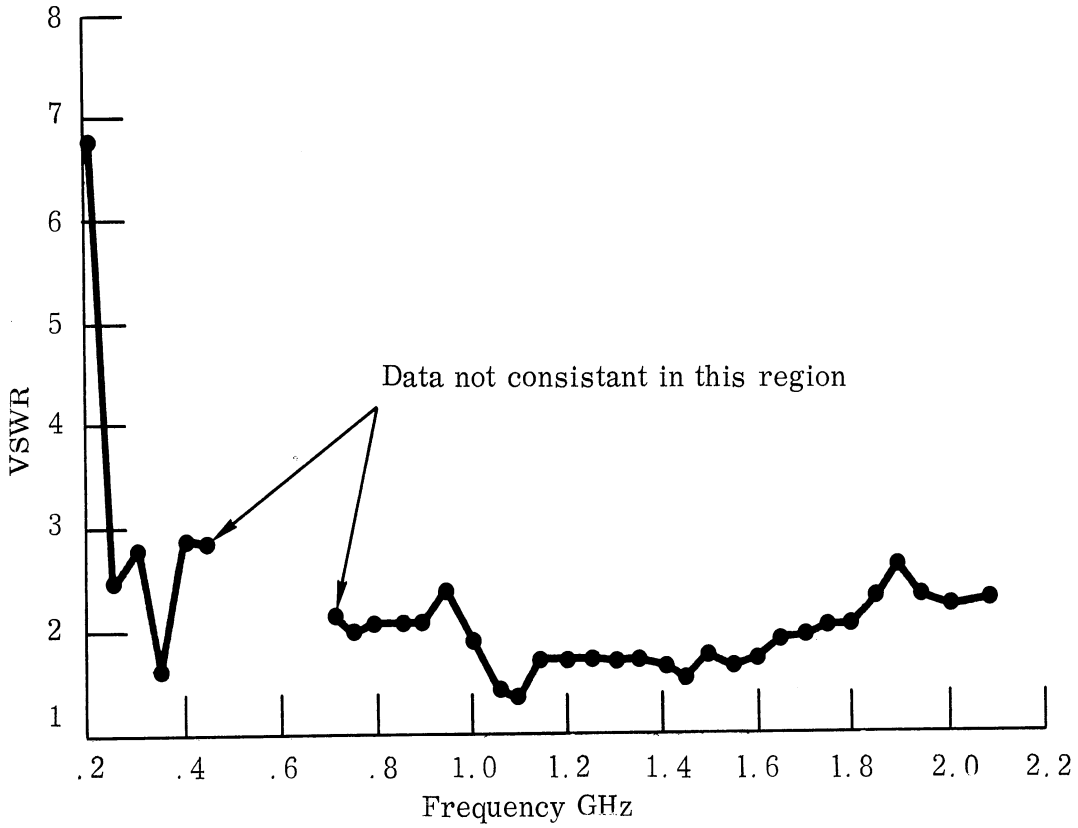

FIG. 3-23: VSWR OF SLEEVE TRAP ANTENNA AND THREE SLEEVES

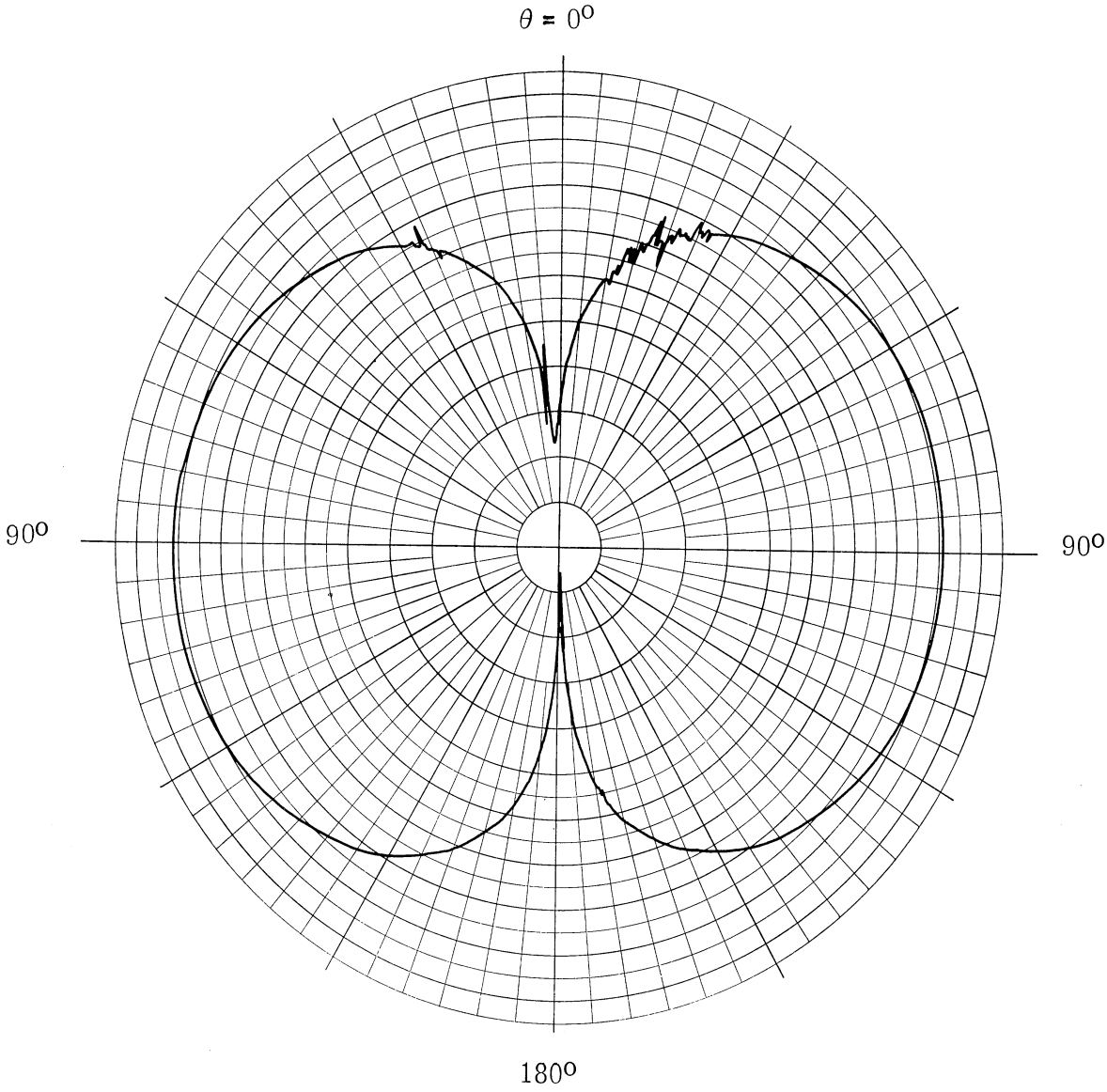

FIG. 3-24: E-PLANE POLARIZATION FOR SLEEVE TRAP ANTENNA AT 100 MHz

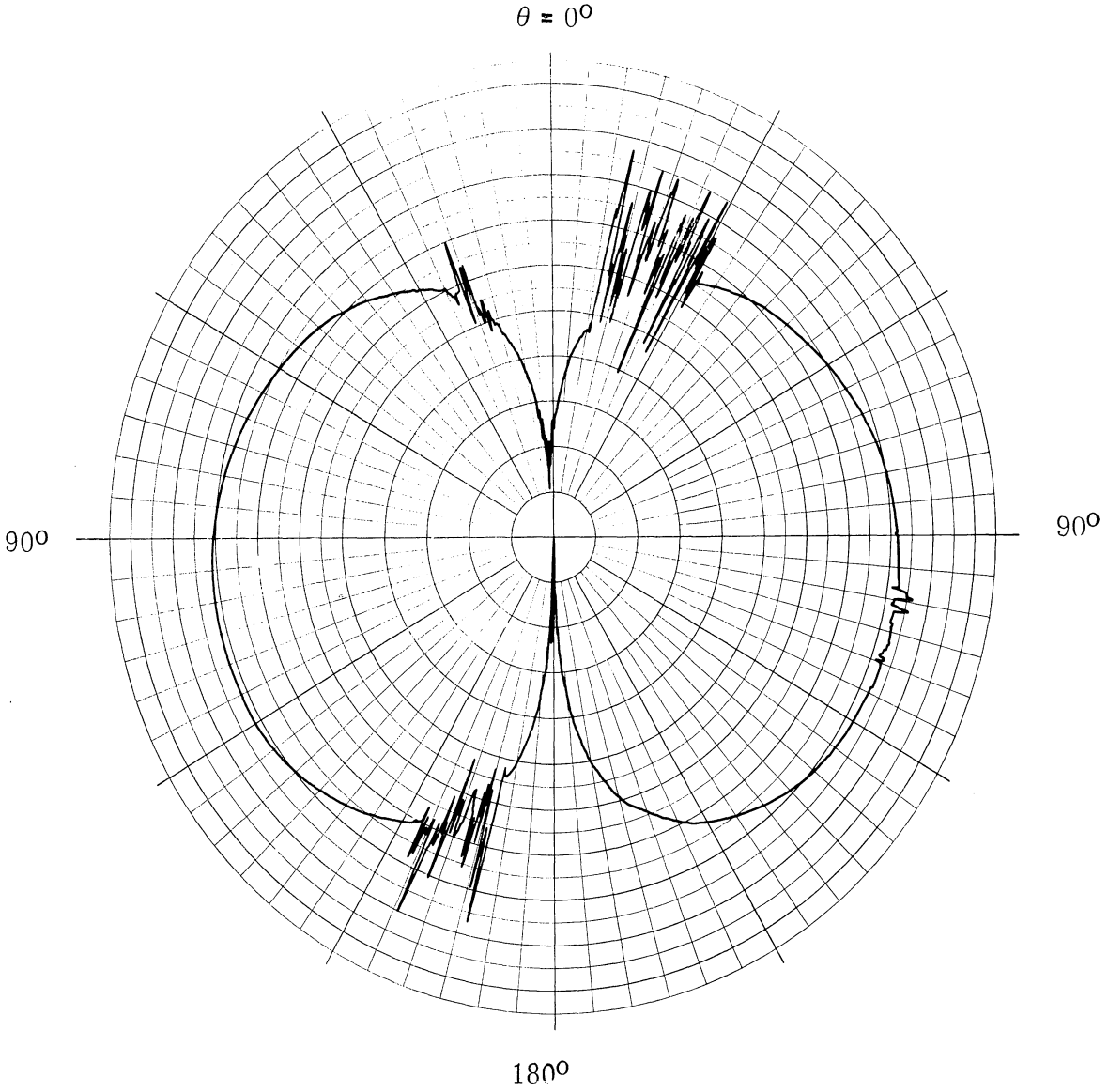

FIG. 3-25: E-PLANE POLARIZATION FOR SLEEVE TRAP ANTENNA AT 200 MHz

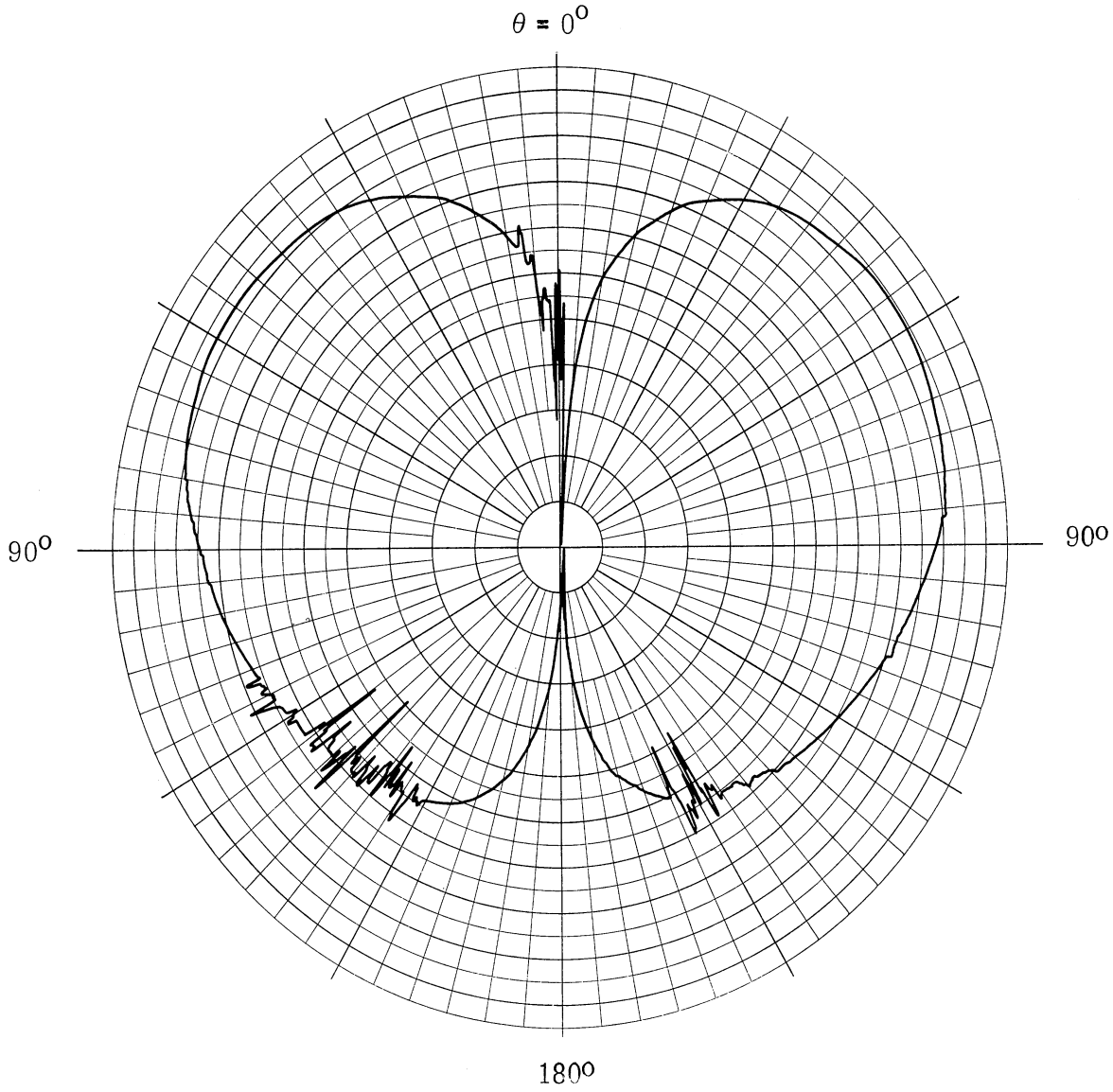

FIG. 3-26: E-PLANE POLARIZATION FOR SLEEVE TRAP ANTENNA AT 300 MHz

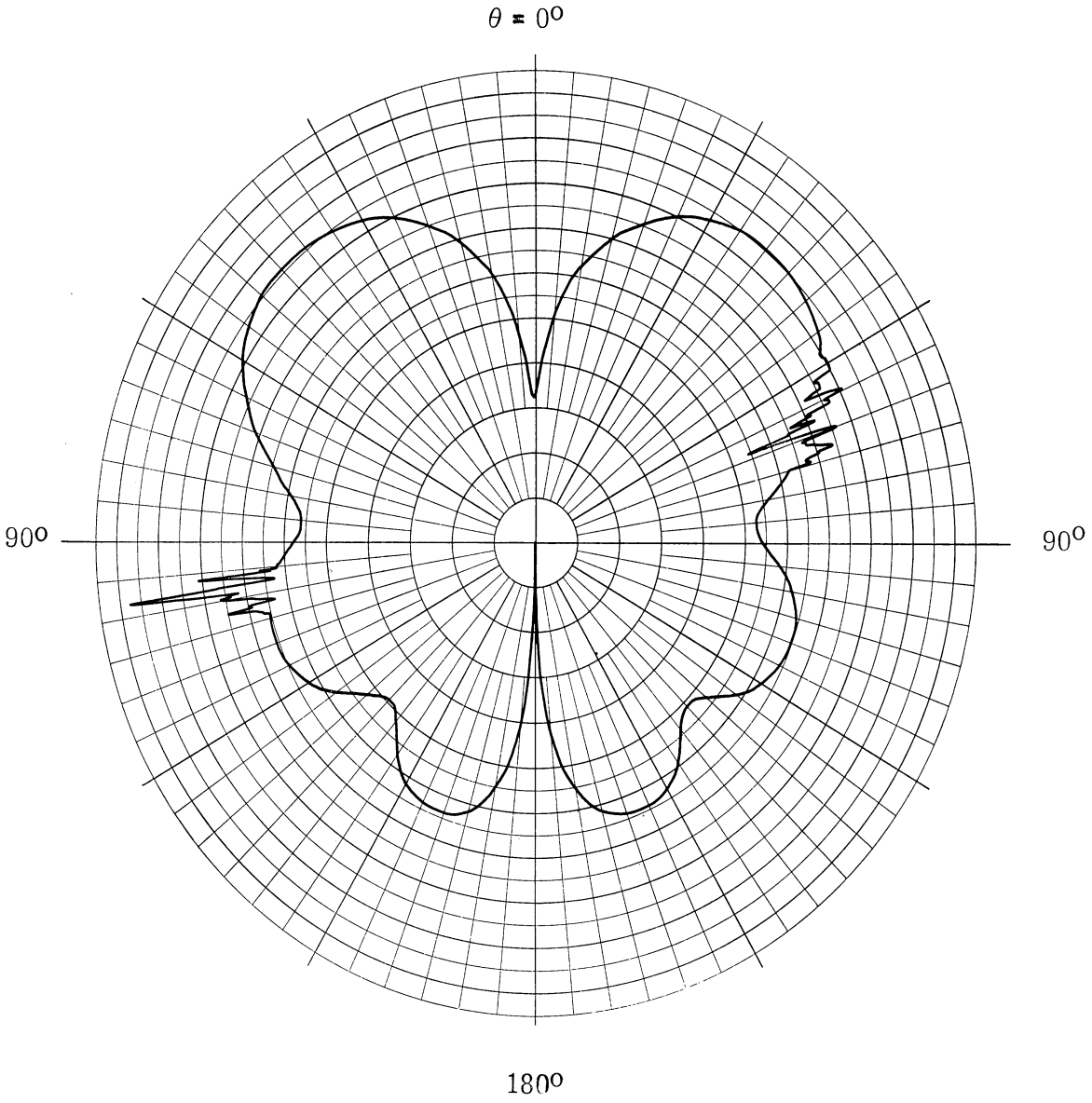

FIG. 3-27: E-PLANE POLARIZATION FOR SLEEVE TRAP MONOPOLE AT 420 MHz

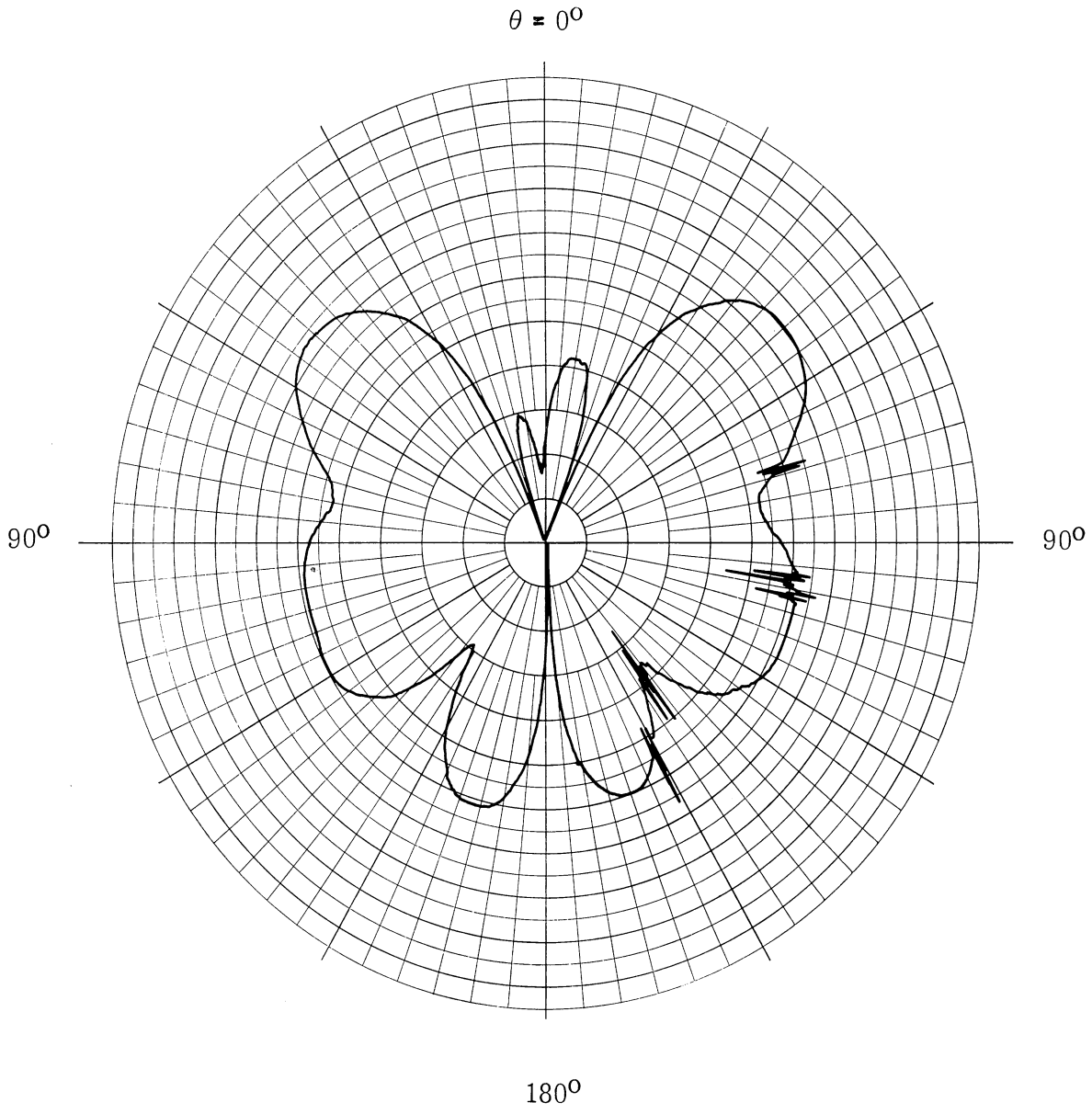

FIG. 3-28: E-PLANE POLARIZATION FOR SLEEVE TRAP ANTENNA AT 500 MHz

frequency band. The recent investigation has been directed towards improving the experimental setup. Initially, impedance data was collected for a $\lambda/4$ monopole mounted over a 4 foot diameter circular ground plane from 1.6 - 4.0 GHz. This data, although within 10 per cent of previous experimental and theoretical work, (Brown, et al 1945) was not felt to be in sufficiently close agreement. Therefore, a large ground plane has been obtained and a new monopole configuration is being fabricated. The new ground plane is a 72" circular flat surface such that it will be approximately 9 wavelengths in diameter at the lowest frequency of interest (1.6 GHz). It has been shown (op. cit.) that consideration must also be given to the terminal point of the antenna to ensure that the transfer of impedance through the connector at the base of the antenna is optimum. Previously a modified UG-30/U double female connector was employed at the base of the monopole as the feed through. This connector had been modified so that it fit flush into the ground plane and the monoploe was then inserted into the female center conductor of the connector. Several problems were experienced in using this configuration, e.g. the transferring of impedance through this connector was a serious problem since the connector is made up of two dielectric spacers and a thin rubber disc. Because of the problems that have been encountered with the UG-30/U connector, a new connector configuration is being obtained. A pair of these connectors, Omni Spectra Model 21011, will be employed to further simplify and improve the data accuracy. One of these will be used with the ground plane to hold the antenna, and the second will be used for obtaining short circuit data. In this way, it will not be necessary to collect data at one point of the transmission line and transfer it through the connector to the base of the monopole.

IV
LOADED LOG CONICAL ANTENNA

Many methods and techniques of reducing the size of conical helix antennas were examined during the period of this contract. Some proved to be practical under limited applications and others that look feasible were not completely explored due to a lack of time. Although the specifications of the contract were not completely met by the prototype, refinement of the techniques to be developed under future effort give promise of a prototype meeting all of the electrical specifications and some further weight reduction. Dielectric and ferrite loading are both practical and feasible if the added weight of these materials can be accepted; a volume reduction approaching 36 per cent has been achieved for the prototype using a combination of dielectric material and resistive loading. The use of metal loading techniques, including metal foil layers, cores and rings looks very promising. Composites of foil and dielectric as well as lumped capacitors and ferrite toroids also show promise. Unwanted side effects that these techniques produce must be studied and suppressed before they become useful. Some progress was made in suppression of these undesirable side effects. A concerted effort was made to study the conical helix antenna mathematically and predict correct behavior.

The prototype was a compromise design. To bring down the weight to a reasonable level, some of the electrical performance was sacrificed. A conical helix that met completely all of the electrical specifications could be fabricated by using more dielectric but it would weigh over 250 pounds.

4.1 Design of Prototype Structure

Figure 4.1 is a picture of the prototype antenna fully assembled and ready for operation. Figure 4.2 shows the antenna disassembled and read for storage. The blocks of material indicated in the picture are pieces of an artificial dielectric produced by Emerson and Cuming, Inc. and fabricated by this laboratory into the

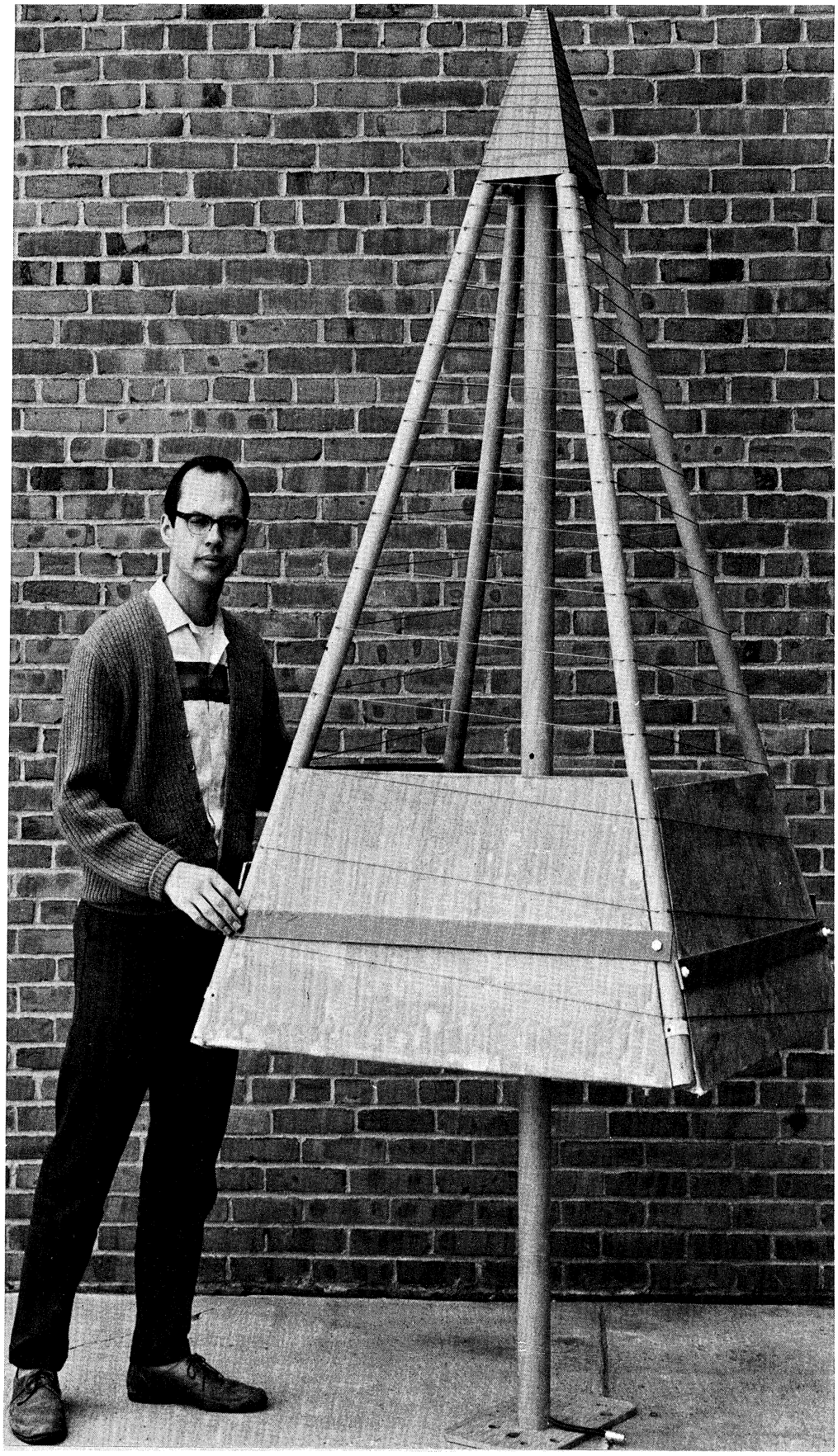

FIG. 4-1: PROTOTYPE ASSEMBLED

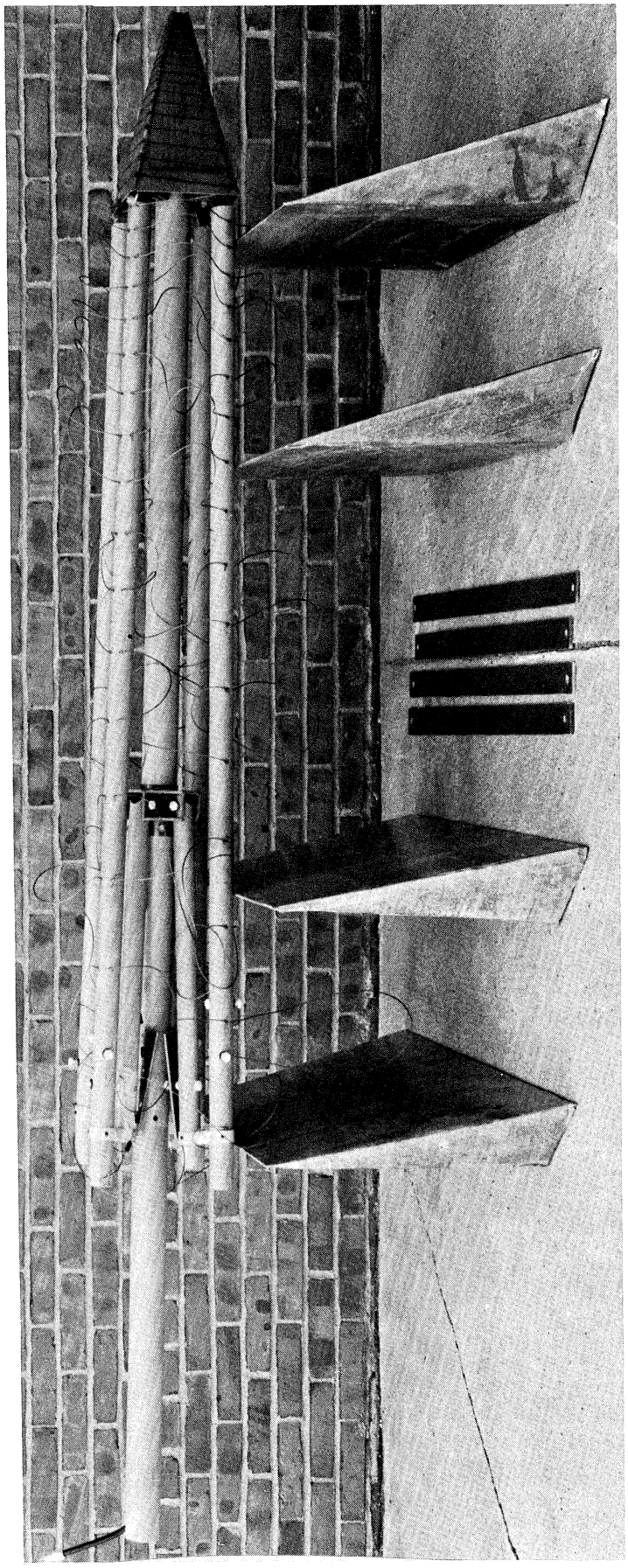

FIG. 4-2: PROTOTYPE DISASSEMBLED

shapes shown. When the antenna is assembled, the dielectric blocks fit into the bottom of the antenna as indicated in Fig. 4-1. Across the back of the antenna is a resistor network that aids the dielectric in reducing the lower frequency of operation of the antenna from 98 to 85 MHz. The experiments that led to the design of the shape of the dielectric loading and the use of resistors connected across the back are described in later sections of this report. However, the mechanical design of the antenna, the fabrication of the dielectric blocks, the design of the balun transformer, and the electrical specifications for the unloaded antenna are covered in this section.

There are difficulties in constructing a log conical helix antenna that is collapsible yet rugged. A structure which is inflatable, like a balloon, could be fabricated but would be subject to deformation by strong enough winds without structural support. The contract monitor ruled out inflatable construction. Other light collapsible structures would necessarily have to be segmented and have struts or ribs. This would force the cross sections of cuts due to planes perpendicular to the antenna axis to be polygonal. Thus a log polygonal helix would be the logical result. Tang and McClelland (June 1962) have done work on log polygonal spiral antennas; a family of antennas similar to the log polygonal helix, which are of interest to this prototype. This reference shows a technique of projecting log conical spiral antennas onto inscribed pyramids which produces antennas with characteristics almost identical to the generating antenna developed on a circular cone.

John Dyson (May 1965) gives an excellent series of design charts for log conical spiral antennas, which are log conical helix antennas that have the conductors scaled with frequency. His design curves were used for designing the generating log conical antenna. Scale model antennas covered later in the report, confirmed the validity of the procedure for designing a square pyramidal helix antenna based on the circumscribed log conical (circular) antenna.

Table IV-1 gives the physical dimensions of both the upper and lower levels of the truncated square pyramidal structure. The weight of the structure is about 14.5 pounds not loaded and about 80 pounds loaded.

TABLE IV-1

DIMENSIONS OF THE PROTOTYPE ANTENNA

Description	Bottom (in.)	Top (in.)
Radius of the circumscribed circle	28.4	0.86
Side of square	40.2	1.21
Distance - base to vertex	78.	2.36
Distance - side to vertex	80.4	2.43
Distance - circle to vertex	83.	2.51

The antenna without dielectric loading was designed to operate from 100 to 1100 MHz. The prototype antenna has a cone angle of 40^{o} instead of 45^{o} as originally planned. The results of the far field patterns on the scale models 221 and 223, described later, indicate that the range of half power beamwidths would have been excessive with a cone angle of 45^{o}. The switch to a cone angle of 40^{o} should not affect the average beamwidth, but it should reduce the variation in the beamwidth about the average. If the variation is still excessive, reducing the cone angle further will correct the problem.

As reported earlier, the wrap angle is 85^{o}. This gives the greatest uniformity among patterns of different frequencies.

The structure of the antenna is designed so that: 1) no member of compression will buckle, and 2) the tensile stress in any shear plane will not exceed the tensile strength under conditions of severe wind loading. The maximum loading occurs if the antenna offers its maximum cross section to the wind. To simplify the static analysis the resulting force was assumed to be borne solely by the member under consideration. No safety factor was used.

On this basis, the structure designed should break in a 25 mph wind at -60° F if the surface of the structure is entirely covered with a backing plane of dielectric loading material. Catastrophic failure would occur at the higher wind velocity if the temperature were warmer or if the plane of the antenna windings were not supported throughout by loading or backing (Jasik 1961). Actually, the structure would not fail unless the wind greatly exceeded 25 mph since the assumed force distribution in the structure is quite conservative. It is thought that wind velocity of 50, or possibly 75 mph would not damage the structure. It is interesting to note that even at 25 mph, the forces caused by wind loading exceed those caused by the weight of any practical dielectric core by two orders of magnitude. The effect of ice loading on the design was not considered.

All material used in the structure, except for bolts, nuts and cable clamps, is NEMA grade G-10 phenolite laminated plastic. The corresponding military grade is MIL-P-18177. The material is an epoxy fiberglass cloth laminate. The material has excellent mechanical and electrical properties. Its tensile and elastic properties are about the same wrought magnesium alloy except it is less ductile. The specific gravity of 1.84 makes it twice as heavy as other phenolite laminates, but its strength to weight ratio is far superior. G-10 has a dielectric constant of about 4.5 and a dissipation factor of approximately 0.01. Its dielectric strength is the same as most common insulators.

The weight of the structure alone is about 14 1/2 lbs. Since standard tube stock is 36", most tubes indicated in the plans are composed of several standard length tubes connected together by butt and intermediate lap joints. The intermediate inside sleeves are short sections of G-10 pipe (which is the next size smaller). Mechanical drawings for the structure of the antenna are in Figs. 4-3 to 4-10.

Fig. 4-3 shows a top view of the antenna frame. As indicated by the drawing, the top of the structure is a pyramid constructed out of 1/16" thick G-10 sheet. This section of the antenna covers the frequency range from about 500 to 1100 MHz. This very rigid structure at the high frequencies was chosen because alignment of the wiring is very critical at higher frequencies due to the short wavelength.

The tip section of the antenna is wound with No. 16 enameled copper wire to reduce the weight of the antenna. The part of the antenna that is collapsible is wound with phosphor-bronze wire. The wire material was recommended by the sponsor because of its low work hardening properties.

Fig. 4-4 shows a section of the structure indicated in the previous figure. Notice that this shows some of the detail of the connection of the structure. Fig. 4-5 is an enlarged view of the tip of the Section A-A.

Figs. 4-6 through 4-10 show details of the hinges. The nylon cable clamps used to make the hinge shown in Fig. 4-6 are connected to the tubing with small nylon bolts and nuts. There aren't necessary, but they prevent the clamps from sliding around the tubes. Figs. 4-7 and 4-8 show what is essentially a simple hinge used to connect the ribs to the rigid tip section of the structure. The extra pieces of sheet stock indicated in Fig. 4-7 are merely to connect the hinge to the tip section.

Fig. 4-9 shows the bottom view of the carriage. This assembly slides up and down the center pole much like an umbrella. However, instead of having a spring operated clip at both the open and closed position, there is a 3/8" nylon bolt that holds the carriage in place at each position.

Fig. 4-10 shows a section of the carriage taken on a plane containing the center pole. Note that the ends of the struts are rounded so that they will pivot freely when the carriage is moved up and down. Note also that the bottom plate perpendicular to the center pole does not cover the compartment containing the rib. This is

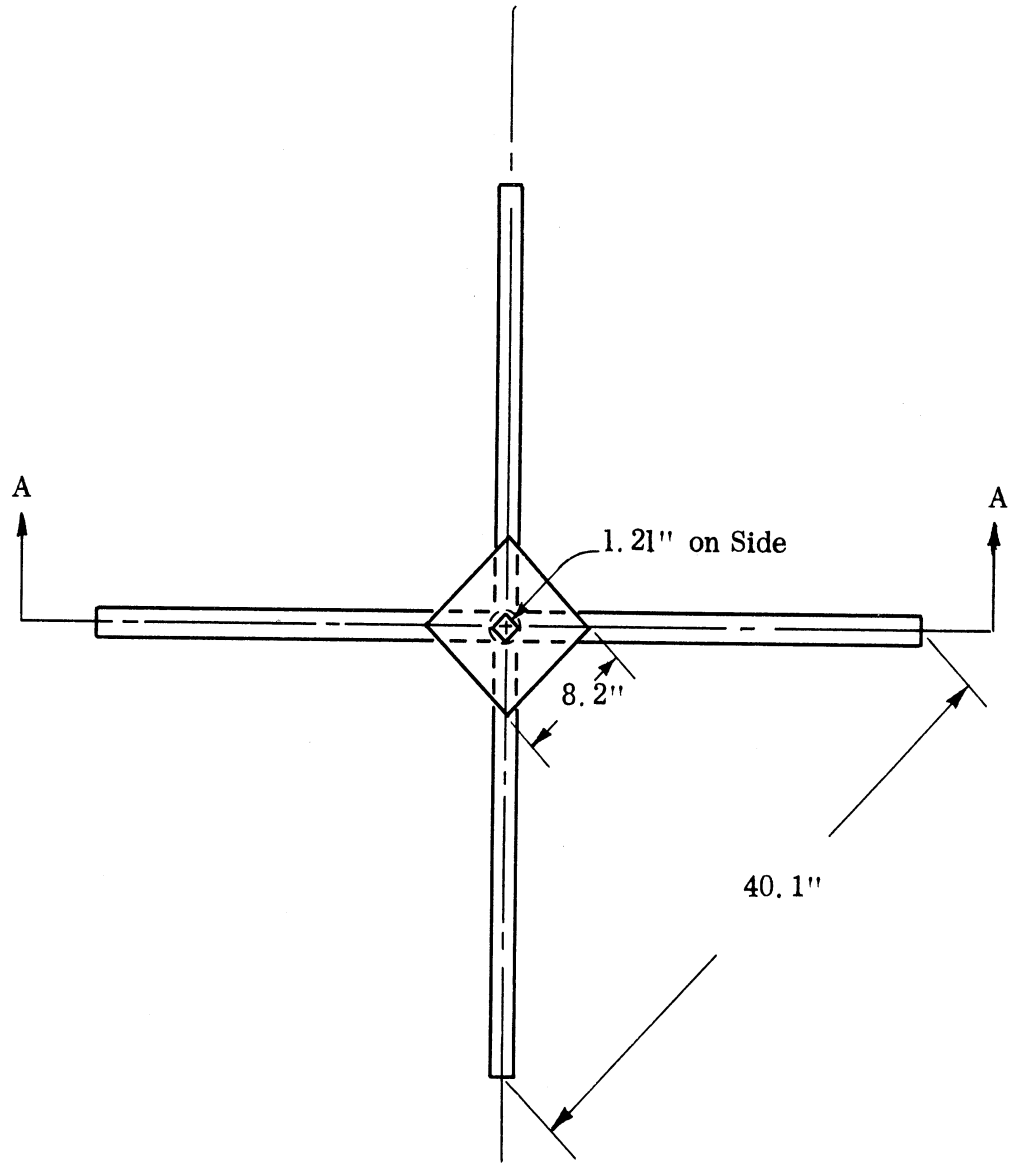

FIG. 4-3: ANTENNA FRAME (TOP VIEW) (1" = 1')

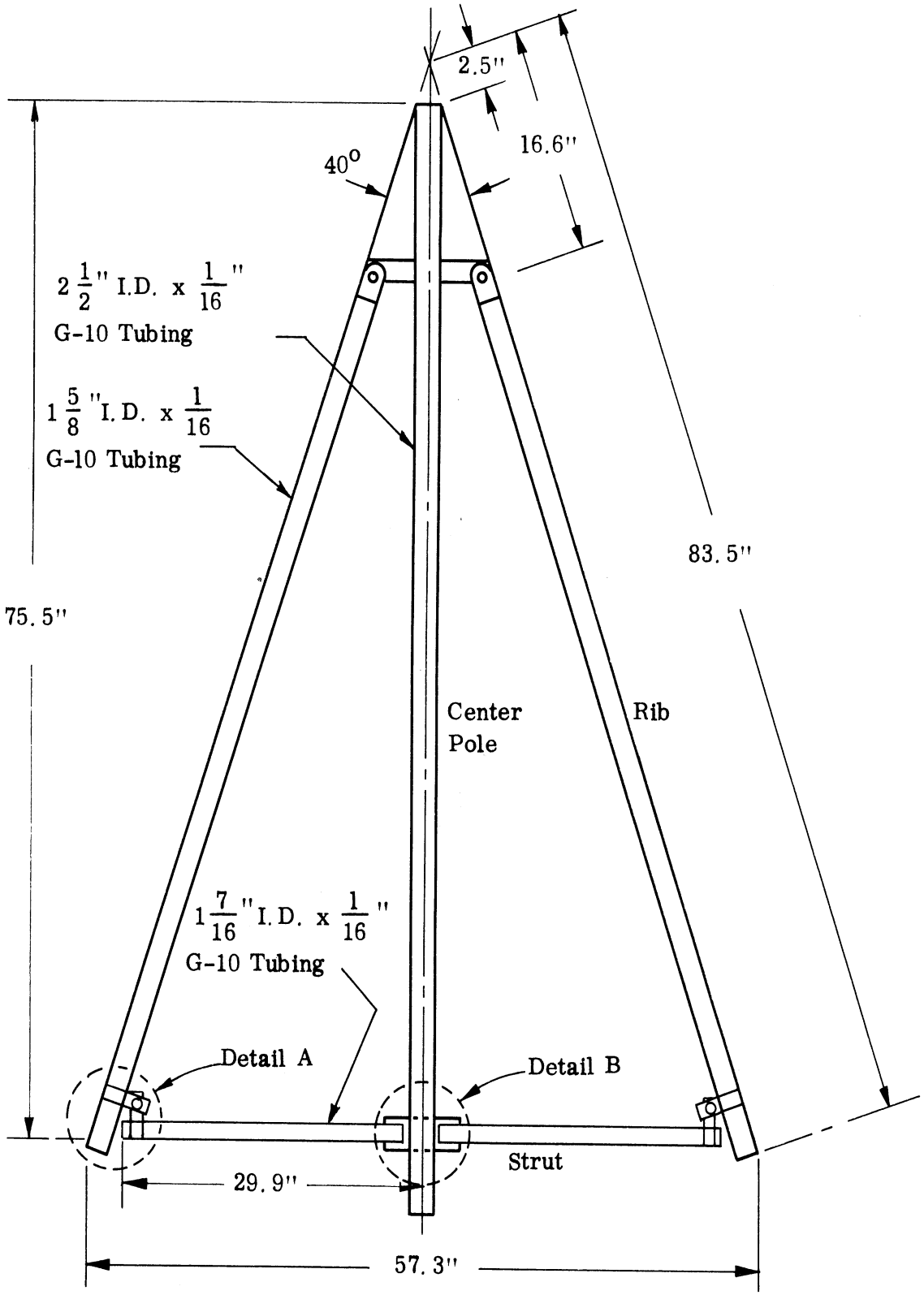

FIG. 4-4: SECTION A-A (1" = 1')

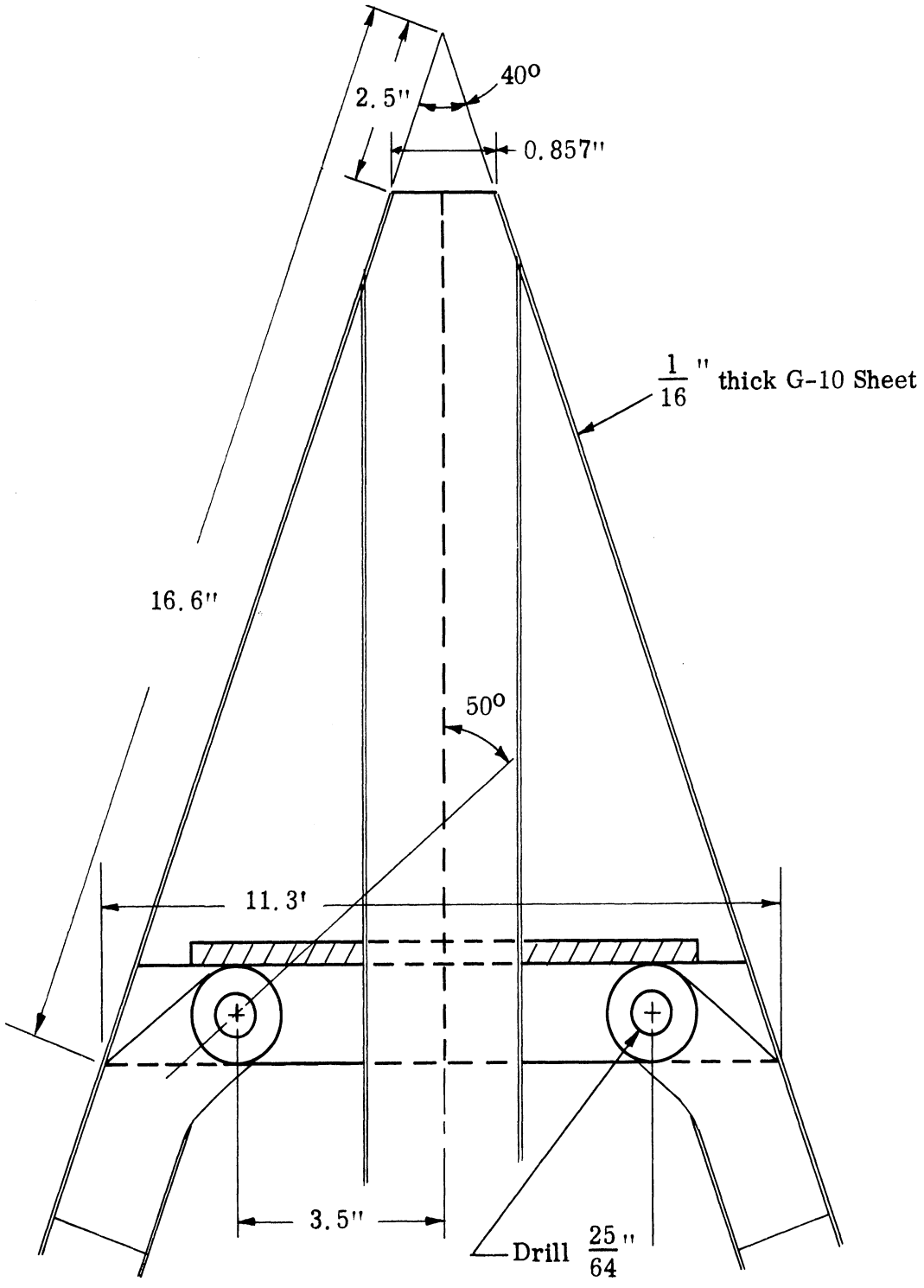

FIG. 4-5: TIP OF SECTION A-A

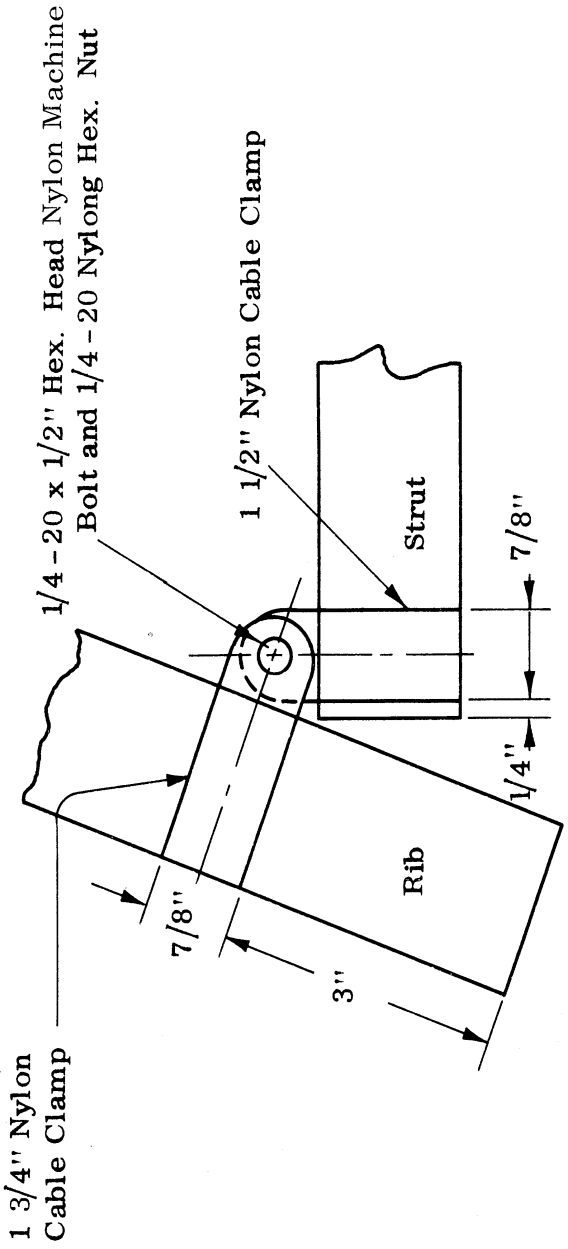

FIG. 4-6: DETAIL A - CONNECTION OF LOWER STRUT TO RIB (FRONT VIEW, HALF SIZE)

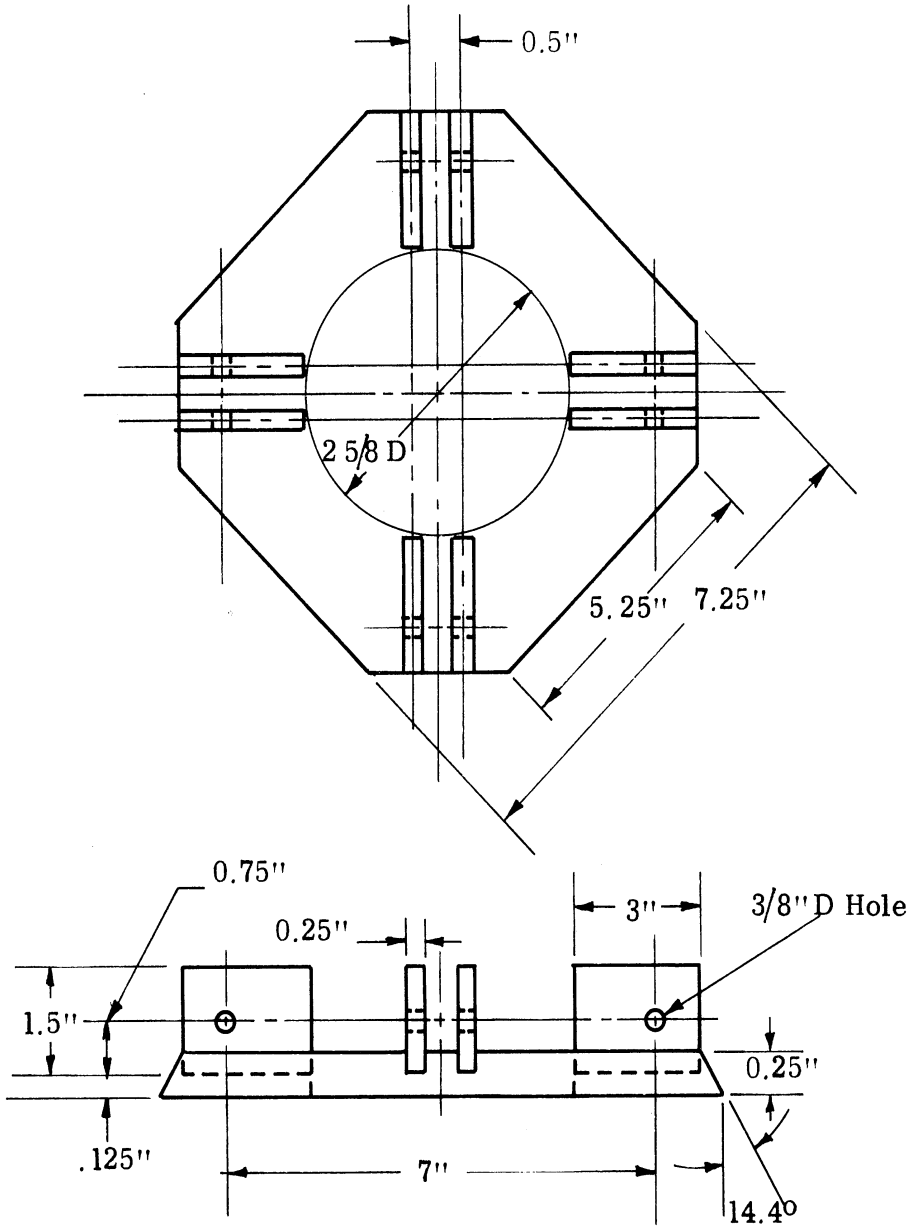

FIG. 4-7: UPPER HINGE

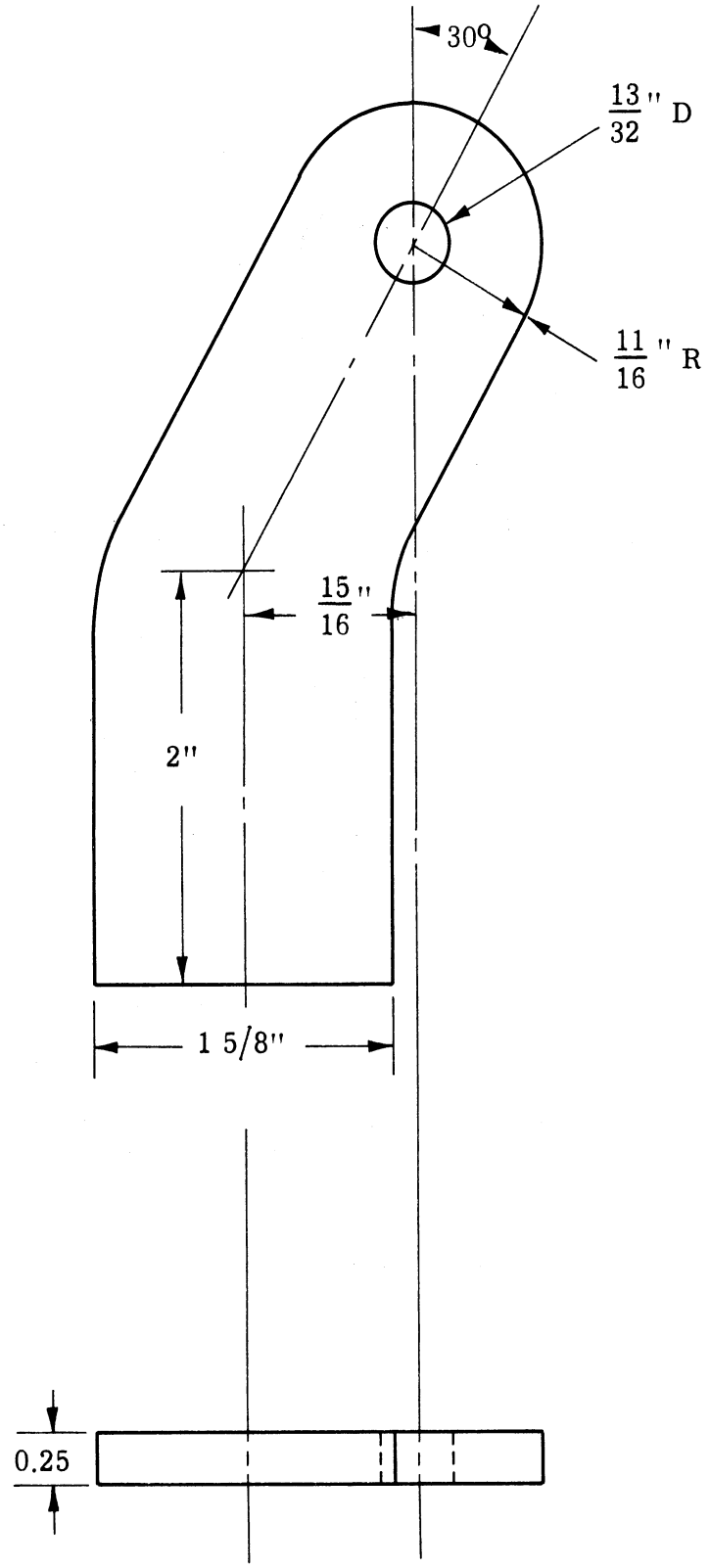

FIG. 4-8: RIB - STRUT CONNECTING ROD (FULL SIZE)

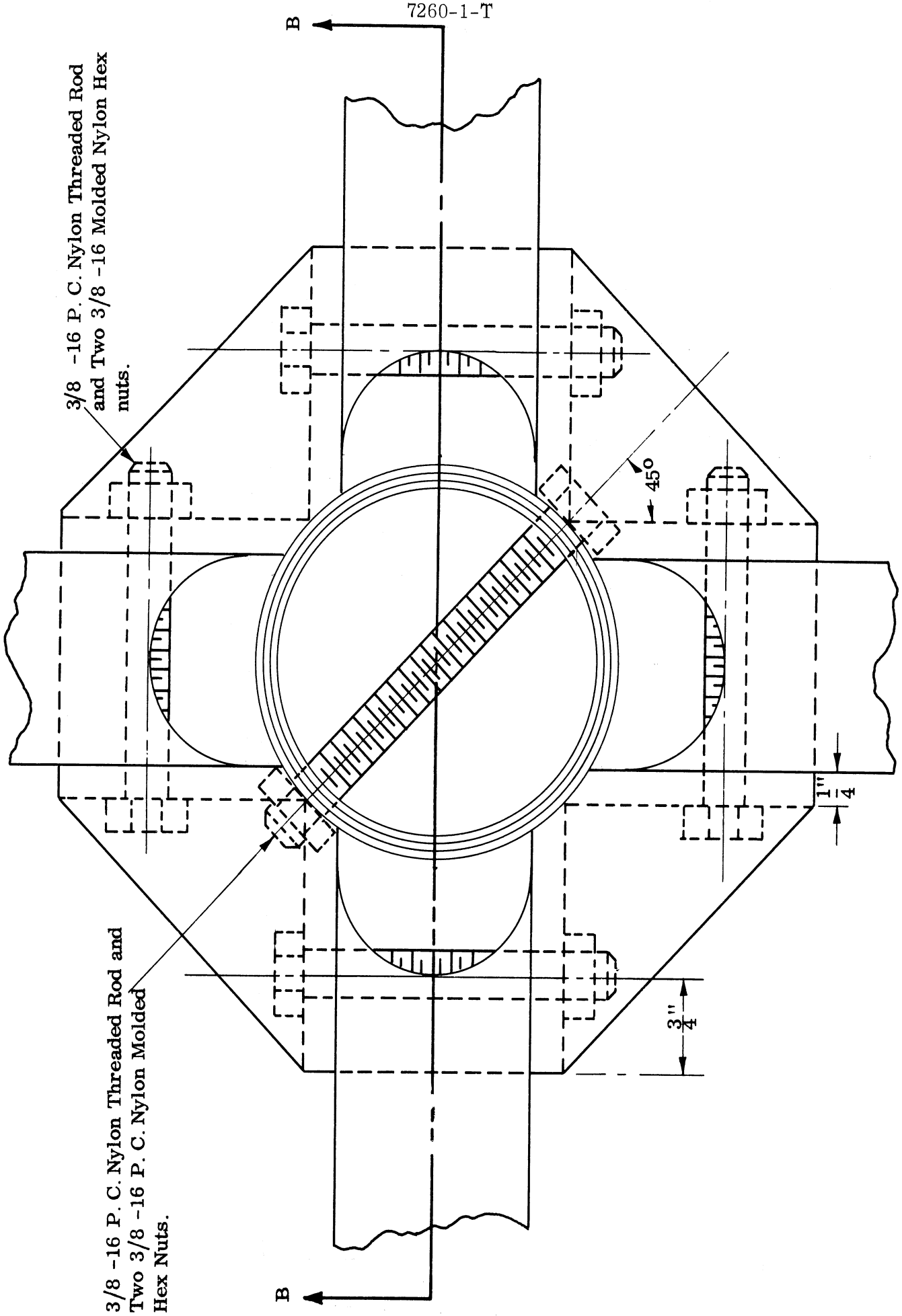

FIG. 4-9: DETAIL B - BOTTOM VIEW

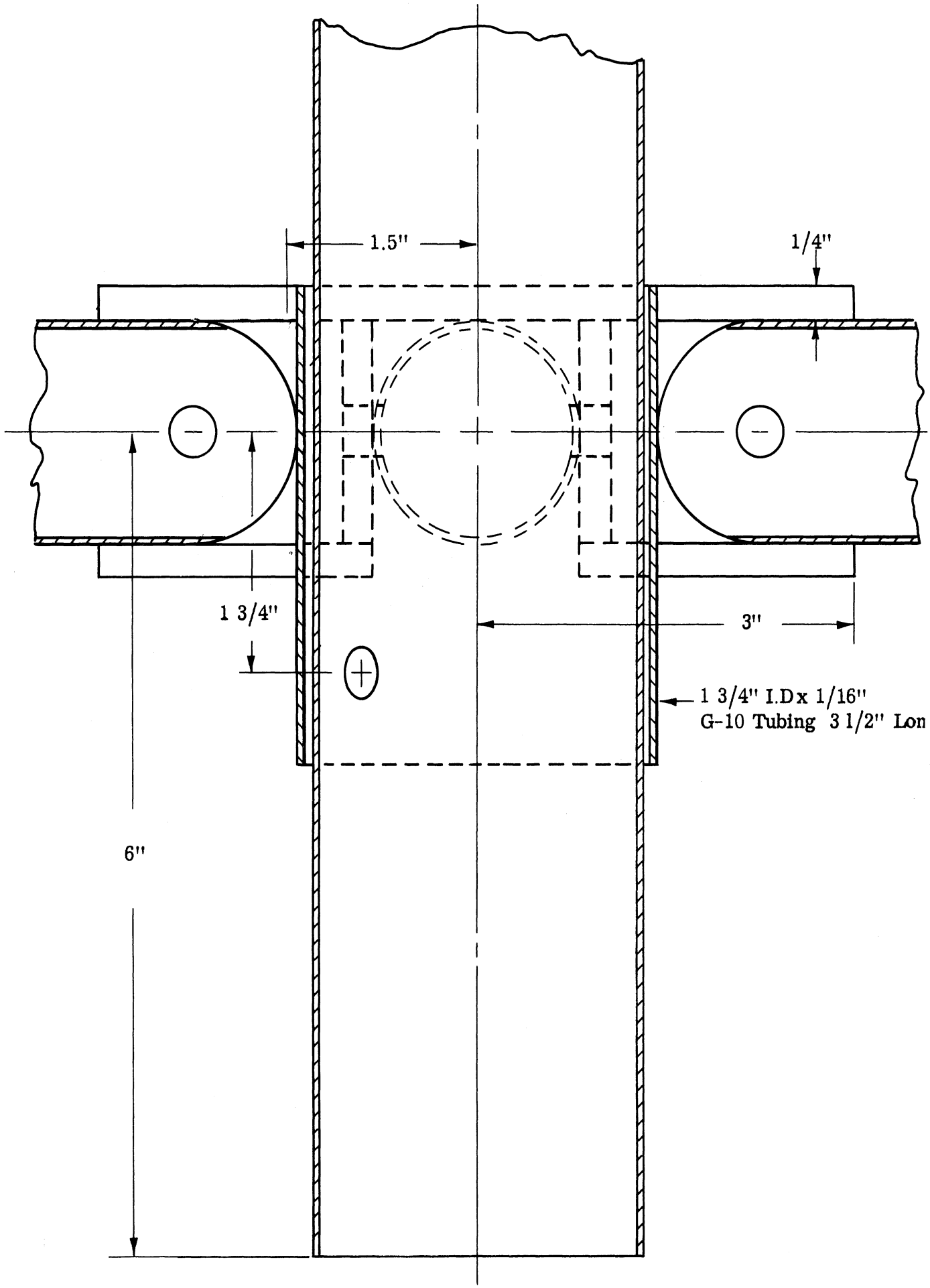

FIG. 4-10: SECTION B-B

deliberately done so that the rib and carriage will clear each other when the antenna is collapsed.

The loading material used is Emerson and Cuming's Eccofoam Flexible Hi-K, which is an artificial dielectric composed of foam and aluminum powder. The material has a dielectric constant of 6, which is the largest available. The material is relatively light (18 lbs/ft^3) but not as light as the 5 lbs/ft^3 advertised. The dielectric material is somewhat difficult to work with. At room temperature, the material is not very elastic. Stresses placed on the material usually result in permanent deformations. However, small deformations will usually work themselves out over a period of several days. Fresh from the factory, the material is tacky and sticks to objects readily. After aging, though, the stickiness disappears. However, the annoying property of the material remains; it sheds aluminum powder over everything it contacts.

Machining the material is difficult, but can be done readily with a little practice. The manufacturer suggests immersing the material in liquid nitrogen before machining. The bath freezes the material solid. However, this technique has several drawbacks. First the machinist must wear special gloves to protect his hands from frostbite. Of course the danger is always present that he will catch the gloves in the machine. Secondly, the heat generated by the friction of cutting causes the material to melt locally. The tool usually binds before large cuts can be made. Consequently, work must be interrupted frequently to refreeze the material. Fortunately for shallow straight line cuts (up to 1") the material can be cut with a very sharp knife or razor blade provided light pressure is used. The prototype dielectric was cut using the latter technique.

The material comes from the manufacturer in 1" x 12" x 12" blocks. These must be cut and bonded together to form the correct loading shape as is shown in

Fig. 4-11. This block is really composed of four blocks which were those shown earlier in the picture of the disassembled antenna. Figure 4-12 shows the dimensions of one of these blocks and how it is composed of five 1" layers of the dielectric. Figure 4-13 shows how each of the five layers is composed of standard pieces that have been precut to the correct shape. Figs. 4-14 a, b, and c indicate how the 15 pieces of dielectric necessary for each block are cut to make up the layers. The use of an assembled block gives the dielectric a nice smooth surface next to the wires so that there is no gap between the wires and the dielectric. This permits the maximum effect of the loading. Even a small spacing can reduce the size reduction properties of the dielectric noticably.

The individual layers of dielectric are glued together with epoxy adhesive. The layers, in turn, are fastened on top of one another with the same epoxy compound, but with a thin layer of fiberglass cloth in between. This adds rigidity to the structure, which, after all, is a sponge-like material. The whole block is wrapped in thin fiberglass cloth and coated with epoxy. This also makes the structure more rigid, but more importantly, it protects the dielectric from minor abrasion, small impact loads, and minor stresses. With careful handling the dielectric should hold up satisfactorily. However, if the dielectric blocks suffer severe physical abuse, they could break or be distorted out of shape. This would greatly impair antenna operation below 100 MHz.

Although not indicated in the drawings, the dielectric blocks are held in place by the ribs, four butterfly clasps, and 1/4" straps which are connected across the face of the pyramid. The butterfly clasps, which are similar to wing nuts, are located at the corners of the base. The pictures in Appendix A, used for assembly instructions, show these in more detail.

Earlier mention was made of a resistance network across the back of the antenna. This network connects the ends of the bifilar winding at the base. As the

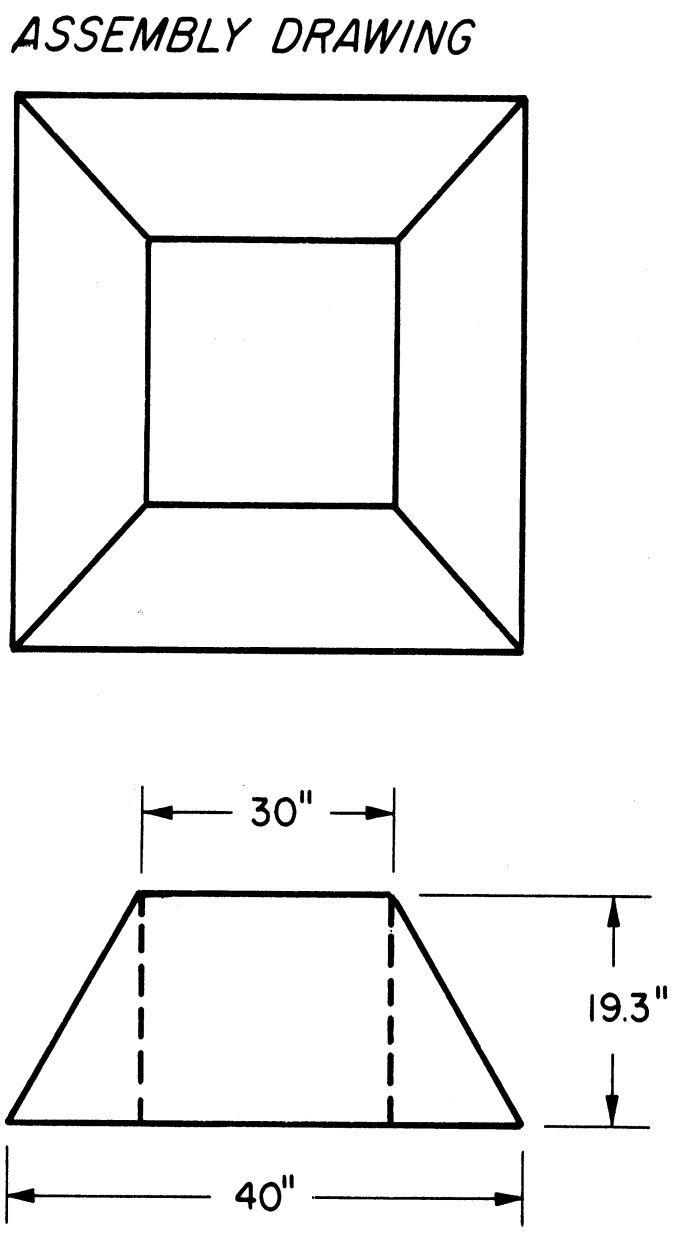

FIG. 4-11: PROTOTYPE DIELECTRIC LOADING

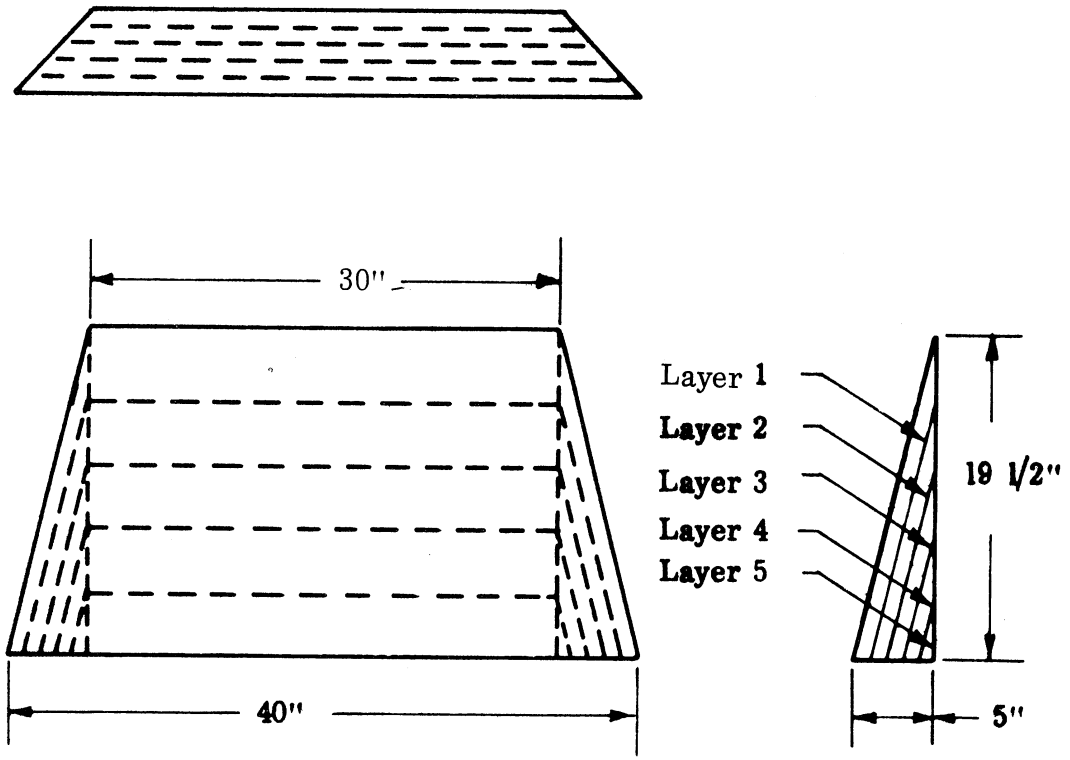

FIG. 4-12: ONE QUARTER OF LOADING FOR PROTOTYPE

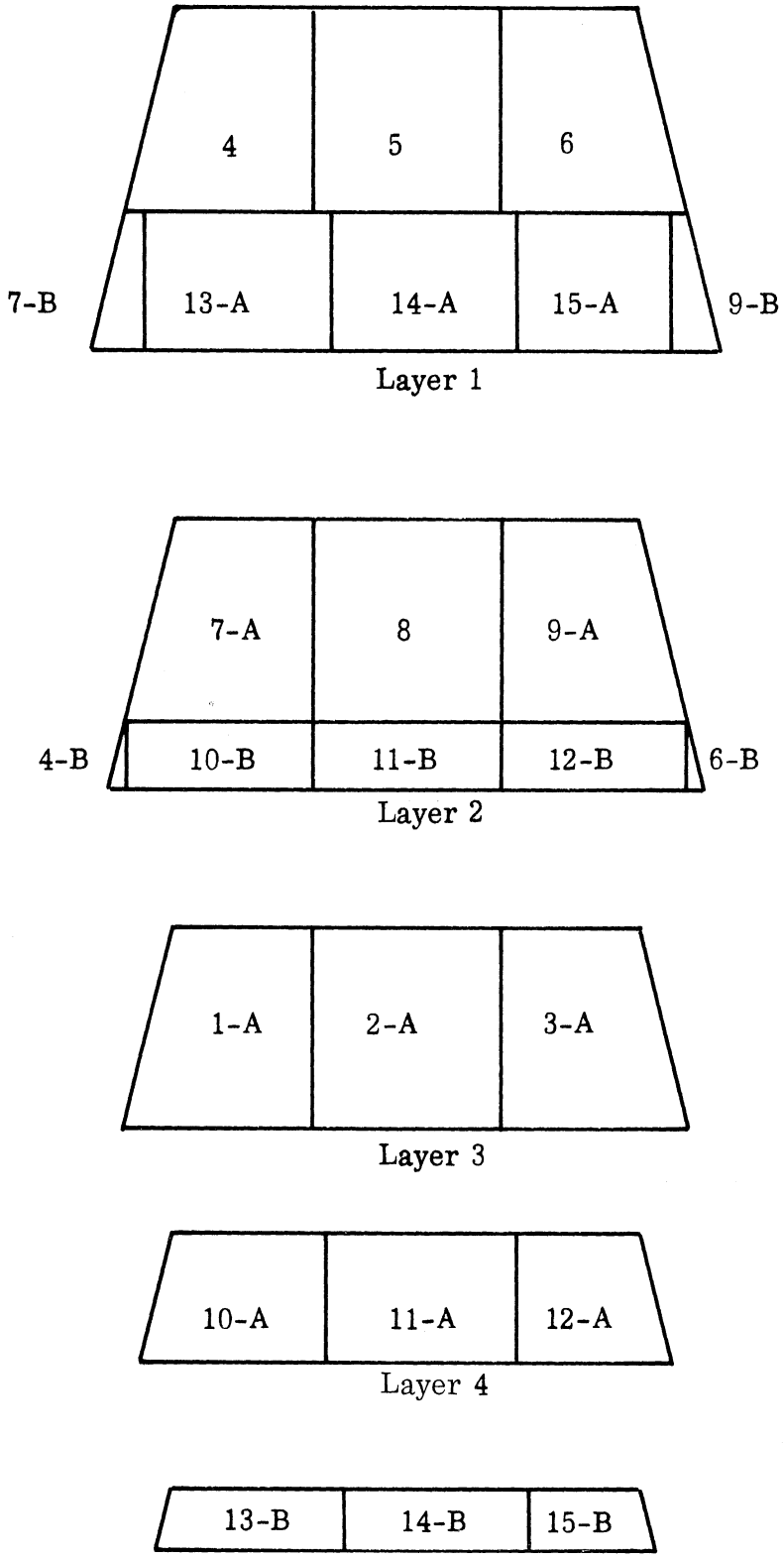

FIG. 4-13: ASSEMBLY OF LAYERS OF DIELECTRIC

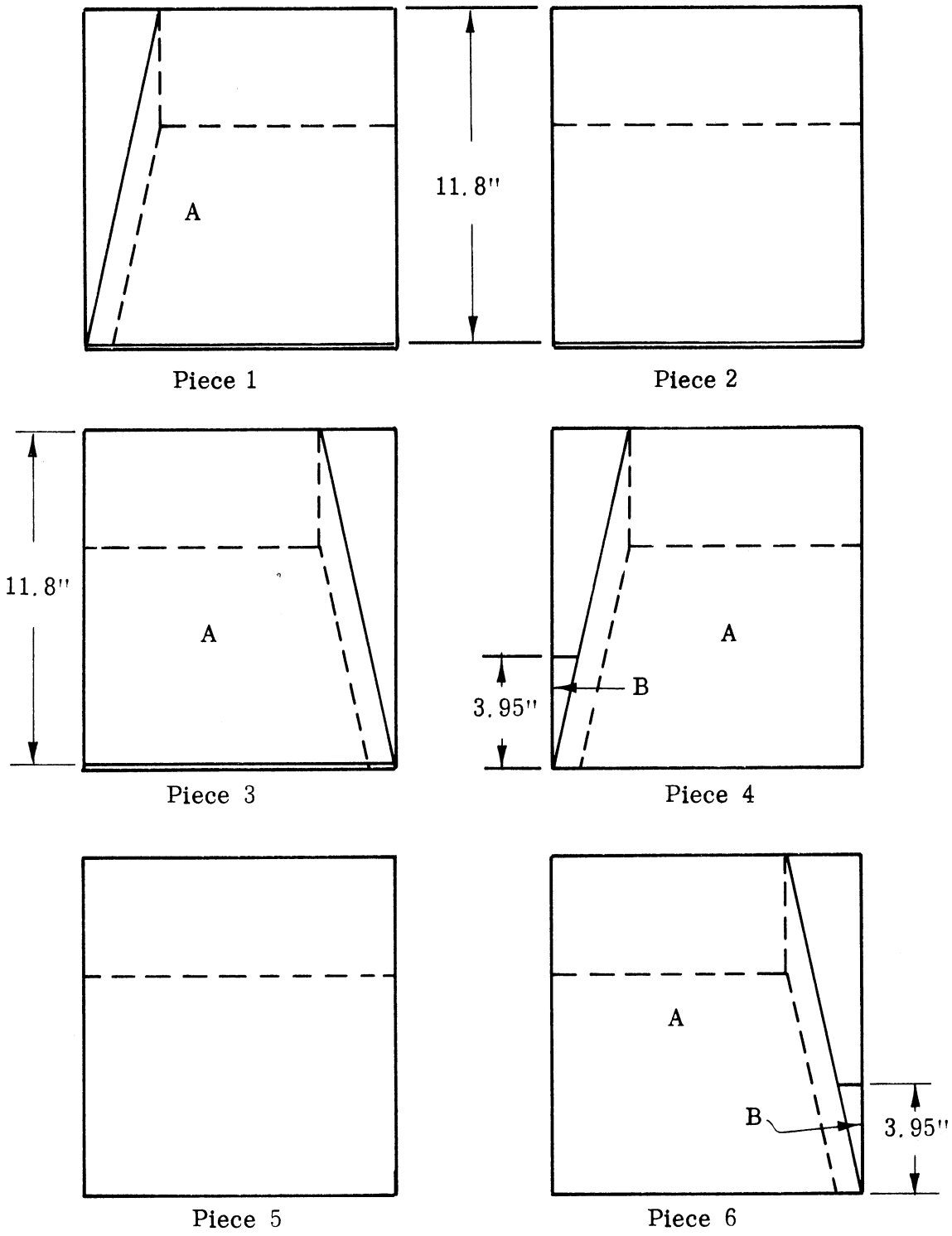

FIG. 4-14A: CUTTING OF 1" x 12" x 12" PIECES OF FLEXIBLE HI-K-6 DIELECTRIC

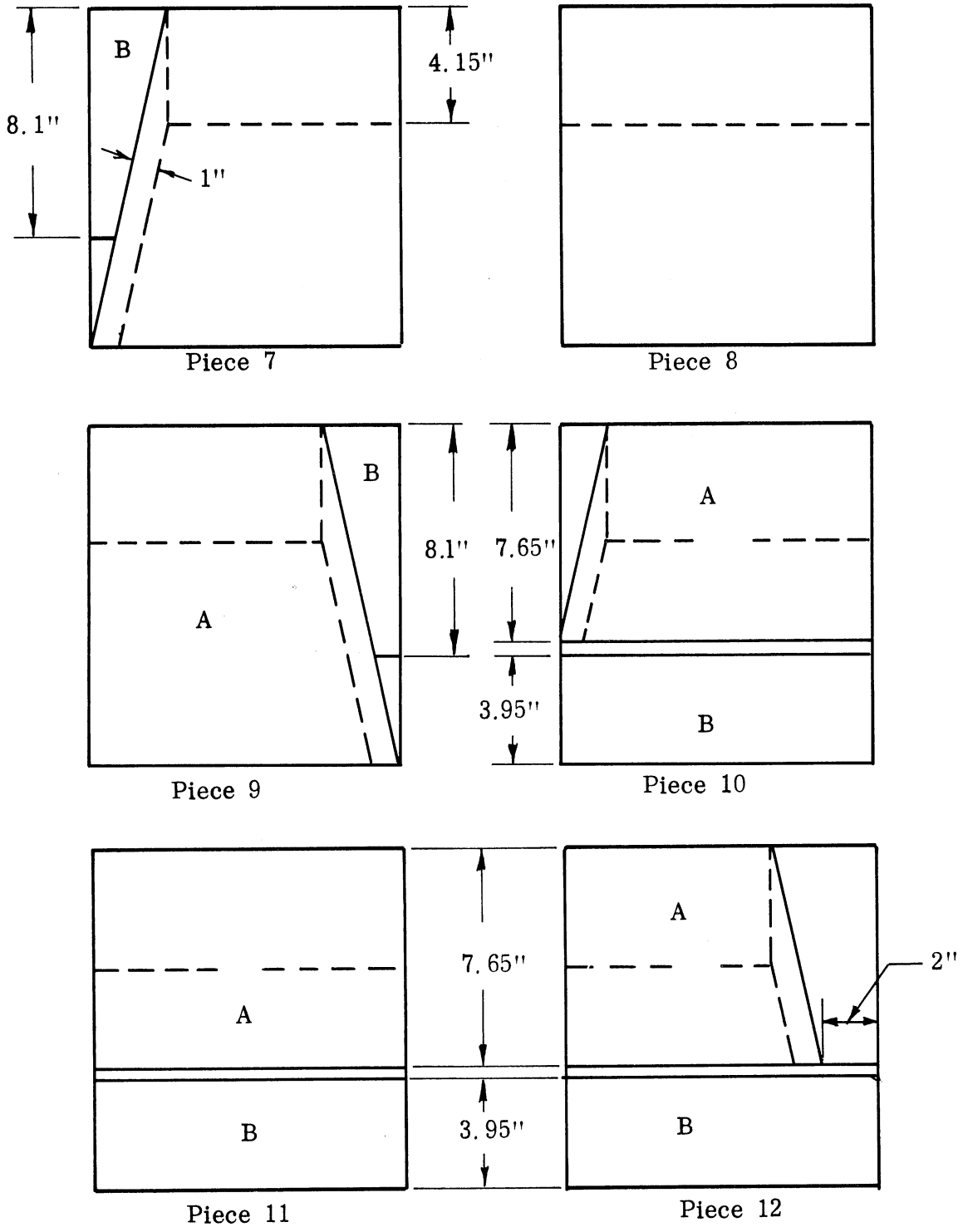

FIG. 4-14B: CUTTING OF 1" x 12" x 12" DIELECTRIC PIECES

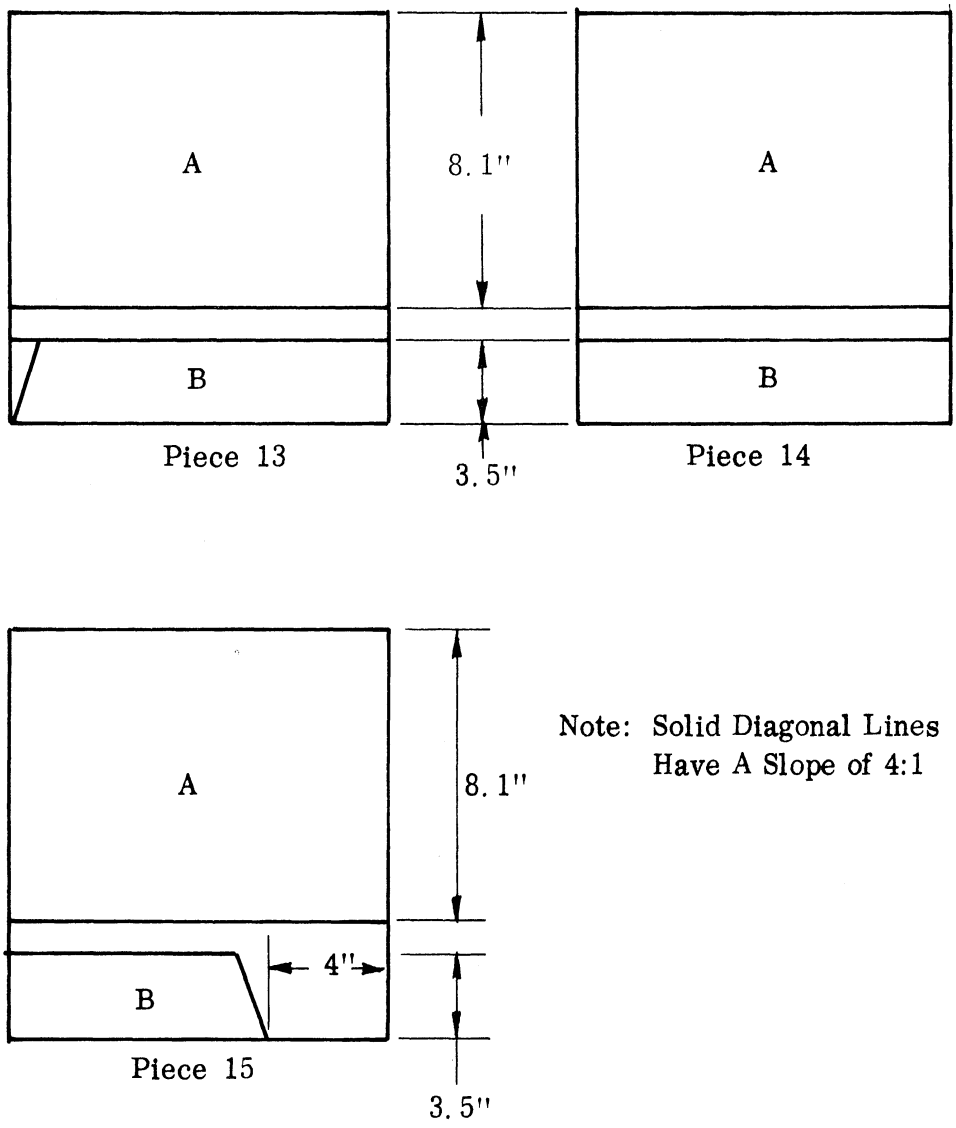

FIG. 4-14C: CUTTING OF 1" x 12" x 12" PIECES OF FLEXIBLE HI-K-6 DIELECTRIC

experiments, which are discussed later show, these resistors absorb some energy that cannot radiate in the mode that gives axial radiation because of the nature of the dielectric-air interface. Because only a small proportion of the antenna (on a basis of frequency) is filled with dielectric (other than air), this excess energy cannot radiate in the backfire direction. However, if it is reflected off the ends of the wire at the base, it will radiate in a backfire mode as it moves towards the tip. This secondary radiation causes a high backlobe.

The resistor network terminates the antenna in what has been experimentally determined to be its characteristic impedance. This prevents the reflection and the consequent secondary radiation. However, if one resistor is used, one can easily show that at about 80 MHz, the wire across the back of the antenna is a resonant dipole antenna. This has been experimentally verified. The reason for using 22, 100 ohm resistors in series is that the wire is broken up into many small dipoles, none of which are resonant below 100 MHz, and each of which terminates more nearly in a conjugate match impedance. If the resultant distribution of the resistance were not done, the resonant dipoles would resonate strongly causing a high backlobe and other undesirable pattern characteristics.

The antenna is center fed at the apex through an Anzac broadband hybrid. An alternative choice of a balun and impedance matching device that can be used is the microstrip device illustrated in Fig. 4-15. The balun is very easy to fabricate. G-10 is used as the dielectric because its high relative permitivity (about 4 compared to other materials which are around 2) permits a reduction in the overall length of the device. A price is paid for this reduced length, however. Much narrower strips of metal must be used to obtain a given impedance. As a result, the output of the device is limited to about 70 ohms instead of 130 to 160 ohms, which is the measured input impedance of antenna 223, a scale model antenna descirbed later.

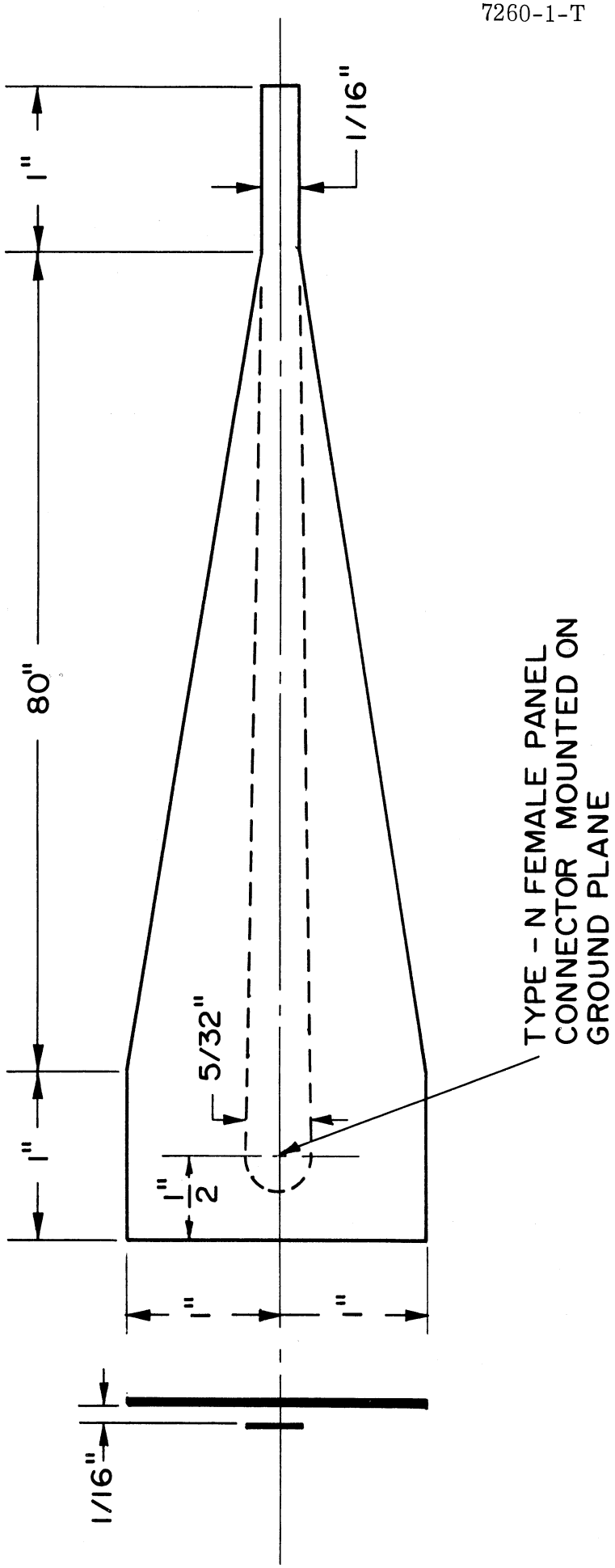

FIG. 4-15: BALUN

A balun built out of 1/8" thick material could have an output impedance closer to 150 ohms without having an output conductor too small for soldering. Unfortunately, such material is not very popular because its greater thickness permits high radiation losses at microwave frequencies. Procuring it in large enough sheets is impossible without a long delivery time. Published sets of impedance curves (Dukes 1958) are very useful in designing such baluns and impedance transformers. The transition section, however, must be at least one half wavelength at the lowest frequency in operation. This is a rule of thumb usually used.

The balun is the same width as the inner diameter of the center pole of the antenna structure and can be fastened inside of it.

4.1.1 Test Results on Prototype Antenna

The tests of the loaded log conical prototype antenna emphasized the low frequencies since the high frequencies were transmitted by the more conventional, unloaded portion of the antenna. Due to the time available, only the most crucial measurements could be made.

The antenna was designed for unloaded operation down to 100 MHz based on curves and formulas from the literature. Starting from this given sized antenna, the electrical performance may be measured and compared to typical data and to the contract's design goals. Throughout, it is understood that "loaded prototype" or "prototype" means with both loading and resistor termination in place; the "unloaded" means with no loading or termination. All antenna patterns are in linear power. The figures referred to are in Appendix C

Figs. C-1 through C-19 show the final antenna patterns taken, while Figs. C-20 through C-28 summarize the data taken. The antenna patterns in Figs. C-1 through C-19 are self explanatory. Note particularly that the patterns of the loaded antenna for 40 and 50 MHz (Figs. C1 and 2) are much better than that of the unloaded antenna,

Fig. C-10. It is felt that the patterns would hold well below 40 MHz. The high frequency patterns have distortions, partly due to construction errors, which can be corrected, and partly due to range problems, since it was necessary to use a new measurement range that had not been completely optimized.

Figs. C-20 and C-21 show that the antenna meets the 90^{o} half-power beamwidth requirements. Figs. C-22 and C-23 show that the backlobe goal of -8 db minimum was met above 90 MHz, but went to -4 db at 50 MHz. However, the backlobe level of the loaded antenna is much better than the 0.5 db for the unloaded antenna. This is the most significant improvement due to loading. The beam tilt is less than 5^{o} except at 70 and 350 MHz, whereas the unloaded antenna shows 8.5^{o} tilt at 50 MHz, as shown in Figs. C-24 and C-25. The axial ratio was not measured in the final configuration, but preliminary measurements showed better than 3 db axial ratios. The directivity and gain are shown in Fig. C-26. In the 300 MHz region, the loading does not affect the active zone and, in fact, was removed for this frequency range for ease of measurement. The difference of 2.5 db between directivity and gain in the 100 - 300 MHz range corresponds to insertion loss due mostly to the hybrid and the feed cable. The added losses at low frequency are associated with an unexpectedly large amount of the current traveling through the active region and being absorbed in the terminating resistor. This is probably due to an insufficient length of loaded region allowed for radiation. The near field measurements predicted a severe problem in shortening the length dimension, in that several humps in the near field amplitude appeared. The total active region length did not scale down like the diameter did. This gain measurement appears to confirm this difficulty in reducing length. Figs. C-27 and C-28 show impedances measured at the input connector to the antenna. The average VSWR is below the 3:1 goal. The mismatch is probably due to the fact that the Anzac balun does not have an optimum input impedance; better tapered matches could easily be made.

The gain measurements indicate that efficiency (gain/directivity) dropped off rapidly, below 70 - 80 MHz, to levels unacceptable according to the contract specifications. Nevertheless, the importance of efficiency depends upon the frequency band. At high frequencies, thermal noise predominates in receivers, and antenna efficiency must be high to obtain sufficient signal noise. At low frequencies, however, sky and ignition noise predominate, meaning that antenna efficiency is relatively unimportant, since both signal and noise are diminished by antenna losses. Jasik (1961, pgs. 25-33) shows that general city ignition noise (when it exists near by) is 30 db above thermal noise at 50 MHz; thus antenna losses of 20 db or so could be simply compensated for by 20 db of amplification without increased noise. Even cosmic noise is about equal to thermal noise at this frequency. Much more important is "noise" due to other unwanted competing signals such as the problem of isolating two signals of the same frequency in a direction finder system. Here directivity is all important and efficiency is unimportant at any reasonably low frequency. In situations such as the above, the prototype antenna, in spite of its losses, may be very useful because of its fairly good low frequency directivity (see, for example, 40 MHz). Whether the major loading effect upon directivity, as these frequencies, is from the dielectric or the resistors is unknown.

Since the contract specifications emphasize both gain and pattern backlobe as criteria, a reduction of the lowest operating frequency from 98 MHz unloaded to 85 MHz loaded has been adopted.

The difference between experiments with $\epsilon = 10$ powder and $\epsilon = 6$ foam dielectric appears greater than theory would indicate, which may imply a dielectric constant for the foam lower than assumed and advertized. This dielectric constant will be measured.

4.2 Size Reduction With Isotropic Materials

The most proven method of size reduction at the beginning of the study was through the use of material loading. From previous studies (Lyon, et al 1964, Shestopalov, 1961), the technique had already been proved experimentally with some theoretical substantiation. During the progress of the work year, therefore, most of the effort was concentrated on this technique. Since conical helix antennas have a well defined "active region" from which radiation emanates, a theoretical explanation of this region may be obtained from consideration of a circular cylindrical helix of the same diameter as this active region. The cylindrical helix has an additional advantage that it has a narrower frequency band than a conical helix, and this shows more clearly the shift of central operating frequency due to loading. The basic studies of the circular cylindrical helix are therefore given first. The next section describes scale model studies of a log-pyramidal antenna.

4.2.1 Basic studies

4.2.1.1 Heuristic explanation

Radiation of a conical helix antenna occurs when the circumference of the antenna is slightly less than a wavelength. The velocity of the current along the wire has been shown theoretically and experimentally to be about the speed of light. Therefore the phasing of the wires along the direction up the slant side of the antenna lags such that backfire radiation occurs. When loading material is present, the phase velocity of the current along the wire decreases, causing a smaller circumference to be one wavelength. This smaller circumference then becomes the active region, phased for backward fire radiation. A reduction in antenna diameter is thus achieved. Approximate formulas (Appendix B) indicate a lineal reduction of

$\sqrt{\frac{\frac{1}{\mu}+1}{\epsilon+1}}$ in diametral size using inside layers.

The reduction of the axial length of the antenna is quite a different matter. The axial length of the antenna must, of course, be much larger than the axial length of the active region. This active axial length is determined by the rate of radiation of the currents. Experiments indicate that this active region length appears to change with the addition of loading (see paragraph 4.2.2.1); however, other peaks in the near field occur indicating incomplete radiation in this first, reduced active region. Theory has not yet provided a confirmation of the axial length of the active region. In the prototype antenna delivered, a 2:1 reduction in total axial length is used. The splitting of the active region into subregions was minimized by use of a partial loading only in the low frequency region.

4.2.1.2 Helix experiments

Basic helix experiments were performed to test the effectiveness of the material loading using layers of various thicknesses. These experiments also served to check the formulas from mathematical models for loading with various values of μ and ϵ. The helix test antennas are specified in Table IV-2. The basic helices were all wound on three epoxy-fiberglass tubes, .04" thick, and fed by infinite baluns using the RG cable shown in the table, stripped of the outer insulation. The balsa wood cores, used to retain layers of the loading material, act like air, with a small dielectric constant. The fiberglass shells also do not seriously effect the radiation due to thinness and a fairly low dielectric constant. The effects of these two materials are shown in Fig. 4-16; only the balsa wood pattern at 300 MHz, far away from resonance, shows a large difference from the air case.

The patterns, when the helices were loaded, are shown in Figs. 4-17 - 4-20 for two different materials and several different layer thicknesses. The patterns are presented in normalized form; thus absolute amplitudes are not shown. Absolute amplitudes, when analyzed separately, turned out to be a very important indicator

TABLE IV-2

SPECIFICATIONS OF HELIX TEST ANTENNAS

	I. D. Number					
	213	214	215	217	218	231
Type	Bifilar	Monofilar	Monofilar	Bifilar	Bifilar	Bifilar
Diameter	4.15"	4.13"	3.85"	4.65"	2.1+	1.1"
Length	10"	10"	14.5"	16"	15"	8"
Conductor	58-U	1/8"cu. tube	*	58-U	174-U	174-U
Turns	6.5	7.0	5	9.5	20	20
Pitch	6.6° (1.5")	.7"	13° 3"	7° (1.8")	6.5° (.75")	6.6° (.4")

* 7 - strand, 14-gauge copper antenna wire

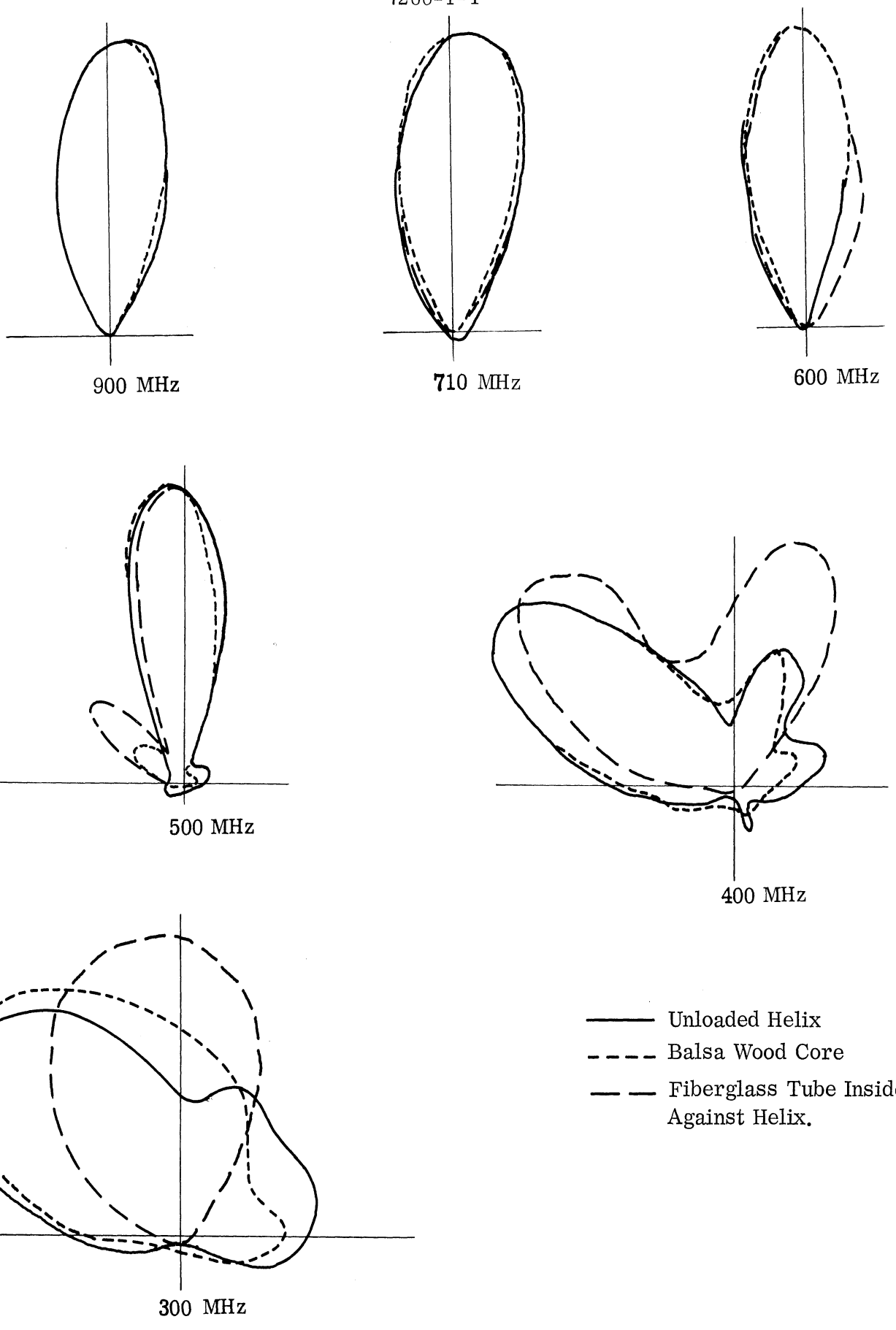

FIG. 4-16: EFFECTS OF BALSA WOOD AND EPOXY-FIBERGLASS ON HELIX ANTENNA, NO. 214, H-PLANE

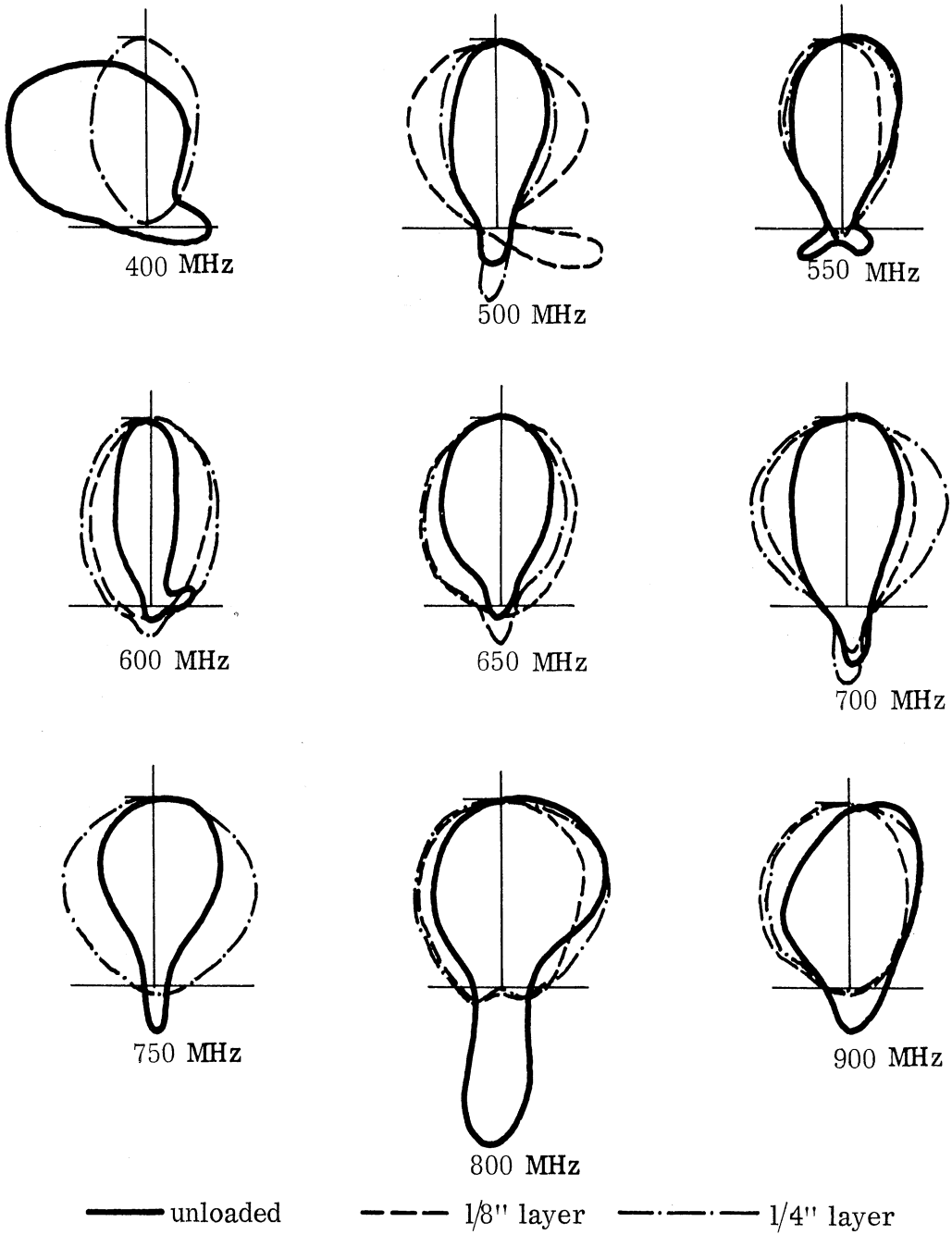

FIG. 4-17: HELIX WITH DIELECTRIC LOADING Plots of E_θ^2, Dielectric ϵ=10. Helix Diameter = 4.5"; Antenna No. 217

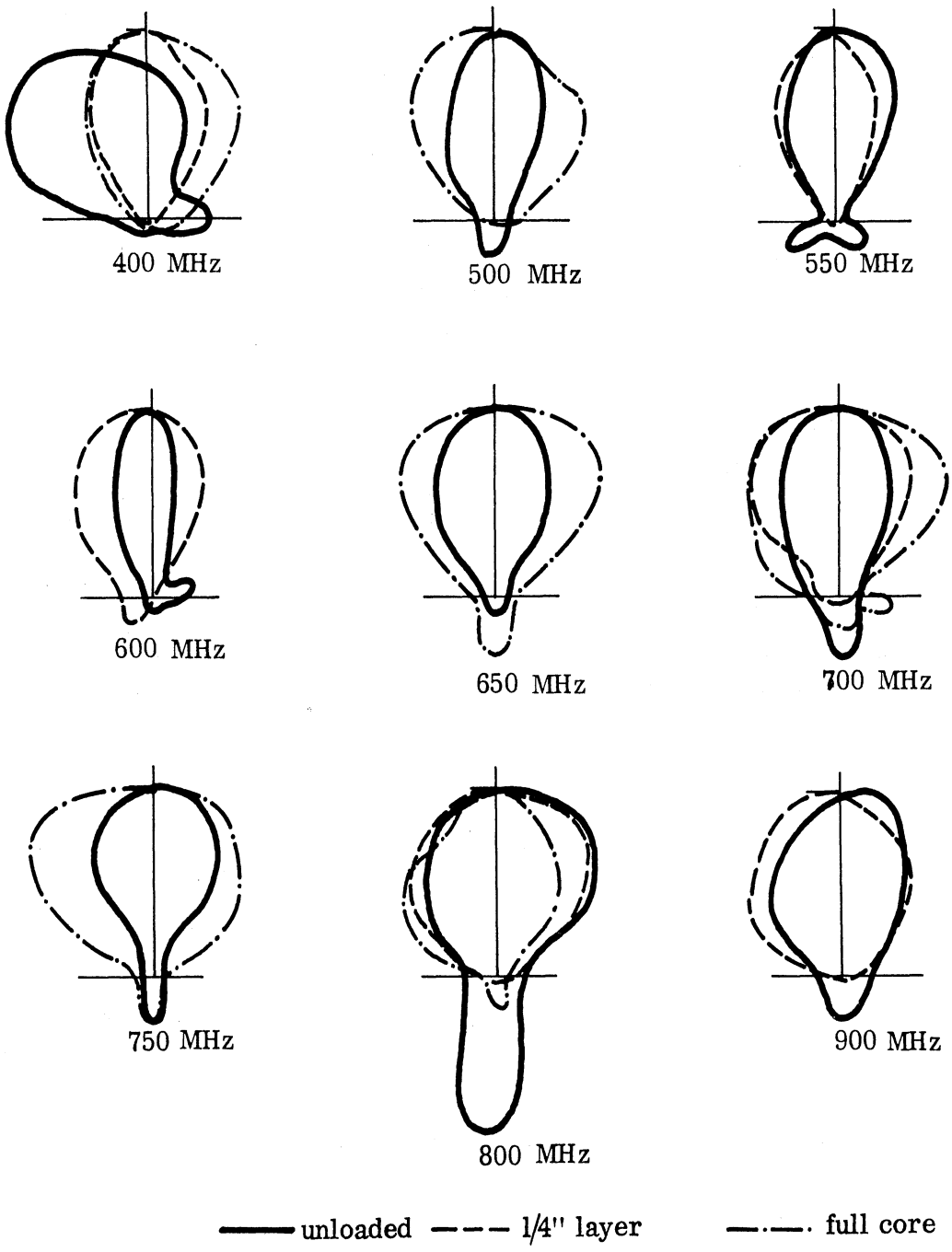

FIG. 4-18: HELIX WITH THICK LAYER FERRITE LOADING
Linear plots of E_ϕ^2. Ferrite μ=2.2, ϵ=3.8, Helix Diameter = 4.5", Antenna No. 217.

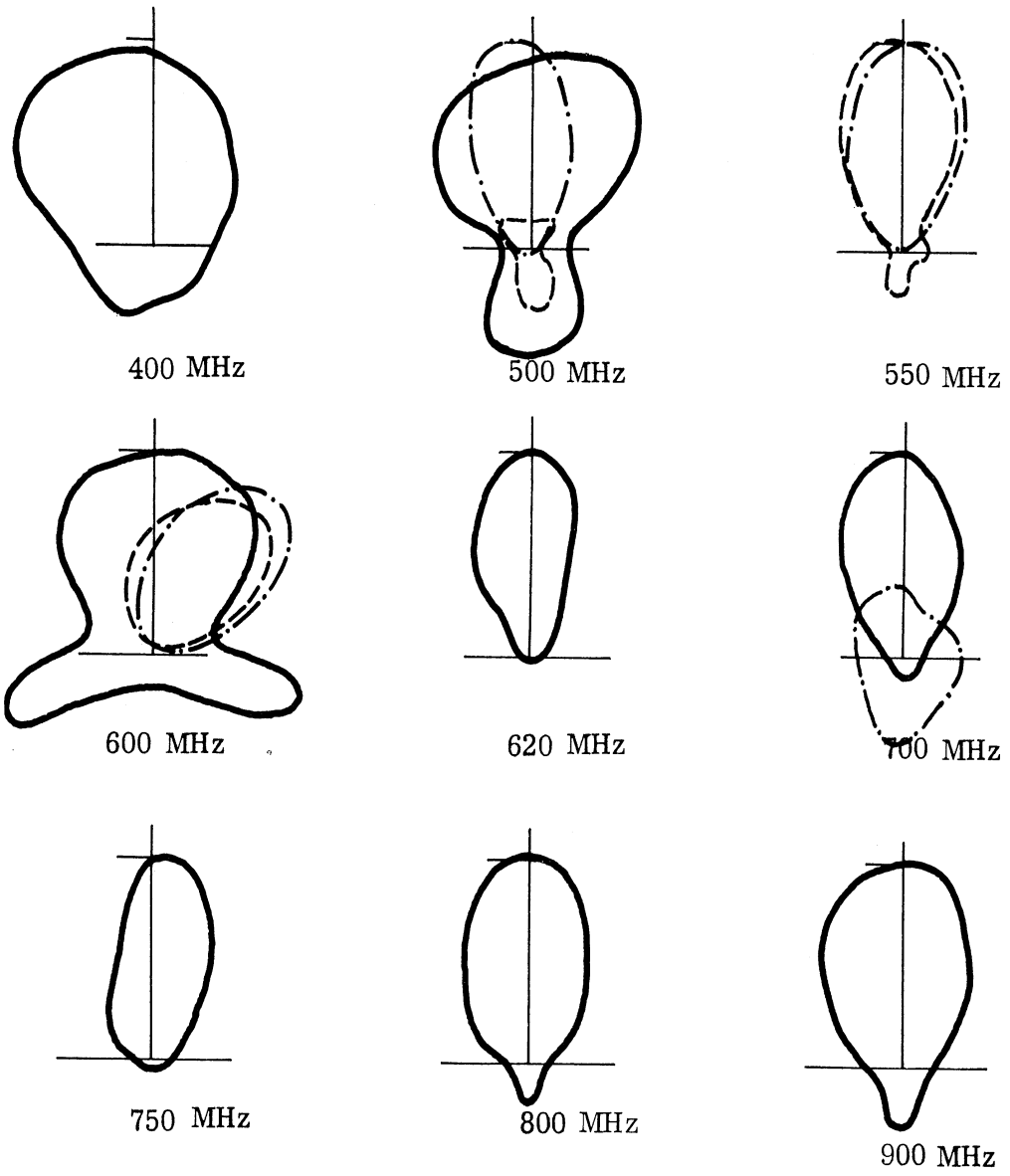

FIG. 4-19: HELIX WITH THICK LAYER FERRITE LOADING
Plot of E_ϕ^2, Ferrite μ =2.2, ϵ = 3.8, Helix Diameter = 4" . Antenna No. 213.

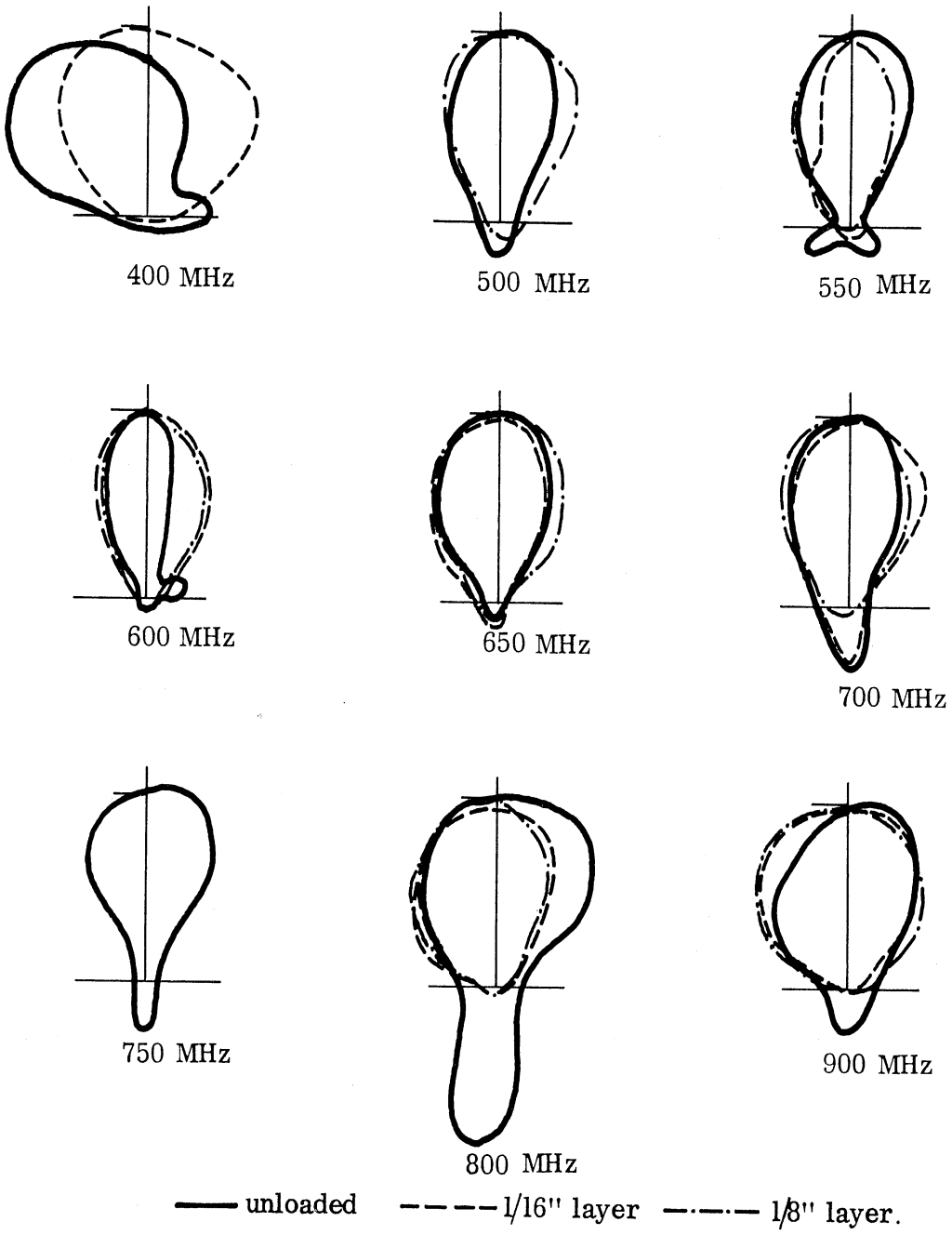

FIG. 4-20: HELIX WITH THIN LAYER FERRITE LOADING
Linear plots of E_ϕ^2, Ferrite μ = 2.2, ϵ = 3.8, Helix Diameter = 4.5". Antenna No. 217

of helix performance. Far field antenna patterns were fairly insensitive to frequency changes, and thus were only poor indicators of the "best" helix operating frequency needed to evaluate loading effects.

Several tentative conclusions may be drawn from antenna patterns and current probe amplitude data, to be reviewed later in the log-pyramid studies.

1) The dielectric ($\epsilon = 10$) was about as effective as the ferrite in lowering the operating frequency for a given size. Rather thin layers of dielectric (0.012λ, 0.25", 1/18 radius) operated well below 400 MHz, similar to ferrite layers of $.012\lambda$.

2) A reduction factor of approximately 0.74 in diametral size resulted from thin layers ($.012\lambda$) of powdered dielectric loading. Further reduction with thicker layers of dielectric can be expected both theoretically and experimentally from examining the ferrite data for thick layers. Material for thicker layers was not available during these experiments, but was used in the later log-pyramid studies. Ferrite layers 0.02λ or greater act essentially as full core loading.

One of the concepts developing out of the rotating dipole equivalent of a helix operating in the 1λ mode was that a dielectric core might be more effective when confined to the center of the helix rather than close to the helix windings. It was hoped that, by keeping the dielectric core in the center only, capacitance between wires on the same side of the helix might be eliminated, thus eliminating additional series capacitance of the equivalent transmission line. The core of dielectric in the center, nevertheless, would provide the shunt capacitance in the equivalent transmission line representation that would assure a slow wave operation. Fig. 4-21 shows the near field of helix No. 217 (4.5" diameter) when loaded with a 3" dielectric core of K-10 material (Emerson and Cuming, Inc., high dielectric powder, $\epsilon = 10$).

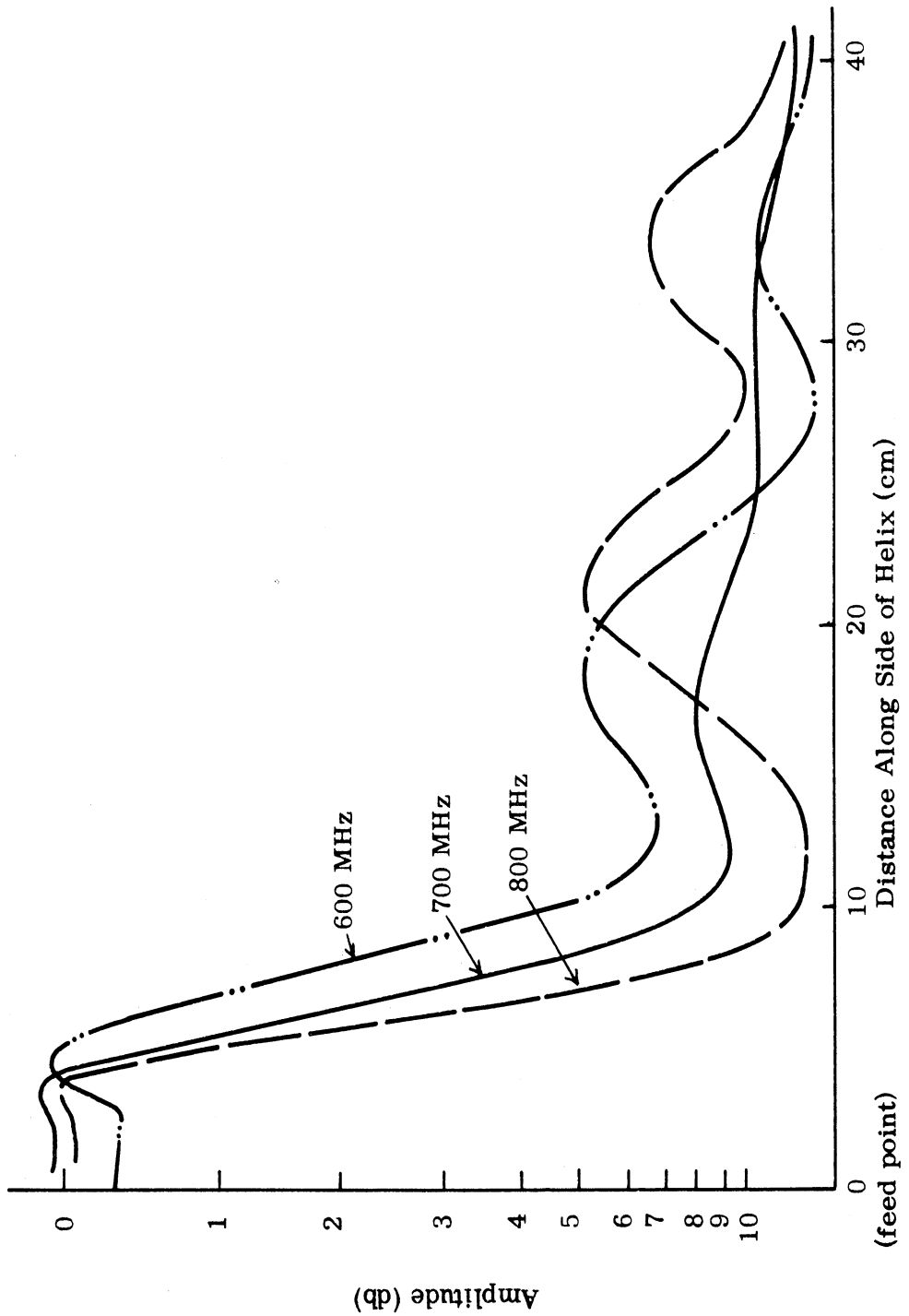

FIG. 4-21: NEAR FIELD OF HELIX NO. 217 (4.5" Dia.)
WITH 3" DIELECTRIC CORE (K-10)

It can be seen that these near fields indicate a center frequency of 700 MHz as in the unloaded helix case. The 800 MHz near field is substantially worse than it was in the unloaded case. The plot indicates that no substantial effect on the helix operation was noticable when a 3" diameter core of high dielectric powder was inserted in the center of the helix, and indicates that less effect is obtained from inserting the dielectric in the center of the helix than from inserting it close to the windings, since earlier experiments had shown substantial shift of frequency when layers of dielectric were used close to the windings.

4.2.2 Log Pyramidal Helix Studies

Scale models of the proposed prototype (designated Antenna No. 221 and 223) were built to investigate tapered bifilar helices with various loadings. Both antennas have a cone angle (2θ) of 45^{o} and a wrap angle (α) of 85^{o}. Both are bifilar wound but 221 is fed with an infinite balun of RG-58 coaxial cable without the outer insulation while 223 is center fed at the tip by a hybrid. Antenna 223 uses No. 16 enameled copper wire as its conductor. Antenna 221 covers the spectrum from 500 to 900 MHz and 223 covers 500 - 3000 MHz. A truncated square pyramid formed of 1/16" thick fiberglass epoxy laminate sheeting supports the windings of 221. Antenna 223, however, is wound on the inside of a square pyramid of 1" styrofoam sheets. This unusual construction gives two advantages; 1) the support of the windings produces almost no loading effect on the antenna, and 2) test loadings of dielectric may be placed next to the windings to produce the maximum reduction of operating frequency. The specifications of these antennas are shown in Table IV-3.

In order to fully understand the operation of these antennas both with and without loading, near field measurements are very valuable. These measurements show the active radiation zone clearly, and thus are sensitive to loading. They will be discussed before the far field results to promote understanding of loading effects.

TABLE IV-3

SPECIFICATIONS OF CONICAL-HELIX ANTENNAS

	ID Number	
Dimension	221	223
Base, Side	9.47"	9.47"
Apex, Side	1.56"	.47"
Height	13.44"	15.38"
Apex (cone) Angle	45°	45°
Pitch Angle	85°	85°
Turns	8.5	14.75
Outer Conductor	58-U	No. 20 Enamel Coated Wire
Feed	Infinite Balun	Wideband Hybrid
Nominal Frequency Range, Unloaded	500-900	500-3000 MHz

Note: Loadings available on either 221 or 223:

L1 - Triangular Cross Section, 0.5 radius at the base tapering to zero with an inside surface parallel to the axis.

L2 - Same as L1, but 0.25 radius

L2 - Modified, constant 0.25 radius from base for 5", then tapering to zero with inside surface parallel to axis.

4.2.2.1 Basic Near-Field Studies

4.2.2.1.1 Probing equipment

The preliminary measurement method used for the near field pattern for helical and log-conical antennas was similar to that of other workers (Dyson, 1965, Patton, 1963). Measurements were made with surface current measurement facilities at Hangar 2, Willow Run Laboratory. The facilities involve an anechoic chamber, a magnetic probe with its carriage system, and a receiver-recorder system. The block diagram of the set-up for the near field amplitude measurement is shown in Fig. 4-22. The details of the anechoic chamber are described fully in the literature (Knott, 1965). The picture of the facility, Fig. 4-23, shows the probe assembly hanging from ceiling. The probe carriage above the ceiling is shown in Fig. 4-24.

The shielded vertical loop probe was used throughout the measurement. It has a diameter of 0.131", and is made from coax line 0.084 cm OD, 21 cm long. The highest frequency used in the measurement was 1600 MHz; thus the pickup error due to E-field is assumed very small (Whiteside, 1962).

The near field phase shift was measured with the set up shown in Fig. 4-25. The attenuator and phase shifter were adjusted to obtain a null on the CRO display; the phase angle was then read from the dial setting of a precision phase shifter. The slotted line was provided for a wider range of measurement.

Since the size of the loop becomes very small relative to the wavelength at lower frequencies, the probe efficiency (also signal-to-noise ration) becomes small. This has made it necessary to change the probe position, (relative to the wavelength) by moving the probe toward the antenna surface in the lower frequency range. The x-y recorder used a time base while the probe was driven by a d-c motor along the axial direction of the antenna. The probe carriage system runs at fairly constant speed, but since it is not regulated nor synchronized to the x-y recorder a small drift can be noted during the measurements. This causes a little inaccuracy in the amplitude plot.

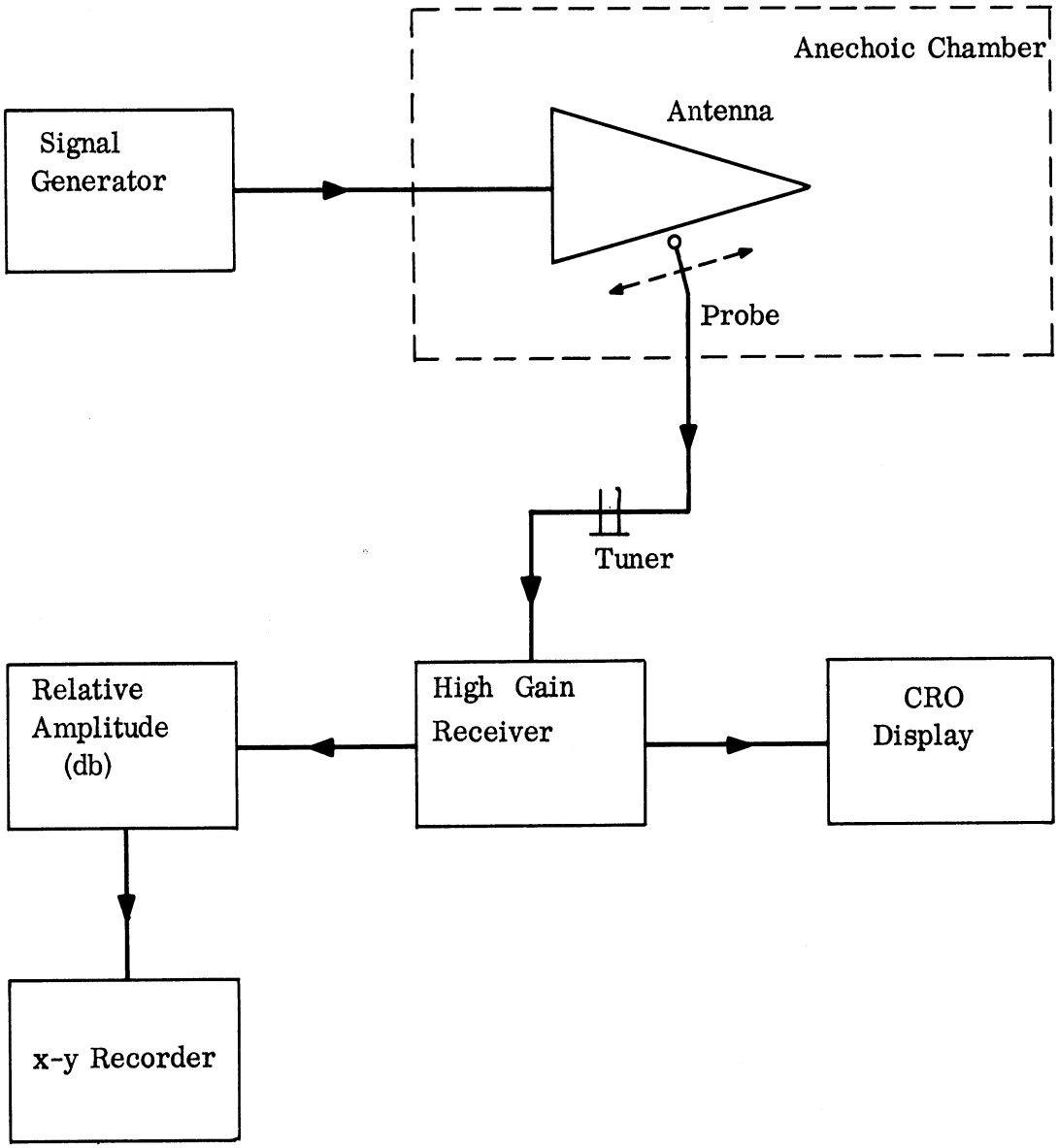

FIG. 4-22: BLOCK DIAGRAM FOR NEAR FIELD AMPLITUDE MEASUREMENTS.

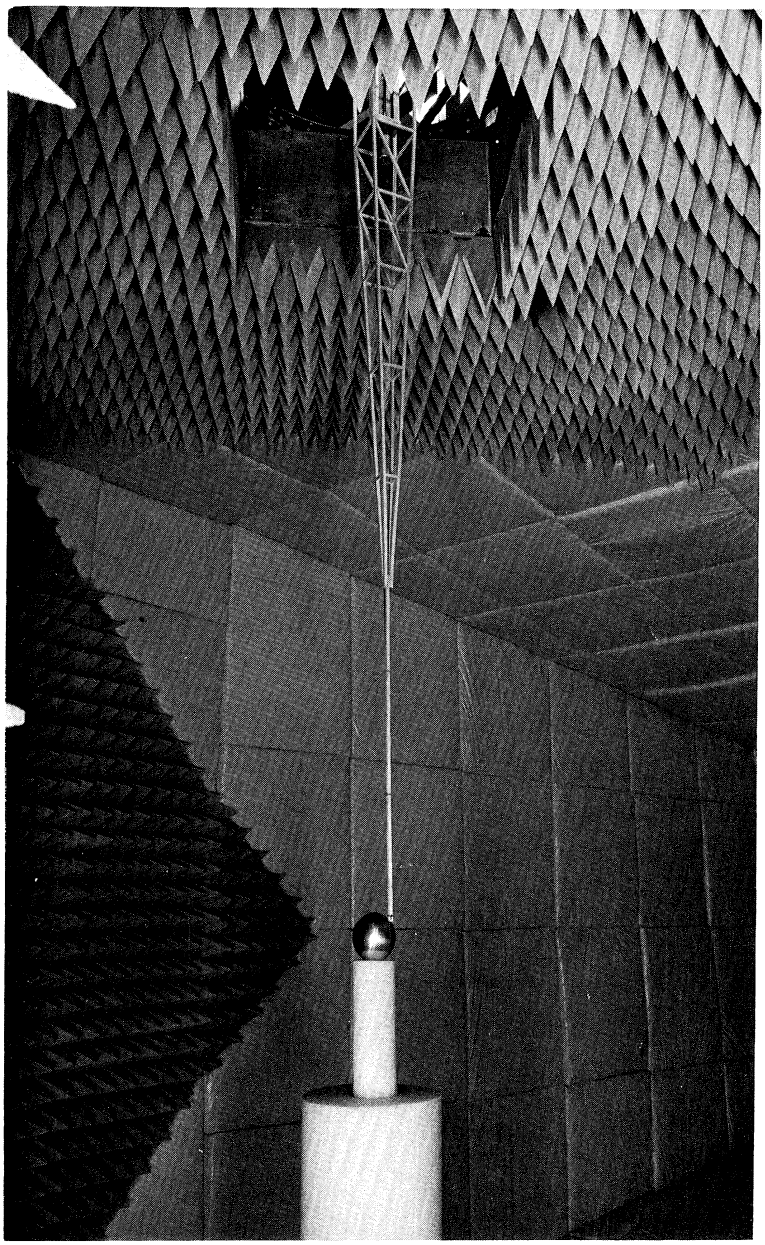

FIG. 4-23: ANTENNA NO. 223 WITH MAGNETIC PROBE ABOVE THE SURFACE; SHOWN IN ANECHOIC CHAMBER

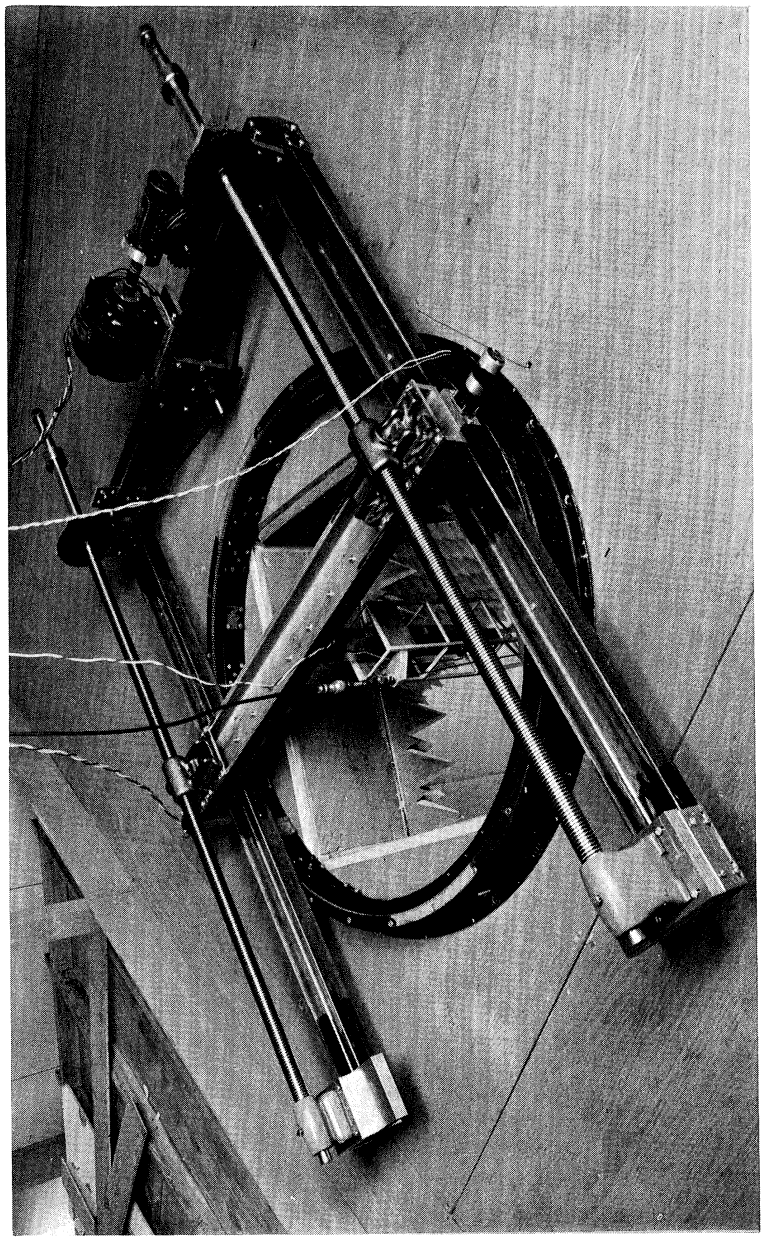

FIG. 4-24: PROBE CARRIAGE SYSTEM ON TOP OF ANECHOIC CHAMGER

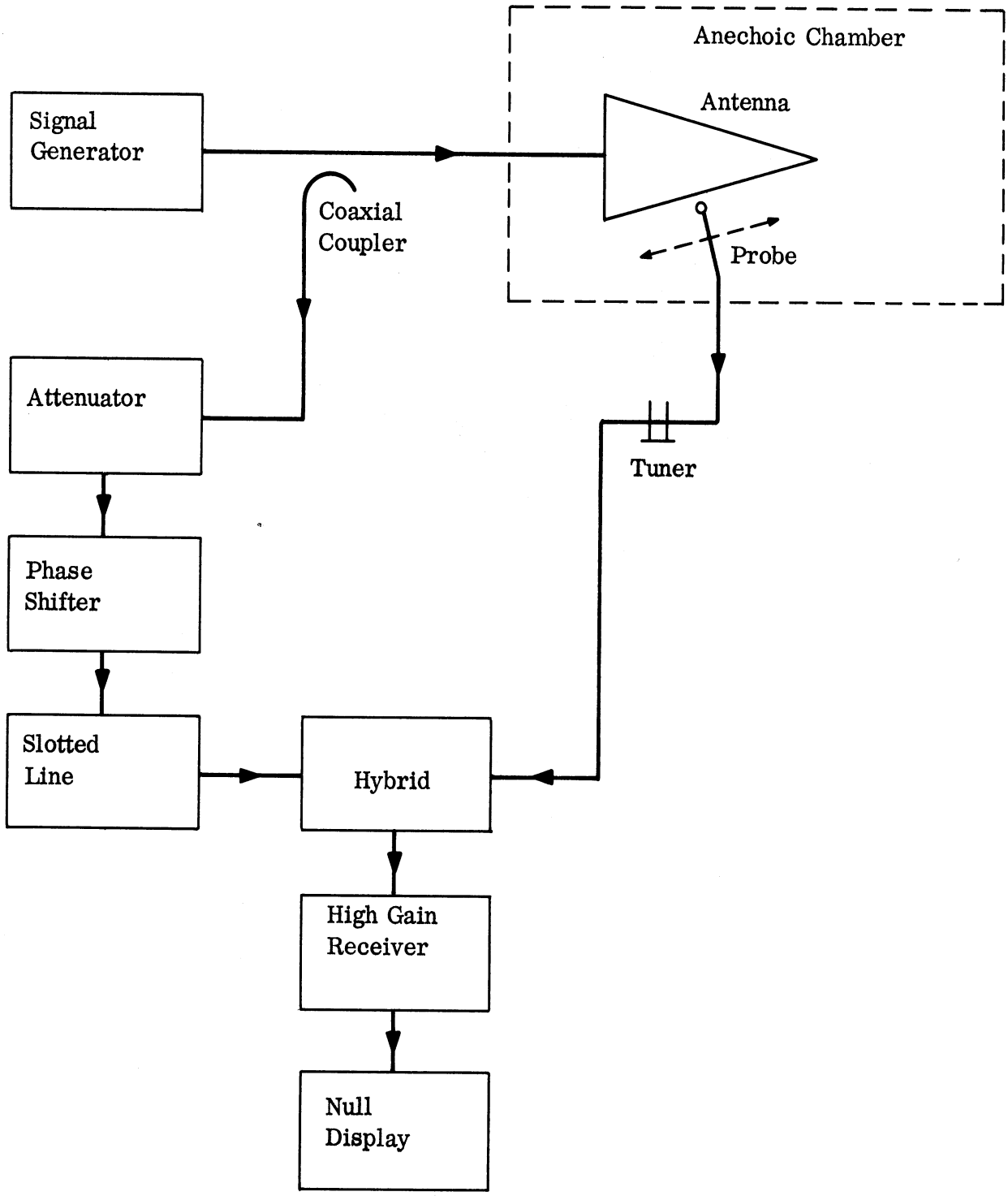

FIG. 4-25: BLOCK DIAGRAM FOR NEAR FIELD PHASE MEASUREMENTS.

In the phase measurement, the probe was placed very close ($\lambda/70$) to the conductor of the antenna (No. 221). Withing the active region the probe pickup was strong enough to easily provide a null in CRO display, but toward the truncated base the pickup signal becomes so weak that the measurement is very difficult; thus the accuracy drops considerably.

4.2.2.1.2 The Probe Position

In order to obtain a meaningful near field amplitude plot, various probe positions were attempted. Figures 4-26 and 4-27 show the effects of the probe position on the shape of the near field amplitude plot for 500 MHz and 900 MHz respectively. When the probe is very close to the conductor, it responds to the amplitude of the current transmitted through the conductor; thus, the amplitude increases sharply whenever the probe passes by the conductor which is quite apparent in Fig. 4-26 when the nearest point of the probe is placed a distance of $\lambda/180$ above the conductor. The average amplitude of the current stays fairly constant until radiation takes place, i.e., the radiation region is where the maximum rate of decrease of the current occurs. As the probe is moved farther from the antenna, the amplitude becomes smooth and the peak seems to move a little toward the base. It is observed that when the probe is placed $\lambda/5 \sim \lambda/20$ above the antenna, the peak of the near field amplitude corresponds very closely to the place where maximum rate of decay of the current occurs. Therefore, this range of probe position has been used throughout later measurements. The optimum position of the probe depends on the frequency, type, and physical size of the antenna. Based on the above observation, the place where peak occurs has been considered to be the center of the radiation region, i.e. the active region. The width of the active region is defined to be the width between 3db points before and after the peak occurs. The active region shifts according to frequency.

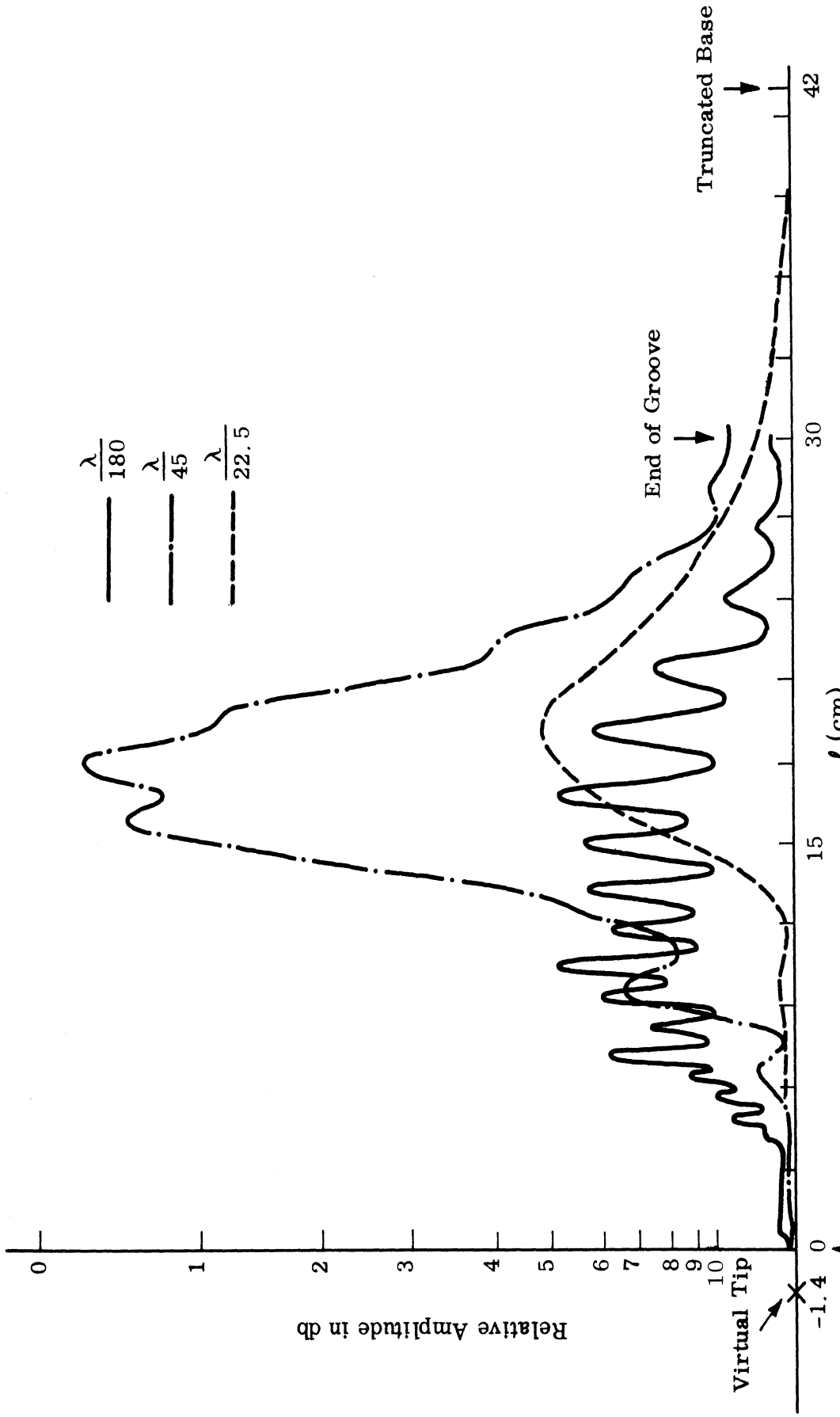

FIG. 4-26: THE NEAR FIELD AMPLITUDE WITH DIFFERENT PROBE POSITIONS AT 500 MHz FOR ANTENNA NO. 223

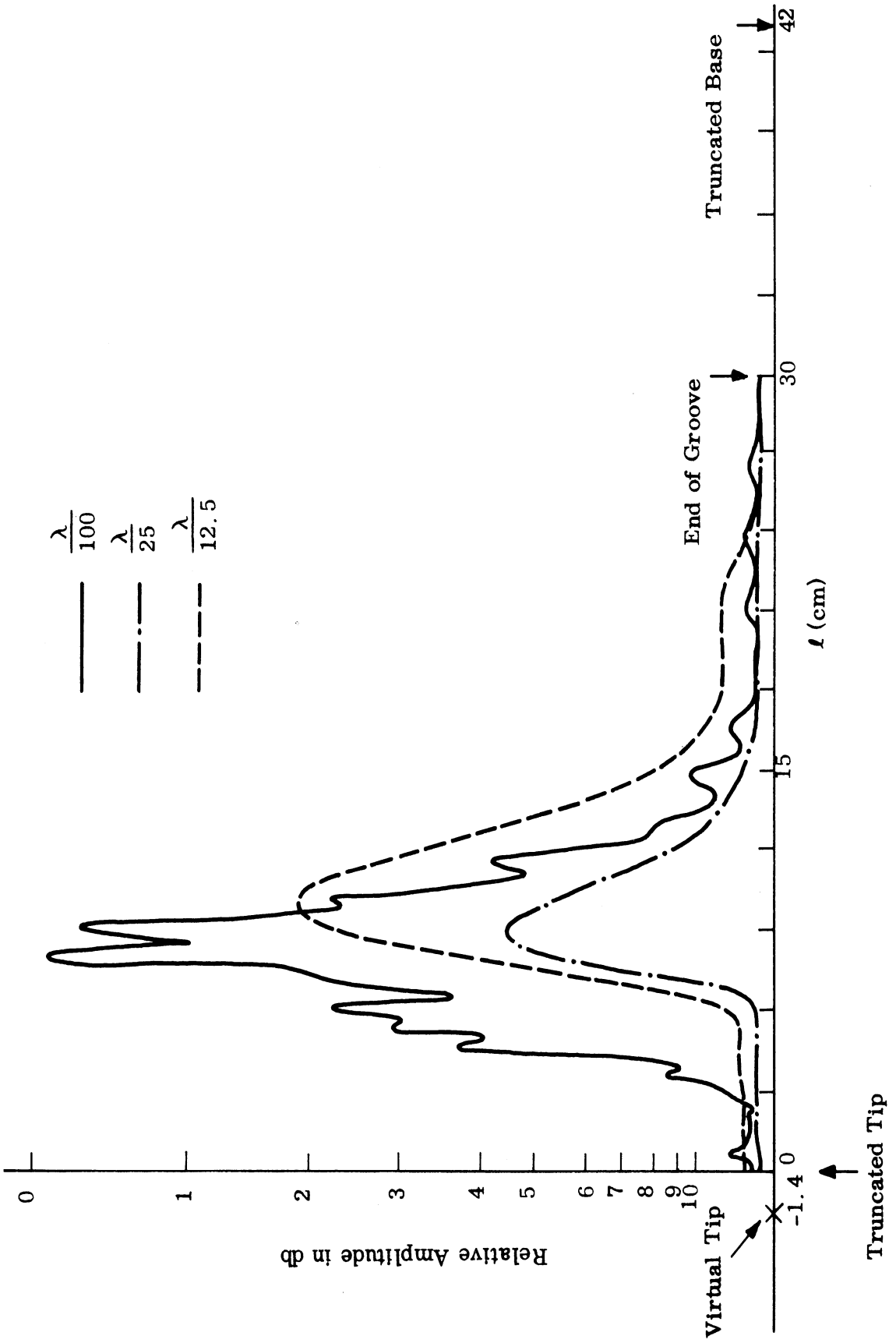

FIG. 4-27: THE NEAR FIELD AMPLITUDE WITH DIFFERENT PROBE POSITIONS AT 900 MHz FOR ANTENNA NO. 223

4.2.2.1.3 The Effect of the Dielectric Loading

The near field amplitude of an unloaded log pyramidal antenna (No. 223) is shown in Fig. 4-28 for three frequencies. The distance of the center of active the region from the virtual tip of the antenna ℓ_a and the width of the active region d_a are tabulated in Table IV-4. It is seen that the location of the peak scales with the frequency as was expected. It is also seen that the width of the active region is fairly constant with respect to the wavelength.

When the dielectric material K-10 ($\epsilon_r = 10$) is placed inside the pyramidal form of No. 223 with a tapered layer of quarter-radius thickness, the near field amplitude changes significantly as shown in Fig. 4-29. The amount of the dielectric material available at the time permitted the loading to extend to 8 cm from the base of the antenna. This discontinuity has resulted in an unusual shape of the near field amplitude near the base of the antenna which may have been caused by the reflection of the propagating wave at the end of the dielectric layer.

The effect of dielectric loading on the near field amplitude is readily seen to be very complex; instead of the very simple shape of the unloaded case, the near field amplitude of a dielectric loaded antenna has at least two major peaks. The distance from the virtual tip to the first peak 1_{a1} and the second peak 1_{a2} together with their respective widths d_{a1} and d_{a2} are tabulated in Table IV-5. At 900 MHz two peaks are so close that d_{a1} and d_{a2} are only crude estimations, while at 300 MHz 1_{a2} and d_{a2} are obscured by the presence of the discontinuity of a dielectric interface. Nevertheless, comparison of Table IV-4 and IV-5 has shown significant effects caused by the dielectric loading. First of all, it is noted that the first peak of the loaded antenna scales with the frequency and is closer to the virtual tip by an average factor of 0.568, while the second peak coincides with the peak of the unloaded antenna. This is a very interesting result observed also for a ferrite loaded zig-zag antenna. The loading seems to split the active region into two major peaks. The amplitude of the first peak is only slightly larger than the second peak at

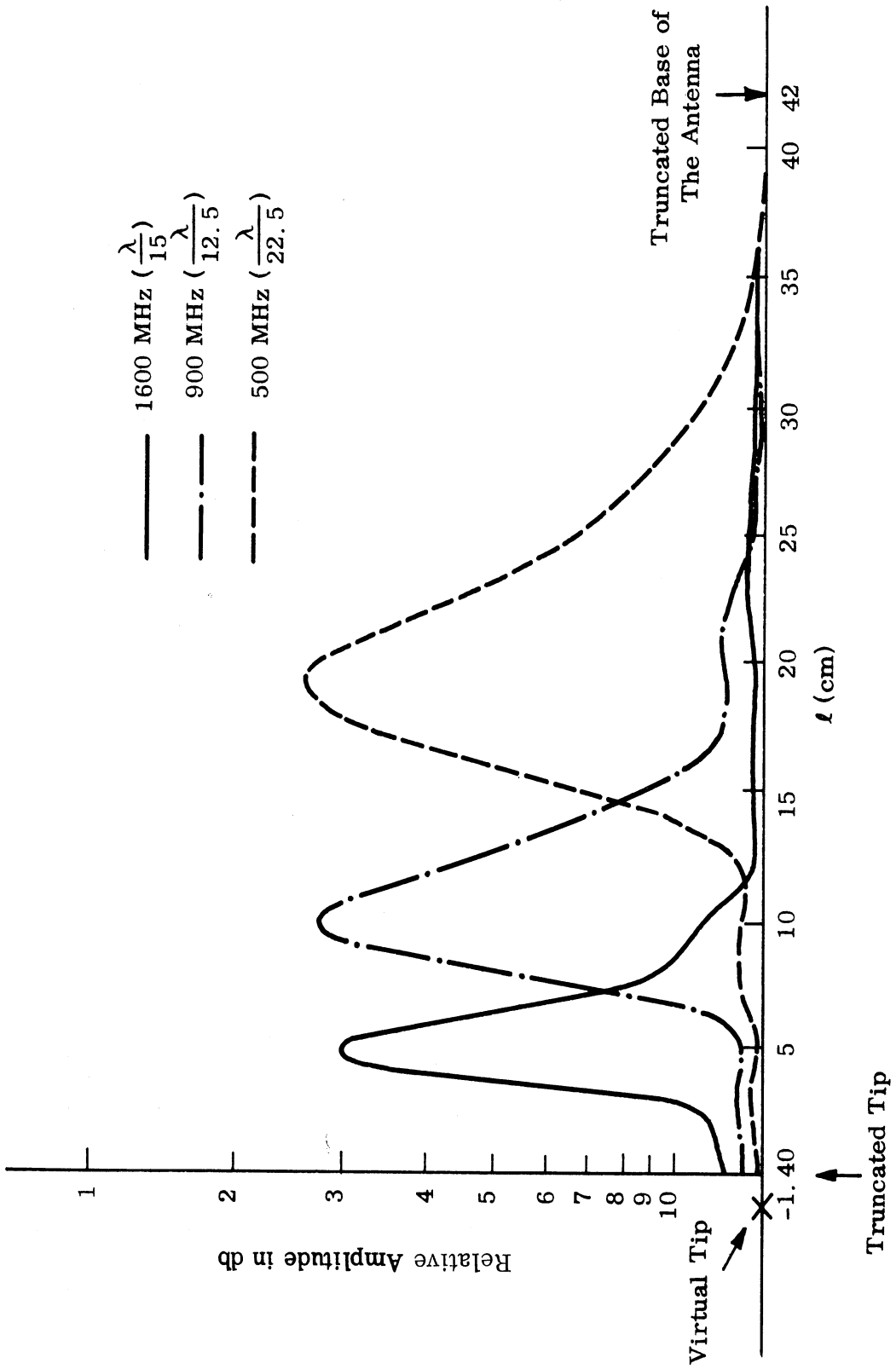

FIG. 4-28: THE NEAR FIELD AMPLITUDE OF ANTENNA NO. 223 WITHOUT LOADING. PROBE POSITIONS ARE INDICATED WITH FREQUENCIES

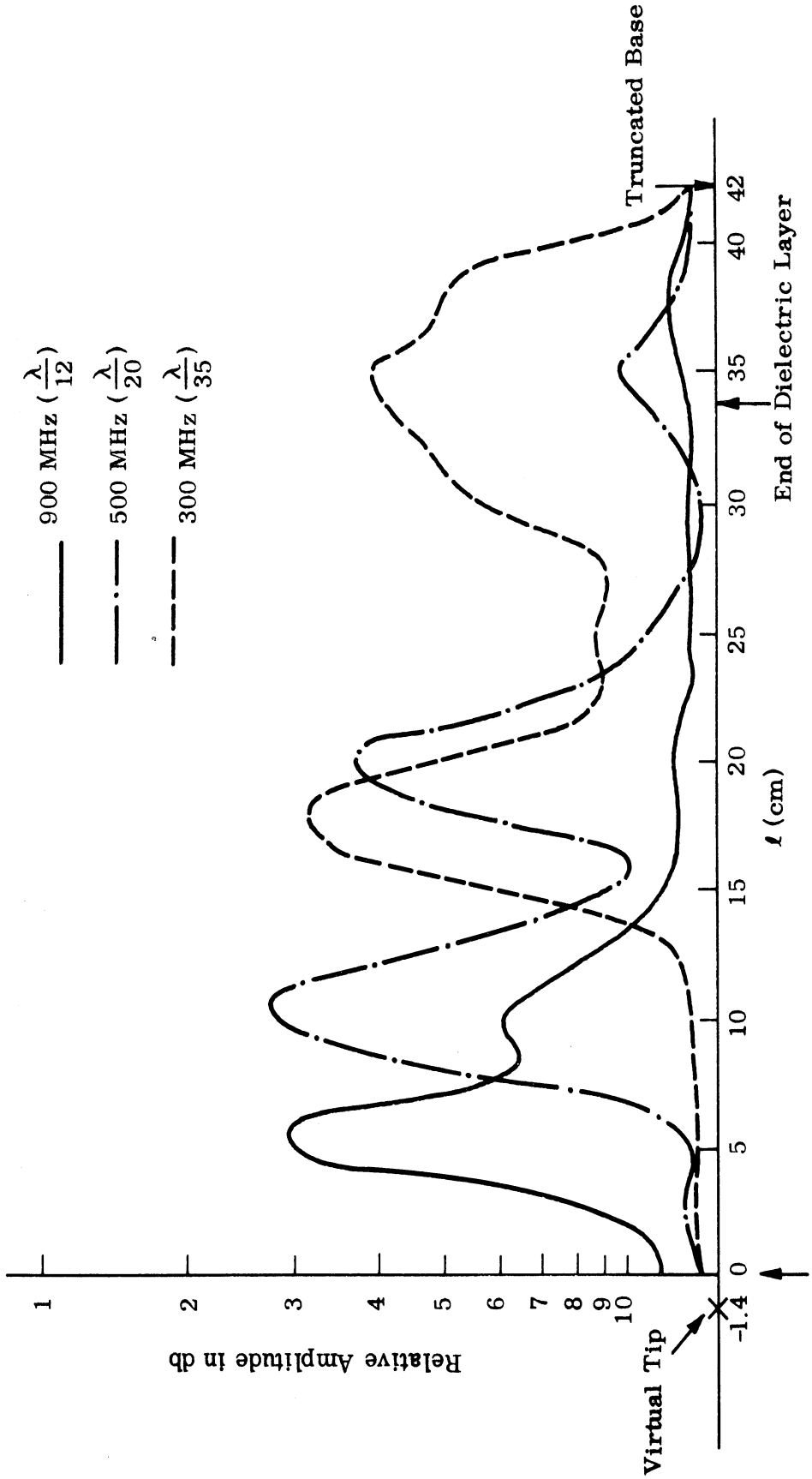

FIG. 4-29: THE NEAR FIELD AMPLITUDE OF ANTENNA NO. 223 WITH DIELECTRIC LOADING. PROBE POSITIONS ARE INDICATED WITH FREQUENCIES

TABLE IV-4

THE ACTIVE REGION FOR ANTENNA NO. 223 WITHOUT LOADING

Frequency f (MHz)	Distance ℓ_a (cm)	Width d_a (cm)	$f \times \ell_a$ (GHz - cm)	$f \times d_a$ (GHz - cm)
1600	6.4	2.9	10.25	4.63
900	11.4	5.1	10.26	4.59
500	20.9	8.8	10.45	4.40

TABLE IV-5

THE ACTIVE REGION FOR ANTENNA NO. 223
WITH QUARTER-RADIUS DIELECTRIC LAYER ($\epsilon_r = 10$)

f (MHz)	ℓ_{a1} (cm)	ℓ_{a2} (cm)	d_{a1} (cm)	d_{a2} (cm)	f x ℓ_{a1} (GHz - cm)	f x d_{a1} (GHz - cm)	f x ℓ_{a2} (GHz - cm)	f x d_{a2} (GHz - cm)
900	6.4	11.4	3.8	5.5	5.76	3.42	10.26	4.95
500	11.9	21.4	5.3	4.5	5.95	2.65	10.70	2.25
300	19.4	36.4	5.5	10.5	5.82	1.65	10.92	3.15

higher frequencies, but the second peak becomes larger as the frequency goes down; eventually the second peak becomes much larger than the first one toward the base of the antenna.

The double-peak character of the inside loaded log pyramidal antenna is quite significant. One reason for this double peak is that the antenna simultaneously operates in both the loaded and unloaded resonance states. It is believed that the loading changes the phase veloctiy of the predominant mode and shifts the active region toward the feeding tip for a backfire radiation. However, the shift of the active region changes the pitch with respect to the wavelength while the width of the active region remains almost unchanged. Therefore, incomplete radiation occurs, and the excess energy, which is loosely coupled to the conductor, travels toward the base on the periphery of the antenna. This energy can be attributed to an excess mode. When the excess mode travels near the place where the unloaded active region was, it may resonate and re-radiate. Since the excess mode is only loosely coupled to the conductor, the inside loading may not have any effect on this second resonance and re-radiation.

The second active region may have very undesirable effects on the far field pattern. If the second peak is smaller than the first peak, the effect is almost negligible. However, if the second peak is comparable to the first one, then depending on the phase difference of the two regions, a broader beam caused by an additional radiating region, or an increase in the back lobe magnitude may occur. Degradations in patterns have been observed in many far-field patterns of some loaded log periodic antennas.

4.2.2.1.4 The phase measurement

Although phase measurements on loaded conical antennas have not yet been made, relative phase shift along the axial surface of antenna No. 221 unloaded can be studied along with its amplitude plot for a better understanding of the active

region. Figures 4-30 and 4-31 show such amplitude and phase combinations at 500 MHz and 900 MHz respectively. The backfire radiation is readily seen from both plots since the phase increases toward the feeding tip at the near peak of the active region.

It is very interesting to note that when the relative phase shift was measured along the conductor for both 500 MHz and 900 MHz, in spite of some inaccuracies mentioned earlier, the phase velocity along the conductor came out to be very close to that of the velocity of light in free space. These are plotted in Fig. 4-32. Other near field measurements appear throughout the report as required for various discussions.

4.2.2.2 Further Measurements of Prototype Scale Models

The pyramidal helix No. 221 has an infinite balun feed, and thus can produce erratic patterns at very low frequencies, when currents travel down the feed. Nevertheless, the antenna had excellent characteristics. In Fig. 4-33, antenna No. 221 was loaded with a tapered loading as shown, in order to load only the large, low frequency end of the spiral, leaving the small high frequency end with its original characteristics. A high dielectric constant (ϵ=10) was used for the loading material. The radiation patterns at a given frequency are better for the loaded condition. From these patterns it can be deduced that for a given frequency of operation the diametral size of the loaded antenna has been reduced by a factor compared to the unloaded size. A slight pattern tilt is observed at 300 MHz for the loaded case. No resistive absorption was used. The near field patterns, shown in Figs. 4-34a and b, are also very good, even below 250 MHz. At all of the frequencies between 250 and 500 MHz a definite improvement with loading over the same antenna with no loading is shown. The far field patterns have low backlobes and beamwidths of about 90^{o}. The near field patterns indicate that the radiation regions for 250 to 500 MHz have moved up the cone. At the lower frequencies, in particular, a more desirable shape is

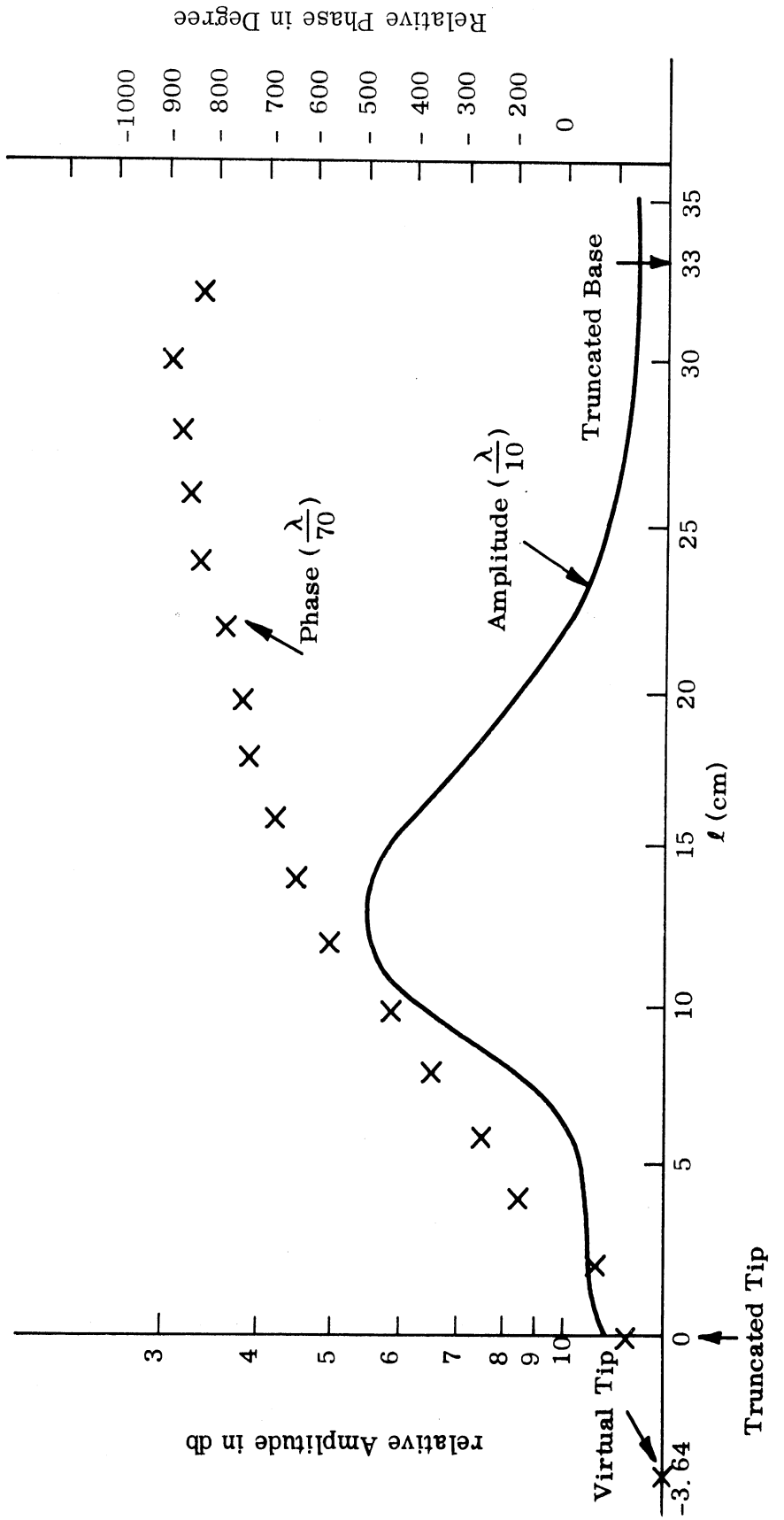

FIG. 4-30: THE NEAR FIELD AMPLITUDE AND PHASE OF ANTENNA NO. 221 AT 500 MHz. PROBE POSITIONS ARE AS INDICATED

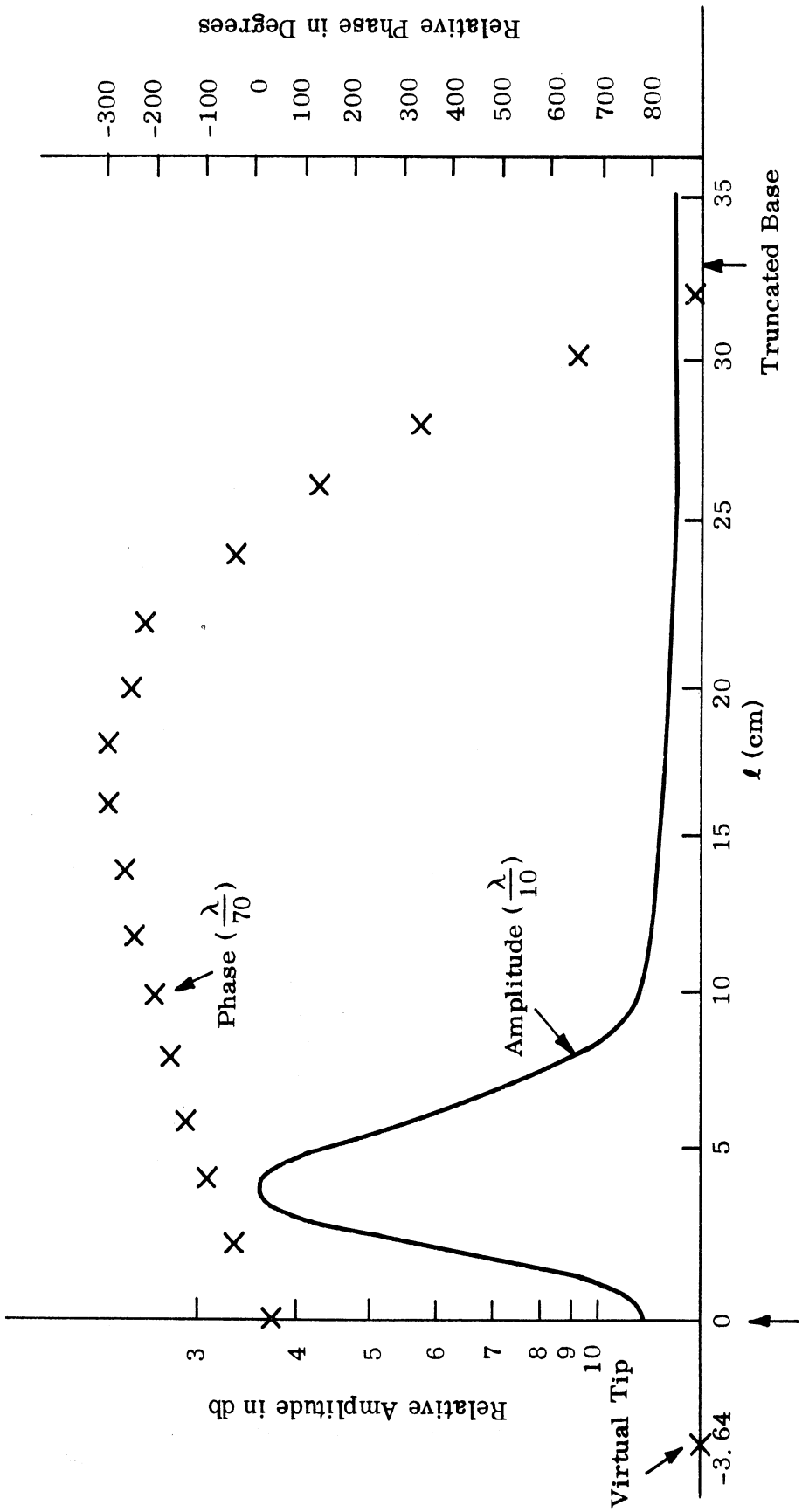

FIG. 4-31: THE NEAR FIELD AMPLITUDE AND PHASE OF ANTENNA NO. 221 AT 900 MHz. PROBE POSITIONS ARE AS INDICATED

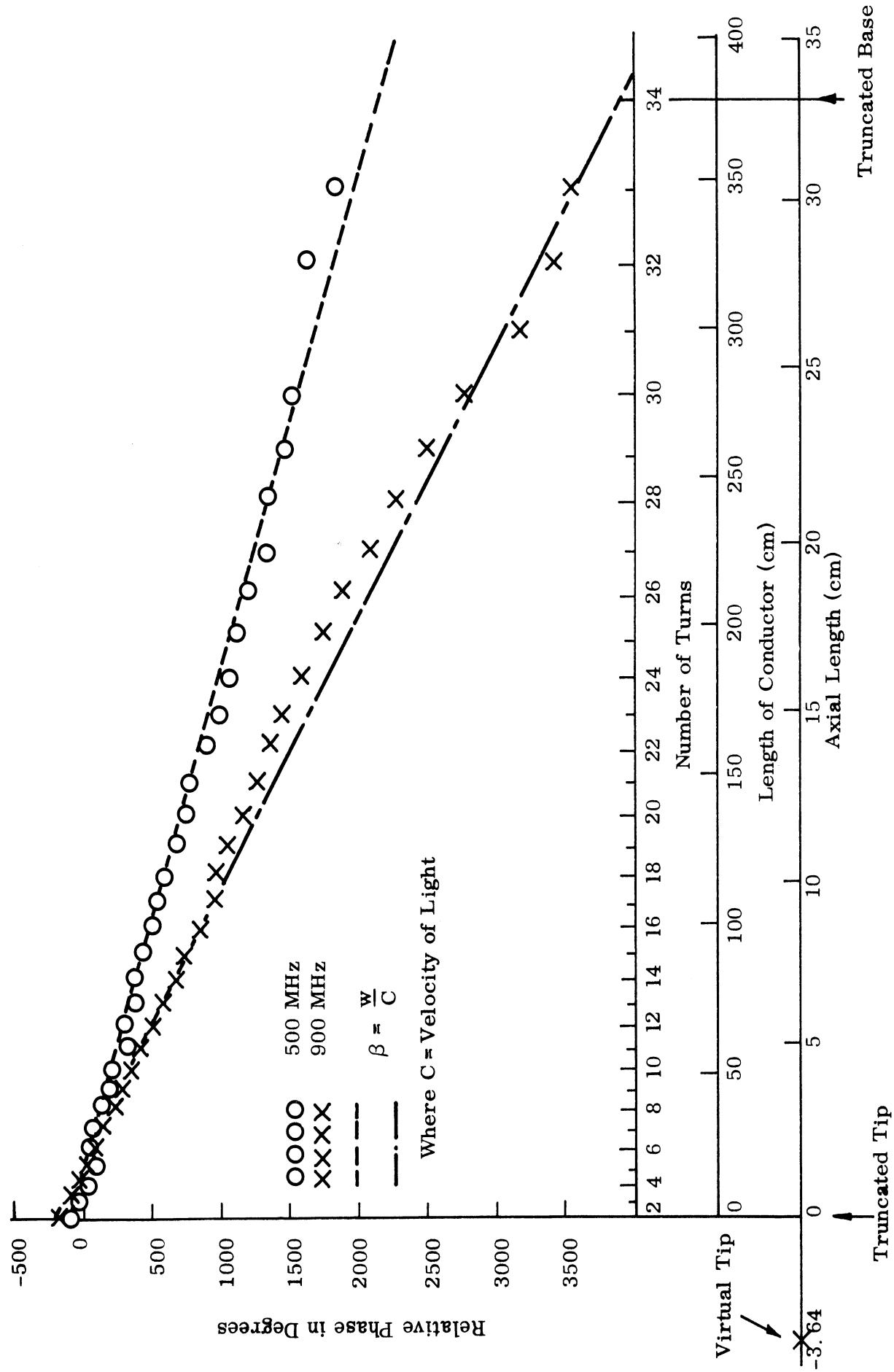

FIG. 4-32: RELATIVE PHASE SHIFT FOR ANTENNA NO. 221 ALONG THE CONDUCTOR (PROBE POSITION IS $\frac{\lambda}{70}$ ABOVE THE CONDUCTOR)

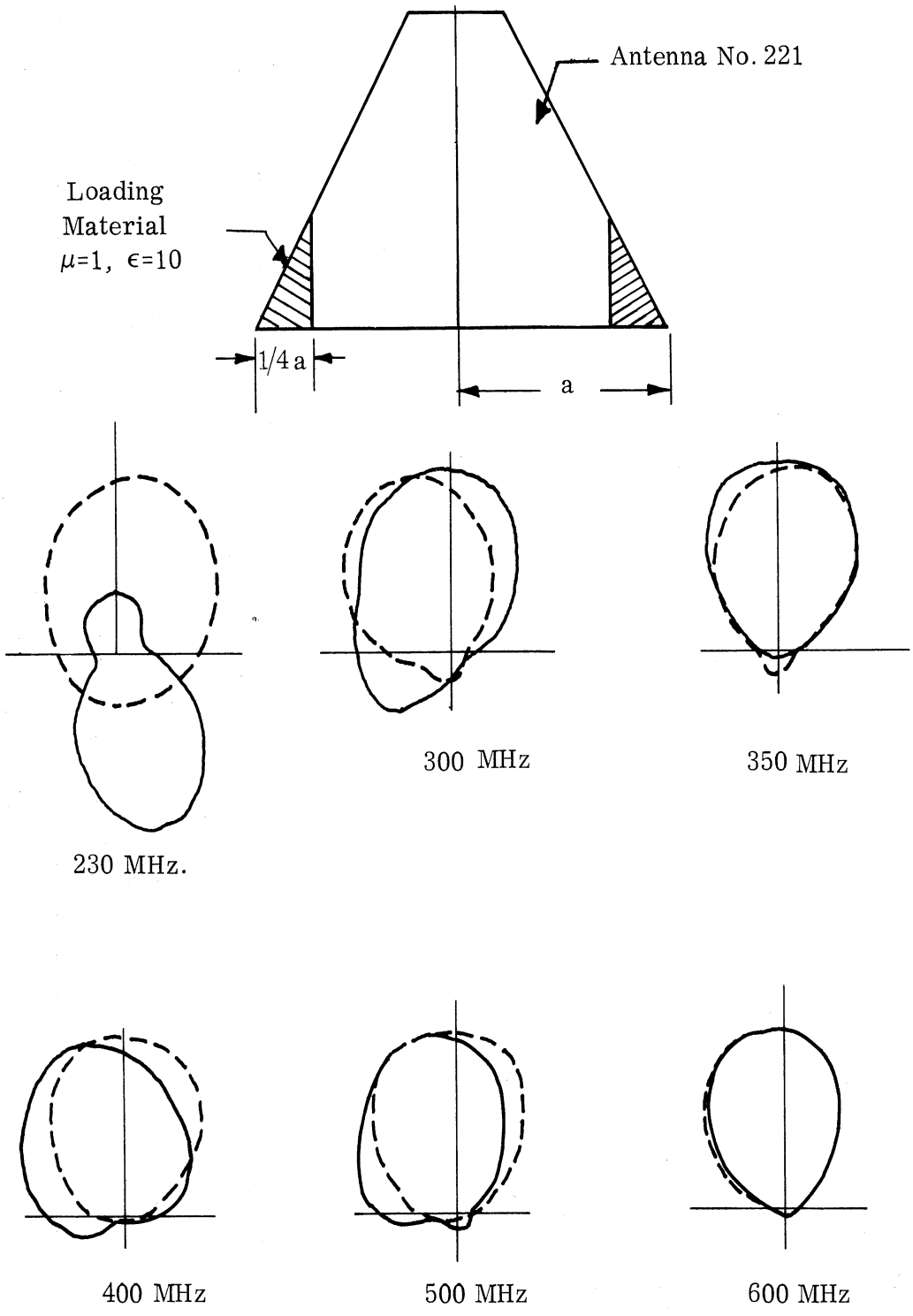

FIG. 4-33: TAPERED LOADING ON PYRAMIDAL HELIX (221), H-PLANE

——— unloaded, — — — — dielectric loaded

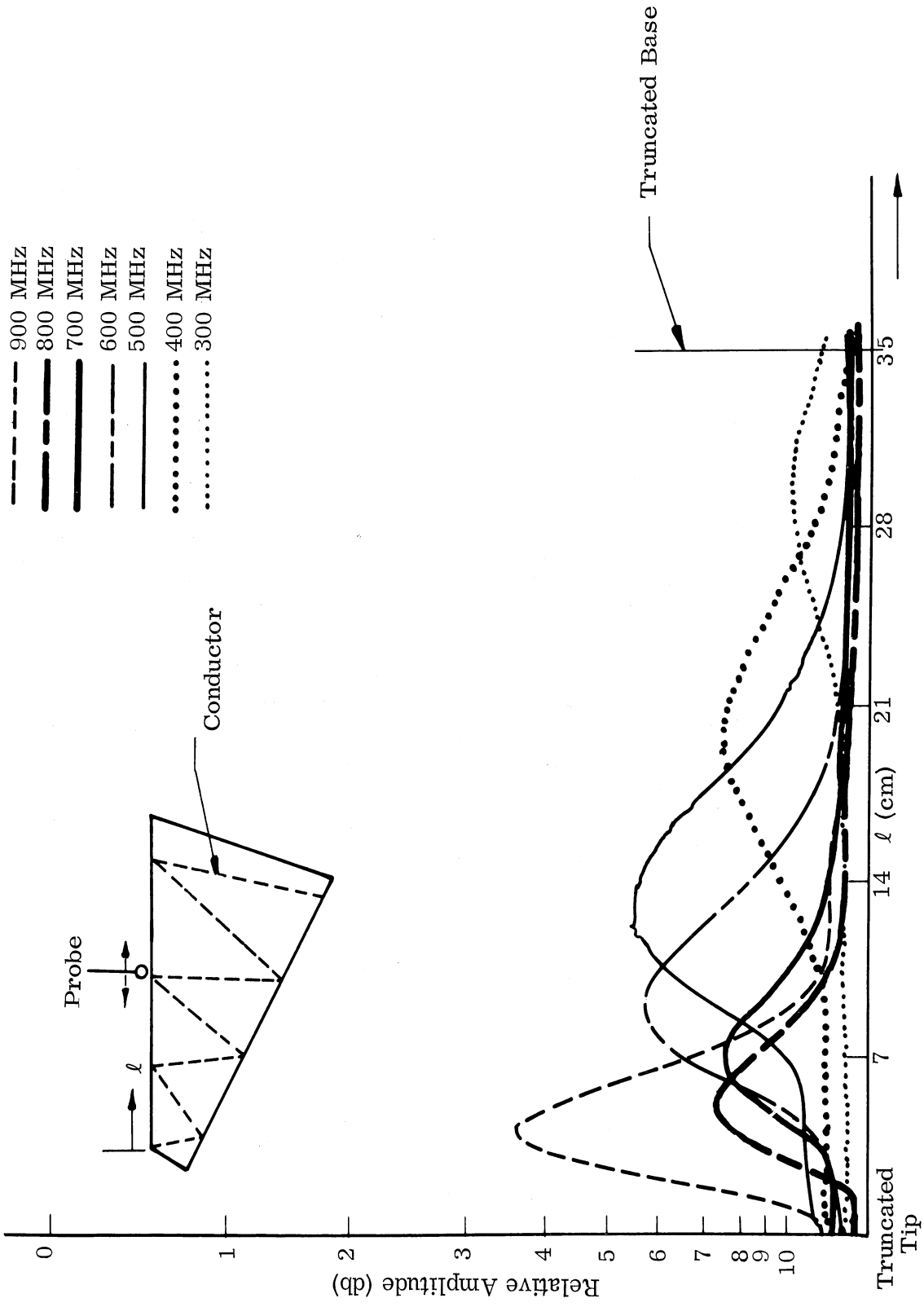

FIG. 4-34a: NEAR FIELD AMPLITUDE OF ANTENNA NO. 221, UNLOADED PROBE POSITION λ/12 ABOVE ANTENNA SURFACE.

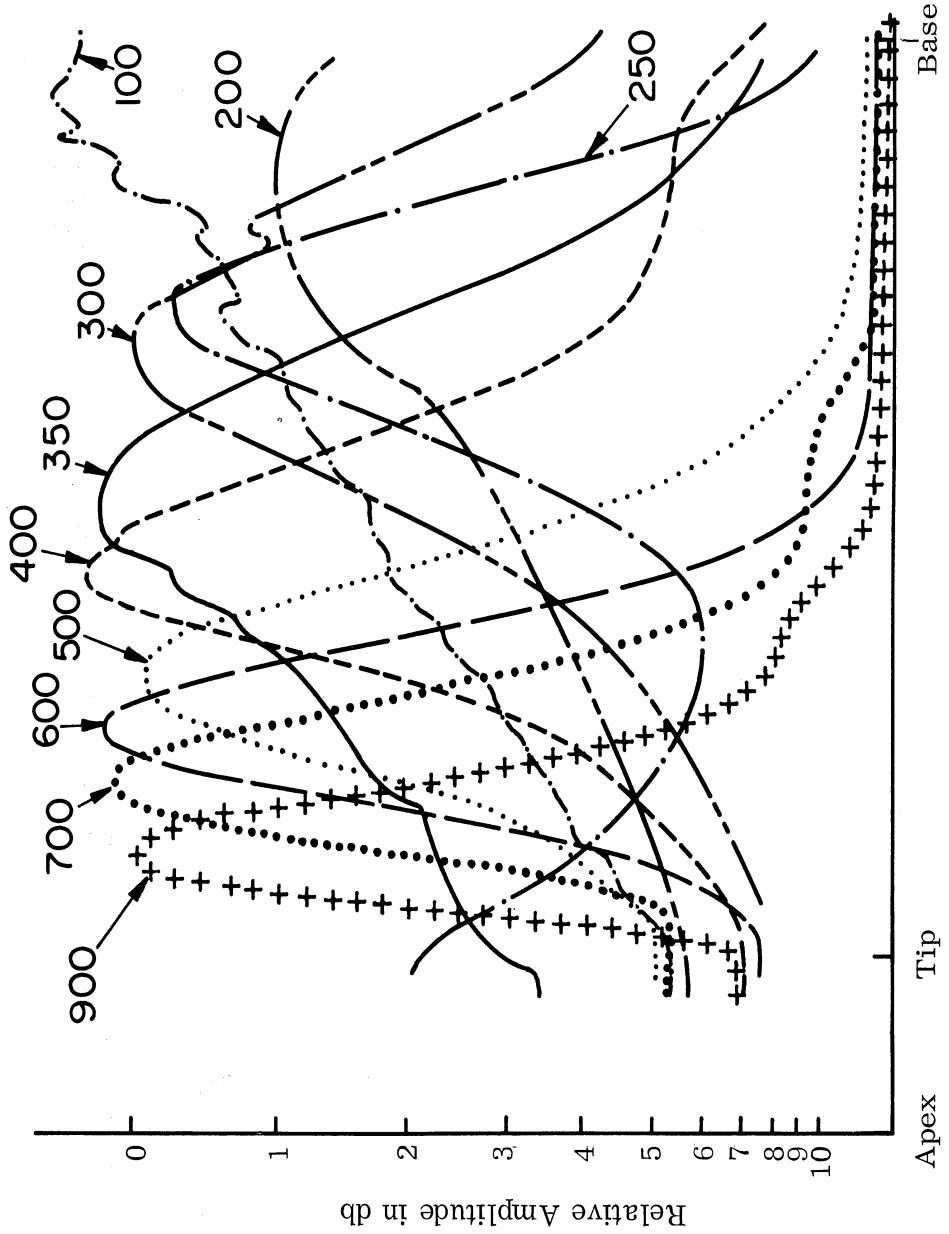

FIG. 4-34b: ANTENNA 221 WITH L2 LOADING OF K-10

observed. The near field patterns were taken at one-tenth of a wavelength from the antenna. This loading gives a reduction factor of about 0.6 to 0.7.

A similar loading on antenna No. 223 resulted in antenna patterns shown in Figs. 4-35 and 4-36. The loading material has a lower dielectric constant ($\epsilon = 6$), and is using the same type of artificial dielectric specified for the prototype. Fig. 4-37 shows the near field of this configuration as compared with the unloaded plots Fig. 4-44.

Figure 4-38 shows the near field patterns at one-tenth of a wavelength probe spacing for antenna No. 223 with the same L2 loading of Flexible Hi-K-6. Note that the taper starts about 0.7 down from the apex to the base of the cone, while from the 0.7 point to the base, the dielectric is a quarter radius thick. The radiation region for 350 MHz moved up the cone. However, the radiation regions for 300 and 400 MHz are very broad. Compared to the previous L2 loading there isn't much improvement in frequency reduction and much more dielectric is used to accomplish essentially the same frequency reduction. In addition, in neither case is the reduction nearly as good as with High-K 10 powder, which leaves some doubt as to the actual G of the Flexible Hi-K.

Near field patterns at a tenth wavelength were taken on an L1 loading of Flexible Hi-K-6 dielectric as shown in Fig. 4-39. As may be recalled, loading L1 is one-half radius thick at the base of the antenna, but tapers to zero thickness one-half of the way down the antenna from the apex to the base. A cross-section of the loading results in a right triangle, one-half radius thick at the base. The antenna radiation regions for 300, 350, 400, 500, and 600 MHz have moved markedly upward. At 700 MHz, the active region is in essentially the same location as in the unloaded case. However, the radiation regions for 300, 350, and 400 MHz are very broad and this may result in undesirable effects. The L1 loading appears more effective than either of the L2 loadings.

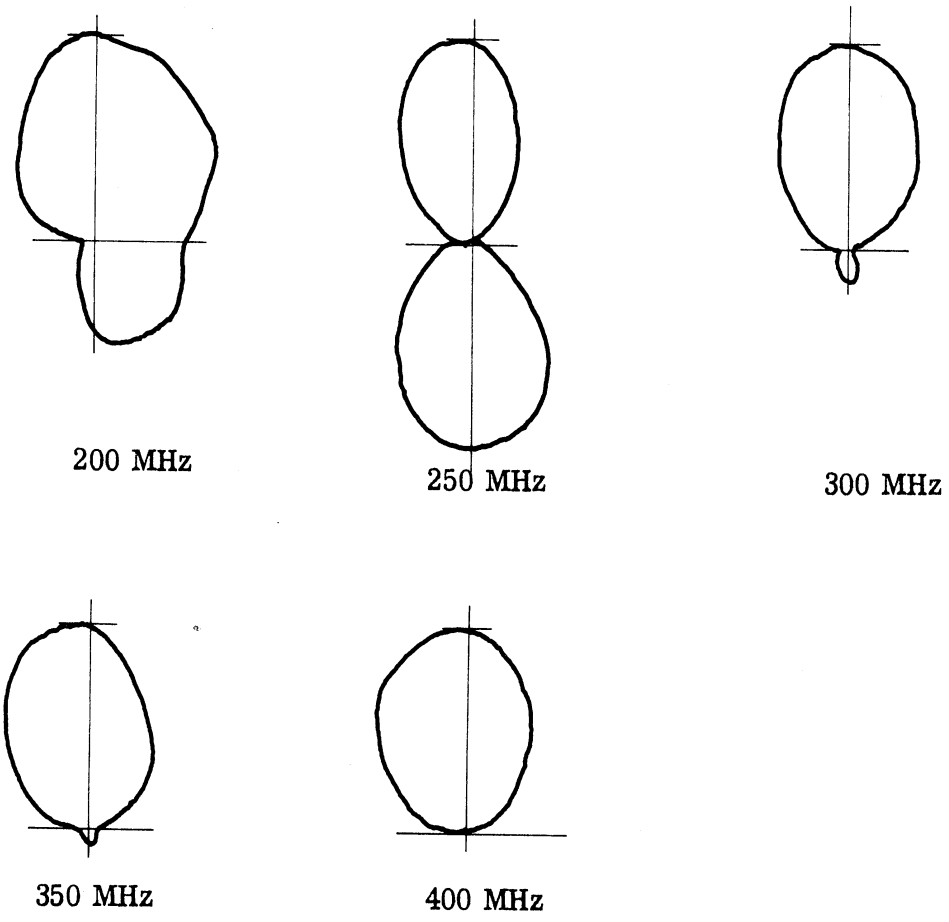

FIG. 4-35: LINEAR POWER PLOTS OF ANTENNA 223
L-2 FLEXIBLE Hi-K-6, VERTICAL POLARIZATION

H-PLANE

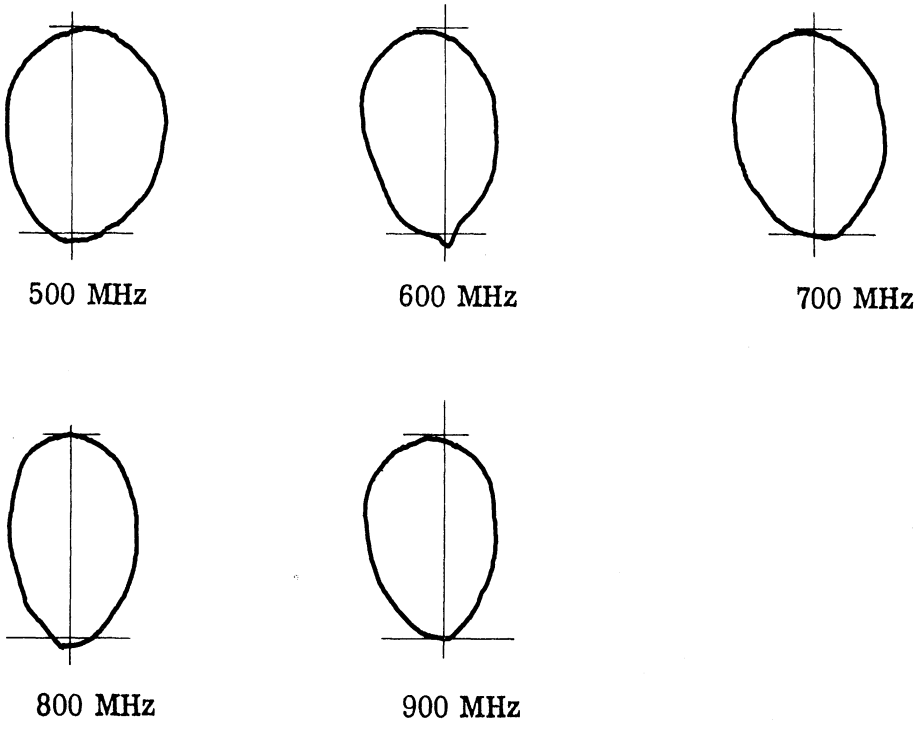

FIG. 4-36: LINEAR POWER PLOTS OF ANTENNA 223
L-2 FLEXIBLE Hi-K-6, VERTICAL POLARIZATION
(continued).

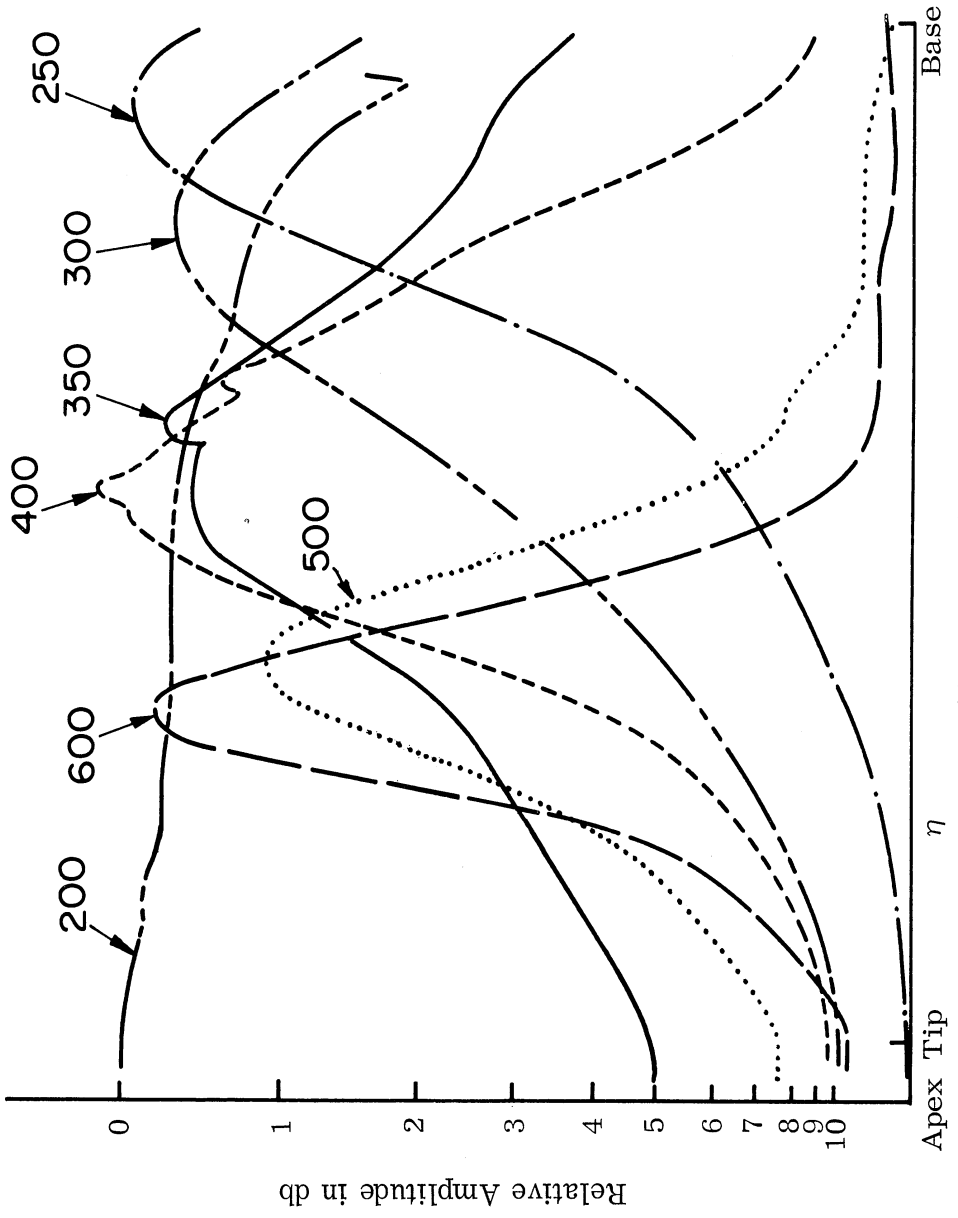

FIG. 4-37: ANTENNA 223 WITH AN L-2 LOADING OF FLEXIBLE HI-K-6.

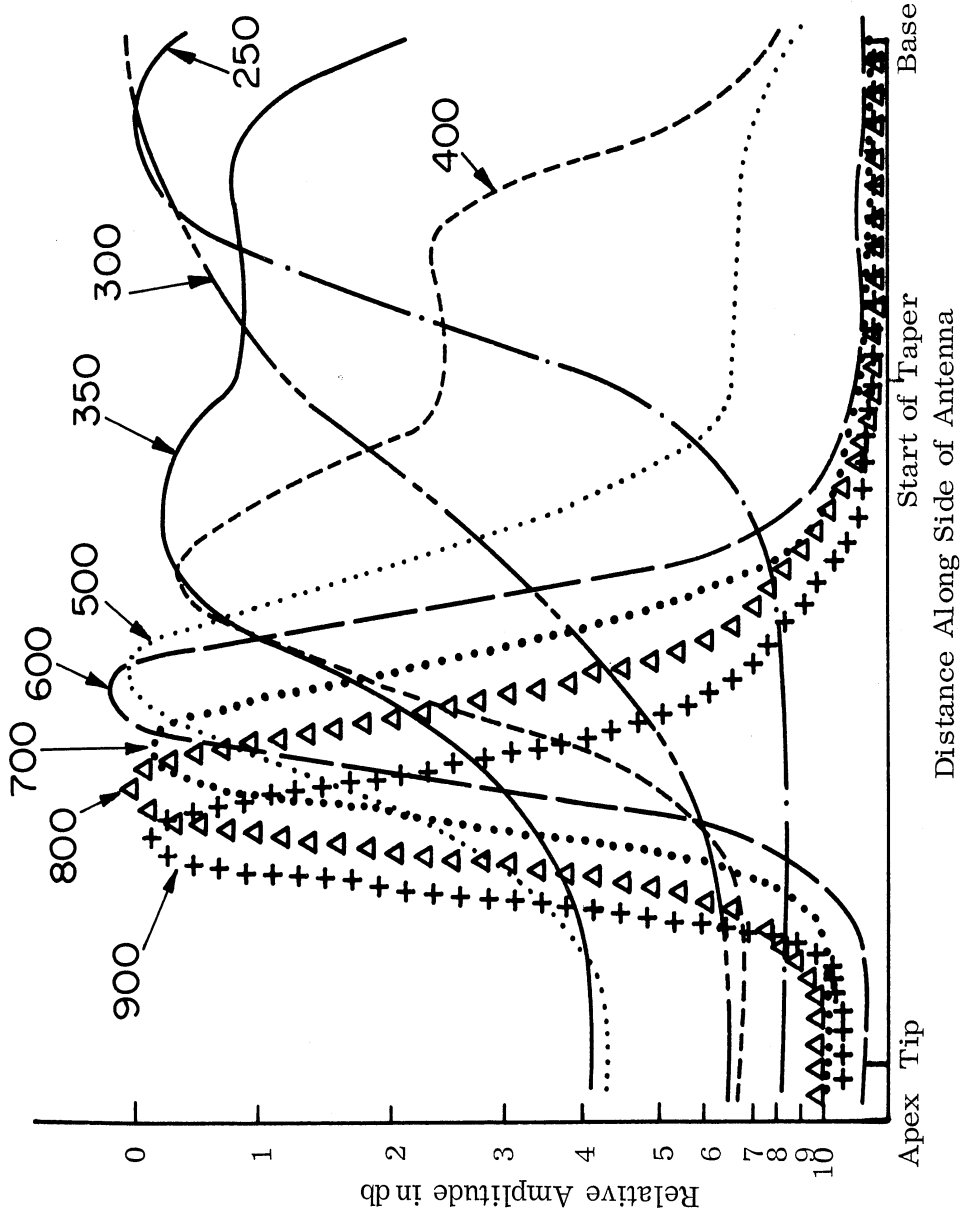

FIG. 4-38: ANTENNA 223 WITH LOADING L2 OF FLEXIBLE HI-K-6 WITH THE TAPER STARTING 5" ABOVE THE BASE.

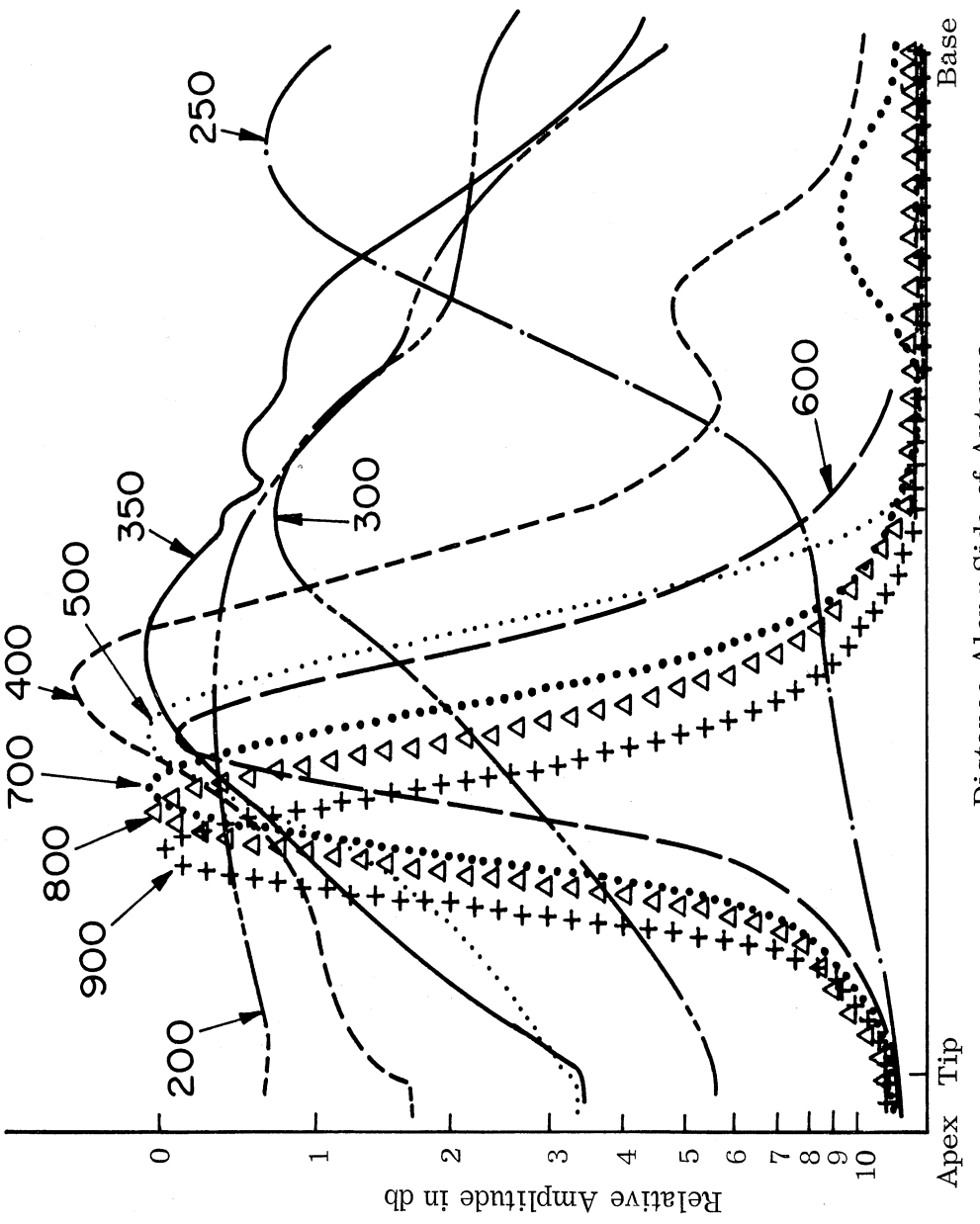

FIG. 4-39: ANTENNA 223 WITH LOADING L1 OF FLEXIBLE HI-K-6.

The L1 loading was the original one specified for the prototype. However, when the manufacturer could not deliver dielectric meeting its own published weight specifications, the L2 loading was used instead. Notice, though, that the L1 loading of a dielectric with a relative permittivity of 6 may possibly result in a reduction factor approaching 0.5 for the lineal dimensions of a conical helix antenna.

More specific listings of the pattern characteristics can be seen in Figs. 4-40 - 4-43. For the tapered base-loading for antenna No. 221 beam tilt when loaded is below 5^{o} except for the 300 - 350 MHz region, and beamwidth remains near 90^{o} to 300 MHz. The patterns of antenna No. 221 for air core were good in the range above 500 MHz; this is in accordance with its design on an unloaded basis. The beamwidth did not exceed 90^{o} by more than 6 per cent. The beam tilt was as much as twice that specified possibly due to rough construction and the infinite balun.

According to beamwidth information the lower cutoff frequency for antenna No. 223 is between 600 - 700 MHz even though the lower dimensions of the antenna are the same as No. 221 (see Fig. 4-42). Antenna No. 221 starts to cut off between 360 - 400 MHz for the same polarization. The near field patterns for antenna No. 223, which were taken at a tenth wavelength probe spacing, look very good (see Fig. 4-44). Notice that the patterns for 500 MHz decays to a very low level by the time the base of the antenna is reached. This indicates that a good far field pattern should be obtained.

A more uniform loading over more of the antenna No. 223 is shown in Fig. 4-45.

Fig. 4-46 gives a summary of the beamwidth and backlobe level of a very interesting experiment. The purpose of the experiment was to determine the reduction occurring when a conical helix was uniformly loaded with a one-quarter radius thick layer of K-10 dielectric. Due to a shortage of dielectric, the lower 8 cm of the layer could not be filled. A significant loading effect was seen, but a breakup of the near field results (Fig. 4-29) which destroys the far fields at 500 - 600 MHz. More study is necessary on the problem of breakup of near field probe patterns.

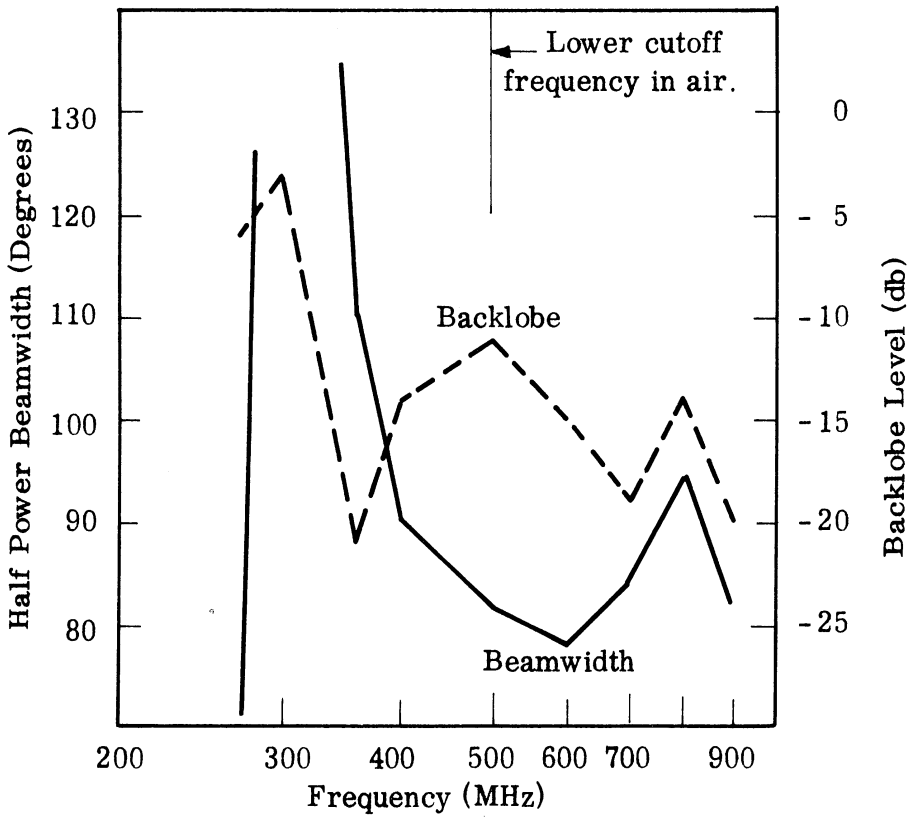

Frequency MHz	VSWR	Half-power Beamwidth Power	Backlobe Level db
270	-	71	- 6
300	-	198	- 3
360	-	110	-21
400	2.5	90	-14
500	1.92	82	-11
600	1.65	78	-15
700	1.89	84	-19
800	2.3	95	-14
900	1.66	82	-20

FIG. 4-40: ANTENNA 221 IN AIR, H-PLANE

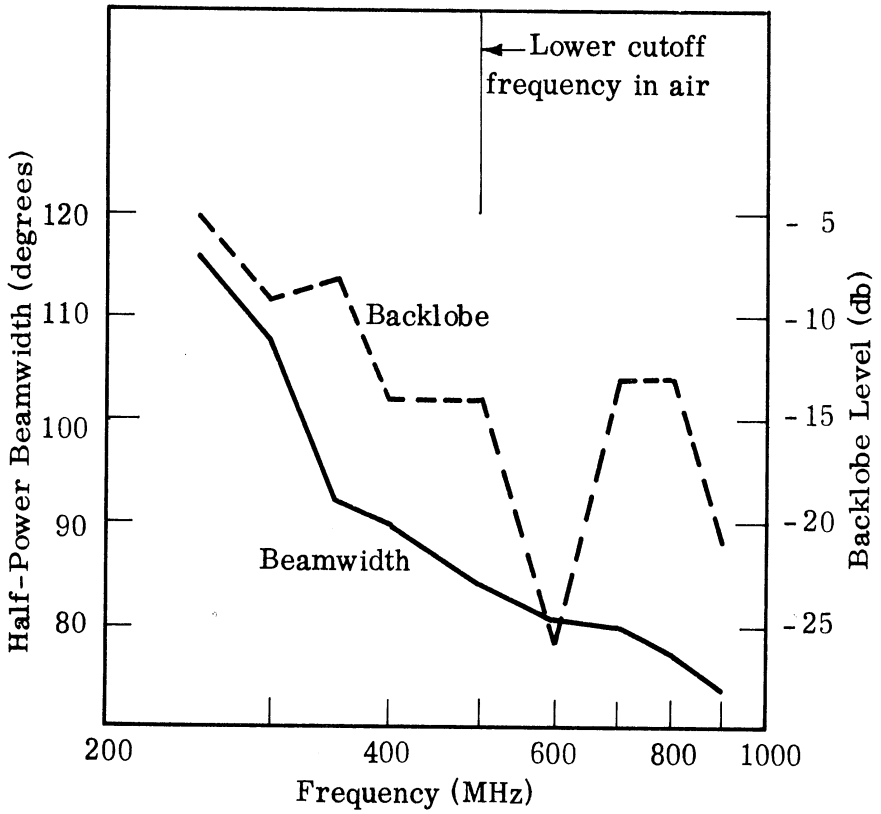

Frequency MHz	VSWR	Half-power Beamwidth Power	Backlobe Level db
250	3.33	116	- 6
300	3.42	108	- 9
350	3.72	92	- 8
400	1.62	90	- 14
500	2.08	84	- 19
600	1.62	80.5	- 26
700	1.48	80	- 13
800	1.28	77	- 13
900	1.25	74	- 21

FIG. 4-41: ANTENNA 221 L2-K10, H-PLANE

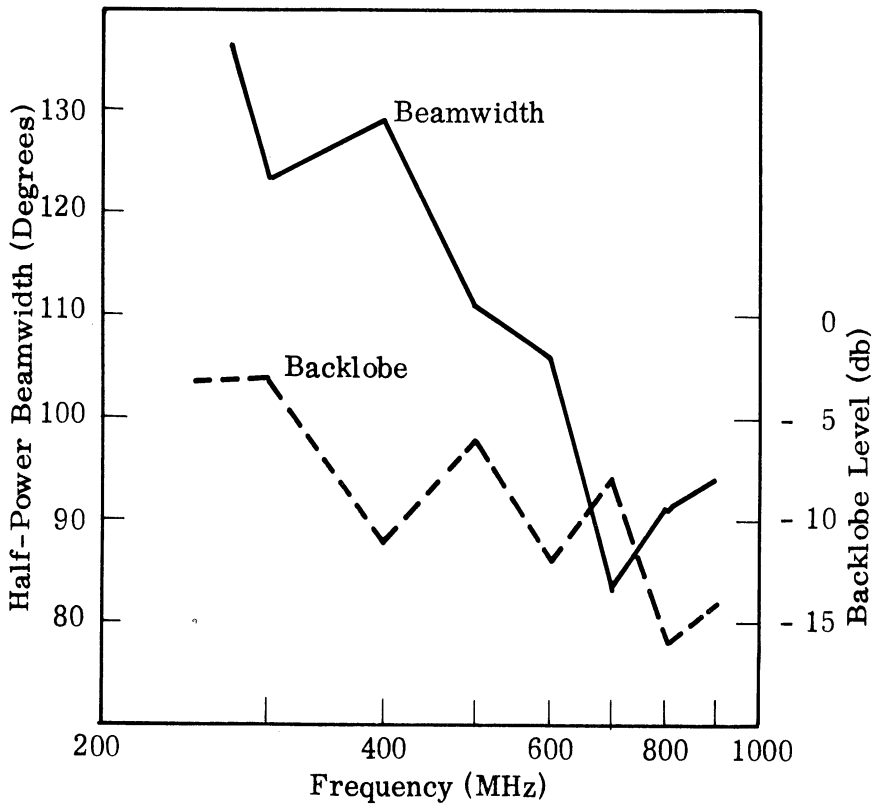

Frequency MHz	VSWR	Half-Power Beamwidth Degrees	Backlobe Level db
250	—	151	- 3.4
300	—	123	- 3
400	1.545	129	- 11
500	1.46	111	- 6
600	1.18	106	- 12
700	1.09	83	- 8
800	1.35	91	- 16
900	1.18	94	- 14

FIG. 4-42: ANTENNA 223 IN AIR, H-PLANE

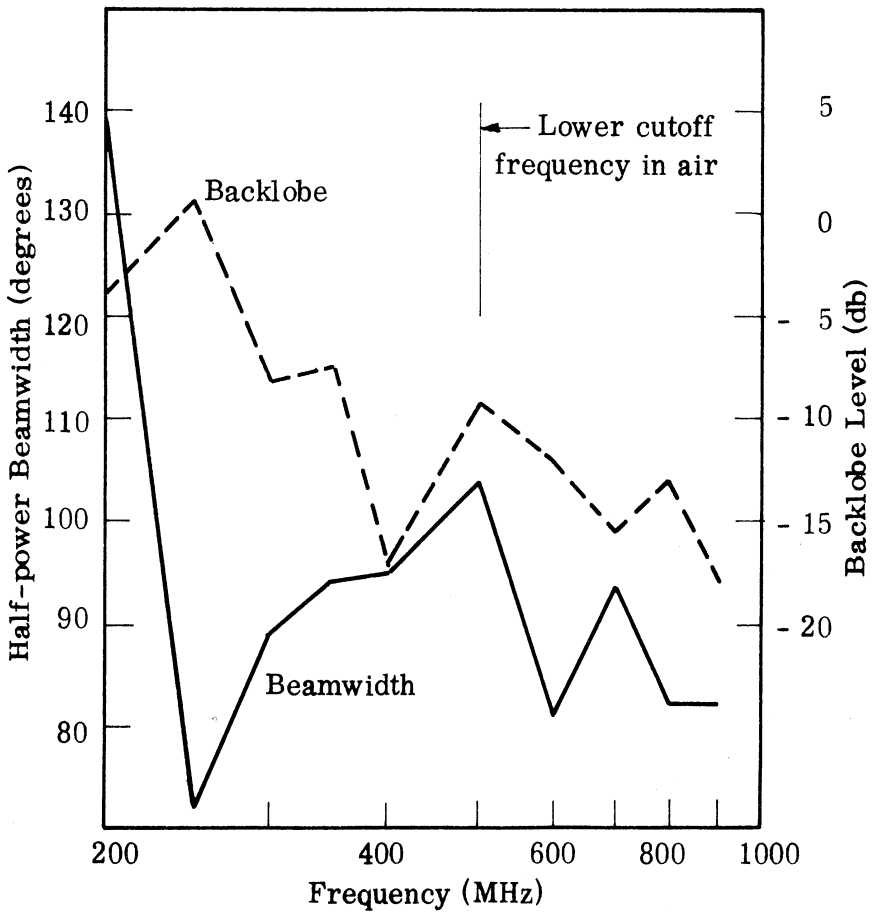

Frequency MHz	Half-power Beamwidth Degrees	Backlobe Level db
200	139	- 2.2
250	72	+ 0.38
300	89	- 8.10
350	94	- 7.48
400	95	- 17.1
500	104	- 9.27
600	81	- 12.04
700	94	- 15.46
800	81	- 13.01
900	81	- 17.95

FIG. 4-43: HALF POWER BEAMWIDTH AND BACKLOBE OF ANTENNA 223 L2-FLEXIBLE HI-K-6 H-PLANE

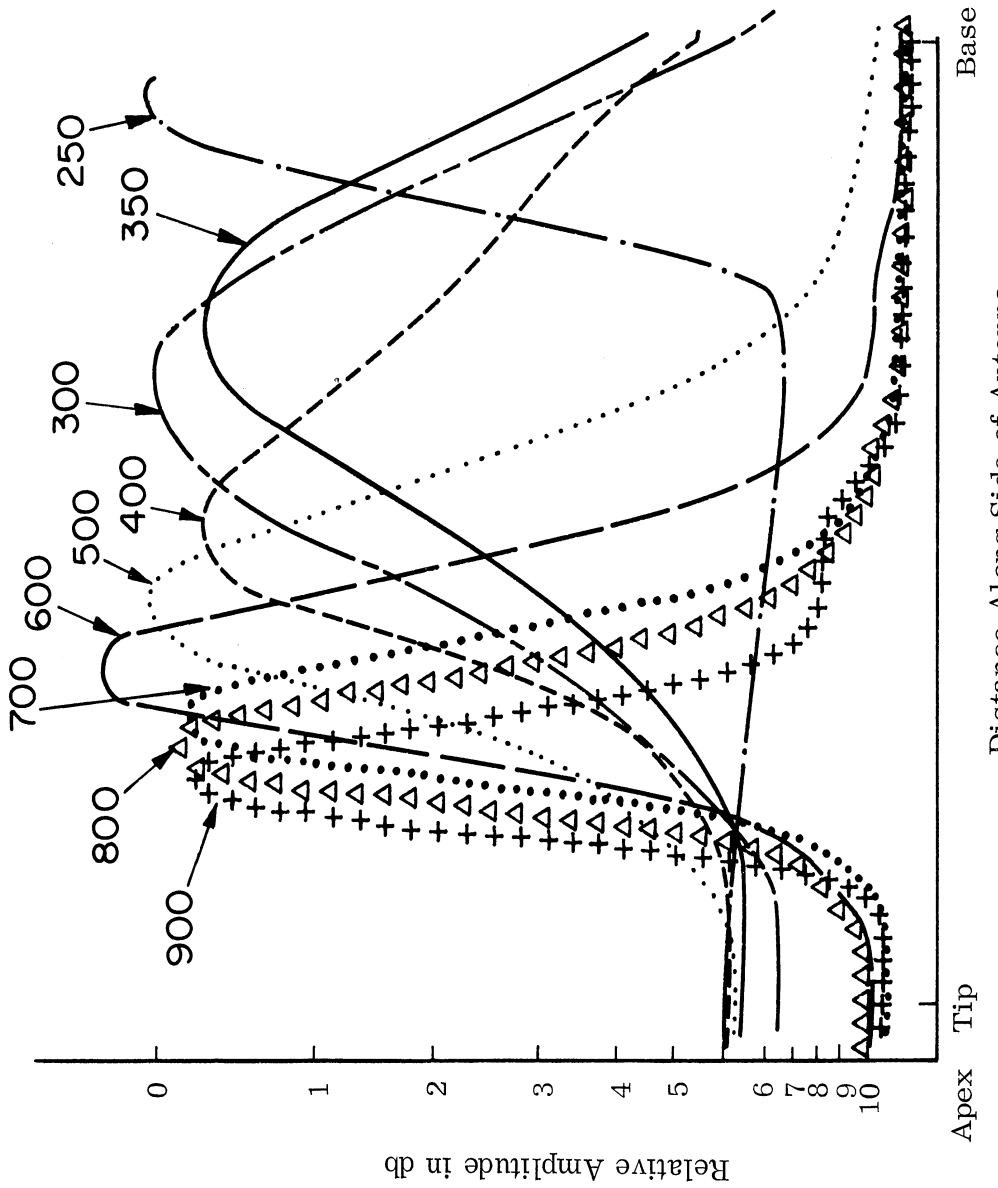

FIG. 4-44: ANTENNA 223 WITH NO LOADING.

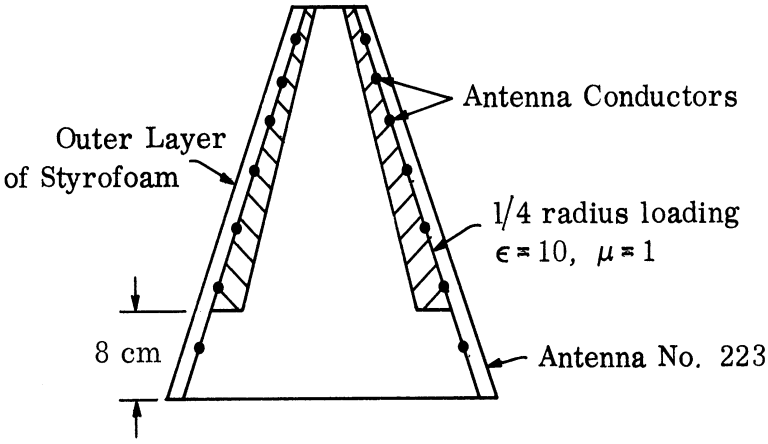

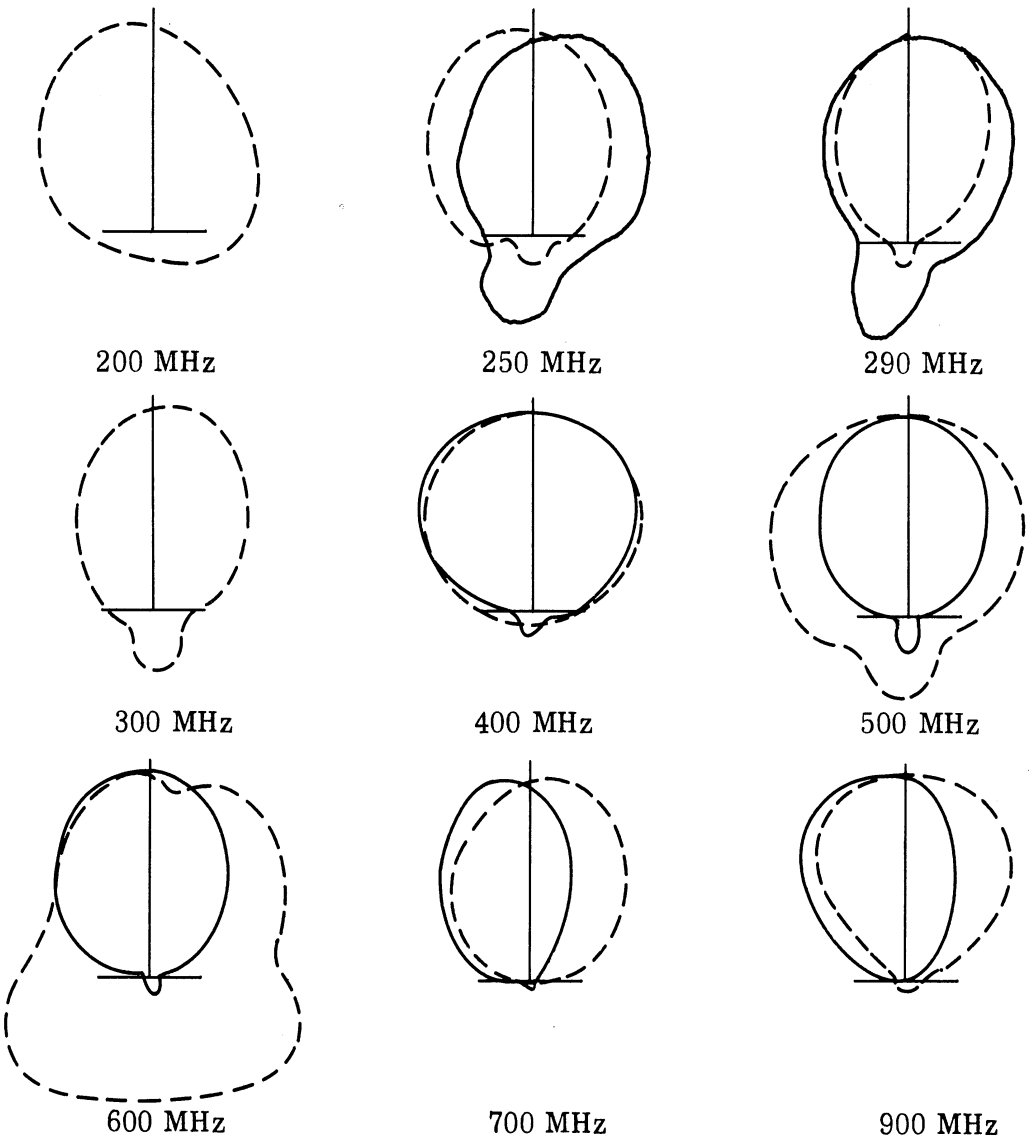

FIG. 4-45: TAPERED LOADING OF PYRAMIDAL HELIX NO. 223

——— Unloaded, ------ Loaded, Plots of $(E_\phi)^2$

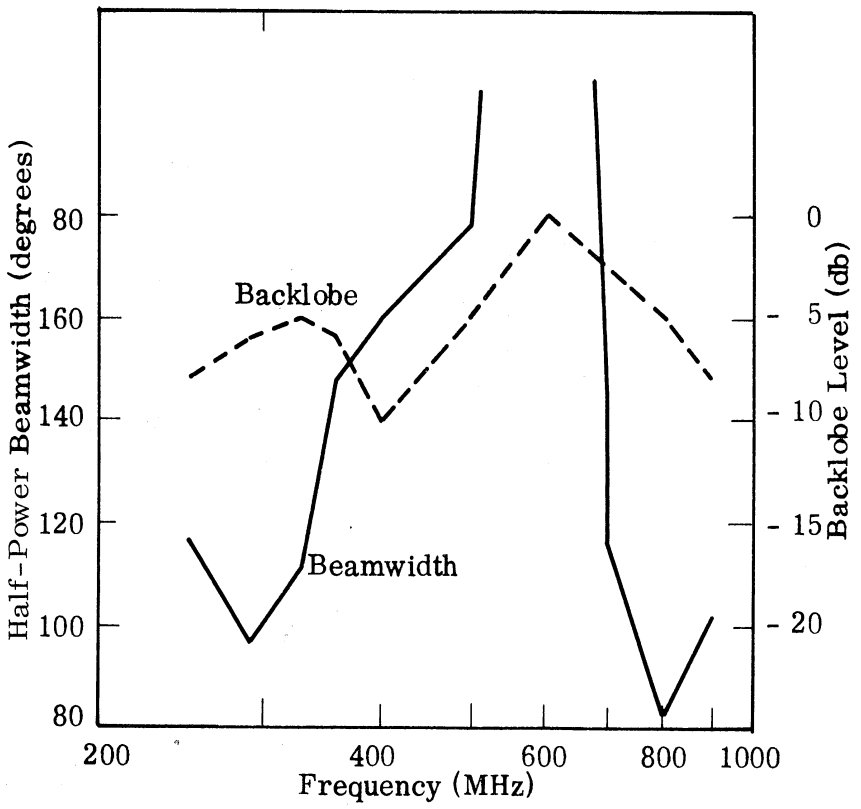

Frequency MHz	Half-Power Beamwidth Degrees	Backlobe Level db
250	117	- 8
290	96	- 6
330	111	- 5
360	148	- 6
400	160	-10
500	178	- 5
600	360	0
700	115	- 9
800	82	- 5
900	102	- 7

FIG. 4-46: ANTENNA 223 WITH 1/4 RADIUS LOADING OF K-10 WHICH STOPS 8 cm ABOVE BASE, H-PLANE

Efficiency on similar loaded helix antennas has been found to be 60 per cent. The directivity of the patterns in Fig. 4-43 is approximately 4-6 db higher than the specified 3 db gain. The VSWR referenced to the 50 ohm input in all tables, is seen to be good.

4.2.2.3 Absorbers

It was found experimentally that the near and far field patterns of the log-pyramidal antennas were being distorted and shifted at the low frequencies by reflections from the base of the antenna. The use of absorbers to minimize these residual currents and fields at the base of the antennas has long been the practice; however, only cut and try methods have been used.

Since this prototype antenna is designed for a minimum size, emphasis has been on the operation near its low frequency end where the active region begins to encounter the base truncation of the antenna. Here, the action of the dielectric loading tends to be obscured by these reflections. Therefore, extensive experiments were made on how best to absorb the currents near the far end of the antenna. Two methods received most attention: 1) resistively terminating the lines forming the antenna by connecting the resistor across the arms, and 2) using a piece of absorber especially designed for this frequency range, sufficiently big to cover the entire back end of the antenna. In all these tests, antenna Nos. 221 and 223 were used in place of the actual prototype. These models were tested with the taper loading, L2 to simulate a scale model of the finished prototype.

Figure 4-47 shows the near field of antenna No. 223 with tapered loading of L2 using the dielectric material High K-Flexible ($\epsilon = 6$) that will be used in the prototype. This first figure, without any absorption at the far end, is used as a reference for the absorption techniques to follow. Of the patterns shown, only 500 MHz can immediately be said to have a good active zone without severe interference. The active zone, which occurs at about 20 centimeters from the tip of the antenna, decays quickly to almost zero near the base of the antenna, as a good pattern should. It

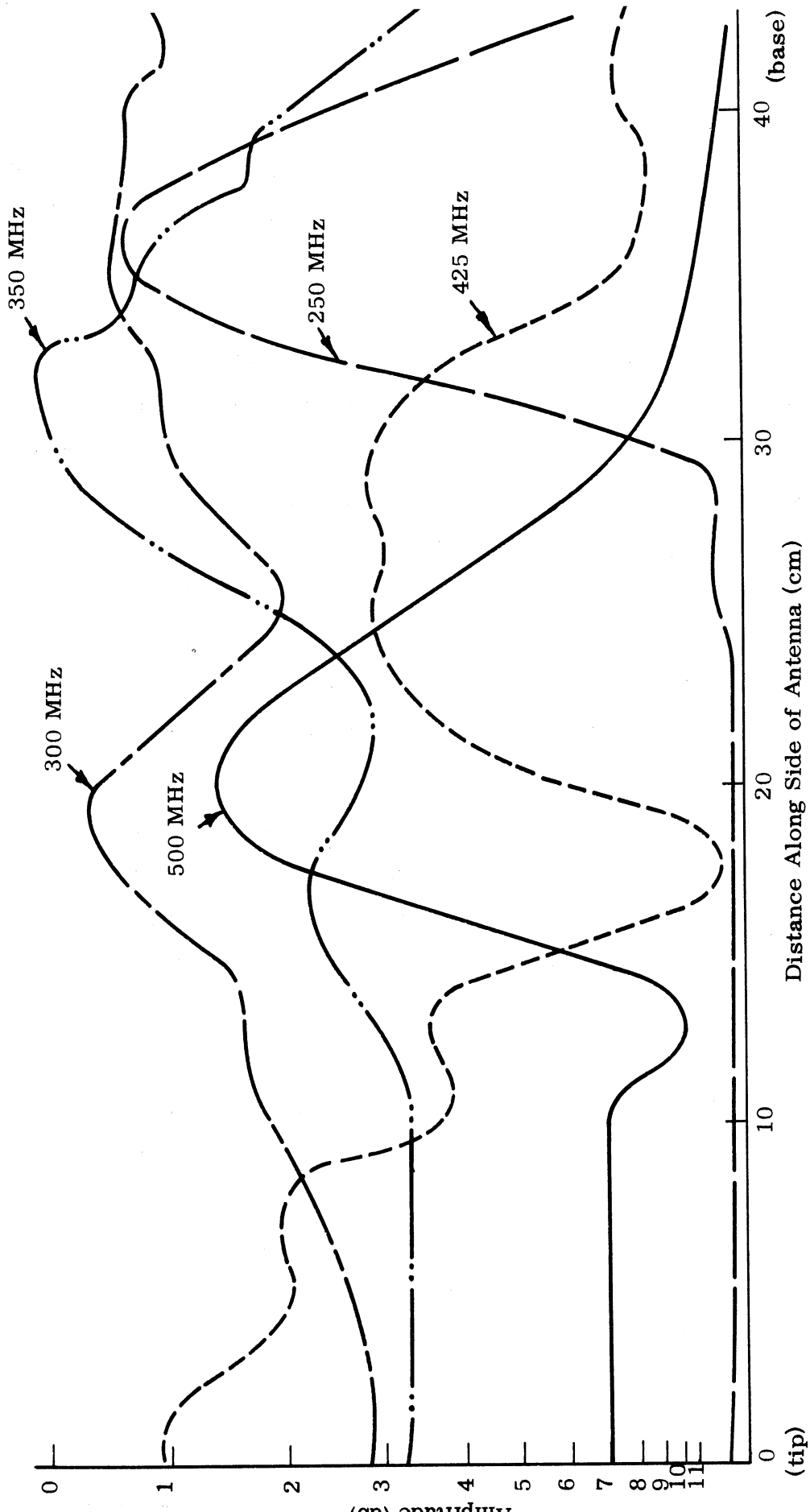

FIG. 4-47: NEAR FIELD WITH TAPERED LOADING (L2) OF DIELECTRIC ($\epsilon = 6$), ANTENNA NO. 223, PROBE DIST. $= \lambda/20$

should be noted that the antenna without loading was designed for approximately 500 MHz operation. The near field shows that 425 MHz is probably very good frequency with this loading due to the rather large active zone centered about 28 cm along the antenna. Nevertheless, the large amplitude of near field near the tip poses a question. It should be noted that the probe spacing used in this experiment was 1/20 of a wavelength rather than the 1/10 of a wavelength used in many of the other experiments. This probe spacing appeared to bring out many of the details of the active zone more clearly than the tenth wavelength one; nevertheless, currents associated with bound waves might also be detected due to its proximity to the conductors. Thus this may be the explanation for the rather large near field at 425 MHz near the tip of the antenna, although even 0, 005λ spacing has been found inadequate to pick up currents very close to the tip. It is also seen that 350 MHz has a fairly large, and high active zone further toward the base of the antenna than 425 MHz, indicating good operation at this frequency. Far field patterns indicate that much lower frequencies (250 - 350 MHz) have reasonable but somewhat degraded forward beams, even though fairly poor near field patterns at 300 MHz were observed, due to reflection of unradiated currents. Notice that a reflected wave at 250 MHz does not result in a completely deteriorated near field pattern as might be expected; that it results rather in a shift of the apparent near field region to a point closer to the tip of the antenna. It may be, however, that this is an interference effect; possibly the lobe seen in the near field is not even a very active region. It must be remembered that the amplitudes are meaningless and only the positions of the near fields are important.

Figure 4-48 shows the near field of Antenna No. 223 with loading as before, but with the important addition of a single 2.2k ohm resistor terminating the wires at the base of the antenna. The probe spacing is the same as in the previous figure. The important thing is that all the frequencies appear to have more defined active regions near the base of the antenna down to 250 MHz, which is below the 500 MHz designed lower frequency without loading. The resistor clearly absorbs some of

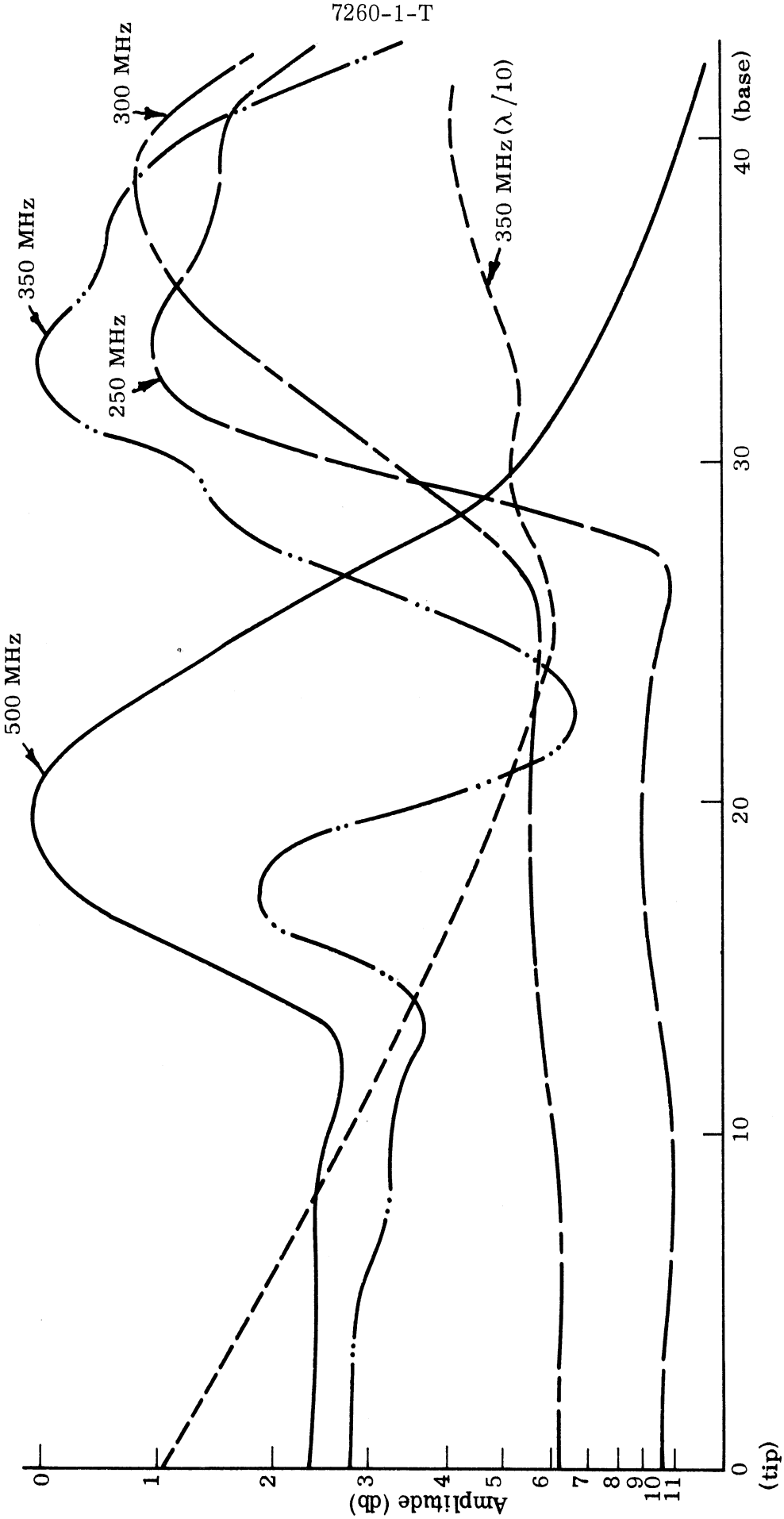

FIG. 4-48: NEAR FIELD WITH TAPERED LOADING (L2, $\epsilon = 6$) AND DIAGONAL 2.2K TERMINATION RESISTOR, ANTENNA NO. 223, PROBE DIST. = $\lambda/20$ EXCEPT $\lambda/10$ FOR 500 MHz AND ONE 350 MHz (SHOWN)

the energy of the incident waves that do not radiate on the first pass of the antenna, preventing reflected waves from forming undesirable interferences on the antenna and breaking up the near and far field patterns.

The effect of the probe spacing on these measurements is clearly seen from the dotted line corresponding to $1/10\lambda$, where $1/20\lambda$ spacing is common to the rest of the measurements on this plot. If the probe is not spaced correctly, the near field character of the antenna can easily be lost. At 500 MHz it is noticed that the close probe spacing produces an indication of amplitude near the tip of the antenna which is known to be associated with the bound wave, since the tip of the antenna is not even close to the loading of the antenna and is known to have a bound wave at 500 MHz.

Figure 4-49 shows the effects, on the far field patterns, of terminating the ends of the bifilar winding in a shunt resistor at the base of the antenna. Notice how the beamwidth and the backlobe go through a minimum at 2200 ohms. In this case, 1/4 watt carbon composition resistors were used. However, substituting 1/2 watt or 1 watt resistors produce no significant difference in the results.

Figure 4-50 shows the linear power plots of antenna No. 223 with an L2 loading of Flexible Hi-K-6 dielectric with a 2200 ohm, 1/4 watt carbon composition resistor connected with the ends of the windings at the base. Figure 4-51 shows the backlobe levels and beamwidths at several frequencies. The patterns at 400 and 500 MHz are almost identical to those for the same antenna and loading, but without the resistor. Consequently patterns above 500 MHz were not taken. Notice that the backlobe is well within the specifications for the prototype, although the beamwidth is outside that expected for 250 MHz. Except for the cone angle, this is a scale model of the prototype.

As a further test of using shunt resistors to suppress unwanted modes, two resistors were connected across the antenna at different locations. A 2200 ohm resistor connected the two ends of the bifilar winding at the base. However, an additional resistor, the value of which was varied to find an optimum, ran across

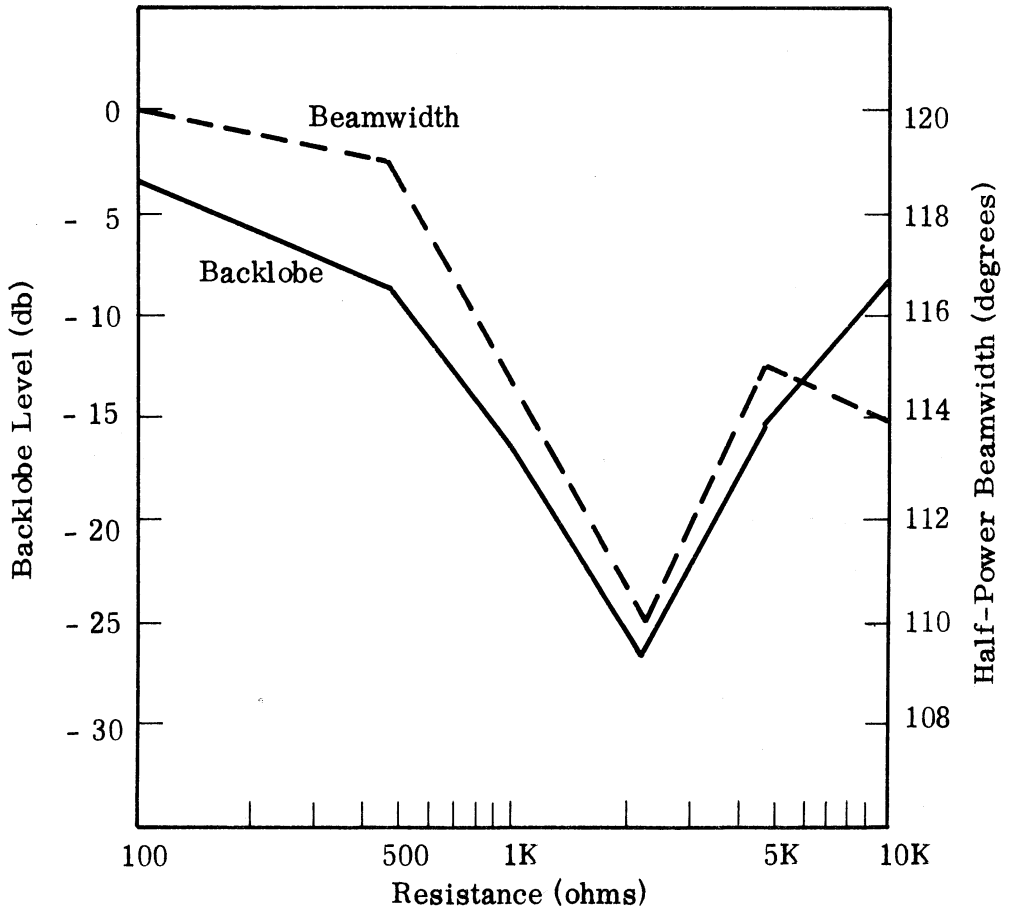

Resistance ohms	Backlobe Level db	Half-Power Beamwidth degrees
100	- 3.48	120
470	- 7.89	119
1K	- 16.53	115
2.2K	- 26.32	110
4.7K	- 15.01	115
10K	- 8 .29	114

FIG. 4-49: EFFECT ON BEAMWIDTH AND BACKLOBE OF 1/4 W CARBON COMPOSITION RESISTOR CONNECTED ACROSS BASE OF ANTENNA 223 L2-FLEXIBLE HI-K-6 AT 250 MHz, H-PLANE

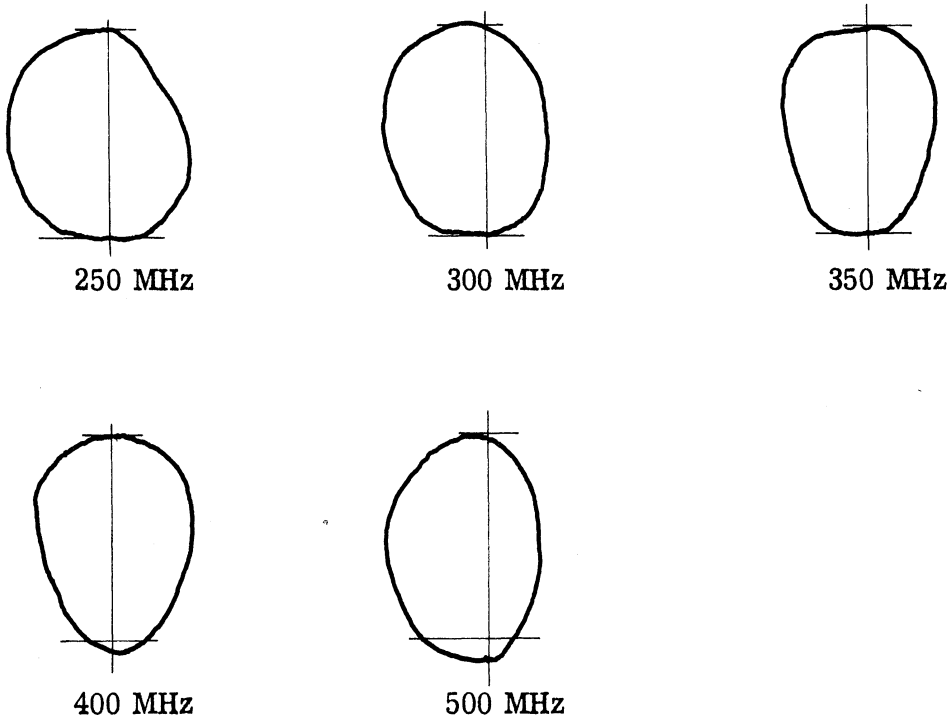

FIG. 4-50: LINEAR POWER PLOTS OF ANTENNA 223 L2 FLEXIBLE Hi-K-6 WITH A SHUNT 2.2K 1/4 W CARBON COMPOSITION RESISTOR ACROSS THE BASE. H-PLANE

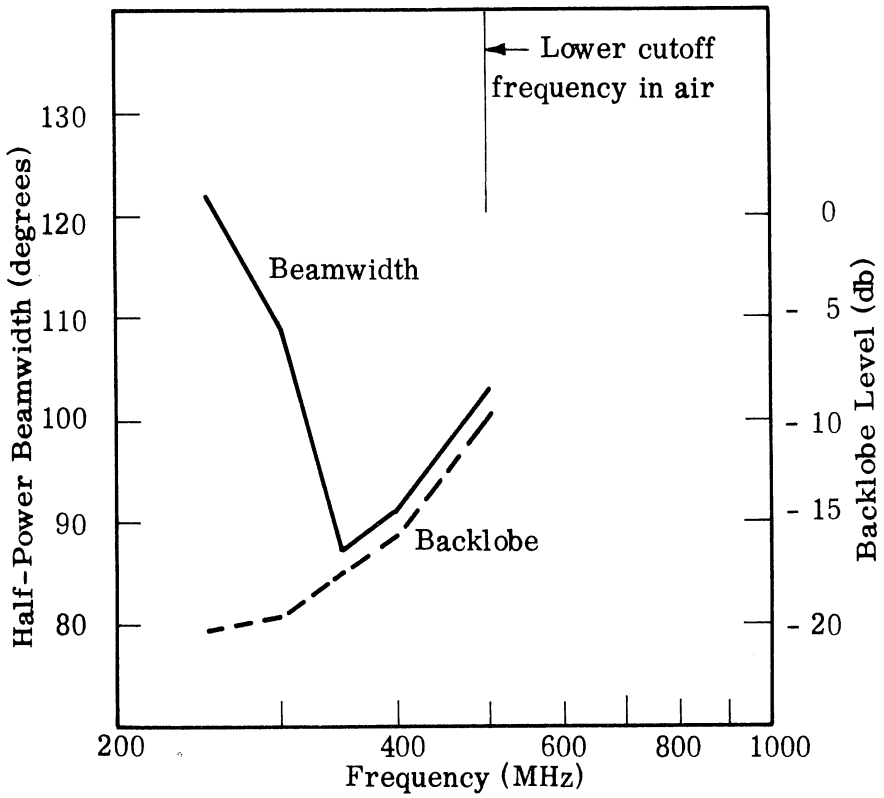

Frequency MHz	Half-Power Beamwidth Degrees	Backlobe Level db
250	122	- 20.21
300	109	- 19.32
350	87	- 17.4
400	91	- 15.68
500	103	- 9.89

FIG. 4-51: HALF POWER BEAMWIDTH AND BACKLOBE LEVEL OF ANTENNA 223 L2 FLEXIBLE HI-K-6 WITH 2.2K, 1/4W CARBON RESISTOR ACROSS BASE; H-PLANE

the base of the antenna, connecting the two bifilar wires a quarter turn from the base. A summary of the data is in Fig. 4-52. Notice that a minimum is reached in the backlobe level around 2200 ohms. However, the level appears to be higher than with one resistor. This is probably a consequence of the large reflections on the range used at 250 MHz. Note though, that the beamwidth does not start to rise until the backlobe level has passed a minimum. It appears, however, that one resistor connected across the base is the best way of absorbing on conical helix antennas with the present weight limitations.

In order to show if the resistor leads themselves were significantly affecting the experiment, rather than the resistor, near fields were taken with the tapered loading on antenna No. 223 and the resistor lead wires in place, but without the resistor connected. The lead wires were thus left open and unconnected. Figure 4-53 shows the near field of such a configuration and shows that indeed the lead wire themselves have a very large influence on the near field patterns of this antenna, probably due to the fact they drastically affect the boundary condition at the ends of the wires and permit a current flow past the critical base region. It may be that capacitance between the wires allowed a current to flow, reducing reflections. Far field patterns for this configuration have not been taken since it is not felt to be as good as the resistor termination.

In order to try the effect of a large sheet of absorber, a panel of WG resistive absorber was obtained from Emerson and Cuming, Inc. This technique is feasible provided that lightweight absorbing materials are used. The Eccosorb WG used in this experiment is a VHF absorber good from 100 - 1000 MHz. No additional published data are available for the material, but is relatively lightweight (8 lbs/ft^3).

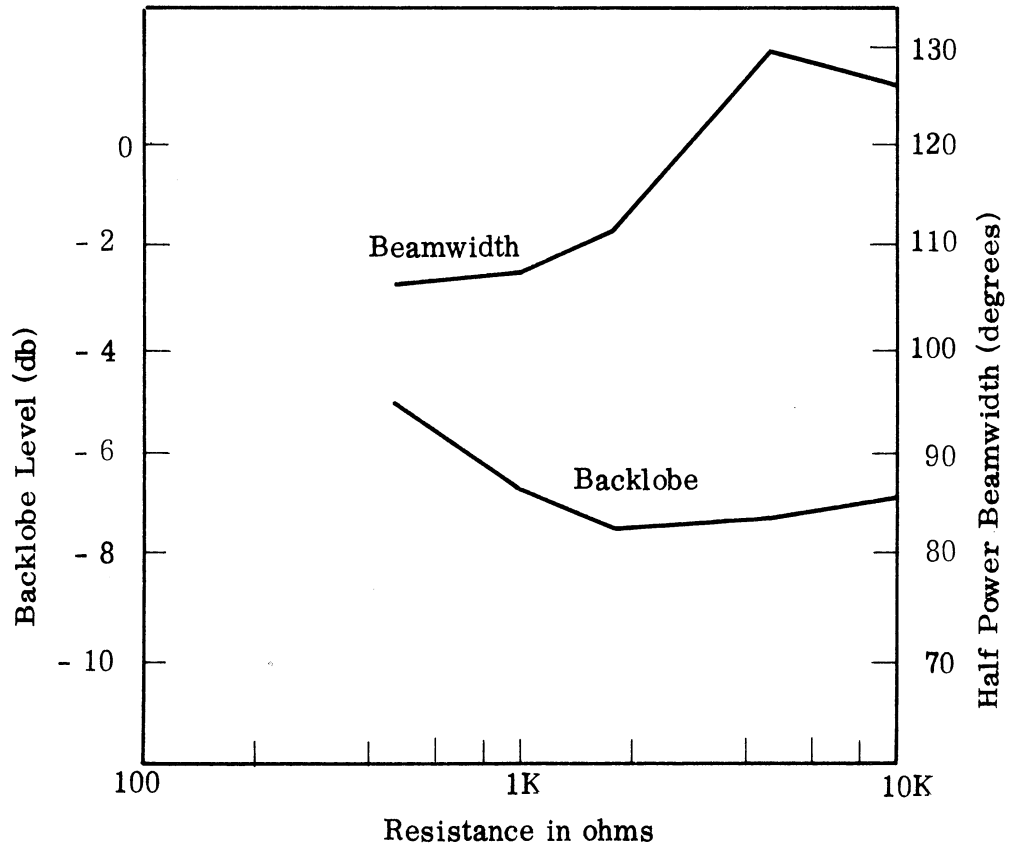

Resistance ohms	Backlobe Level db	Half Power Beamwidth Degrees
470	- 4.89	107
1K	- 6.61	108
1.8K	- 7.40	112
4.7K	- 7.2	129
10K	- 6.76	126

FIG. 4-52: EFFECT ON BEAMWIDTH AND BACKLOBE OF TWO 1/4W CARBON RESISTORS CONNECTED ACROSS BASE OF ANTENNA 223 L2 FLEXIBLE HI-K-6 AT 250 MHz H-PLANE

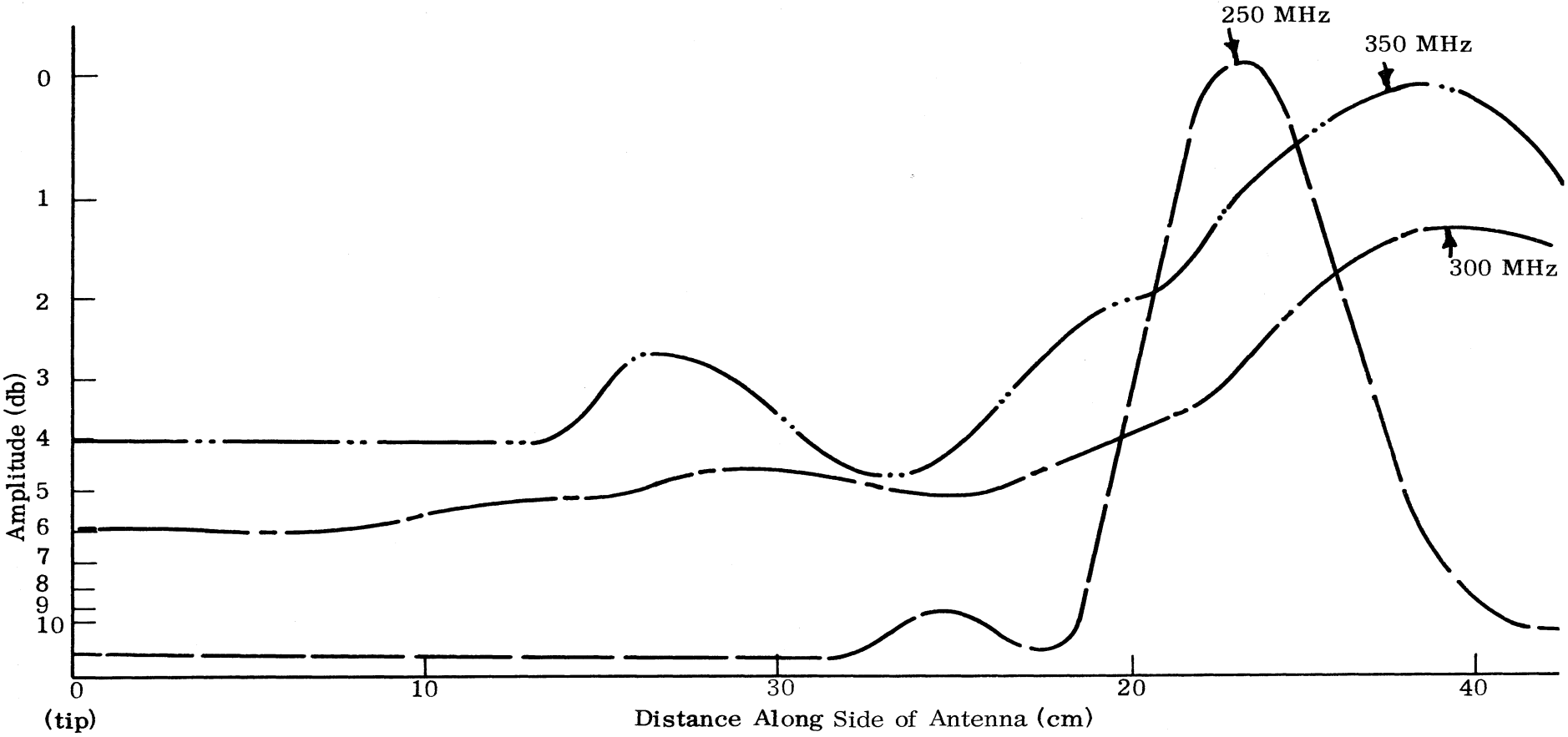

FIG. 4-53: NEAR FIELD WITH TAPERED LOADING, (L2, $\epsilon = 6$) AND RESISTOR LEAD WIRES, NO. RESISTOR, ANTENNA NO. 223, PROBE DIST. = $\lambda/20$

Fig. 4-54 shows near field measurements of Antenna No. 223 loaded with L2 loading as before, but with a panel of WG absorber on the back and without the resistor termination. This panel of absorber should be capable of absorbing the forward traveling near fields at the base of the antenna, preventing reflections. This figure demonstrates that the active zone near field characteristic is greatly enhanced by the use of this slab of WG absorber on the back of the antenna. At the very low frequencies, 250 - 300 MHz, the near fields are improved more by this technique than by the resistor loading if one used clarity of near field zone and smoothness of the curves as a measure. Nevertheless, this large slab of WG absorber would be impractical as an absorber on the prototype due to its size and weight. The resistor itself performs fairly well in absorbing the incident current wave.

In order to see the combined effect of both types of absorption, the resistor termination and the slab of absorber were placed at the base of antenna No. 223 and more near fields patterns were taken as shown in Fig. 4-55. This figure, for the first time, shows a completely orderly progression of near field active zones with frequency, starting with the lowest frequency of 250 MHz and proceeding in smooth fashion to 500 MHz. Thus, it is seen that either method of absorption causes a much more defined active region than the antenna without base absorption. Both types of absorption together produce the best antenna. Fig. 4-56 shows the effect of having the absorber slab of "WG" on the back of antenna No. 223 along with the resistor lead wires, but without the resistor being connected. The near field is better than that shown in Fig. 4-53 without the absorber, due to less reflection. However, the leads make quite a difference from the "absorber-only" case, Fig. 4-54. Extensions of the wires on the back of the antenna make quite a difference; further investigation of this phenomenon could be useful.

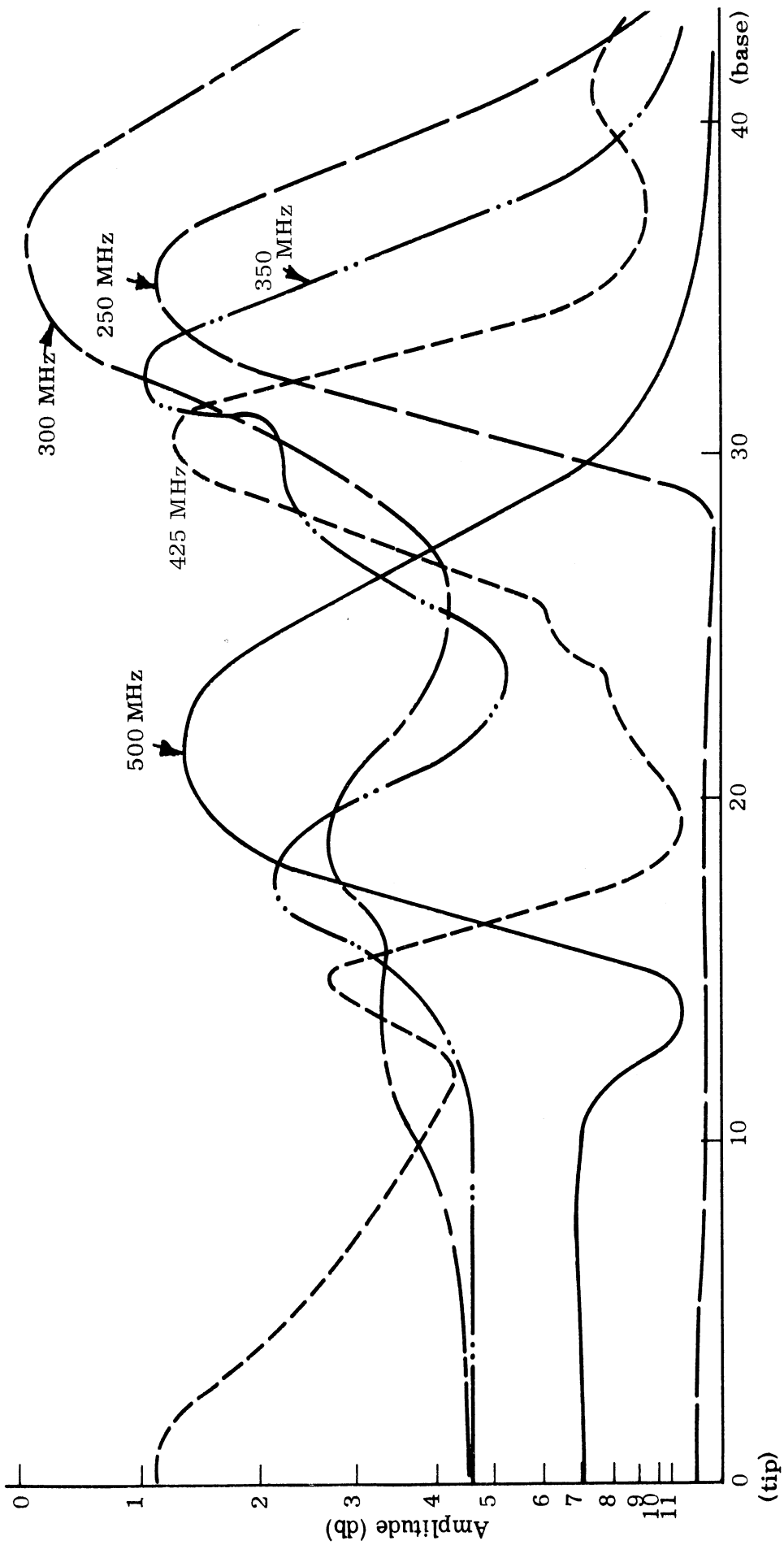

FIG. 4-54: NEAR AMPLITUDE WITH TAPERED LOADING (12, $\epsilon = 6$) AND ABSORBER (WG) COVERING BACK OF ANTENNA, ANTENNA NO. 223, PROBE DIST. = $\lambda/20$

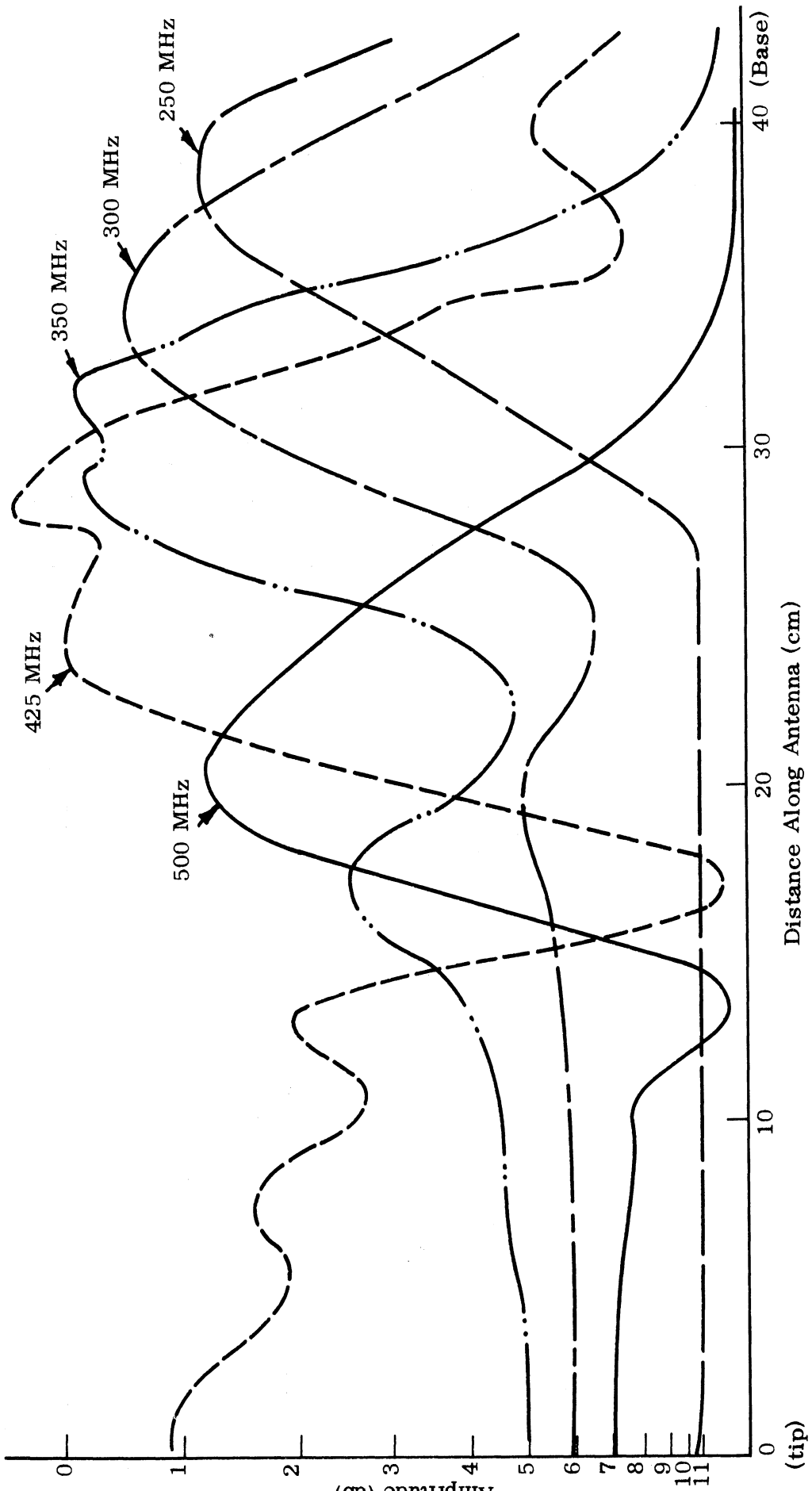

FIG. 4-55: NEAR FIELD WITH TAPERED LOADING (L2, $\epsilon = 6$), TERMINATING RESISTOR (2.2K), AND ABSORBER (WG) ON BACK, ANTENNA NO. 223, PROBE DISTANCE = $\lambda/20$

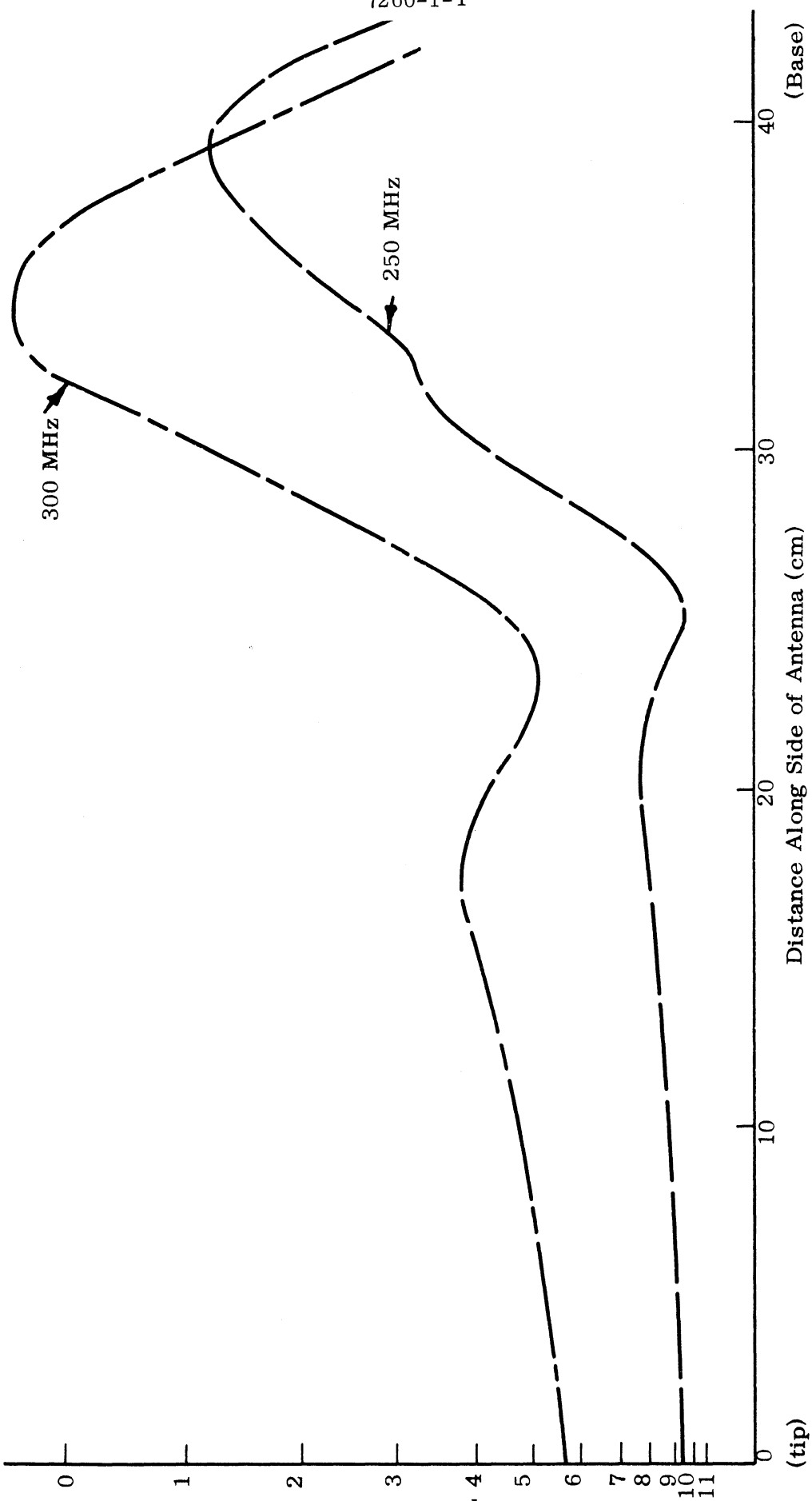

FIG. 4-56: NEAR FIELD WITH TAPERED LOADING (L2, $\epsilon = 6$), ABSORBER (WG) ON BACK, AND RESISTOR LEADS, NO RESISTOR ANTENNA NO. 223, PROBE DIST = $\lambda/20$

Figs. 4-57 and 4-58 show the effects, on far field patterns, of placing a 3 inch thick square of Eccosorb WG absorbing material, which is 10 inches on a side, over the base of antenna No. 223. If these results are compared with the data for the same antenna without absorber, using Figs. 4-35 - 36 and 4-42 - 43, improvement in the backlobe level and half-power beamwidth is detected. Notice that the beamwidth of the antenna stays close to the design level of 90^{o} in the 250 to 500 MHz frequency range. Except at 300 MHz the backlobe is well below the specified level of 8db.

The previous experiments were all with antenna No. 223. The effect of absorption of the wave on antenna No. 221 was also tried in preparation for an outside loading of dielectric on antenna No. 221. Outside loading could not be employed on antenna No. 223 since it has a large layer of polyfoam on the outside of the antenna. Fig. 4-59 shows the near field of antenna No. 221 with tapered loading of L2 as was used in antenna No. 223, but without any absorption at the base of the antenna. It must be remembered that antenna No. 221 has an infinite balun connected to the base of this antenna, so that it is essentially different from antenna No. 223 which has no connections to its base but is fed only from its tip. Nevertheless, the near fields of antenna No. 221 show reasonably clear near fields down to 350 MHz with some perturbation of the 300 MHz curve, perhaps due to reflections, and definite perturbations of the 250 MHz curve due to the reflection at the base of the antenna. Notice that this antenna reflection might occur from only one arm, since the other arm could permit energy leakage down to the generator along the infinite balun. Fig. 4-60 shows the near field of antenna No. 221 with tapered loading and a terminating resistor of value 2.2K. The near fields of this antenna are much better than the no resistor case; the near fields are sharp, smooth and progressive with frequency as one would expect in a good log periodic antenna. Fig. 4-61 shows the near fields, of No. 221, with tapered loading and resistor termination as before and

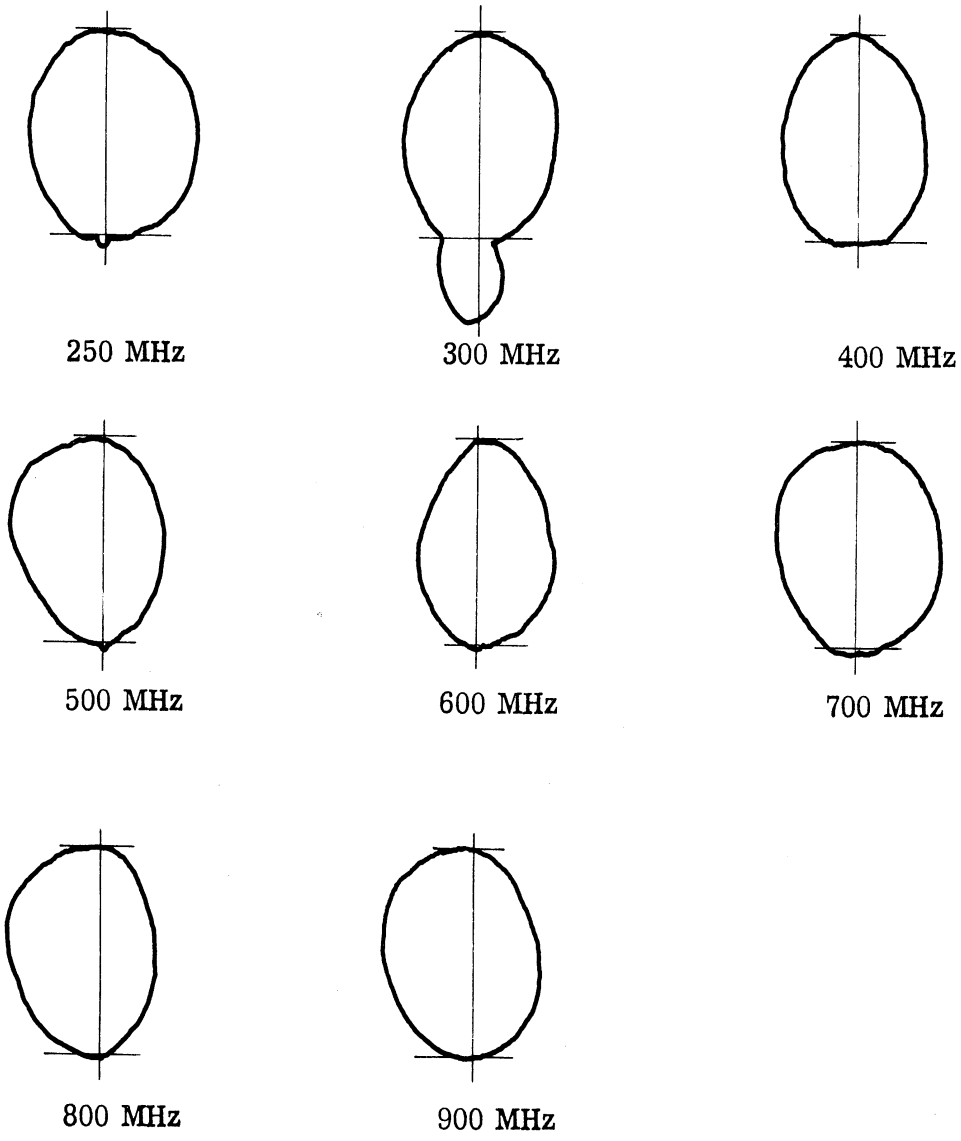

FIG. 4-57: LINEAR POWER PLOTS OF ANTENNA 223 L2 OF FLEXIBLE Hi-K-6 WITH 3"x10"x10" PIECE OF ECCOSORB W. G. ON BACK. H-PLANE

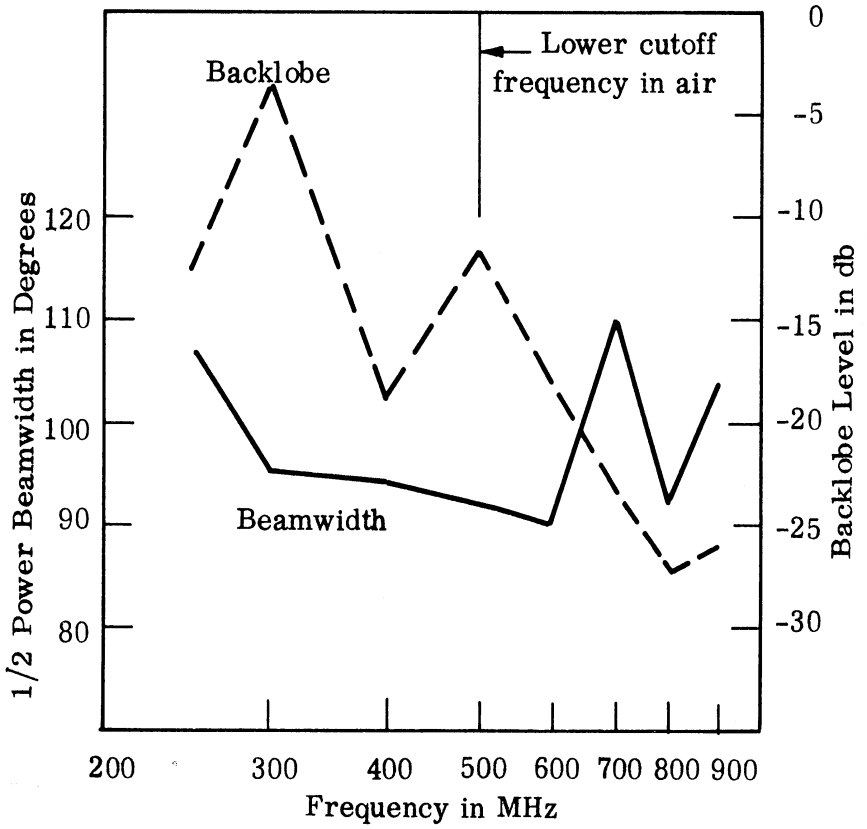

Frequency (MHz)	1/2 - Power Level (Degrees)	Backlobe Level (db)
250	107	-12.15
300	95	- 3.64
400	94	-18.98
500	92	-11.82
600	90	-18.06
700	110	-23.34
800	92	-27.23
900	106	-26.02

FIG. 4-58: 1/2 POWER BEAMWIDTH AND BACKLOBE LEVEL OF ANTENNA 223 - L2 - FLEXIBLE HI-K-6 WITH A 3" x 10" x 10" PIECE OF ECCOSORB WG ON THE BACK, H-PLANE

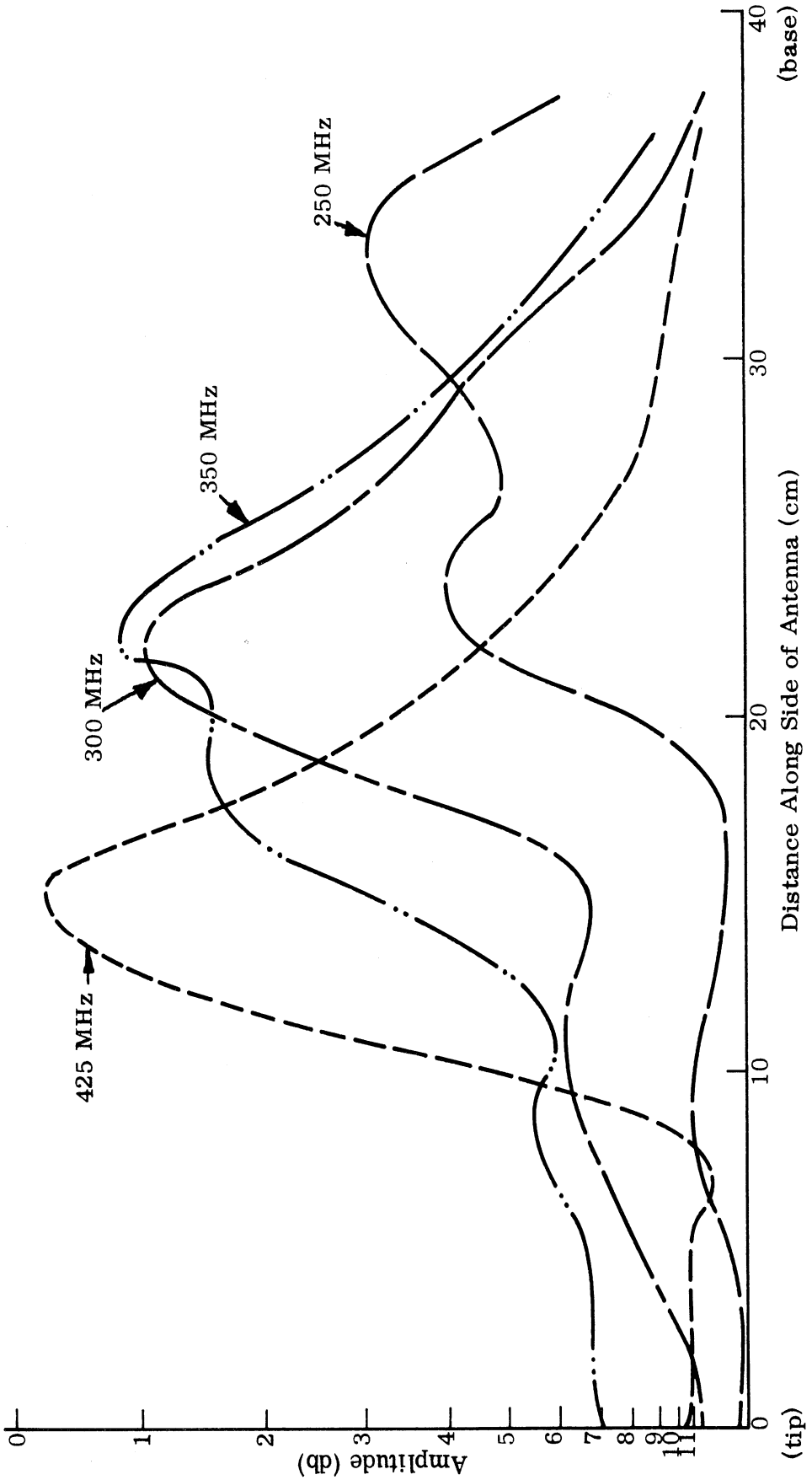

FIG. 4-59: NEAR FIELD WITH TAPERED LOADING (L2, $\epsilon = 6$), ON ANTENNA NO. 221, PROBE DISTANCE = $\lambda/20$

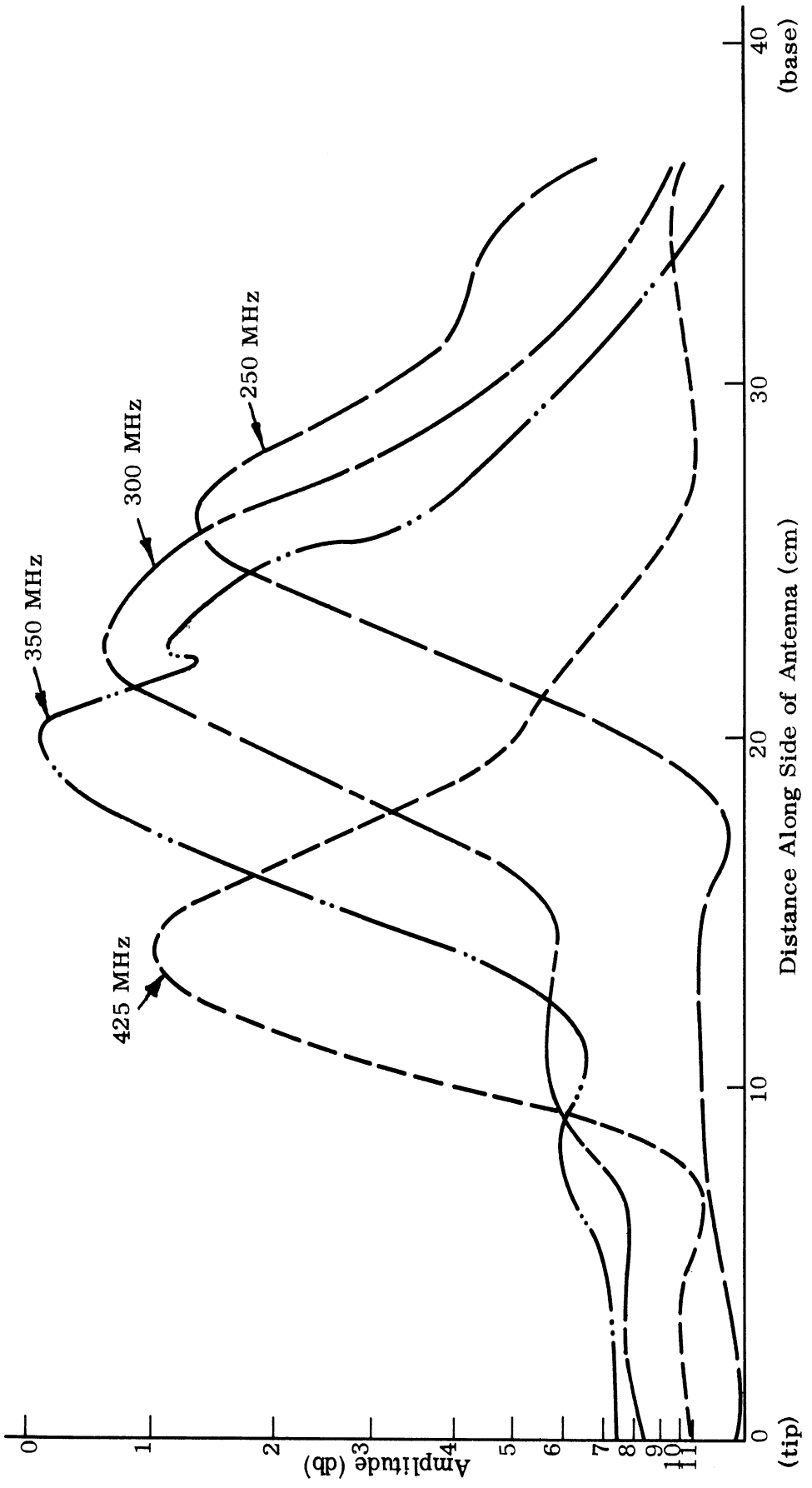

FIG. 4-60: NEAR FIELD WITH TAPERED LOADING (L2, $\epsilon = 6$), AND TERMINATING RESISTOR (2.2K) ANTENNA NO. 221, PROBE DIST. = $\lambda/20$

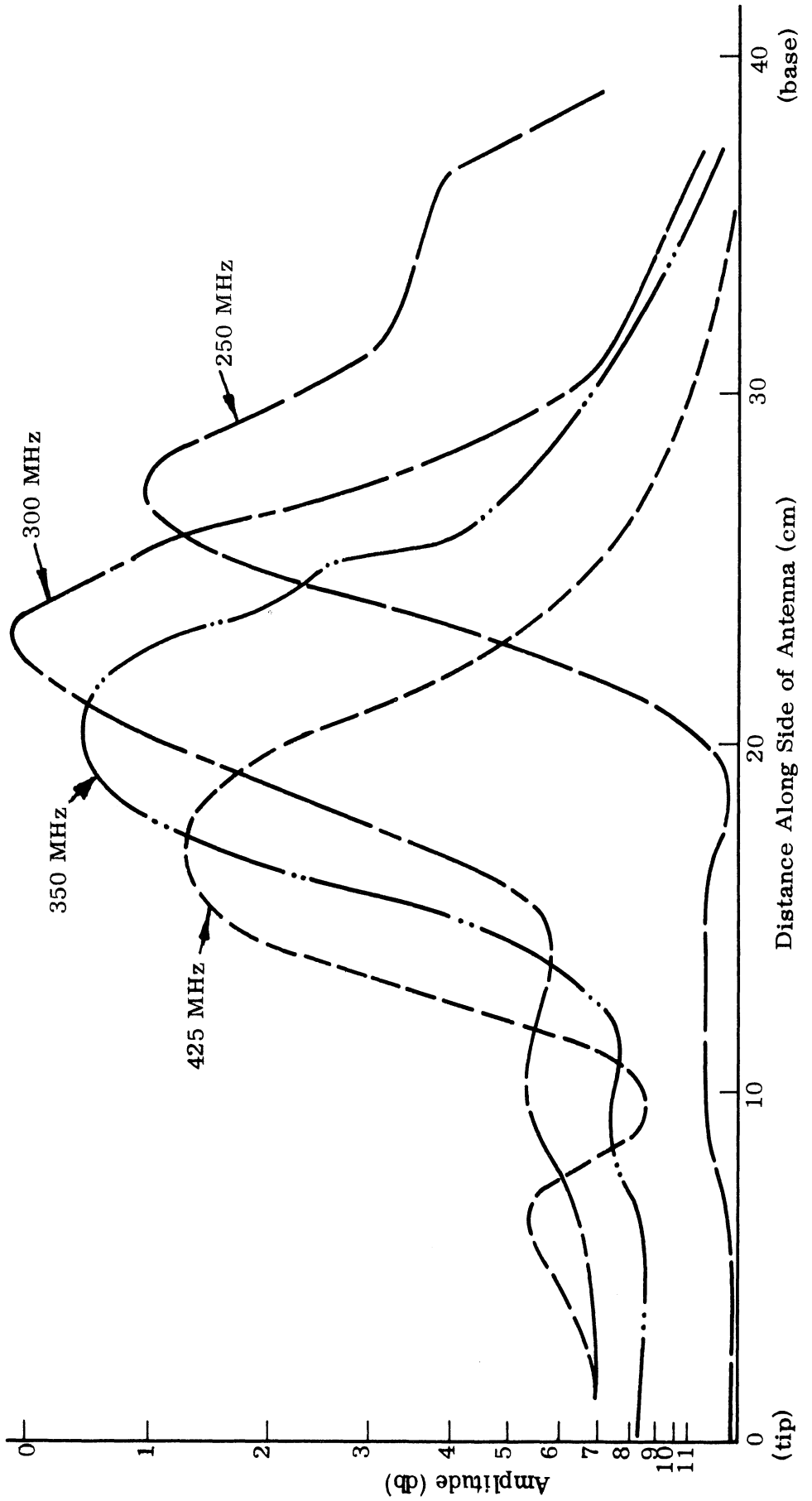

FIG. 4-61: NEAR FIELD WITH TAPERED LOADING (L2, $\epsilon = 6$), TERMINATING RESISTOR (2.2K), AND ABSORBER (WG) ON BACK, ANTENNA NO. 221, PROBE DIST. = $\lambda/20$

in addition a slab of "WG" absorber, such as used in antenna No. 223 absorber investigation. The figure shows that no substantial improvement in characteristics is noted with the addition of the slab of "WG" absorber on the back of this antenna and that the resistor itself was sufficient to produce good clear near field patterns. Next, an L2 loading of dielectric (High-K Flexible) was placed both inside and outside this antenna to determine if superior characteristics could be gained by additional loading on the outside of the windings as well as inside. It should be remembered that the L2 loading inside is already very thick and that the loading provided by this inside method may already be near the best that can be afforded within the very drastic taper. Nevertheless, theory indicated that a considerable advantage would be achieved by having dielectric both inside and outside the windings and close to them. Fig. 4-62 and 4-63 show the near field results when antenna No. 223 is loaded with both inside and outside L2 loadings. Fig. 4-62 is without a terminating resistor; Fig. 4-63 is with a resistor (2.2K) in addition to absorb reflections. It can be seen from both figures that no substantial change in the position of the near field maximum occurs for 425 and 350 MHz. It must be remembered that amplitudes have been approximately normalized; only near field shape is significant here. The peak of the 300 MHz near field has been moved only by several centimeters to the left. Somewhat more important is that the decay of the 300 MHz curve is considerably more rapid and almost complete near the base of the antenna. Also, at 250 MHz the near field is considerably wider and better shaped. Nevertheless, it is felt that the outside loading is not worth the additional weight at this time. Further tests below 250 MHz should be made to establish the lowest possible frequency of operation with loading both inside and outside.

4.3 Other Size Reduction Techniques

Although the material loading method was chosen for the prototype since it is the only proven method of reduction so far, other promising methods exist. Some

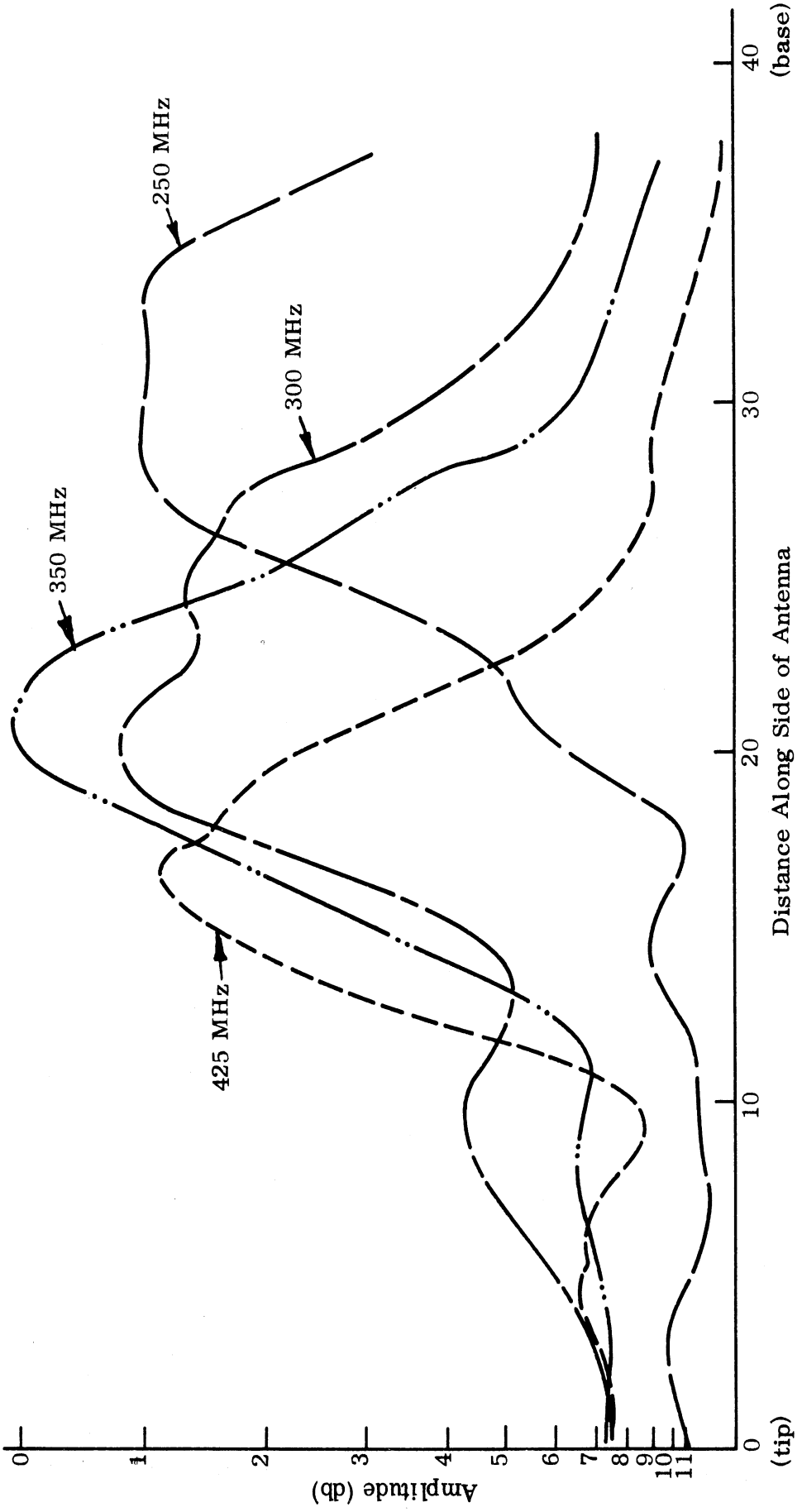

FIG. 4-62: NEAR FIELDS WITH LOADING (L2, $\epsilon = 6$), INSIDE AND OUTSIDE ANTENNA NO. 221, PROBE DIST. = $\lambda/20$

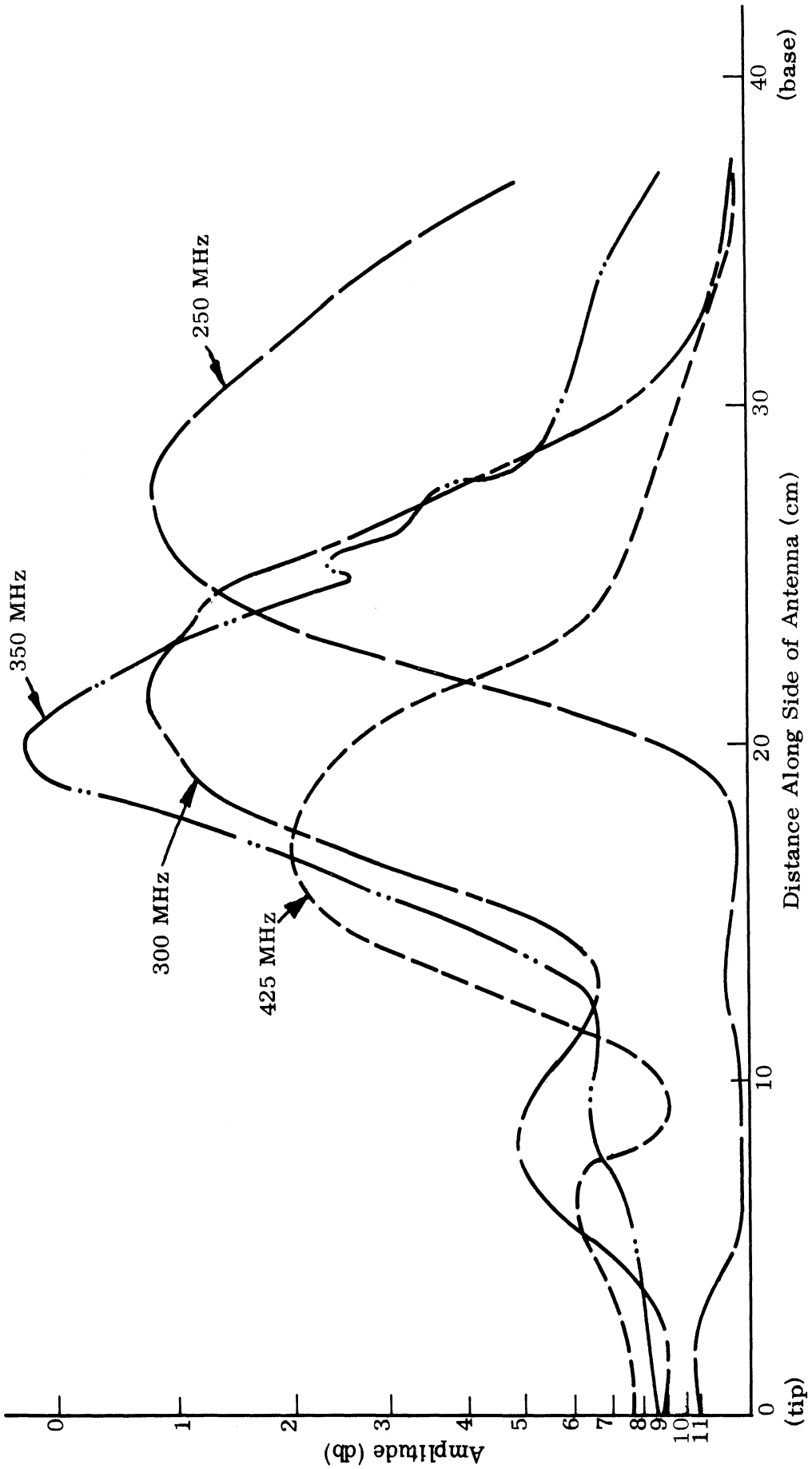

FIG. 4-63: NEAR FIELDS WITH TAPERED LOADING INSIDE AND OUTSIDE AND RESISTOR (2.2K) TERMINATION, ANTENNA NO. 221, PROBE DIST. = $\lambda/20$

initial experiments were performed on a few of these.

All of these loading methods are based on viewing the bifilar helix as a transmission line and attempting to slow the velocity on this transmission line using classical transmission line TEM wave concepts. The validity of such a model has never been proven. Nevertheless, the speed of current along the wire is almost exactly the speed of light at all frequencies; this is at least approximately true even in the middle of radiation regions. This is the speed of a TEM wave. Other modes travel either slower or faster than the speed of light. In addition, by studying the "tape helix" mathematical model (Sensiper, 1951 and Klock, 1963), it is found that for very thin conductors, the higher order modes rather than the radiating mode control the phase velocity of the current along the wire. These higher order modes are bound so closely to the surface of the helix that it may be regarded as a plane surface, resulting in the so called "plane-helix" models. In addition, these higher order modes require the current velocity to be almost the speed of light, when the helix is unloaded. Also, since the higher order modes cling tightly to the helix, there is hope that lumped element concepts may apply as they do in ordinary transmission lines where the field is highly localized.

4.3.1 Helix conductor

If the concept of slowing the current phase velocity on the wires, independent of the radiation, is valid, then other slow wave techniques might be employed rather than just discrete loadings. For example, the helix itself could be used as the conductor of a larger conical helix or helix antenna. One experiment was tried by designing a coiled conductor wrapped on a polystyrene tube, as a basic conductor. The coiled conductor was designed according to standard calculations of helices. If the coil diameter is too small ($< .1\lambda$), no reduction in velocity along the coiled conductor would occur. Nevertheless, after wrapping this coiled conductor around

a cylinder in the form of a bifilar helix antenna, no good radiation patterns at any frequency were recorded. Additional study is necessary to properly assess this technique; it is still considered promising.

V
CONCLUSIONS AND RECOMMENDATIONS

The horn employed as the primary feed for each of the reflectors discussed in this report was a broadband ridged horn having a design parameter similar to those noted by Walton and Sundberg (1964). In the event of further development of the broadband constant beamwidth reflector antenna, it is suggested that consideration be given to the use of a horn which has a slightly larger aperture and longer throat than the present horn. The aperture should be increased approximately 25 per cent and its length doubled. Increasing the aperture size would help to narrow the far field pattern of the primary feed thus reducing the effective size of the secondary reflector. The purpose for increasing the length of the horn is to minimize phase errors in the aperture distribution. This would further reduce the half power beamwidth and side lobes of the far field radiation pattern of the primary feed. Consideration should also be given to the possibility of minimizing side lobes in the E-plane of the ridged horn by employing a corrugated structure similar to that reported by Peters, et al (1965).

Three reflector configurations were considered by the University of Michigan which were the solid parabolic reflector, the doily reflector, and the wire grid structure. Of the three types considered, the foily reflector (parabolic reflector with circular holes) appeared to be the most promising. As a continuation of this work, in a development stage, consideration must be given to the arrangement of the holes of the doily reflector. The principal design of the reflector should be to have a solid metallic portion in the central region of the reflector. The solid section is to effect an aperture of adequate size to produce the desired half power beamwidths at the highest design frequency. For example, in our case, the desired constant half power beamwidth was 18 degrees and therefore, a 5 inch section was required in

the center. Around the solid portion many holes must be drilled. The holes near the central region should be approximately 0.6λ in diameter at the highest frequency of interest. These holes should be placed close together and arranged to avoid symmetry in the structure. The hole diameters should increase as the radius from the center of the reflector to the outer edge increases. It is recommended that at least 10 hole sizes be employed with the largest hole being approximately 0.6λ in diameter at the lowest frequency of interest. It was noted in the text that the holes should be non-symmetrically spaced around the center, and further they should be closely packed. A gradual transition from the small holes to the larger ones is necessary. For example, at the higher frequencies where the large holes cannot be as closely packed one should include holes of smaller diameters to reduce as much of the reflecting surface as possible. A suggested technique for drilling the holes is shown in Fig. 5-1. During this study, it has been learned that much of the metallic surface can be removed without seriously affecting the electrical characteristics of the reflector (provided the holes are arranged non-symmetrically) when used as a broadband constant beamwidth structure.

The present design employs an asymmetrical parabolic reflector having an F/D ratio of 0.25, i.e. F = 13 inches and D = 48 inches. This has been found to be an optimum design criteria since either reducing or increasing the ratio would require one to respectively increase or decrease the aperture size of the primary feed. Changing the aperture size is undesirable since the present feed has an aperture $\lambda/2$ at the lowest frequency of interest and if made smaller the feed would become inefficient. Further, if the aperture size is increased the horn will have to be made longer thus increasing the cost associated with the fabrication of the ridges.

Further study of the wire grid will require the grid structure to be mounted in a free space environment or on a low dielectric ($\epsilon_r \leq 1.06$) supporting structure. Another concept that one might give consideration is the use of a metal grating.

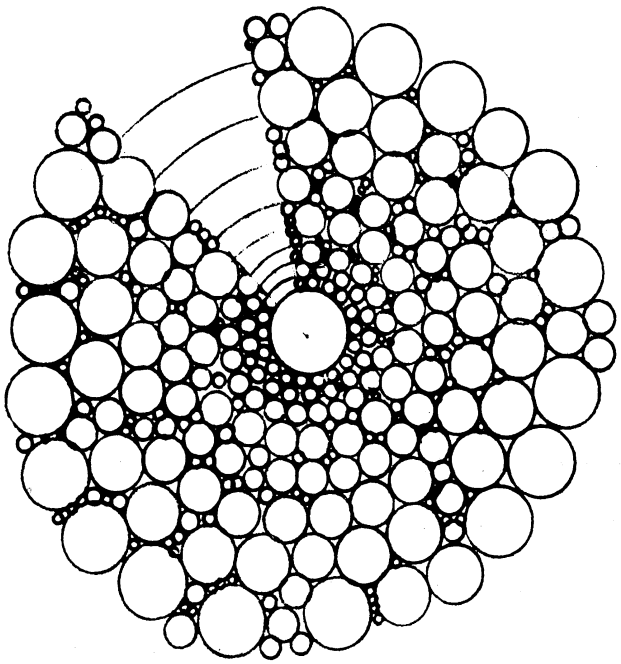

FIG. 5-1: SUGGESTED HOLE LOCATION FOR CONSTANT BEAMWIDTH DOILY REFLECTOR

Here the grating spacing could be adjusted to have electrical characteristics similar to those suggested for the wire grid structure in Section II. However, it is felt that either of these would tend toward a more complicated structure than the doily and for this reason is not recommended as the preferred antenna configuration.

To ensure that accurate data is collected it will be important that a relatively accurate test fixture be designed and fabricated to support both the reflector and primary feed. The present test frame is felt to have been relatively crude out of necessity. The crudeness of the test frame is justified because of the many changes that were required during the feasibility study. It is felt the feasibility of the concept has been demonstrated. For example, the feed configuration is well established, such that future work can concentrate on using only the ridged horn concept. Further the reflector configuration has been established, i.e. it must be an asymmetrical parabolic reflector having an F/D ratio of 0.25 and non-symmetrically perforated with holes varying in size from 0.6λ at the highest frequency of interest to 0.6λ at the lowest frequency of interest. Future development work should employ a precise test frame to simplify and expedite the study. It is suggested that future development work be directed towards devoting approximately four months to optimizing the horn configuration, three months to the design and fabrication of the test frame and five months to design, fabricate and evaluate the secondary reflector. It is suggested that three dimensional pattern data be collected for the purposes of evaluating the secondary reflector.

A broadband omnidirectional antenna has been designed, fabircated and tested and found to satisfy the requirements of the technical guidelines of the present contract. The double cage antenna (bird cage) is 20" diameter, and 34 1/2" tall. However, because of the delicate nature of the antenna, it has been encased in a low dielectric foam material to add mechanical strength. The entire antenna including

the foam structure has been tested from 100 - 1000 MHz and found to have VSWR characteristics of less than 3 : 1 and good omnidirectional pattern characteristics in the $\theta = 90^{o}$ and θ variable planes. The antenna consists of two broadband elements, which are the bird cage and a conical ground plane. The bird cage is felt to be a true broadband element. However, the conical ground plane is not since it is electrically small as noted in the text.

To overcome the stray radiations from the lead-in, it is recommended that the size of the ground plane be increased to minimize currents coupled from the ground plane to the lead-in. However, with a larger ground plane, the pattern characteristics of the antenna structure will change from those noted in the text. In the event the antenna is used in close proximity to the earth, there is the probability that the patterns in the vicinity of the earth will change such that they will exhibit a lobing structure in the upper half plane. It is recommended that a short investigation be made to determine the theoretical pattern characteristics of the bird cage and similar antennas in the presence of the earth. This study should be conducted with the antenna located at several heights above the ground, e.g. in two foot increments from two feet to ten feet above the ground.

Some preliminary study has been initiated on an antenna configuration to satisfy the requirements of the follow-on work. This antenna consists of several axially symmetric tubes, one inside the other. The initial investigation has shown that it exhibits VSWR characteristics similar to those noted for the manipole structure.

To further satisfy the requirements of the follow-on work (to obtain a physically small antenna that operates in the frequency range of 100 - 1000 MHz) a further study is being conducted to better understand the coupling phenomenon that takes place in the manipole structure. The present study has been limited to an investigation of the impedance characteristics of a single monopole antenna, and it is recommended

this study be continued so that the mutual coupling effects of the manipole structure can be better understood.

Some size reduction of the log conical helix antenna has been achieved. The prototype of such an antenna is being shipped to the sponsors. The methods of reducing the size of an antenna through the use of dielectric loading are exemplified in the prototype which has been constructed.

It can be concluded that the dielectric loading methods permit the design of a log conical antenna well within the prescribed limits of beamwidth at most spot frequencies throughout the entire operating range of the antenna. Likewise, the impedance variation with such a loaded antenna is sufficiently restricted so that a reasonable average standing wave ratio such as listed in the specifications, can be achieved. Actually, the VSWR averaged considerably less than the specified average value of VSWR.

The actual prototype exemplifies the reduction in size that can be achieved by the use of dielectric and resistive loading. With available dielectric loading materials it has been shown experimentally, that a volume reduction of at least 36 per cent can be achieved. Unfortunately, weight reduction with currently available loading materials is very difficult. The prototype antenna supplied under this contract does not meet the specified weight objective.

It is observed that the specified back load level, 8 db down from the forward main lobe can be approached for designs using dielectric loading throughout most of the very extended frequency range of such an antenna. The specifications are not fully met in the frequency range of 50 MHz up to 100 MHz. It is possible that some of this is due to defects of the range used in measuring the back lobe. A false level of back lobe may have been obtained through the reception of range scatter through the main lobe. In the continuing effort, such possibilities will be minimized at these low frequencies.

Radiation patterns have been obtained for the prototype both with and without loading. It can be concluded that the pattern of the unloaded log conical helix is closely indicative of the pattern of the loaded log conical helix corresponding to a downward shift of the operating frequency for the loaded version of the antenna. The gain measurements of the antenna have been taken; apparently there is a considerable reduction in the radiating efficiency at the extreme lower end of the specified operating range of frequency. However, an analysis of the data indicates a very respectable efficiency for all those values of frequency above 100 MHz.

There appears to be no serious beam tilt introduced by the dielectric loading. Any observed beam tilt, even of small magnetude is attributed to unwanted range reflections, and small construction errors.

In overall it can be concluded that worthwhile reductions in size while still preserving the property of wide frequency of operation can be obtained for log conical helical antennas through the use of dielectric and resistive loading. There is promise that further reductions in size for this antenna can be achieved through additional means of loading including combinations of dielectric materials, ferrite materials, and metallic materials. Periodic inductive and capactive elements also give promise of futher reductions in size. Some of these possibilities have been mentioned in the main body of this report.

Continuing work in the development of loaded log conical antennas will have as an objective to reduce the weight of the antenna. This weight reduction conceivably can be obtained through one or more means. One such mean is to utilize for loading, an artificial dielectric material built up of metal foil or metal particles and some type of carrier material. It is anticipated that in some of the uses of artificial dielectric, the metal foil will be used in layers. Indications are that an anisotropic permittivity may be extremely useful for loading log conical antennas. The use of a coiled conductor for winding the log conical antenna will be subjected to very thorough

studies. This coiled conductor may utilize internal loading within the core to achieve phase retardation. A further approach for future work will be to consider the importance of the loading material between adjacent turns on the antenna. So far, the loading has been underneath the metal conductors of the antennas.

A major objective in the continuance of the loaded log conical antenna work will be to further reduce the size of such an antenna. The reduction of size may be possible through one of the means which is cited in the previous paragraph. In addition, new dielectric materials may offer further reduction in size. So far a rather restricted range of permittivity has been utilized for loading purposes with dielectrics. An attempt will be made to extend the range of permittivity and also to consider materials with permeability as well.

APPENDIX A
INSTRUCTIONS FOR PROTOTYPE LOADED LOG CONICAL ANTENNA

Assembly.

1. Loosen and remove the nylon bolt holding the carriage to the center pole.

2. Slide the carriage down the center pole, opening the structure much as one would an umbrella, checking to assure the antenna wires are free, until the carriage lines up with the bottom hole in the center pole. (See Figure A-1)

3. Insert the nylon bolt removed earlier and secure the carriage tightly to the center pole.

4. Connect the straps made out of sheet stock to the sides of the pyramid using the nylon bolts furnished. Make sure the number on the strap corresponds to the number on the face of the tip of the antenna. (See Figure A-2)

5. Insert the blocks of dielectric one at a time. Make sure that the number on the dielectric block corresponds to the number on the strap and to the number on the same side of the tip. If the block does not fit snugly without forcing it, do the following:

   a. Check to see if the numbers on the pieces match up and that none of the pieces have been interchanged accidently.

   b. Check the bolts and make sure they are tightened properly. All four pieces are cut to fit properly in their correct position.

6. After each block has been inserted, turn the butterfly clasp at the base of the pyramid to hold each block securely in place. (See Figure A-3)

7. Connect the antenna to the transmitter with a 50 ohm cable. (See Figure A-4)

Precautions.

1. Handle the blocks of dielectric carefully even though they have been encased in fiberglass to protect them. DO NOT DROP, KICK, HIT, or in any other way

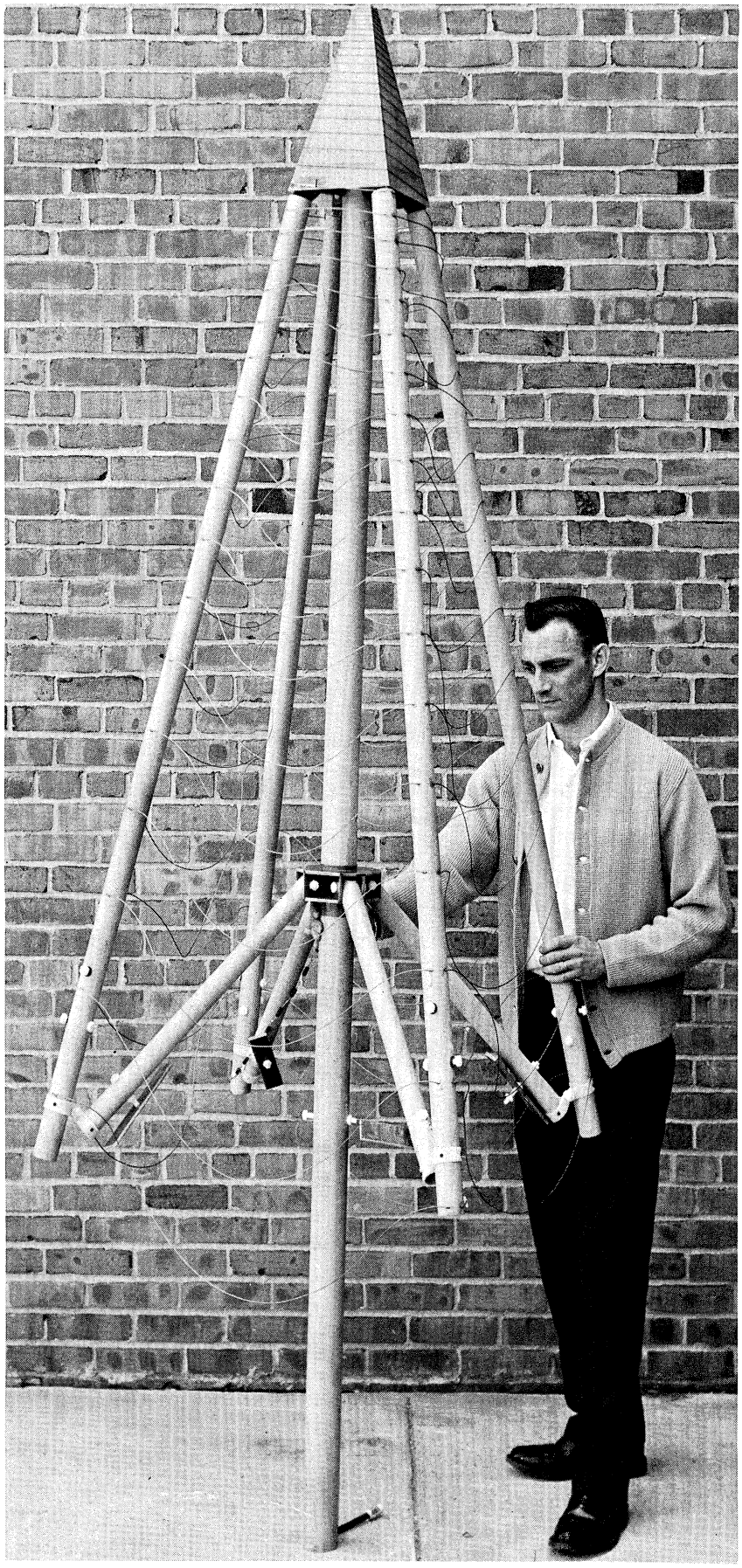

FIG. A-1: ERECTING THE ANTENNA

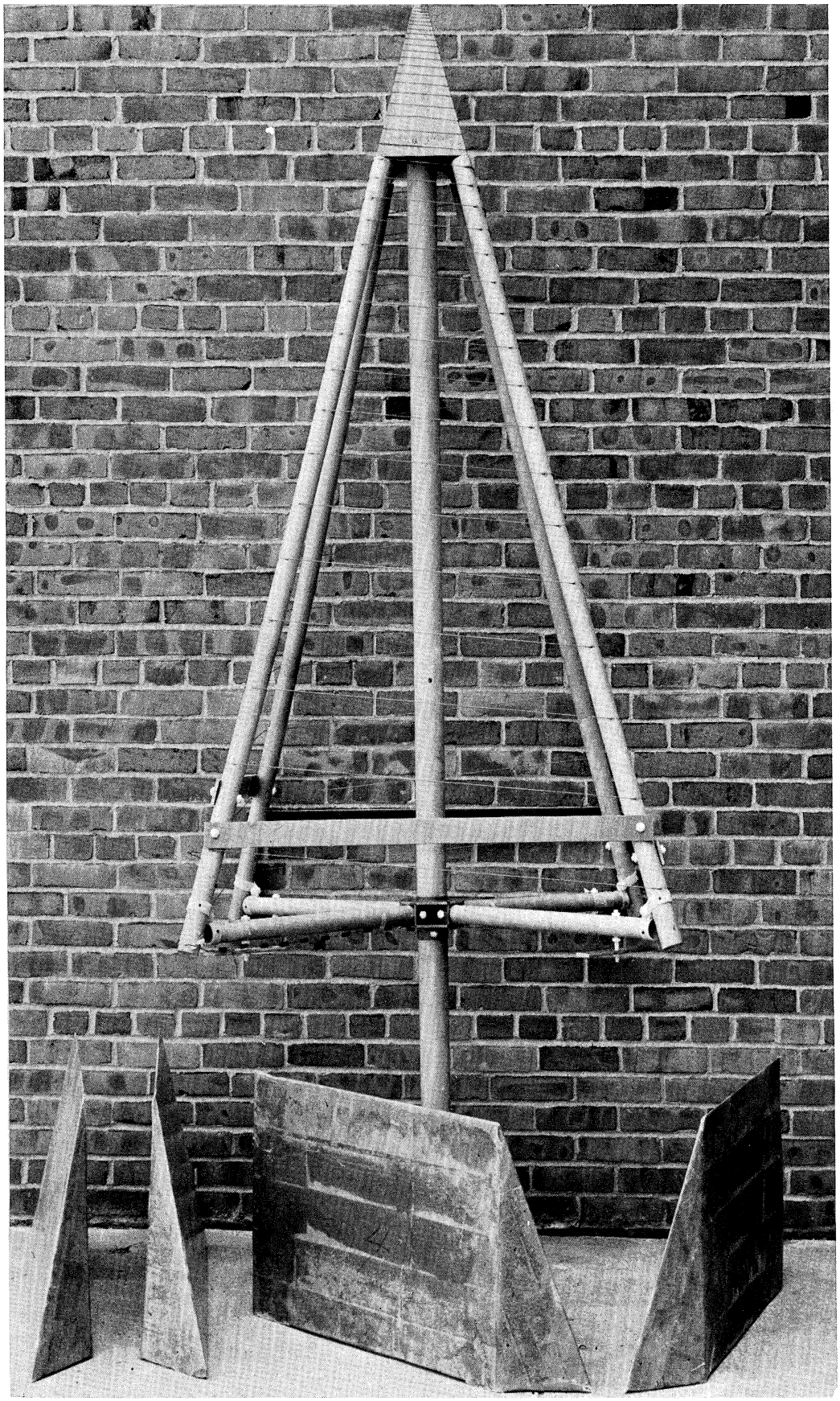

FIG. A-2: ERECTED ANTENNA WITH LOADING BLOCKS

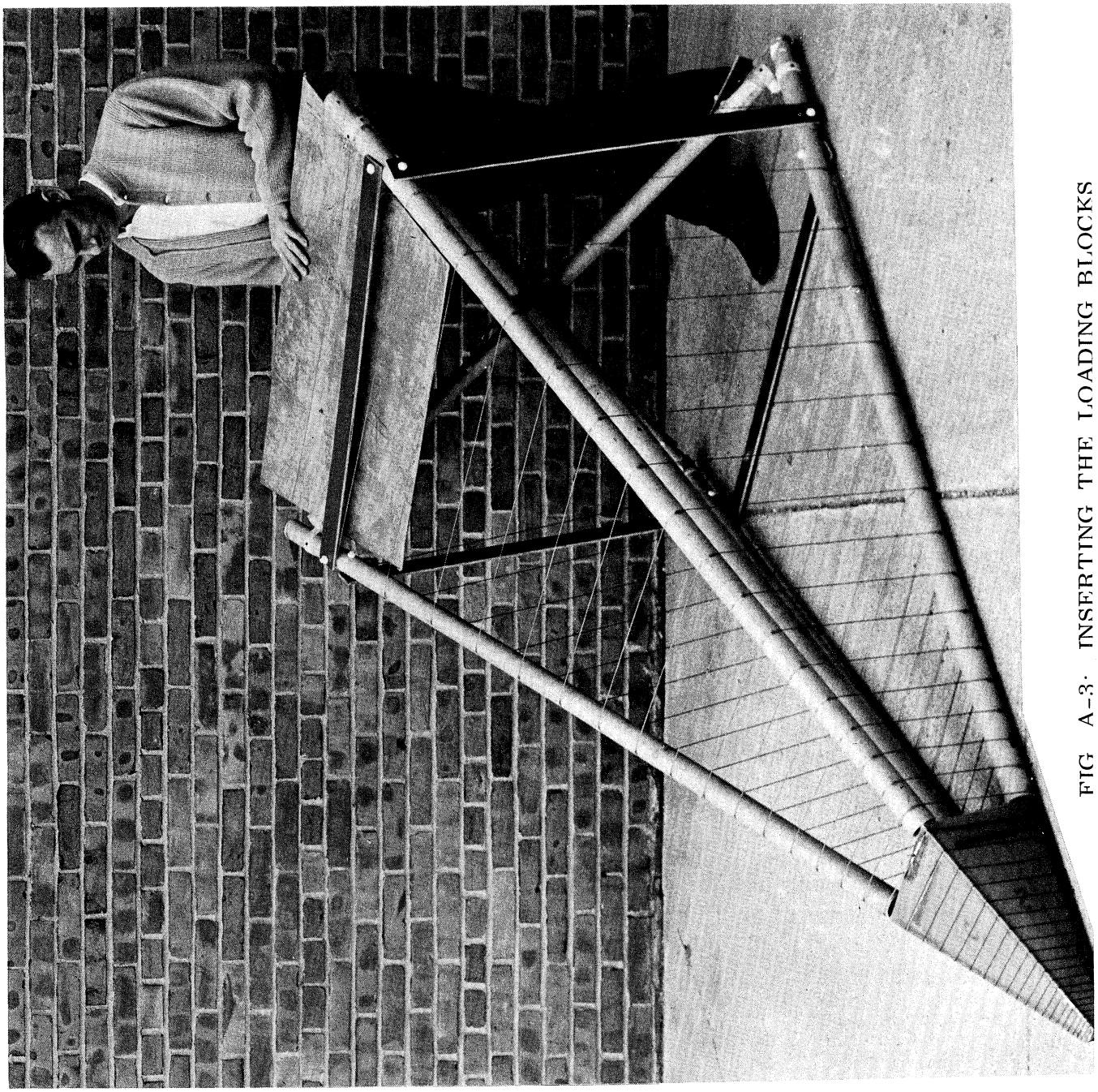

FIG A-3· INSERTING THE LOADING BLOCKS

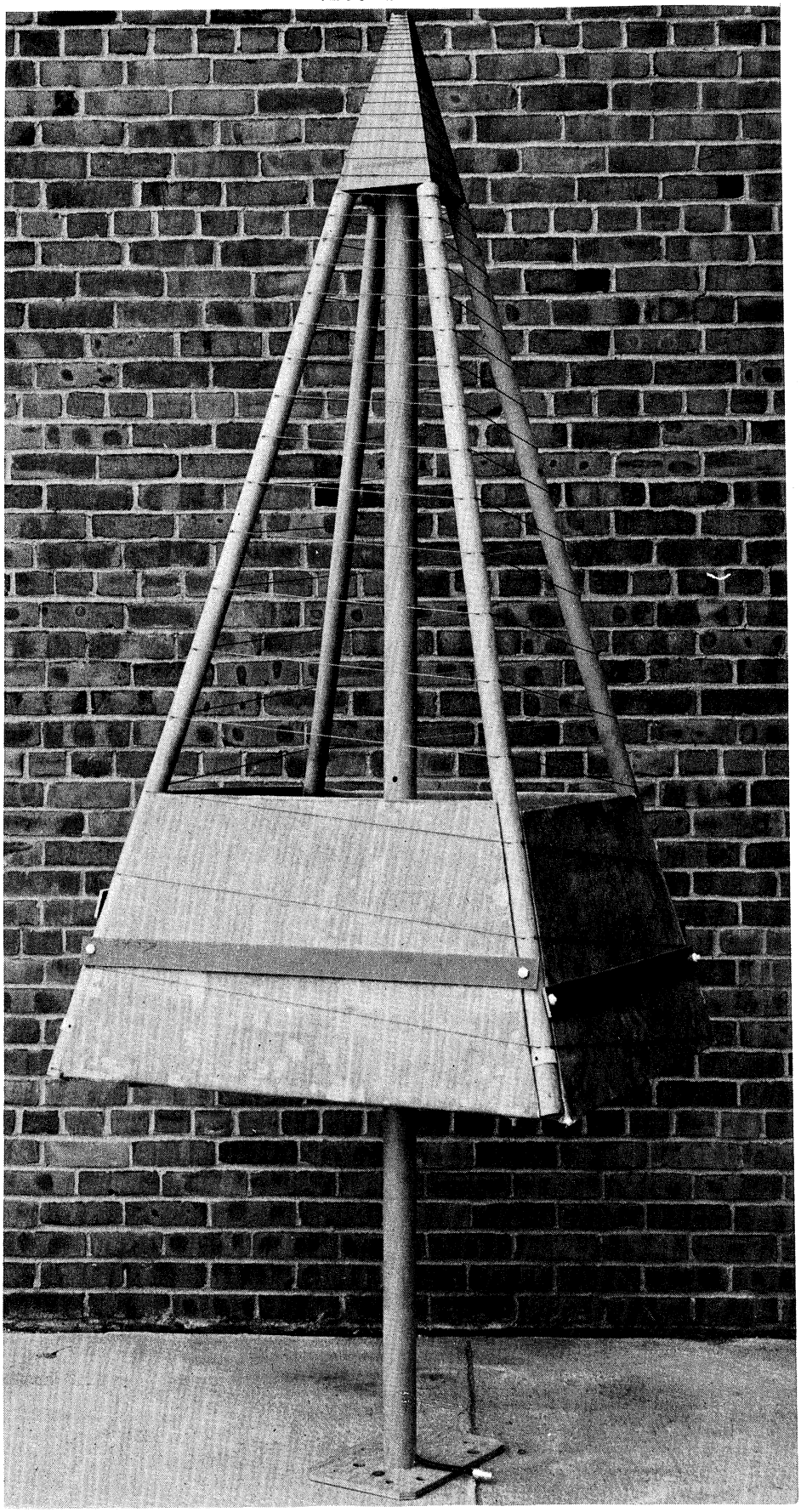

FIG. A-4: THE FINISHED ANTENNA

treat the blocks so that they will be compressed or subject to sudden impact. The resulting deformation will not come out and will greatly impair the operation of the antenna.

2. DO NOT ALLOW THE DIELECTRIC TO BECOME WET. The dielectric blocks are composed of a sponge-like material. If the blocks come in contact with water, they will absorb it readily. This will drastically alter the properties of the antenna and could lead to its destruction under high power.

3. If the blocks do become wet, let them dry thoroughly in a warm dry place. Let them dry for at least two days if just the surface is wet and for at least a week if the blocks become thoroughly soaked. DO NOT HEAT THE BLOCKS TO DRY THEM. This will destroy the dielectric, even though the surface may appear undamaged.

Disassembly.

Perform the inverse operations in the reverse order shown for assembly.

APPENDIX B
THEORY OF HELIX PROPAGATION

An approximate solution may be obtained to the problem of the propagation constant on a helix with a loading material inside or outside. This propagation constant is of great value since it describes the phase of the currents along the helix which in turn is a factor in the size of the antenna for optimum radiation.

Several mathematical models of a helix exist, the "tape" helix and the "sheath" helix, which is the crudest and simplest model. The sheath helix allows current flow at every point on a cylinder, but only in the direction of the helix wires. However, the wire size does not enter in the calculation. This model results in a decoupling of the various modes that can exist on the helix, so that each may be calculated separately, making the mathematics relatively simple.

The present interest is in the $n = -1$ mode useful in endfire radiation, rather than the $n = 0$ mode used in several other loaded sheath studies (Tien, 1953; Suhl and Walker, 1954; Hair, 1964). The $n = -1$ mode allows more general asymptotic expressions to be used than for the $n = 0$ mode; the $n = -1$ asymptotic expressions give a simple approximation valid for any sized helix, at least in the slow wave (β real) region.

The sheath helix supports two sets of modes, TE and TM. Using Figure B-1 to define the geometry, the axial electric and magnetic fields of each mode may be represented as (Hong, 1965):

$$H_z^{i,e} = A_n^{i,e} \begin{cases} I_n(\gamma^i r) \\ K_n(\gamma^e r) \end{cases} e^{-j\beta z - jn\theta} \quad \begin{matrix} r \leq a \\ r \geq a \end{matrix} \qquad \text{(B.1)}$$

and

$$E_z^{i,e} = B_n^{i,e} \begin{matrix} I_n(\gamma^i r) \\ K_n(\gamma^e r) \end{matrix} e^{-j\beta z - jn\theta} \begin{matrix} r \leq a \\ r \geq a \end{matrix} \qquad \text{(B.2)}$$

with

$$\gamma^e = \sqrt{\beta^2 - k_o^2}, \qquad \gamma^i = \sqrt{\beta^2 - k_o^2 \epsilon_r \mu_r}$$

and

$$k_o = \omega \sqrt{\mu_o \epsilon_o}.$$

I_n and K_n are modified Bessel functions of order n, and the superscripts i and e refer to inside and outside, respectively. The boundary conditions at $r = a$ are: the component of the magnetic field parallel to helical paths is continuous, the component of the electric field normal to helical paths is continuous, and the parallel component of the electric fields are zero. Determining the electric and magnetic fields with Eqs. (19) and (20), and then using these boundary conditions at $r = a$, one finds that in order to have a non-trivial solution, the following determinantal equation must be satisfied:

$$\frac{K_n(\gamma^e a)}{K_n'(\gamma^e a)} - \frac{k_o^2 a^2 (\gamma^e a)^2 \cot^2\psi}{\left[(\gamma^e a)^2 - n\beta a \cot\psi\right]^2} \cdot \frac{K_n'(\gamma^e a)}{K_n(\gamma^e a)} = A \frac{1}{\mu_r} \frac{I_n(\gamma^i a)}{I_n'(\gamma^i a)} \qquad \text{(B.3)}$$

$$\frac{k_o^2 a^2 (\gamma^e a)^2 \cot^2\psi}{\left[(\gamma^e a)^2 - n\beta a \cot\psi\right]^2} \cdot \frac{\gamma^e}{\gamma^i} \epsilon_r \frac{I_n'(\gamma^i a)}{I_n(\gamma^i a)}$$

with

$$A = \frac{(\gamma^e)^3}{(\gamma^i)^3} \cdot \left[\frac{(\gamma^i a)^2 - n\beta a \cot\psi}{(\gamma^e a)^2 - n\beta a \cot\psi} \right]^2 . \qquad \text{(B. 4)}$$

For slow waves radial propagation constants are almost equal to β, and we can approximate $\gamma^i = \gamma^e = \gamma$.

For this approximation, asymptotic values for some of the Bessel Functions for large n may be used, even for $n = -1$, (Watkins, 1958), which gives a dispersion equation

$$\frac{K_n'(\gamma_n a)\, I_n'(\gamma_n a)}{K_n(\gamma_n a)\, I_n(\gamma_n a)} = -\frac{\left[\beta_n^2 a^2 - n\beta a \cot\psi\right]^2}{(c^2 k^2 a^2)\, a^2 a^\beta \cot^2\psi} \qquad \text{(B. 5)}$$

where $c^2 \cong \frac{1+\epsilon}{\frac{1}{\mu}+1}$ for $n \geq 1$, and not too large (< 10). This is the dispersion equation for a sheath helix in air, with the factor $c = 1$ in air. Thus the size frequency parameter, when a loaded sheath helix is considered, is scaled from its free space value by

$$\frac{1}{c} = \sqrt{\frac{\frac{1}{\mu}+1}{\epsilon+1}} . \qquad \text{(B. 6)}$$

In addition, the more exact theoretical solutions, as well as experimetnal data (Dyson, 1964), yield for very narrow conductors.

$$\frac{k_o a}{\beta_o a} = \sin\psi . \qquad \text{(B. 7)}$$

Thus it is natural to assume the scaling of $k_o a$ remains, yielding:

$$\frac{k_o a}{\beta a} = \sqrt{\frac{1 + \frac{1}{\mu_r}}{1 + \epsilon_r}} \sin\psi \, . \qquad \text{(B.8)}$$

B.2 Size Reduction for Bifilar Helices

Dyson (1965) has shown that the propagation constant obtained from the sheath model can be applied for analysis of bifilar helix. He has also shown that for a conical helix with a narrow cone angle $(2\theta_o)$, analysis of a cylindrical helix can be used with a slight modification. For a conical helix, Eq. (B.8) is modified as

$$\frac{k_o a}{\beta a} = \sqrt{\frac{1 + \frac{1}{\mu_r}}{1 + \epsilon_r}} \sin\psi \cos\theta_o \, . \qquad \text{(B.9)}$$

From Eq. (B.8), we obtain the Brillouin diagram for a bifilar helix (see Fig. B-2). As frequency changes, the progagation constant β varies along the line:

$$\frac{k_o a}{\beta a} = \sqrt{\frac{1 + \frac{1}{\mu_r}}{1 + \epsilon_r}} \sin\psi \, .$$

When this line meets with the line given by $\frac{k_o a}{\cot\psi} = 1 - \frac{\beta a}{\cot\psi}$, the phase of the radiated fields from each element of the helical antenna is lined up such that a backfire radiation occurs (Jones and Mittra, 1965). Figure B-2 shows that as the frequency increases further, the radiation pattern changes from backfire to broadside, then to endfire.

The required size of a cylindrical bifilar helix for backfire radiation can be obtained from the solution of the following two equations (Hong, 1965):

$$\frac{k_o a}{\beta a} = \sqrt{\frac{1 + \frac{1}{\mu_r}}{1 + \epsilon_r}} \sin\psi \qquad \text{(B.10)}$$

$$\frac{k_o a}{\cot\psi} = 1 - \frac{\beta a}{\cot\psi} \quad .$$

The solution of Eq. (B.10) is

$$k_o a = \frac{\sqrt{\frac{1 + \frac{1}{\mu_r}}{1 + \epsilon_r}} \cos\psi}{1 + \sqrt{\frac{1 + \frac{1}{\mu_r}}{1 + \epsilon_r}} \sin\psi} \quad . \qquad \text{(B.11)}$$

Therefore the ratio between the linear sizes of loaded and unloaded helices becomes

$$\frac{a \text{ (with arbitrary } \epsilon_r \text{ and } \mu_r)}{a \text{ (with } \epsilon_r = \mu_r = 1)} = \frac{\sqrt{\frac{1 + \frac{1}{\mu_r}}{1 + \epsilon_r}} (1 + \sin\psi)}{1 + \sqrt{\frac{1 + \frac{1}{\mu_r}}{1 + \epsilon_r}} \sin\psi} \quad . \qquad \text{(B.12)}$$

In a similar manner, the active region of a conical bifilar helix for backfire radiation can be predicted from the following formula:

$$k_o a = \frac{\sqrt{\frac{1+\frac{1}{\mu_r}}{1+\epsilon_r}}\cos\psi \cdot \cos\theta_o}{1+\sqrt{\frac{1+\frac{1}{\mu_r}}{1+\epsilon_r}}\sin\psi \cdot \cos\theta_o} \qquad \text{(B.13)}$$

with $2\theta_o$ = cone angle.

In Eq. (B.13) 2a is the diameter of the cross section of the cone in the region where helical elements become active and radiates. The linear size reduction factor for a conical helix is

$$\frac{a\,(\text{arbitrary } \epsilon_r \text{ and } \mu_r)}{a\,(\epsilon_r = \mu_r = 1)} = \frac{\sqrt{\frac{1+\frac{1}{\mu_r}}{1+\epsilon_r}}(1+\sin\psi \cdot \cos\theta_o)}{1+\sqrt{\frac{1+\frac{1}{\mu_r}}{1+\epsilon_r}}\sin\psi \cdot \cos\theta_o} . \qquad \text{(B.14)}$$

For fairly small pitch angle, ψ, the solution gives the simple size reduction factor

$$\frac{a\,(\text{arbitrary } \epsilon_r \text{ and } \mu_r)}{a\,(\epsilon_r = \mu_r = 1)} = \sqrt{\frac{1+\frac{1}{\mu_r}}{1+\epsilon_r}} . \qquad \text{(B.15)}$$

Remember that all the formulas given depend upon the assumption, $\mu\epsilon < 10$ approximately, and are only approximate even then.

The reduction factor (B. 15) for the three materials most used in the experiments, is given in Table B-1.

TABLE B-1

REDUCTION COEFFICIENTS

ϵ	μ	(B. 15)
10	1	.43
6	1	.54
3. 77	2. 2	.55

The factors have been approached by the experimental results shown in this report, offering some verification.

Further work on the effect of layer thickness on size reduction is available for the sheath and in the slow wave region only. However, recent work in tape helices shows that the higher modes have a great influence on the phase velocity of the current in the active region, thus making the true effect of loading layer thickness a difficult and unsolved theoretical problem. The experiments in this report indicate that fairly thick (. 25 radius) loadings behave like full core loading.

APPENDIX C

FINAL DATA - LOG CONICAL ANTENNA

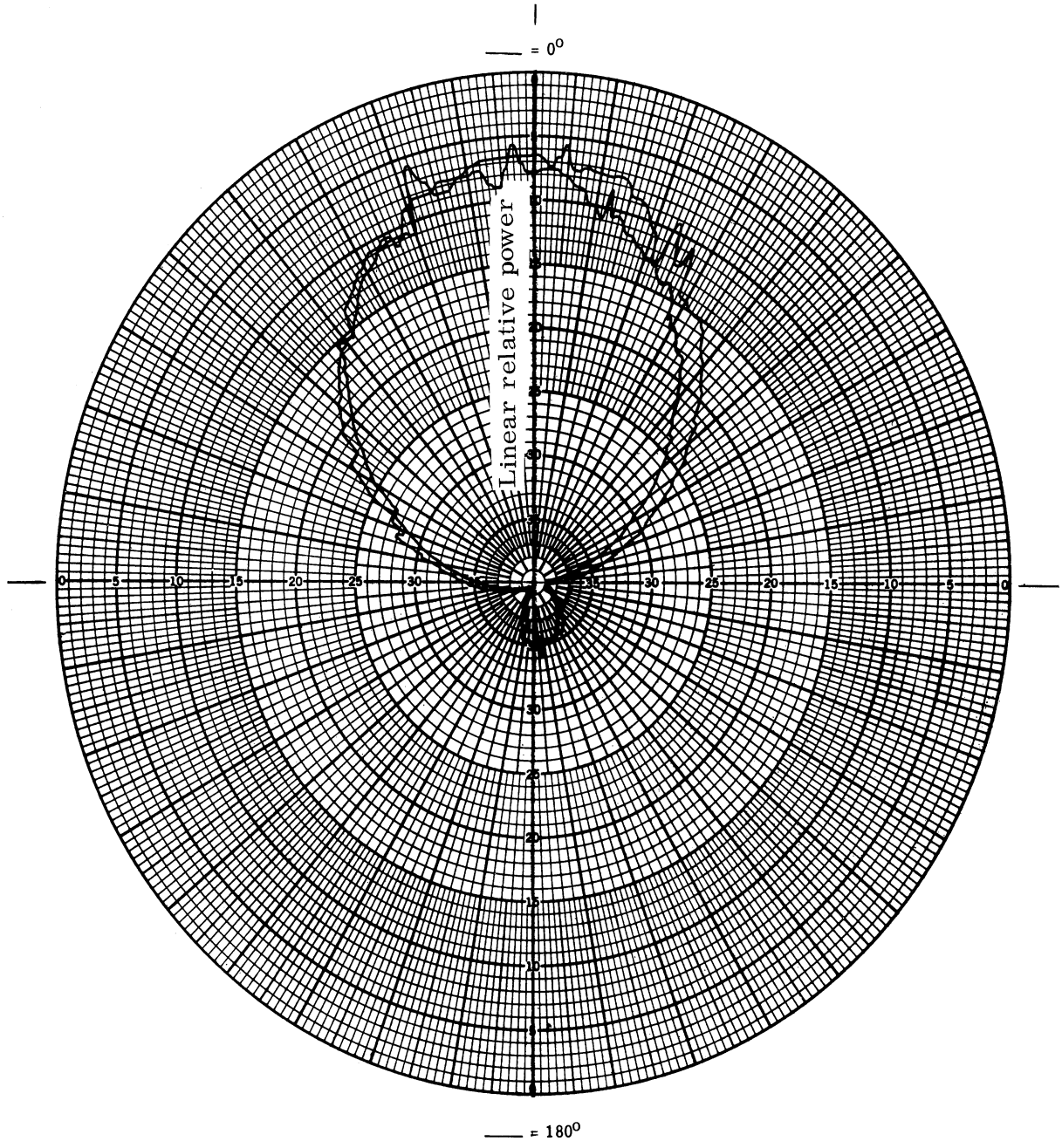

FIG. C-1: LOADED LOG CONICAL ANTENNA, 40 MHz, E-PLANE

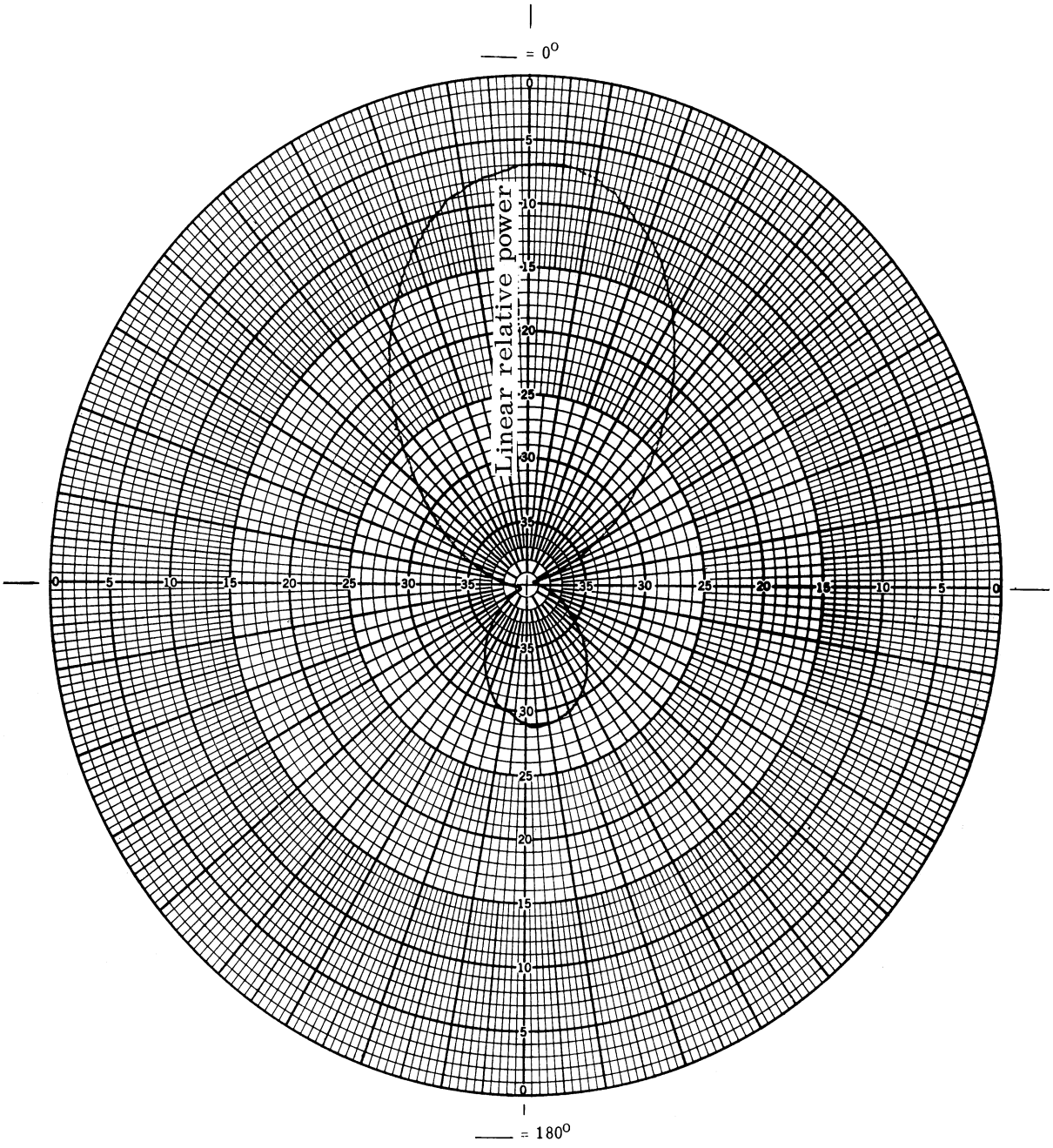

FIG. C-2: LOADED LOG CONICAL ANTENNA, 50 MHz, E-PLANE

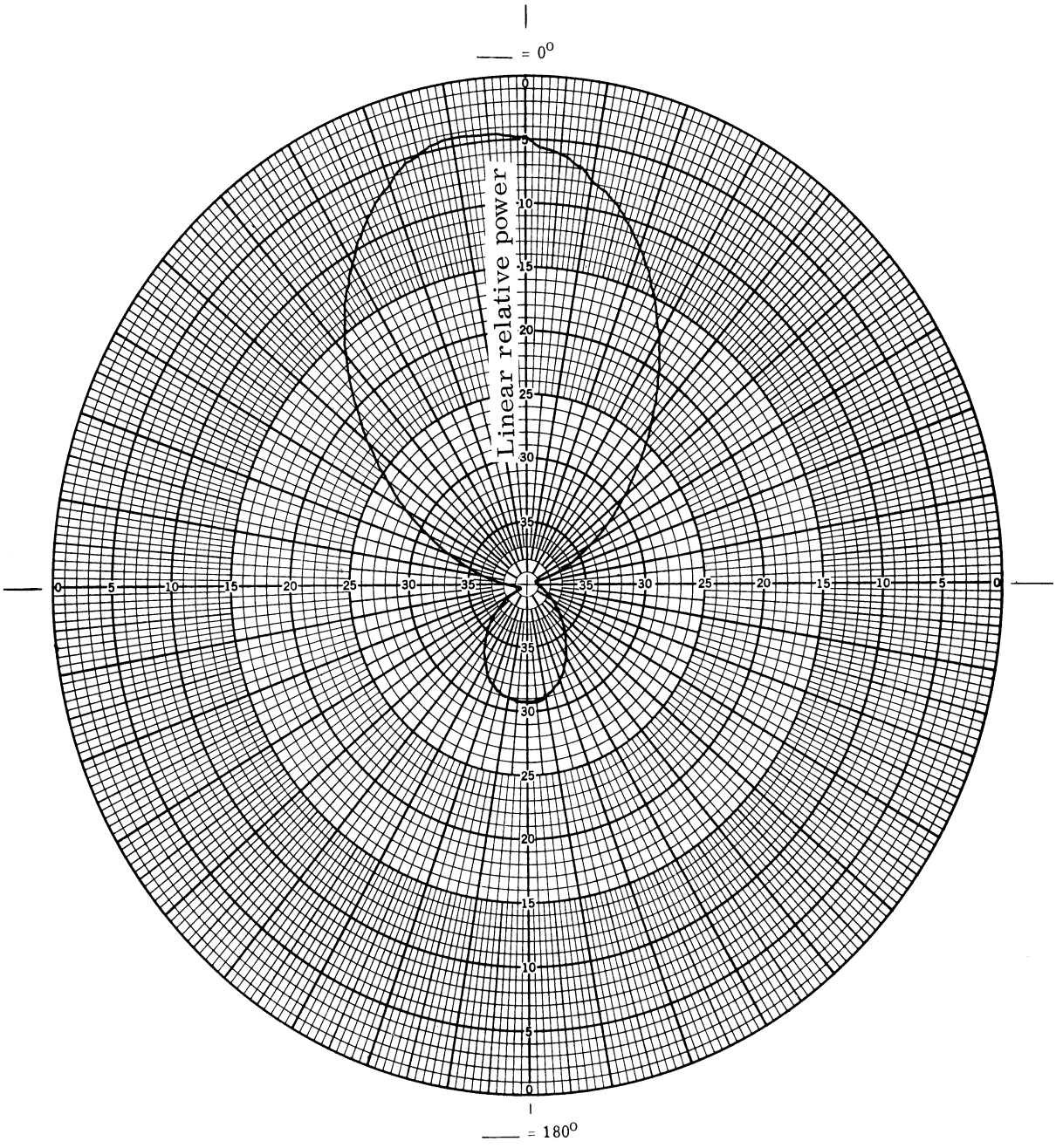

FIG. C-3: LOADED LOG CONICAL ANTENNA, 65 MHz; E-PLANE

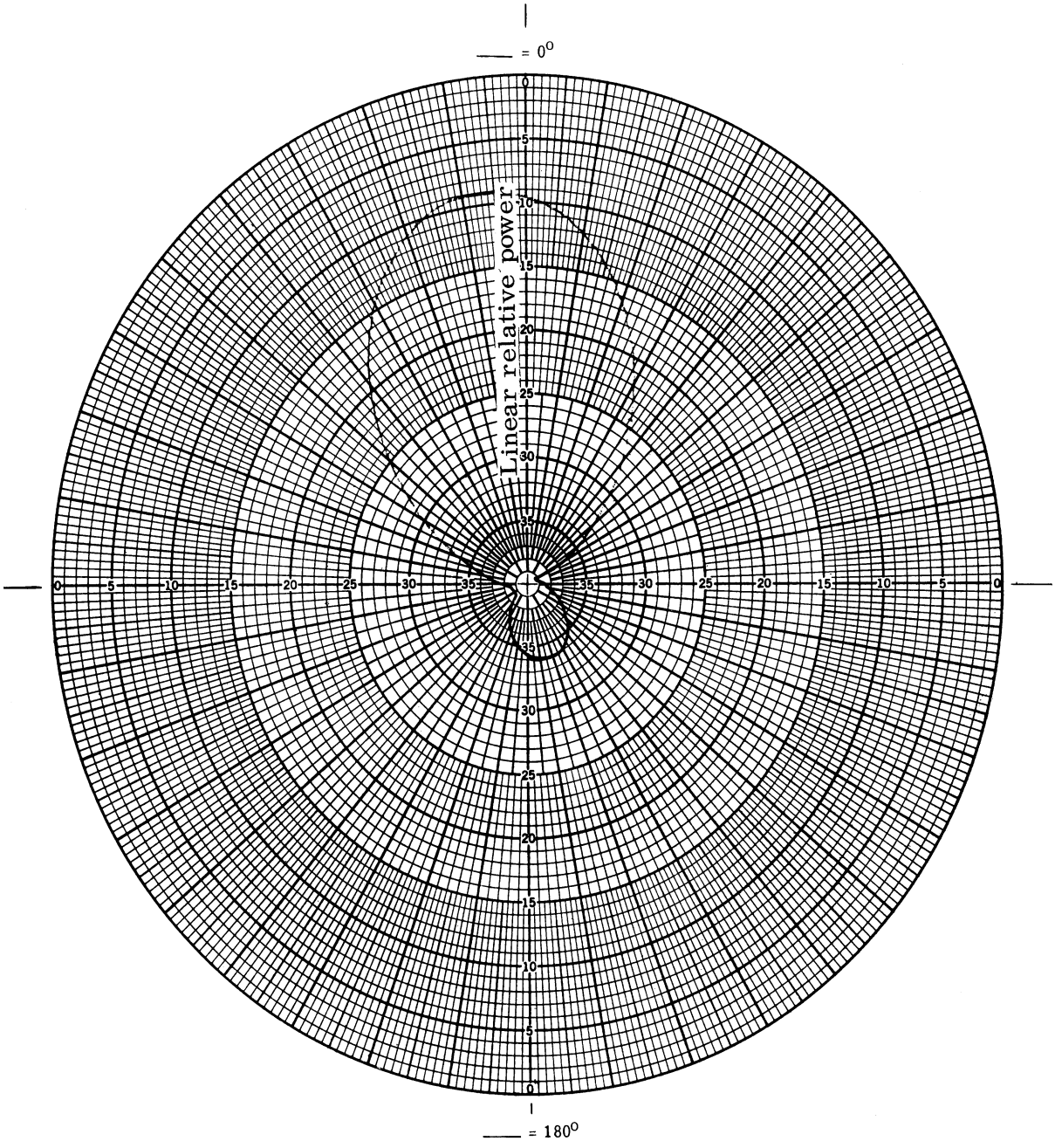

FIG. C-4: LOADED LOG CONICAL ANTENNA, 70 MHz, E-PLANE

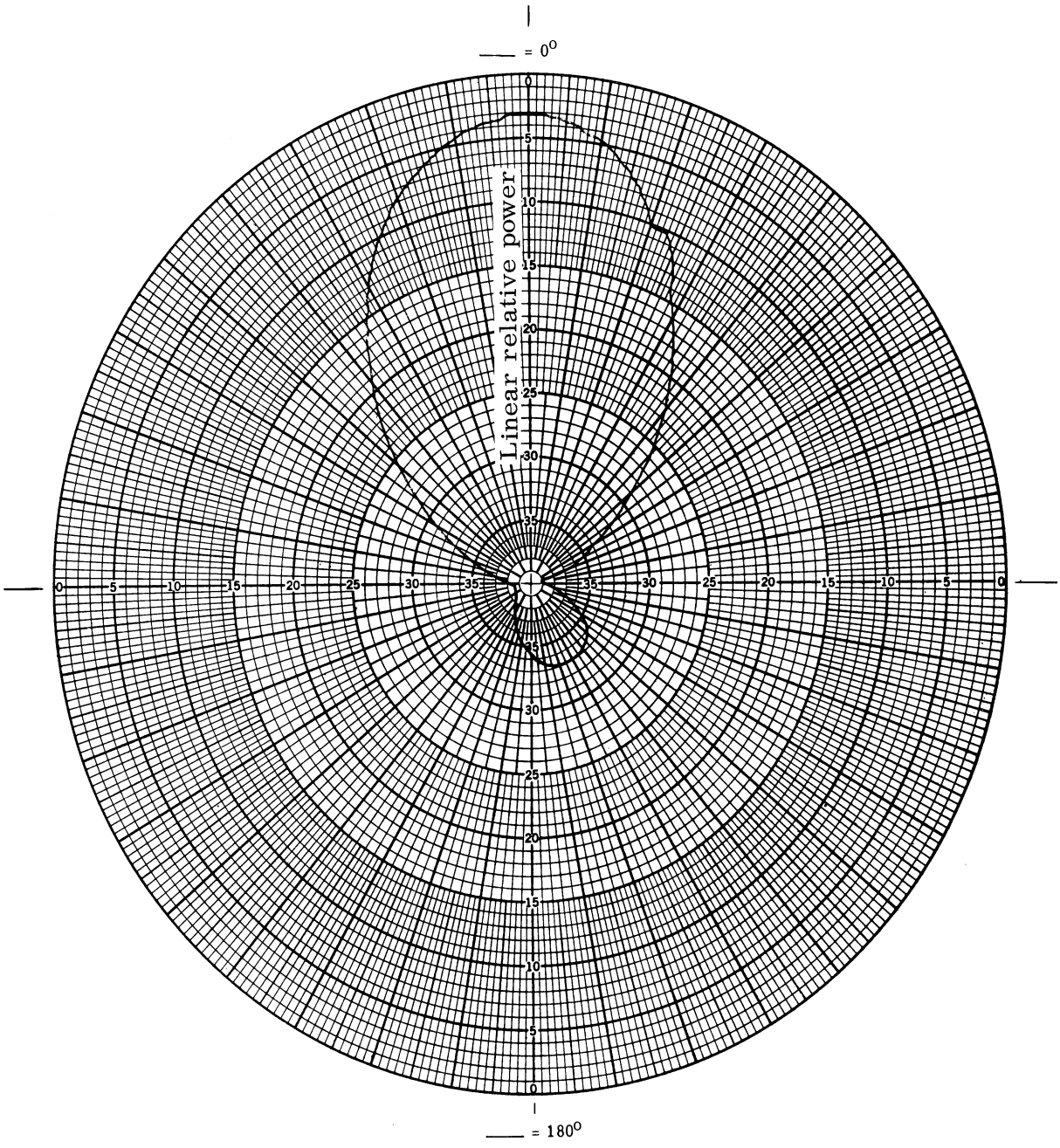

FIG. C-5: LOADED LOG CONICAL ANTENNA, 80 MHz, E-PLANE

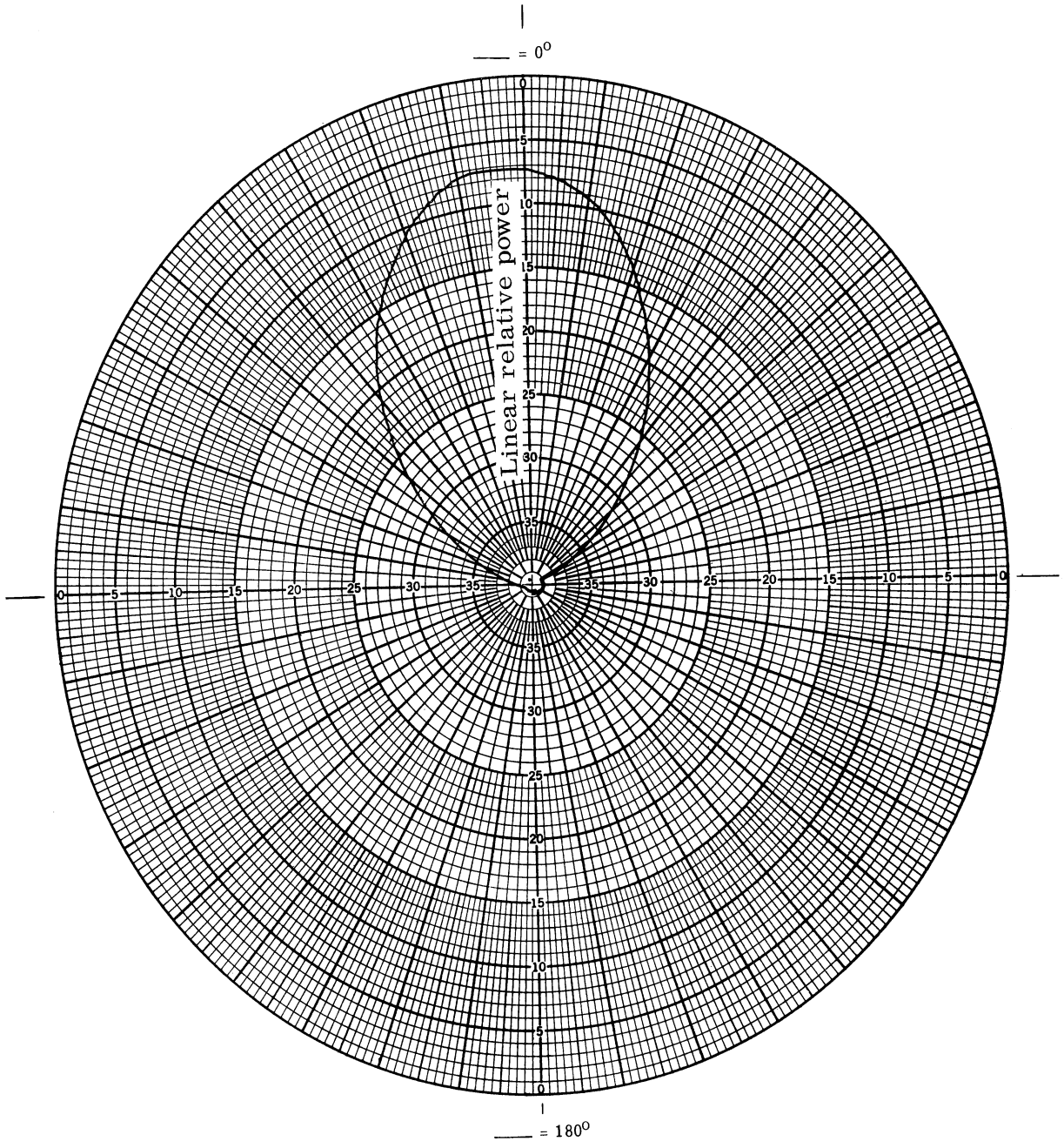

FIG. C-6: LOADED LOG CONICAL ANTENNA, 150 MHz; E-PLANE

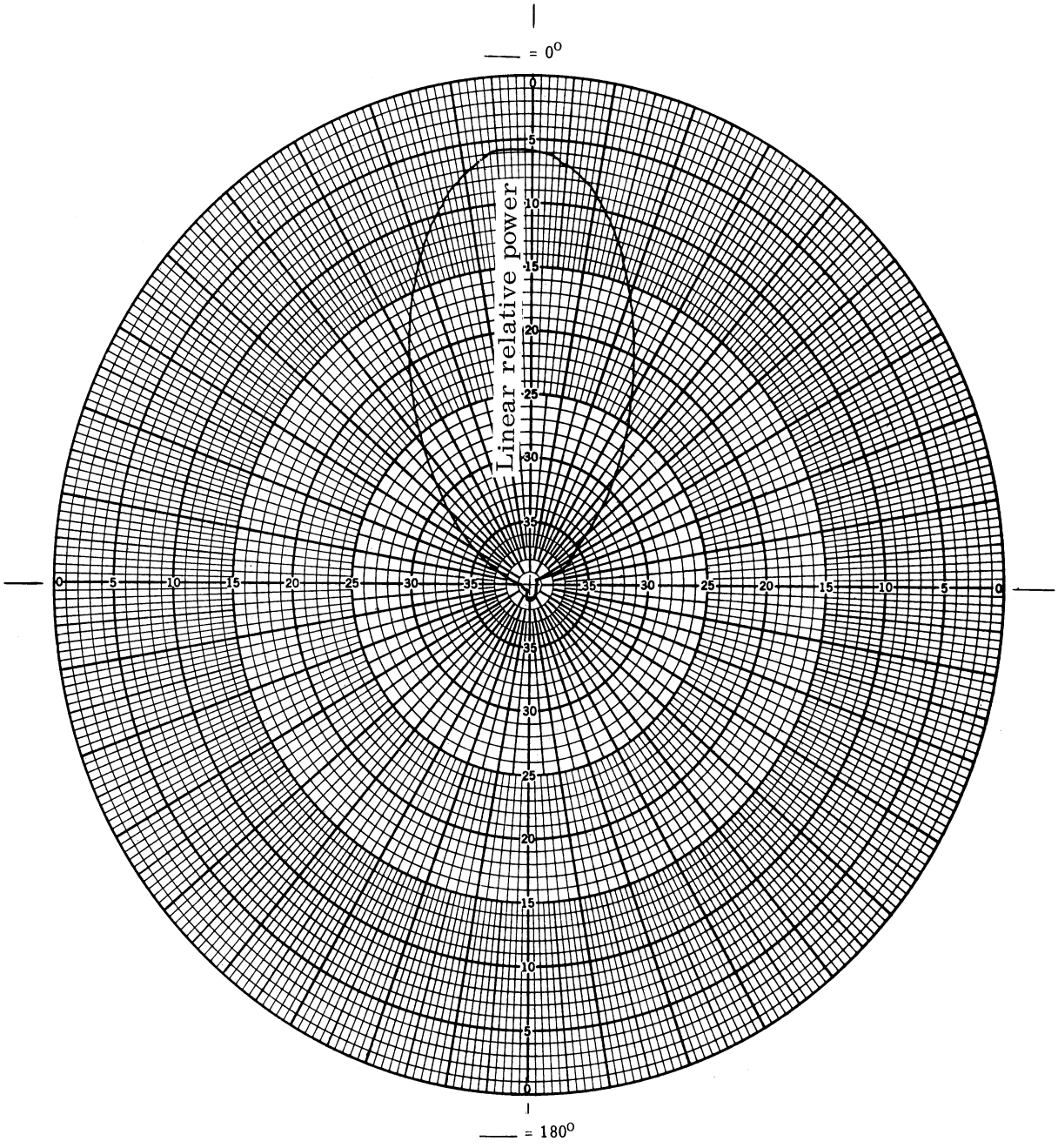

FIG. C-7: LOADED LOG CONICAL ANTENNA, 300 MHz, E-PLANE

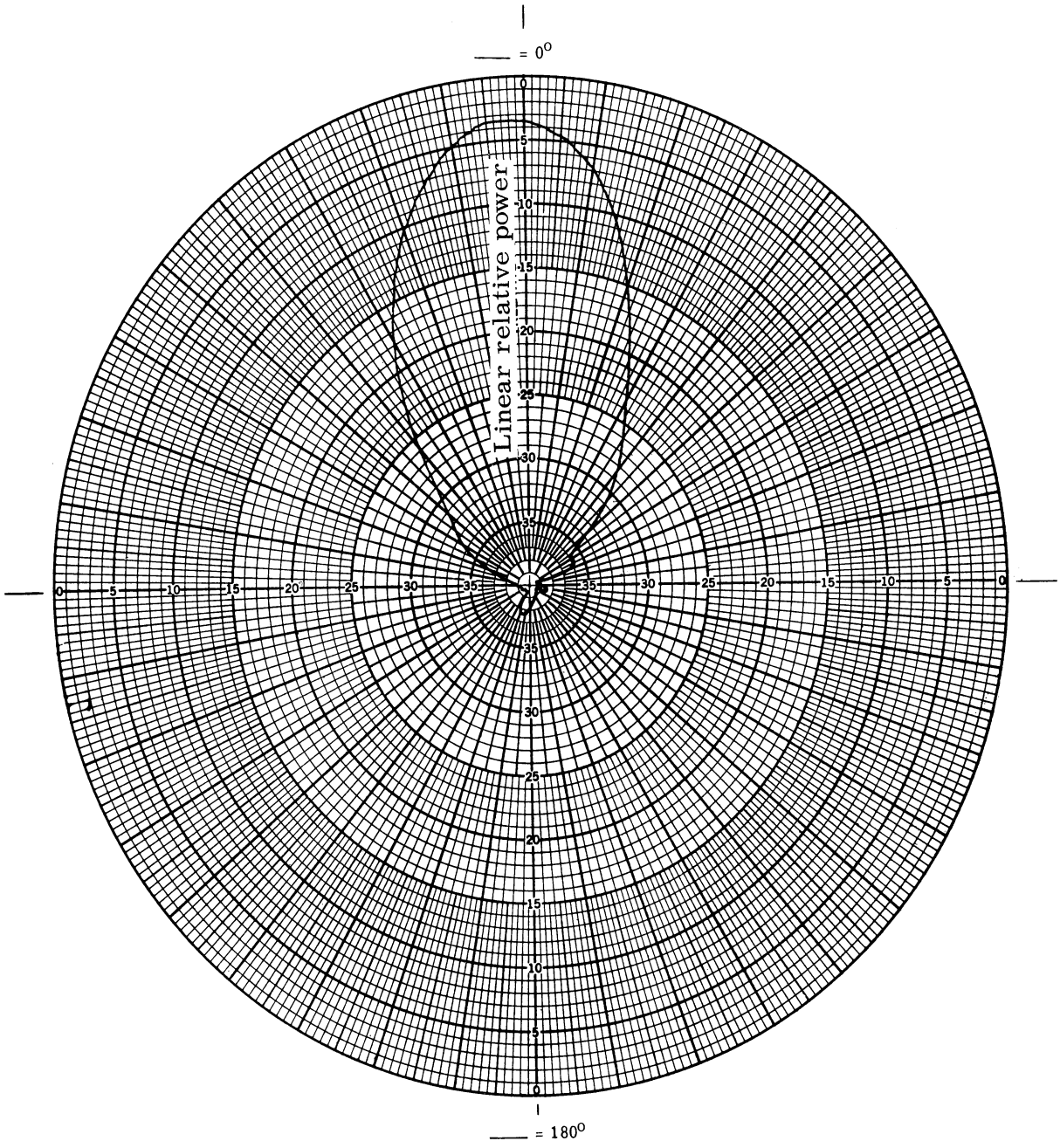

FIG. C-8: LOADED LOG CONICAL ANTENNA, 500 MHz
TERMINATING RESISTORS OMITTED, E-PLANE

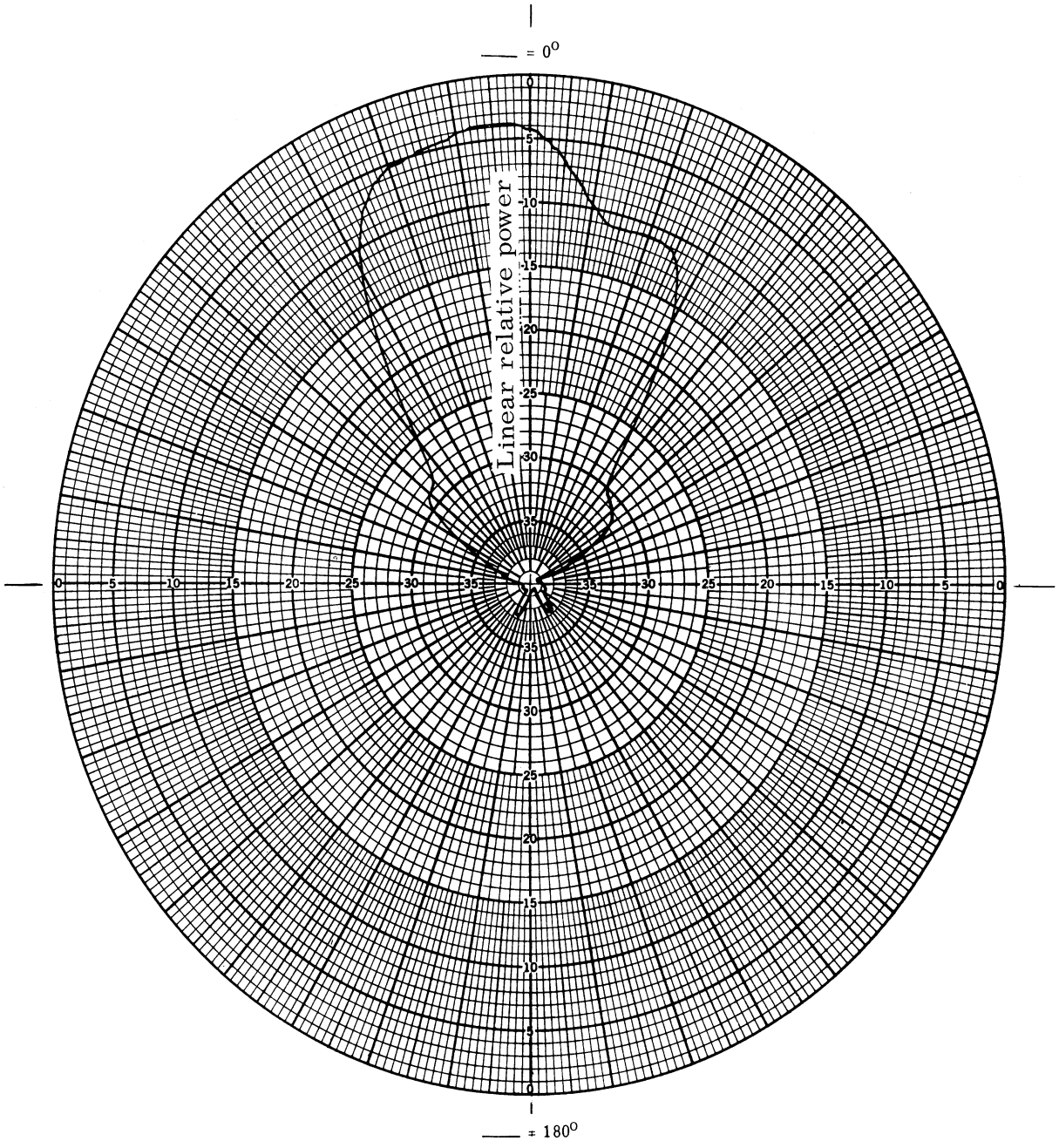

FIG. C-9: LOADED LOG CONICAL ANTENNA, 500 MHz, E-PLANE

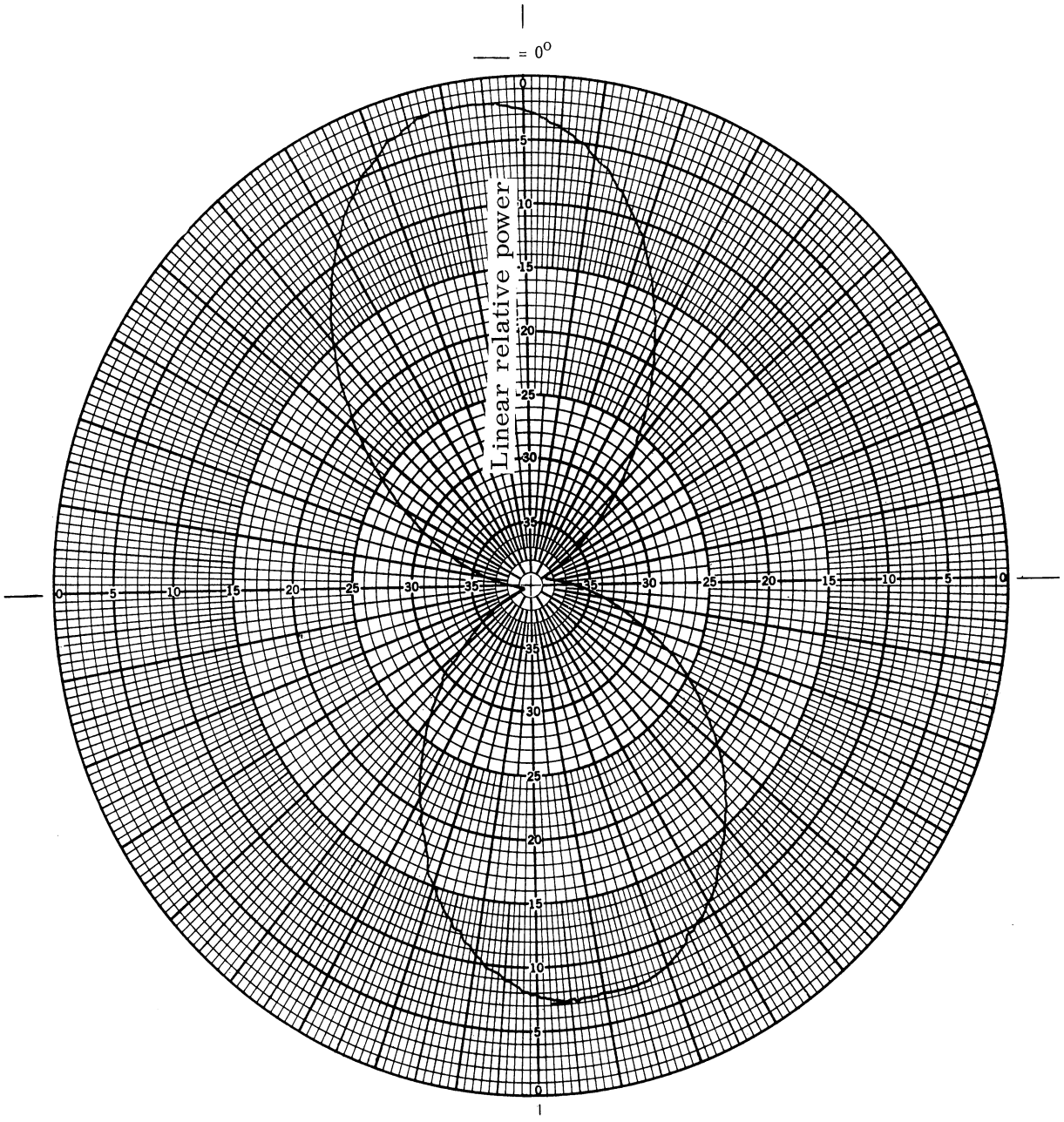

FIG. C-10: UNLOADED LOG CONICAL ANTENNA, 50 MHz, E-PLANE

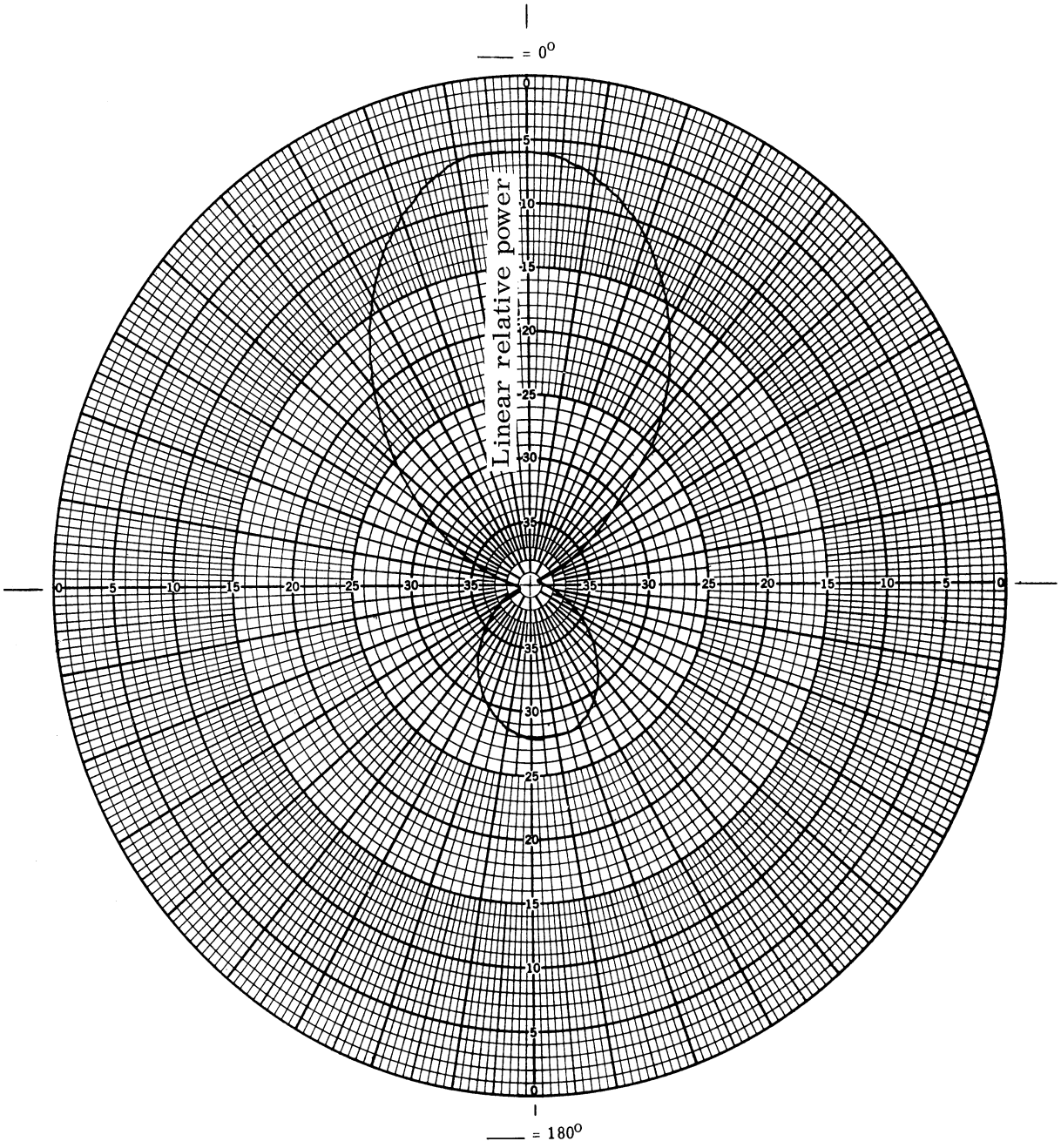

FIG. C-11: UNLOADED LOG CONICAL ANTENNA, 80 MHz, E PLANE

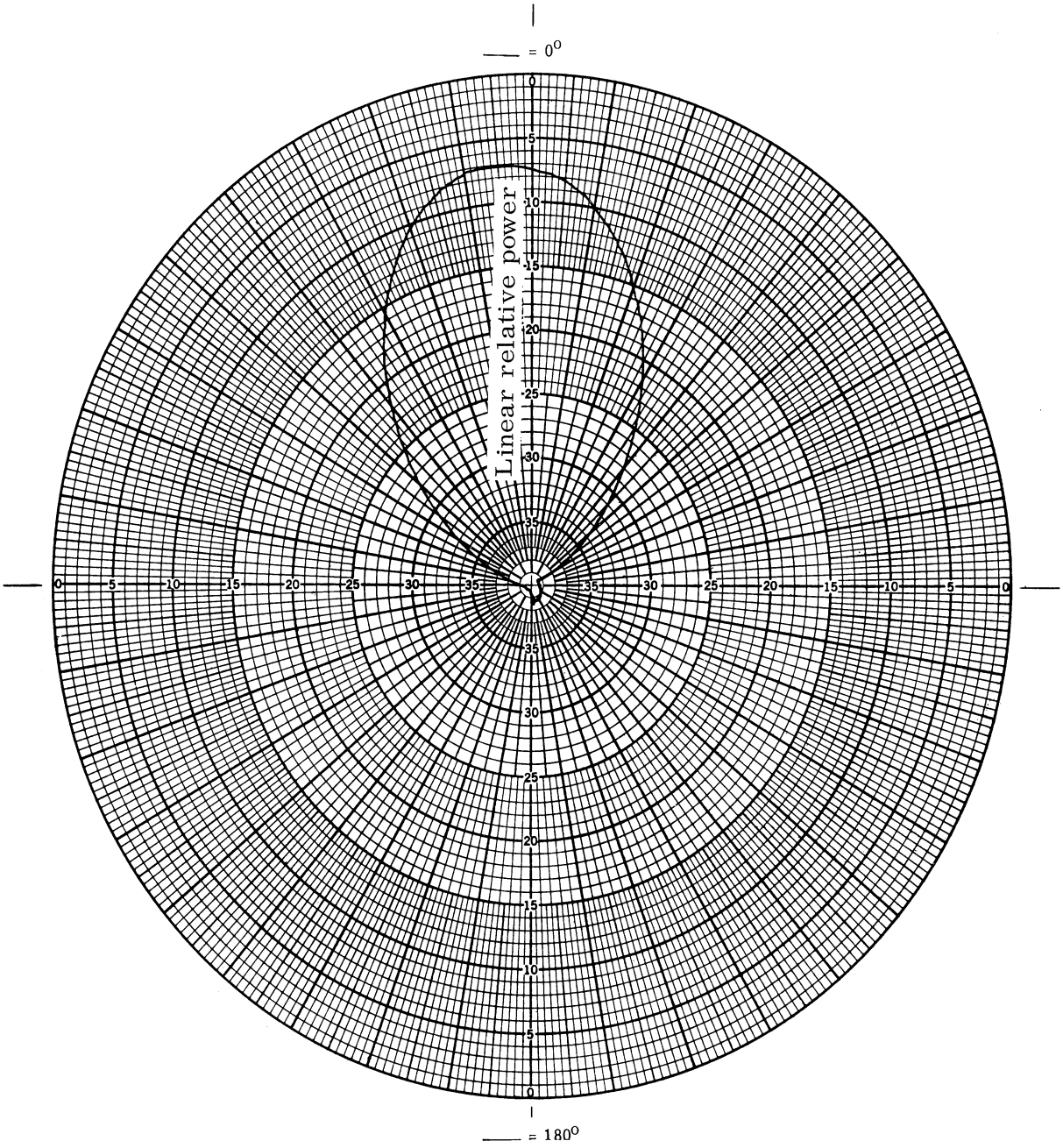

FIG. C-12: LOADED LOG CONICAL ANTENNA, 150 MHz, E-PLANE

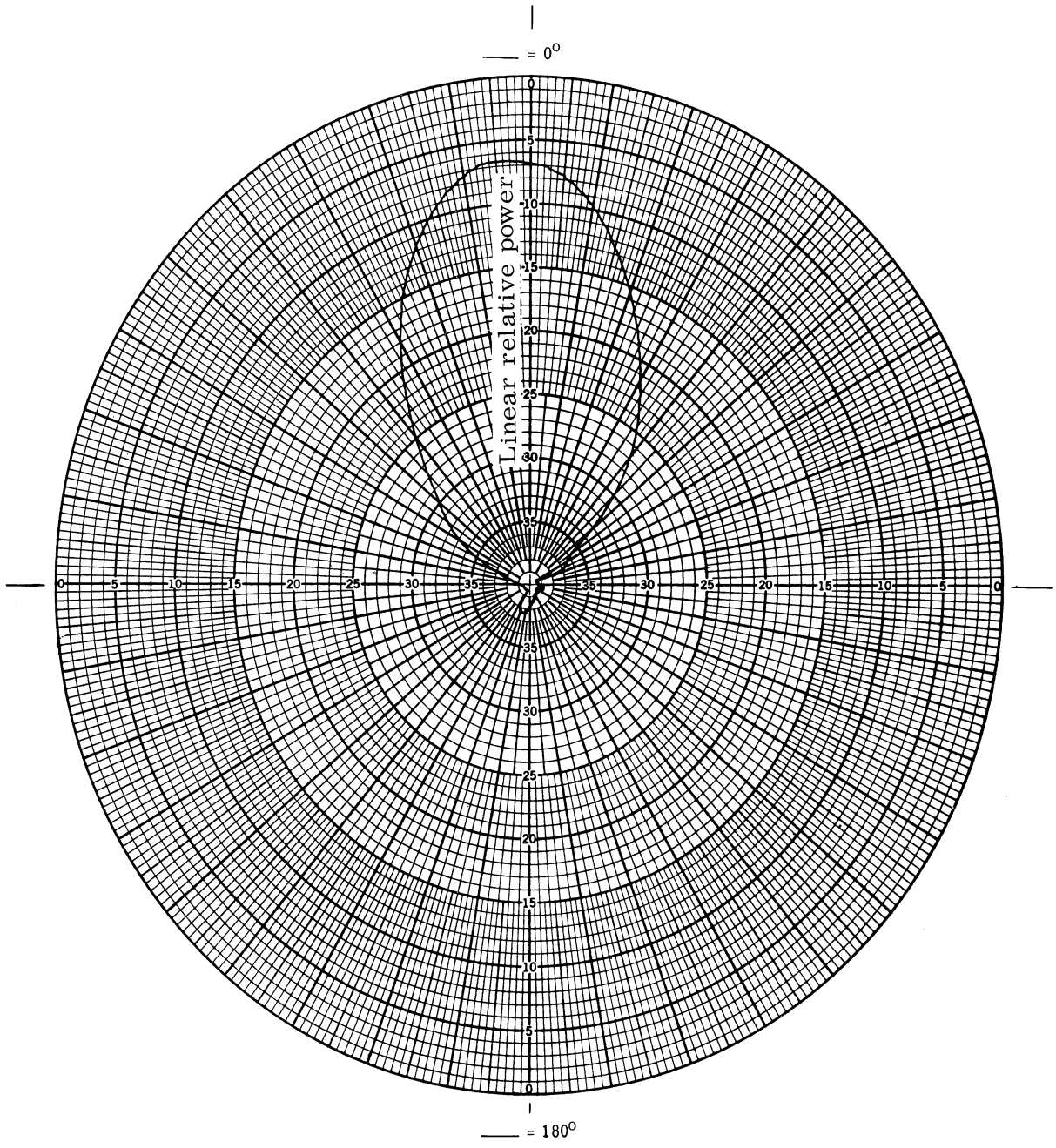

FIG. C-13: UNLOADED LOG CONICAL ANTENNA, 300 MHz; E-PLANE

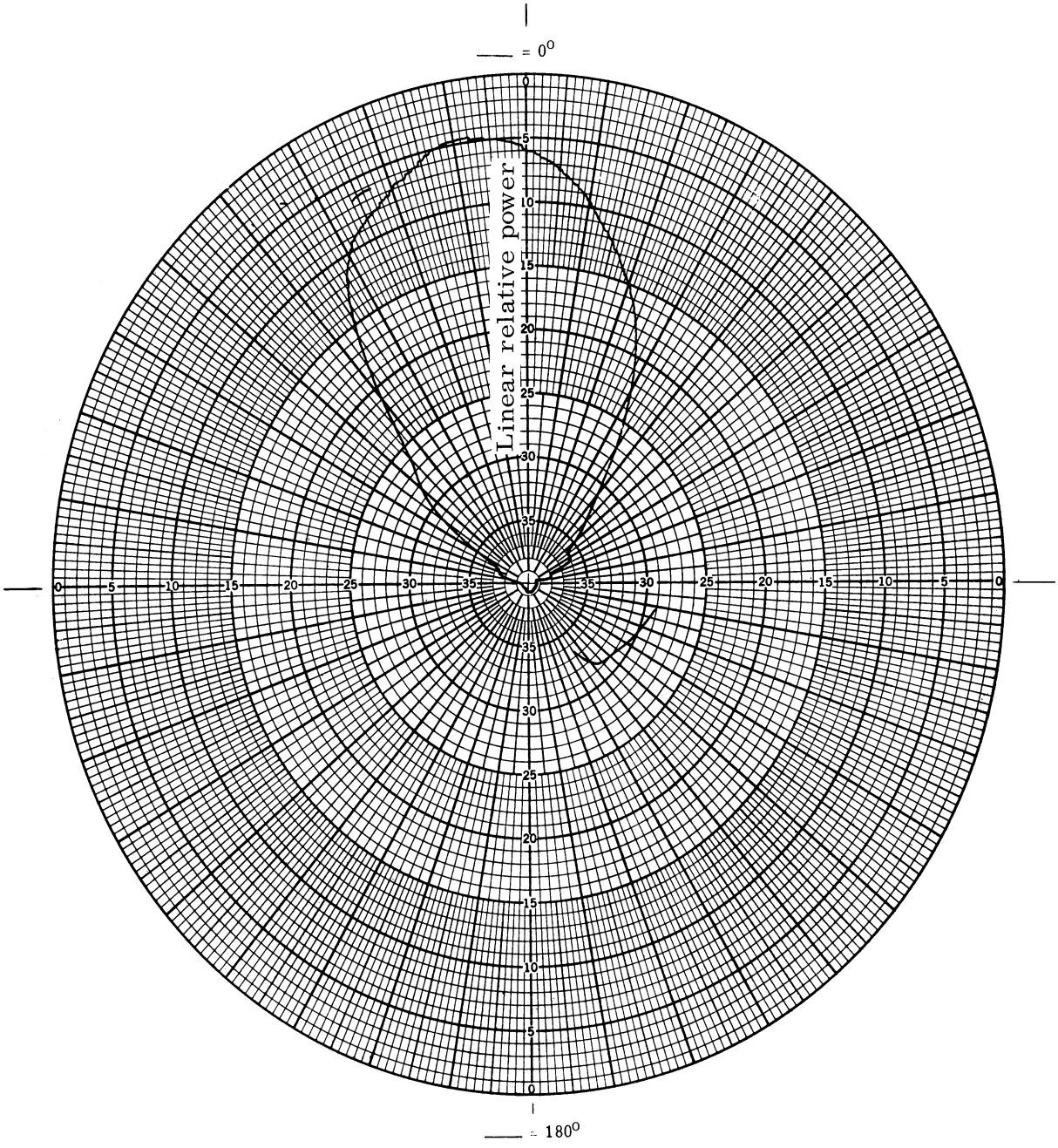

FIG. C-14: UNLOADED LOG CONICAL ANTENNA, 500 MHz, E-PLANE

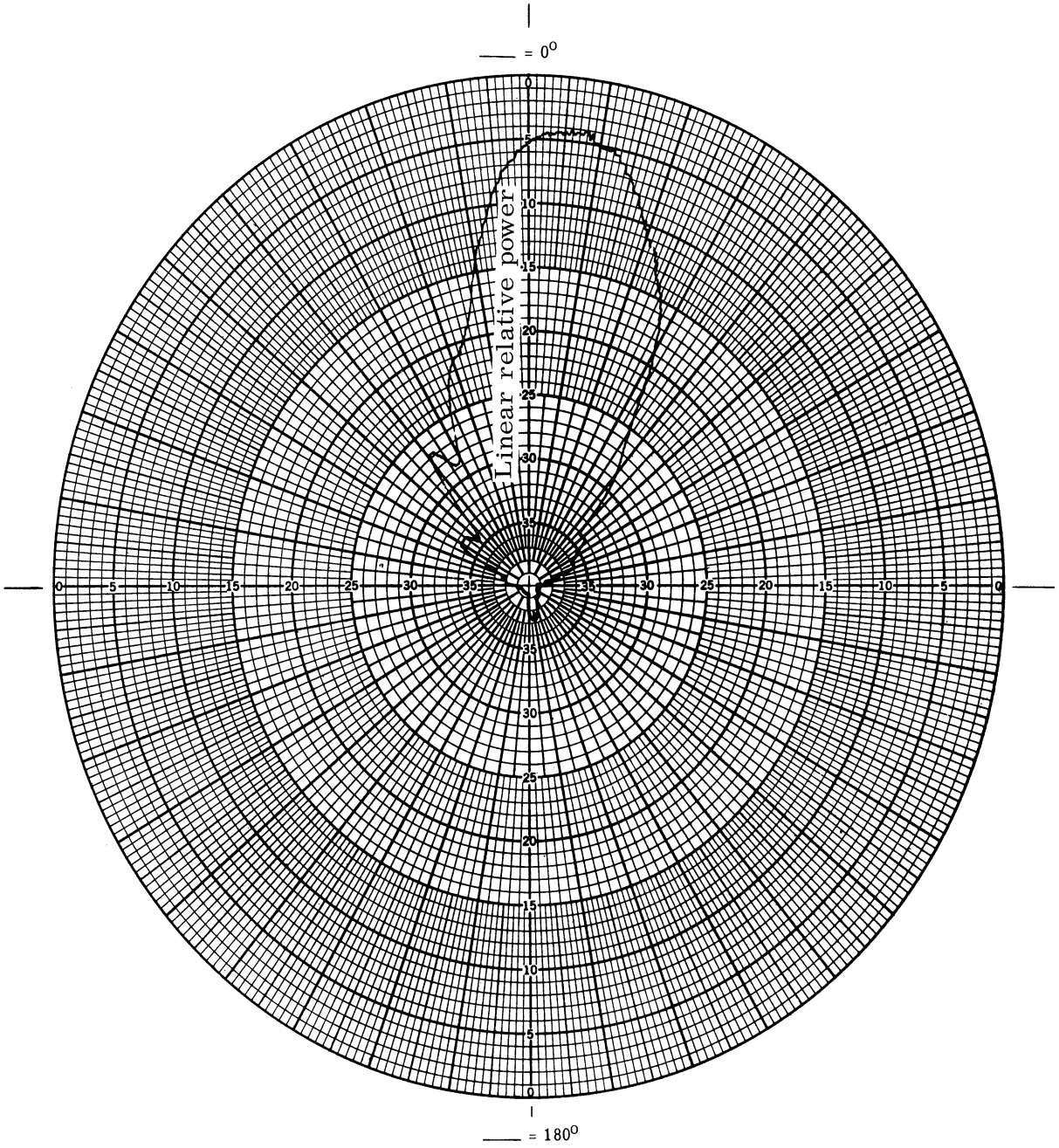

FIG. C-15: UNLOADED LOG CONICAL ANTENNA, 750 MHz; E-PLANE

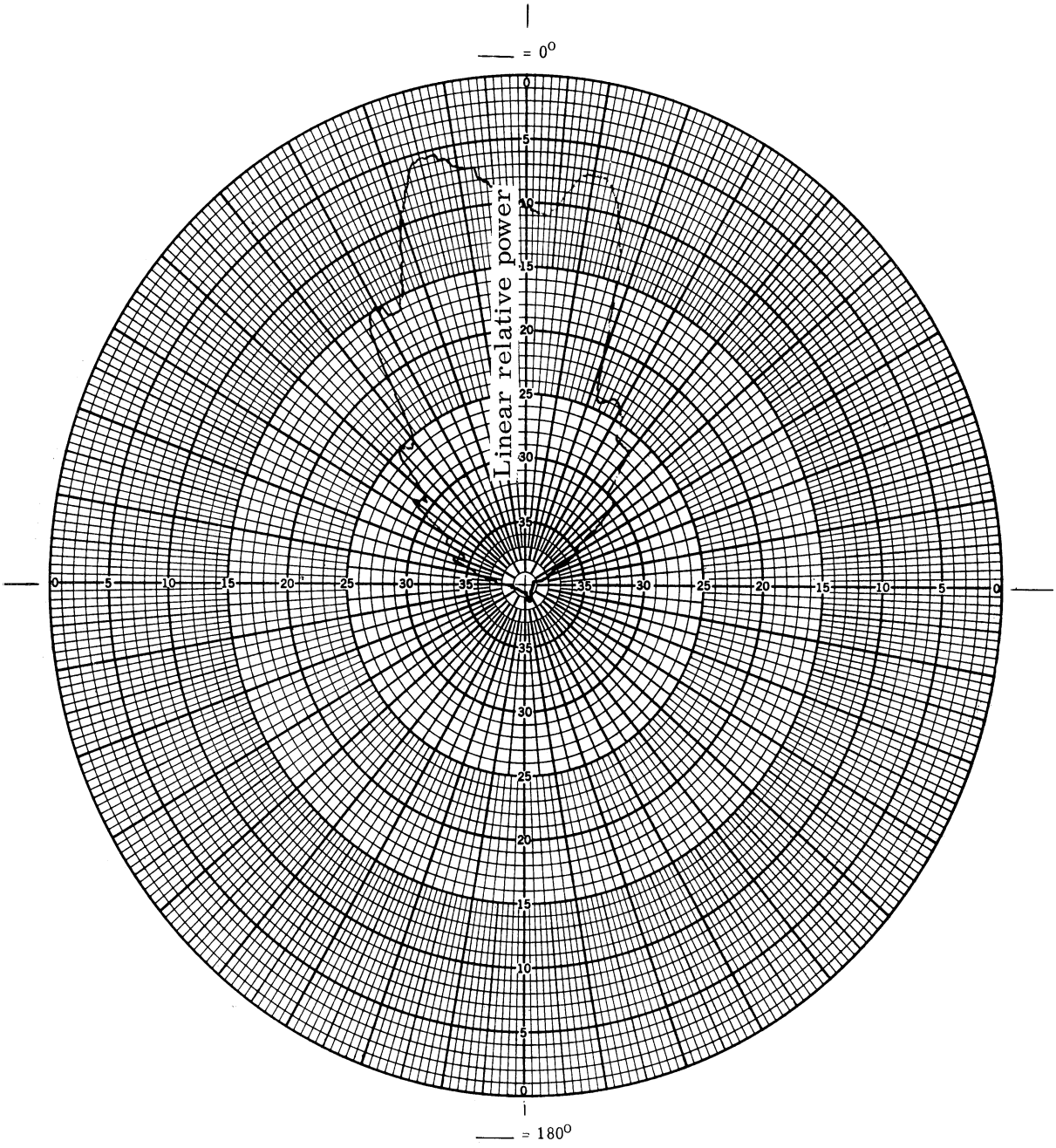

FIG. C-16: UNLOADED LOG CONICAL ANTENNA, 950 MHZ; E-PLANE

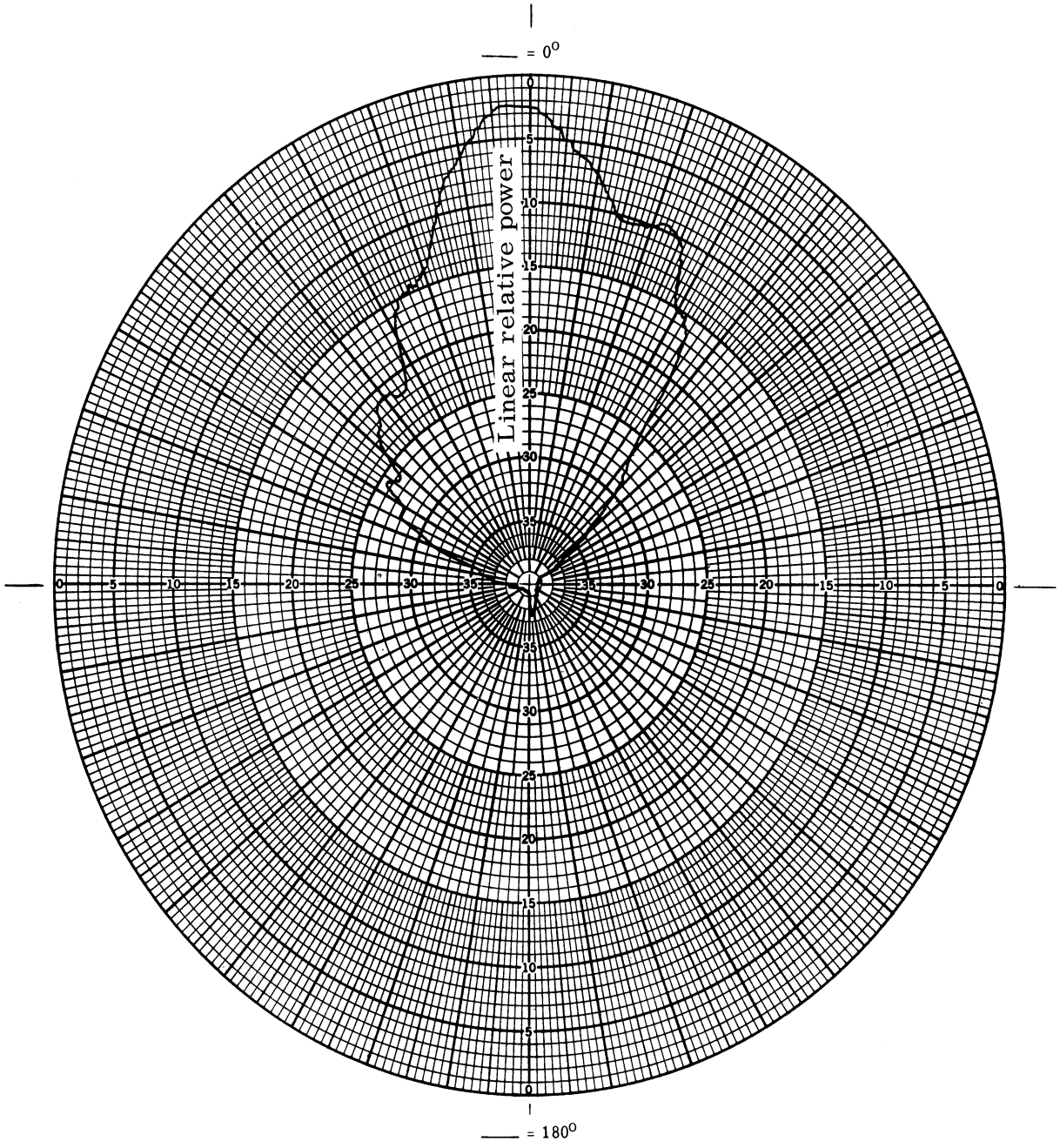

FIG. C-17: UNLOADED LOG CONICAL ANTENNA, 1100 MHz, E-PLANE

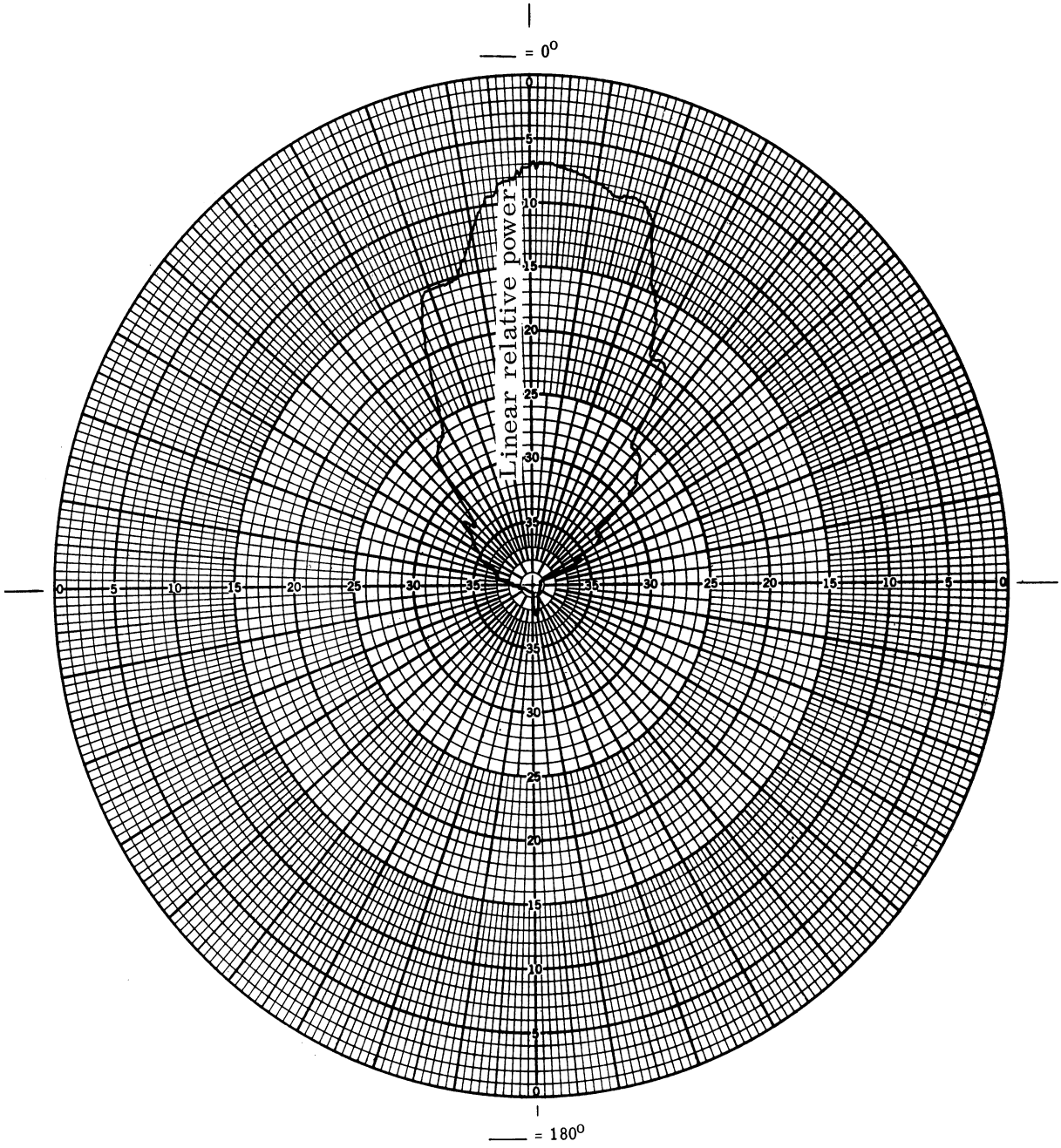

FIG. C-18: UNLOADED LOG CONICAL ANTENNA, 1300 MHz, E-PLANE

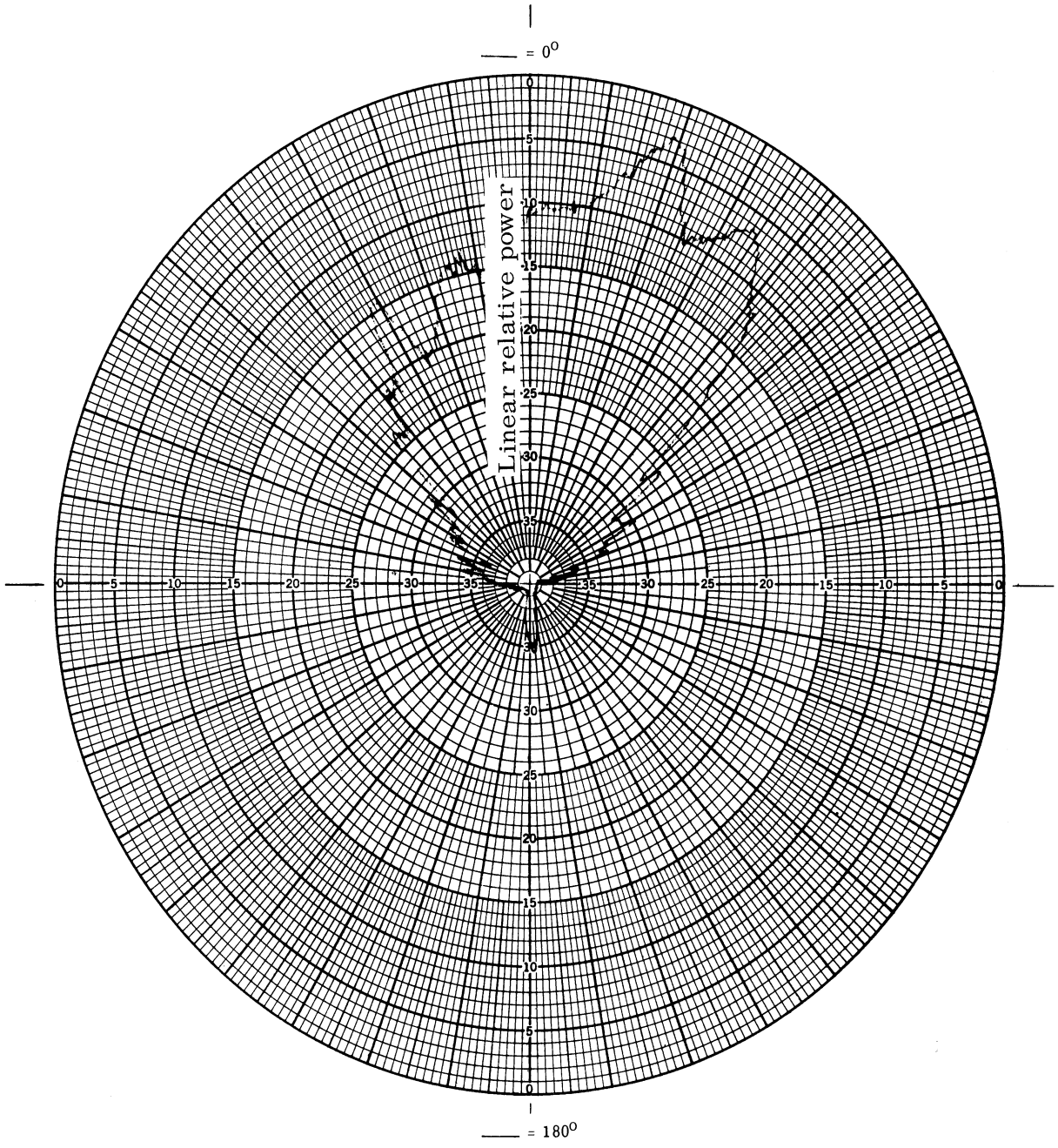

FIG. C-19: UNLOADED LOG CONICAL ANTENNA, 1500 MHz, E-PLANE

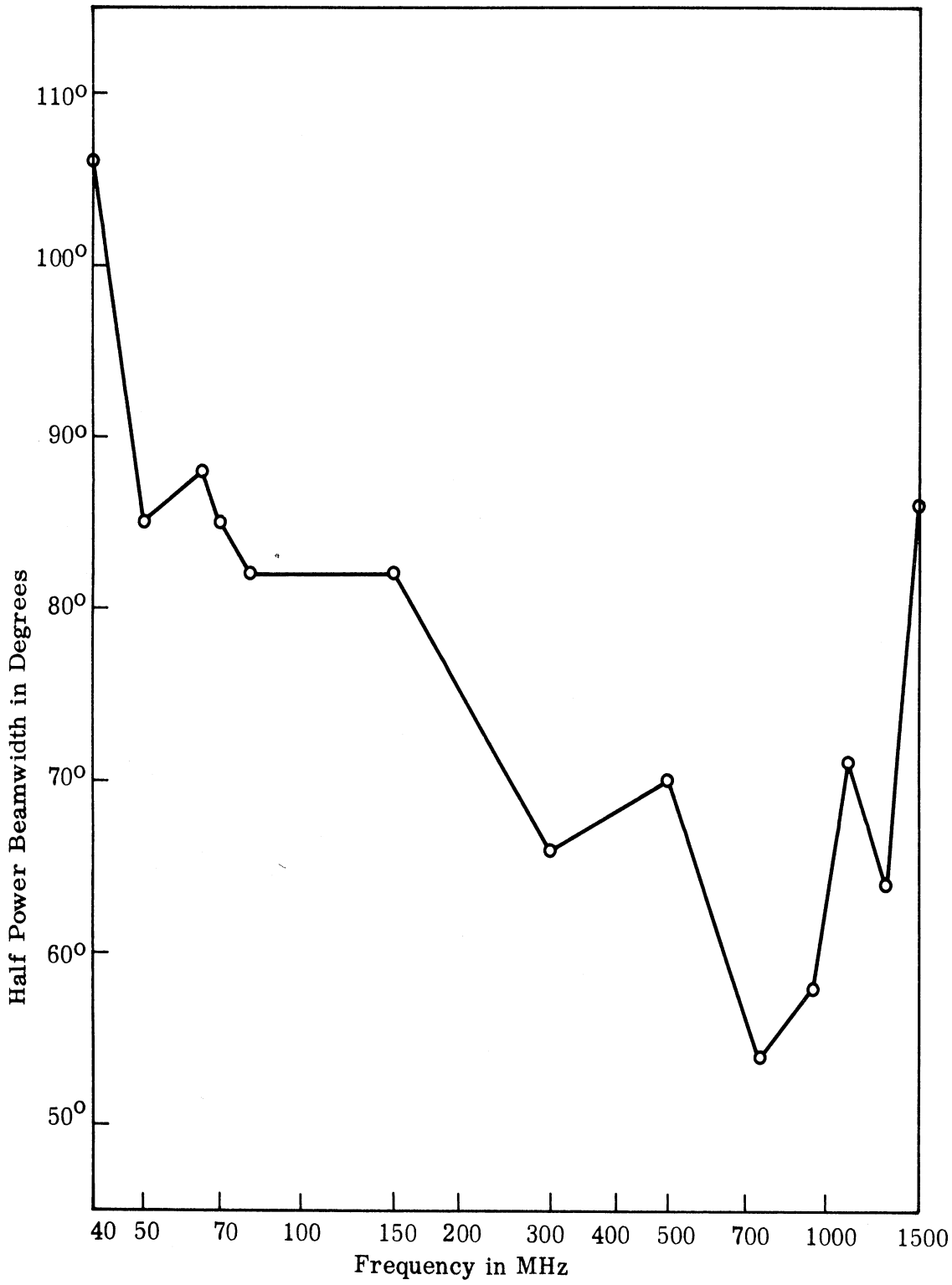

FIG. C-20: HALF POWER BEAMWIDTH OF PROTOTYPE, E-PLANE

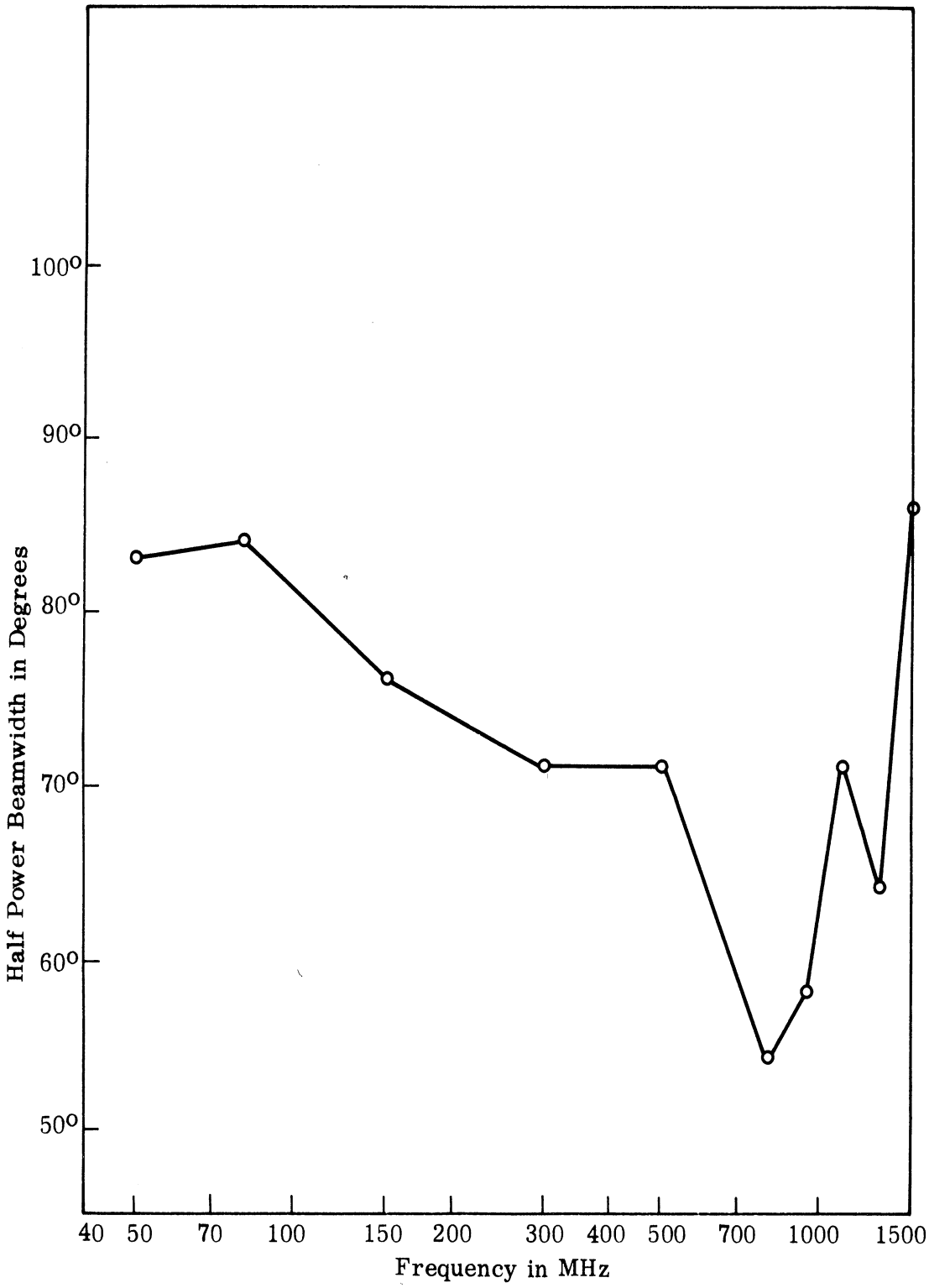

FIG. C-21: HALF POWER BEAMWIDTH OF THE UNLOADED PROTOTYPE, E-PLANE

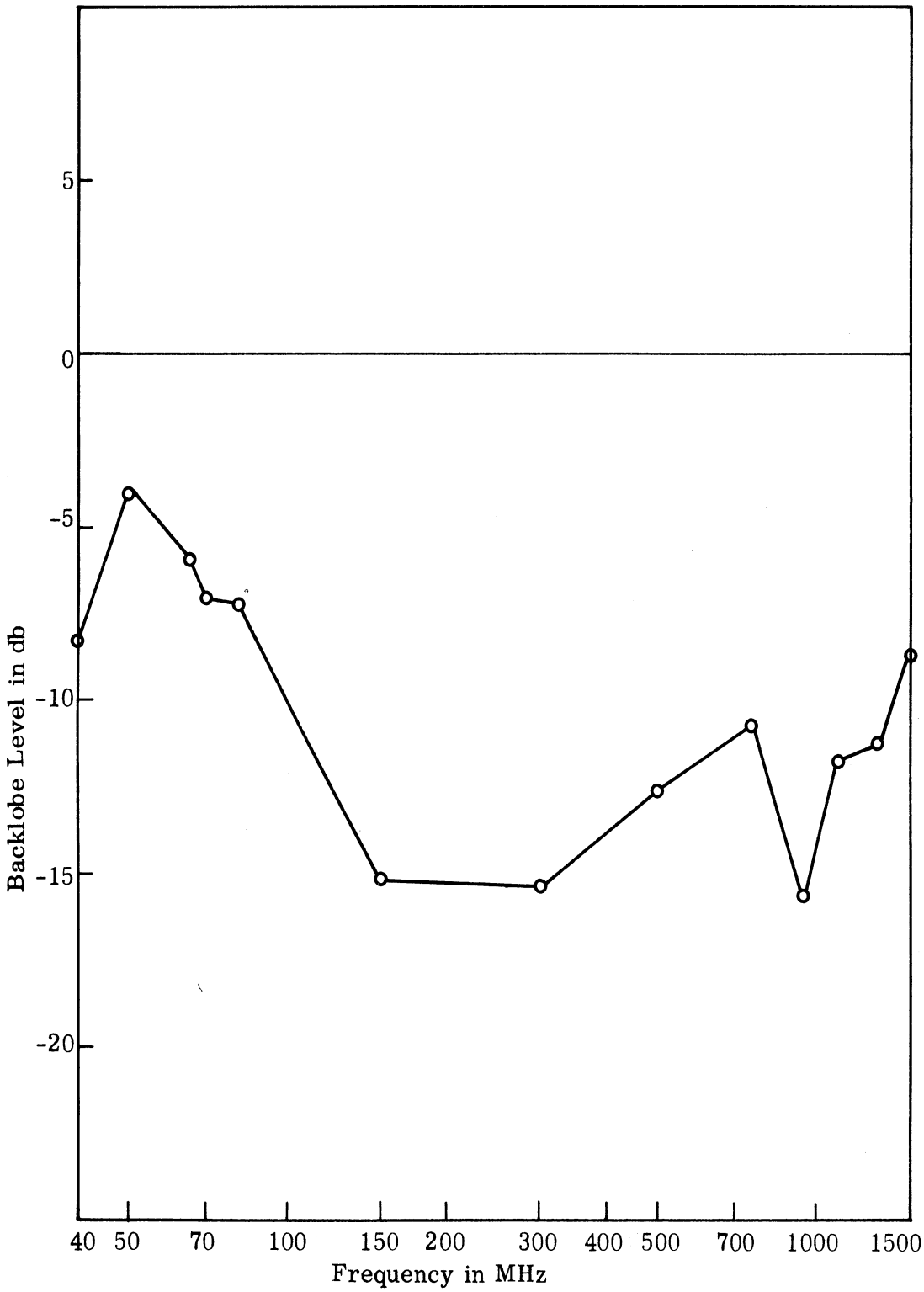

FIG. C-22: BACKLOBE LEVEL OF PROTOTYPE, E-PLANE

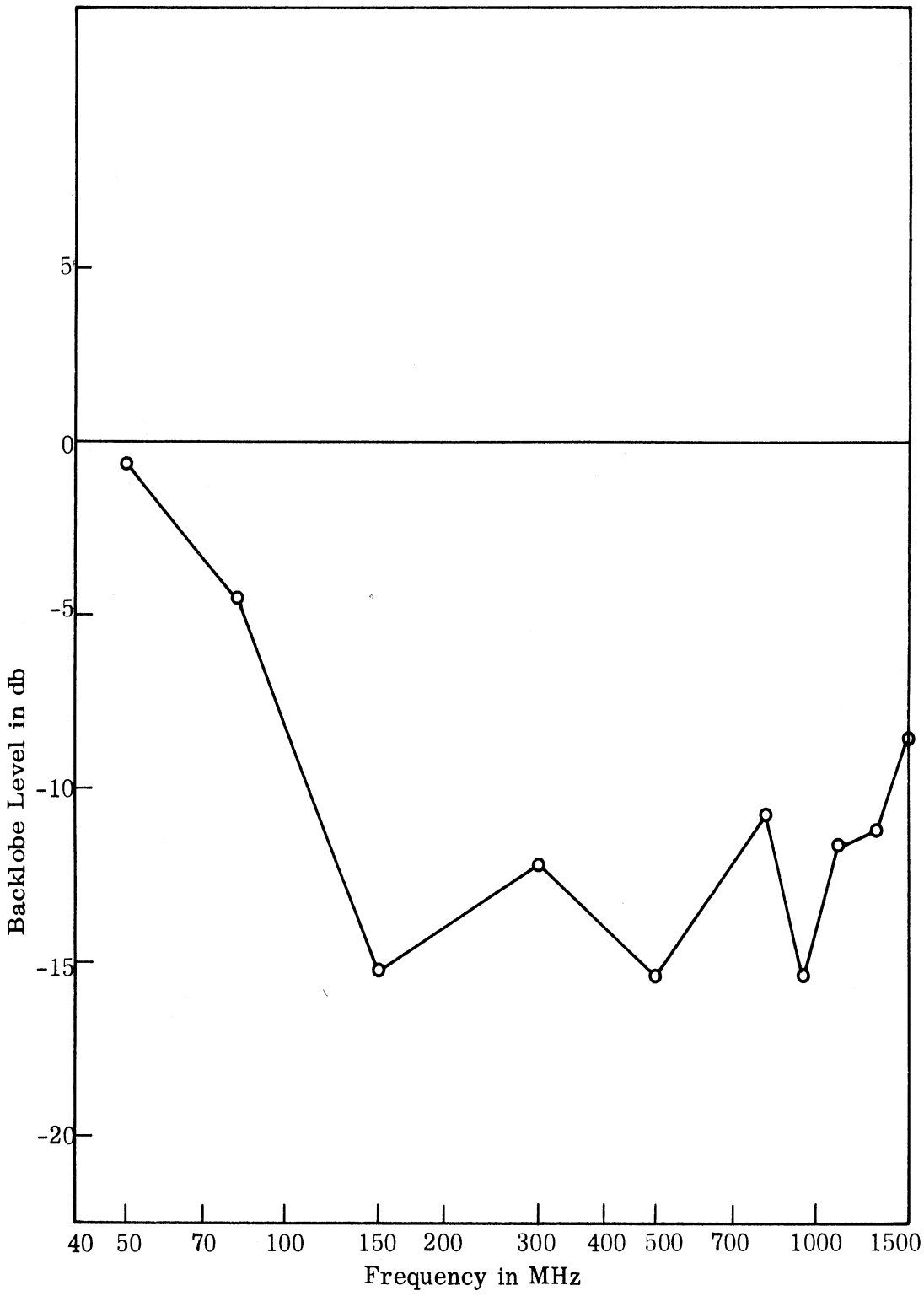

FIG. C-23: BACKLOBE LEVEL IN db OF THE UNLOADED PROTOTYPE, E-PLANE

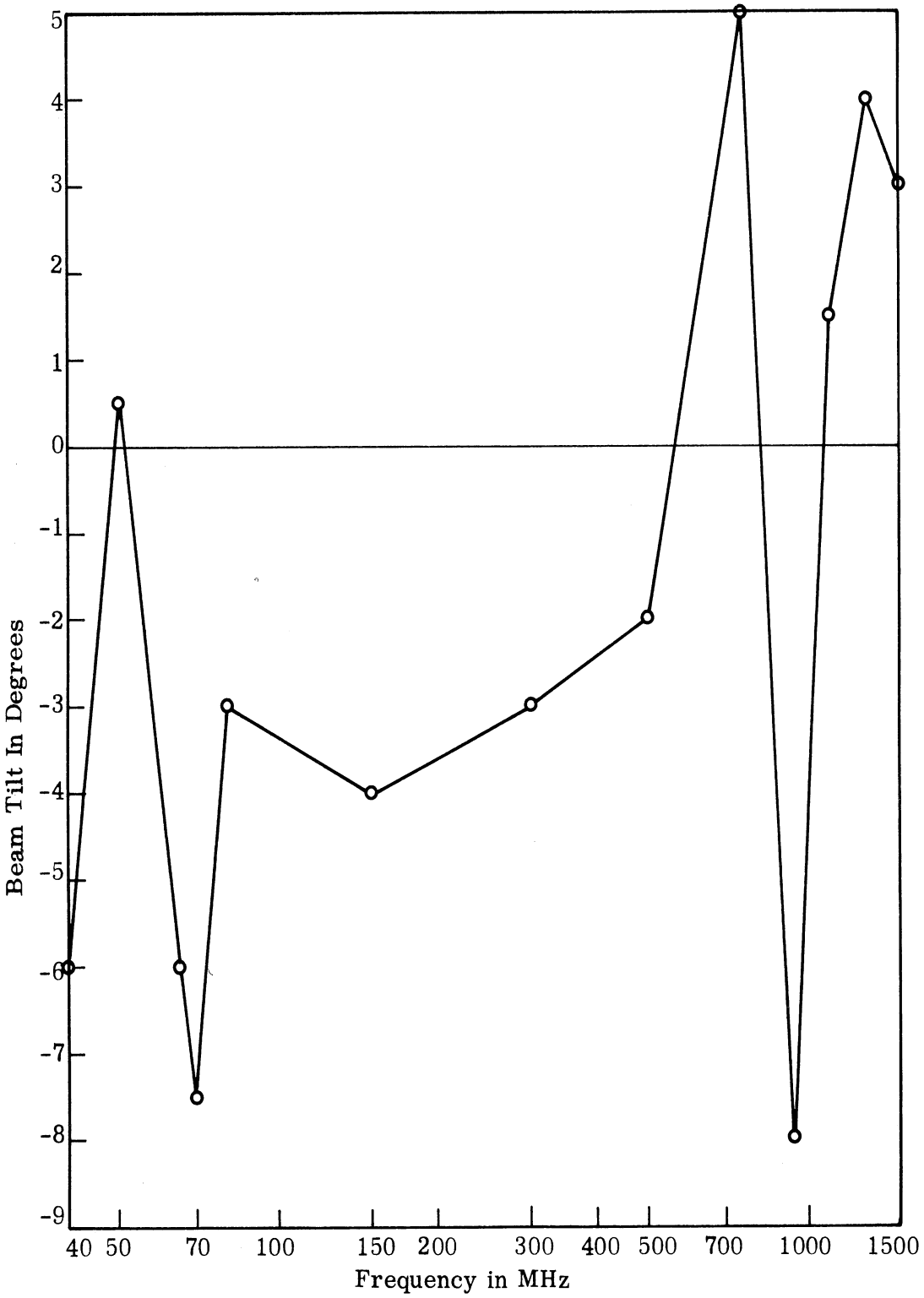

FIG. C-24: BEAM TILT OF PROTOTYPE, E-PLANE

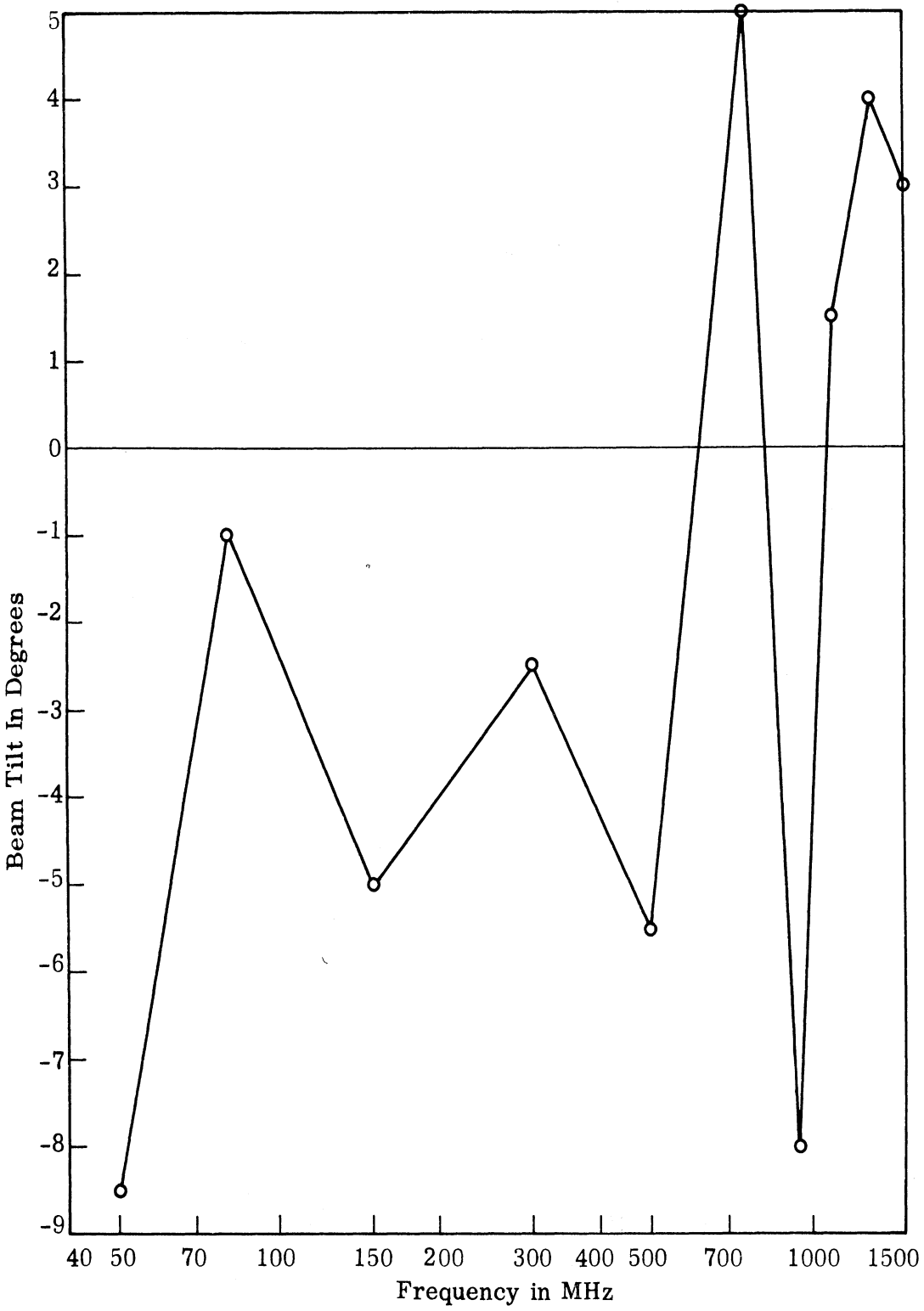

FIG. C-25: BEAM TILT OF UNLOADED PROTOTYPE, E-PLANE

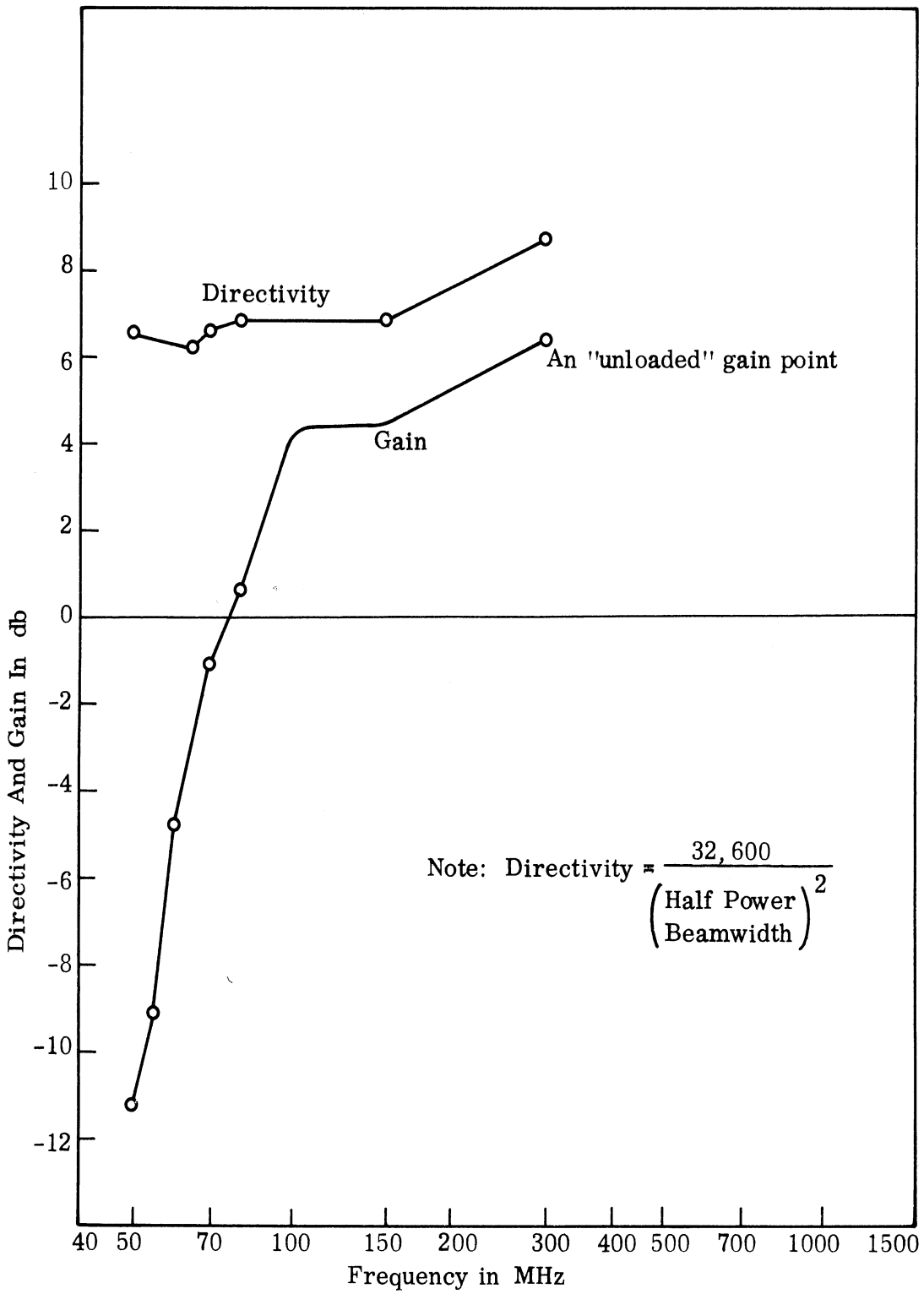

FIG. C-26: DIRECTIVITY AND GAIN OF PROTOTYPE WITH RESPECT TO AN ISOTROPIC SOURCE; E-PLANE

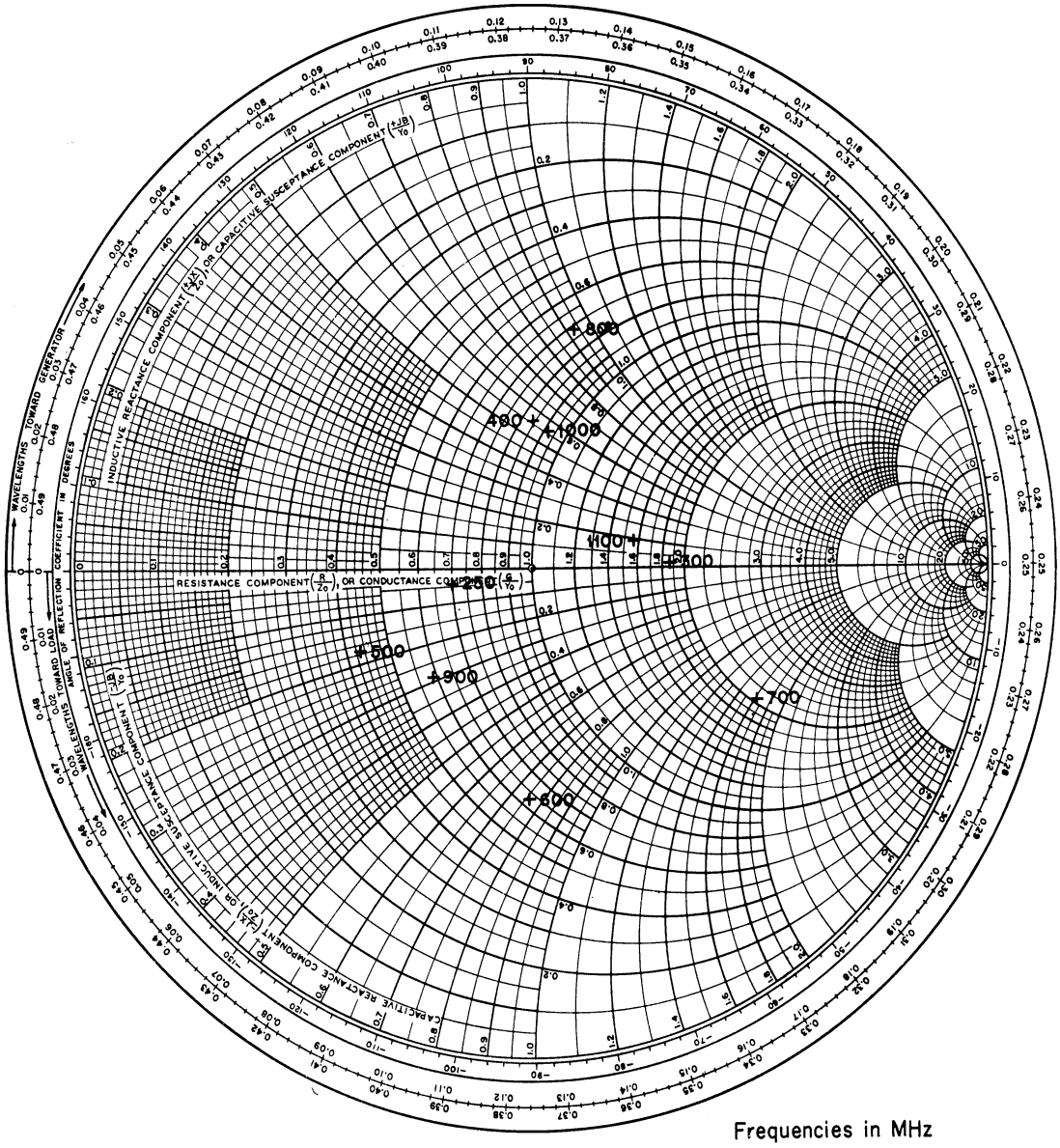

FIG. C-27: IMPEDANCE OF LOADED LOG CONICAL ANTENNA, HIGH FREQUENCIES

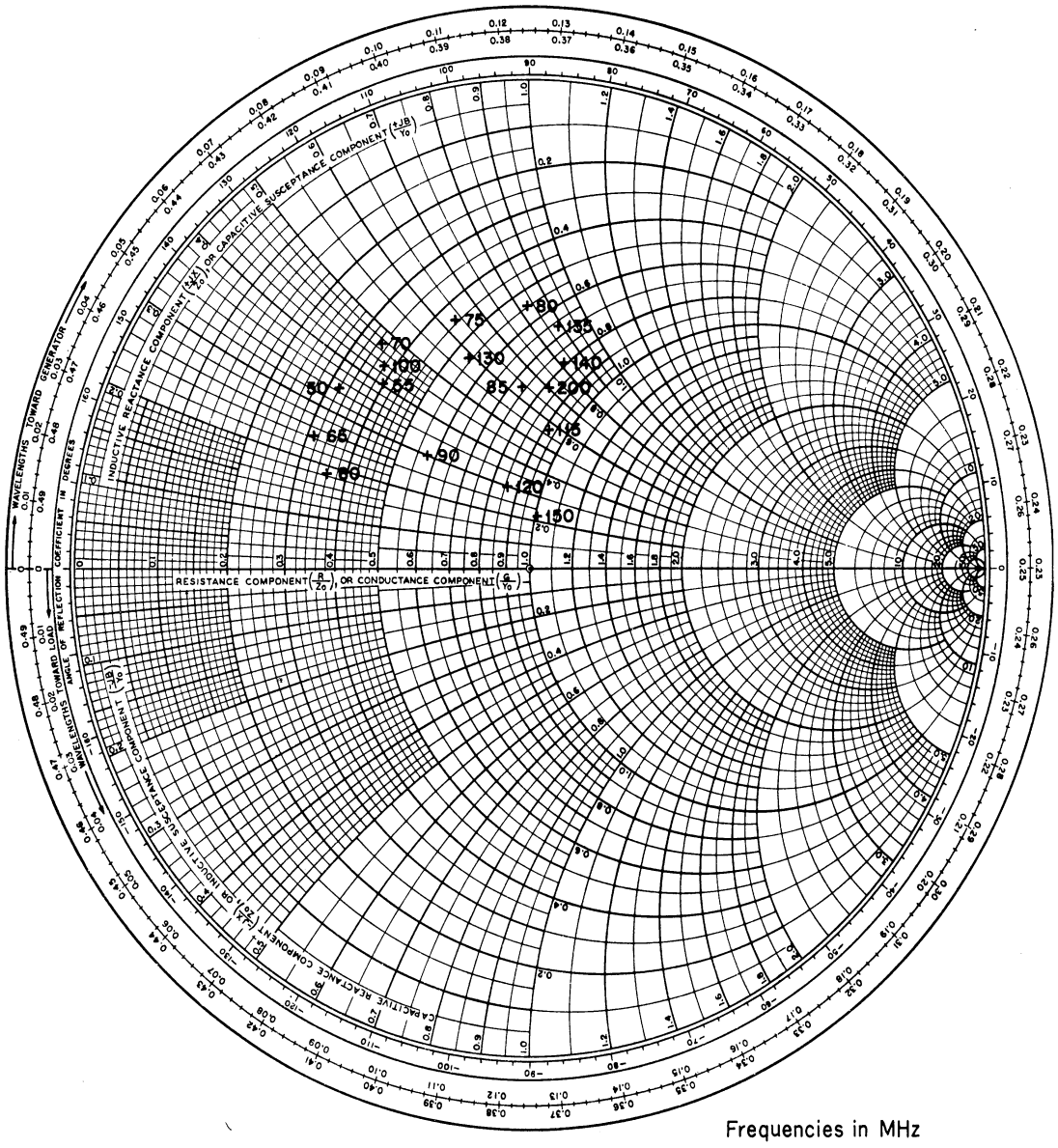

FIG. C-28: IMPEDANCE OF LOADED LOG CONICAL ANTENNA, LOW FREQUENCIES

REFERENCES

Brown and Woodward, Jr., (1945), "Experimentally Determined Impedance Characteristics of Cylindrical Antennas," Proceedings of I. R. E., April 1945.

Cohn, A. and A. W. Maltese, (1961), The Lincoln Laboratory Antenna Test Range, Microwave Journal, 1961.

Condon, E. V., and Odishaw (1958), Handbook of Physics, McGraw-Hill, New York.

Dukes, J. M. C. (1958), "The Application of Printed-Circuit Techniques to the Design of Microwave Components," Proceedings of the Institution of Electrical Engineers (London), 105, Part B, No. 20, pp. 155-172, March.

Dyson, J. D. (1965), "The Characteristics and Design of the Conical Log-Spiral Antenna," University of Illinois Antenna Laboratory Report No. 65-4.

Ferris, J. E., et al (1965a), "Broadband Antenna Techniques Study," Second Quarterly Report ECOM 0126302 Under DA 28-043 AMC 01263(E), The University of Michigan Radiation Laboratory Report 7260-2-Q.

Ferris, J. E., et al (1965b), "Broadband Antenna Techniques Study," Third Quarterly Report ECOM 01263-3 Under DA 28-043 AMC 01263(E), The University of Michigan Radiation Laboratory Report 7260-3-Q.

Hair, H. H. (December 1964), "Development of Helical Phase Shifters," General Electric Company, Final Report prepared for MIT Lincoln Laboratories.

Hong, Soonsung (1965), "Size Reduction of Bifilar Helical Antennas by Loading with Magneto-Dielectric Materials," The University of Michigan Radiation Laboratory Internal Memorandum No. 7260-504-M.

Hopfer, Samuel (1955), "The Design of Ridged Waveguides," MTT Vol. 3, No. 5, October, 1955, pp. 20-29.

Jasik, H (1961), Antenna Engineering Handbook, McGraw-Hill, New York, 9.

Klock, (1963), "A Study of Wave Propagation of Helices," University of Illinois, PhD Dissertation 64-2914.

Knott, E. F., V. V. Liepa, T. B. A. Senior, "A Surface Field Measurement Facility," Proc. IEEE, 53, pp. 1105-1107.

Lyon, J. A. M., et al (1965), "Study and Investigations of UHF-VHF Antenna," The University of Michigan Radiation Laboratory Report 5549-1-F, AFAL-TR-65-64.

Patton, W. T. (1965), "The Backfire Bifilar Helical Antenna," University of Illinois Technical Antenna Laboratory, Report No. 61, AD 289 084.

Peters, L., Jr. and T. E. Kilcoyne, (1965), "Radiating Mechanisms in a Reflection Antenna System," IEEE Electromagnetic Compatibility, Vol. EMC-7, No. 4, December 1965, pp. 368-374.

Sensiper, S. (1951), "Electromagnetic Wave Propagation on Helical Conductors," Massachusetts Institute of Technology, Report 194.

Shestopalov, V. P., A. A. Bulgakov and B. M Bulgakov (1961), "Theoretical and Experimental Investigations of Helix-dielectric Aerials," Radio. i. elek, 6.

Suhl, H. and Walker, L. R. (July 1954), "Topics in Guided Wave Propagations Through Cyromagnetic Media," Bell Systems Technical Journal, 33, pp. 939-986.

Tang, C. H. and O. L. McClelland (1962), "Polygonal Spiral Antennas," University of Illinois Antenna Laboratory Report No. 57.

Tien, P. K. (1953), "Traveling Wave Tube Helix Impedance," Proc. IRE, 41, No. 11, pp. 1617-1623.

Walton and Sundberg, (1964), "Broadband Ridged Horn Design," Microwave Journal, Vol. 7, No. 3, March 1964.

Watkins, D. A. (1958), Topics in Electromagnetic Theory, John Wiley and Sons, New York.

Whiteside, H. (1962), Electromagnetic Field Probes," Harvard University Cruft Laboratory Technical Report 377.

DISTRIBUTION LIST

Address	Copies
Defense Documentation Center Attn: TISIA Cameron Station (Bldg. 5) Alexandria, Virginia 22314	20
Office of Assistant Secretary of Defense (Research and Development) Attn: Technical Library, Rm. 3E1065 Washington, D. C. 20315	1
Director, U S Naval Research Laboratory Attn: Code 2027 Washington, D. C. 20390	1
CO and Director, U S Navy Electronics Laboratory Attn: Library San Diego, California 92101	1
AFSC Scientific / Technical Liaison Office U S Naval Air Development Center Johnsville, Pennsylvania 18974	1
Systems Engineering Group (SEPIR) Wright-Patterson AFB, Ohio 45433	1
Electronic Systems Division (AFSC) Scientific / Technical Information Division ESTI L. G. Hanscom Field Bedford, Massachusetts 01731	1
Air Force Cambridge Research Laboratories Attn: CRXL-R L. G. Hanscom Field Bedford, Massachusetts 01731	1
Chief of Research and Development Department of the Army Washington, D. C. 20315	1
C. G., U. S. Army Material Command Attn: R and D Directorate Washington, D. C. 20315	2

Commanding General
U. S. Army Electronic Command
Attn: AMSEL-KL-EM
Fort Monmouth, New Jersey 07703 — 1

C. G., U.S. Army Combat Development Command
Communications - Electronics Agency
Fort Huachuca, Arizona 85613 — 1

Commanding General
U. S. Army Security Agency
Attn: IADEV
Arlington Hall Station
Arlington, Va. 22207 — 3

C.O., Harry Diamond Laboratories
Connecticut Ave and Van Ness St., N.W.
Washington, D.C. 20438 — 1

C.G., U. S. Army Electronic Proving Ground
Attn: Technical Library
Fort Huachuca, Arizona 85613 — 1

C.G., U. S. Army Electronics Command
Attn: AMSEL-WL-S
Fort Monmouth, New Jersey 07703 — 3

C. G., U. S. Army Electronics Command
Attn: AMSEL-RD-DR
Fort Monmouth, New Jersey 07703 — 1

C. G., U. S. Army Electronics Command
Attn: AMSEL-RD-ADT
Fort Monmouth, New Jersey 07703 — 1

C. G., U. S. Army Electronics Command
Attn: AMSEL-RD-ADO-RHA
Fort Monmouth, New Jersey 07703 — 1

C. G., U. S. Army Electronics Command
Attn: AMSEL-RD-LNA
Fort Monmouth, New Jersey 07703 — 1

C. G., U. S. Army Electronics Command Attn: AMSEL-RD-LNR Fort Monmouth, New Jersey 07703	1
Dir., Material Readiness Directorate, AMSEL-MR U. S. Army Electronics Command Fort Monmouth, New Jersey 07703	
C. O., U. S. Army Electronics R and D Activity Attn: SELWS-AJ White Sands, New Mexico 88002	1
Chief, U. S. Army Electronics Laboratories Mountain View Office P. O. Box 205 Mountain View, California 94042	1
U. S. Army Electronics Laboratories Liaison Officer Rome Air Development Center Attn: RAOL Griffiss AFB, New York 13442	1
U. S. National Bureau of Standards Boulder Laboratories Attn: Library Boulder, Colorado	1
Total	49

UNCLASSIFIED

Security Classification

DOCUMENT CONTROL DATA - R&D

(Security classification of title, body of abstract and indexing annotation must be entered when the overall report is classified)

1. ORIGINATING ACTIVITY *(Corporate author)*
The University of Michigan
Radiation Laboratory, Dept. of Electrical Eng.
Ann Arbor, Michigan 48108

2a. REPORT SECURITY CLASSIFICATION
UNCLASSIFIED

2b. GROUP

3. REPORT TITLE
Broadband Antenna Techniques Study

4. DESCRIPTIVE NOTES *(Type of report and inclusive dates)*
Interim Report No. 1 - 1 January - 15 April 1966

5. AUTHOR(S) *(Last name, first name, initial)*
Ferris, Joseph E., Lyon, John A.M., Rassweiler, George G., Smith, Dean L., Wu, Pei R., Zimmerman, Wiley E.

6. REPORT DATE	7a. TOTAL NO. OF PAGES	7b. NO. OF REFS
June 1966	230	24

8a. CONTRACT OR GRANT NO.
DA 28-043-AMC-01263(E)

b. PROJECT NO.
5AO-21101-A902-01-08

c.

d.

9a. ORIGINATOR'S REPORT NUMBER(S)
7260-1-T

9b. OTHER REPORT NO(S) *(Any other numbers that may be assigned this report)*
ECOM-01263-4

10. AVAILABILITY/LIMITATION NOTICES
Each transmittal of this document outside the Department of Defense must have prior approval of CG, U.S. Army Electronics Command, Fort Monmouth, New Jersey Attn: AMSEL-WL-S

11. SUPPLEMENTARY NOTES

12. SPONSORING MILITARY ACTIVITY
United States Army Electronics Command
Fort Monmouth, New Jersey 07703

13. ABSTRACT: Work on the design, fabrication and testing of three broadband antennas is described. The antenna types are: (1) high-gain constant beamwidth, (2) omnidirectional and (3) loaded conical helix.

During this reporting period, an experimental study has been conducted to determine techniques by which a parabolic reflector may be broadbanded such that a constant beamwidth secondary major lobe can be achieved. From this study it has been found that if circular holes are placed in the reflector in a random fashion and a broadband horn is used as a feed, a beamwidth variation of less than 2:1 for a frequency bandwidth of 8.3:1 can be achieved.

A cage antenna has been designed, fabricated and tested to satisfy the requirements of the broadband omnidirectional antenna task. The antenna exhibits good omnidirectional patterns across the frequency range of 100-1000 MHz, and the VSWR is less than 3:1 for the same frequency range.

One of the primary objectives of this research activity has been the design of a conical helix antenna covering the frequency range from 50 MHz to 1.1 GHz with a size reduction over conventional unloaded designs. The design and description of a prototype are included in this report. Data on the experimental test of this prototype including a comparison with specifications are also included. Although the weight of the prototype is considerably in excess of that specified, some size reduction has been accomplished.

DD FORM 1 JAN 64 1473

UNCLASSIFIED

Security Classification

14. KEY WORDS	LINK A		LINK B		LINK C	
	ROLE	WT	ROLE	WT	ROLE	WT
BROADBAND CONSTANT BEAMWIDTH OMNIDIRECTIONAL SIZE REDUCTION WEIGHT REDUCTION BEAM SHAPING LOADED CONICAL HELIX CAGE ANTENNA						

INSTRUCTIONS

1. ORIGINATING ACTIVITY: Enter the name and address of the contractor, subcontractor, grantee, Department of Defense activity or other organization *(corporate author)* issuing the report.

2*a*. REPORT SECURITY CLASSIFICATION: Enter the overall security classification of the report. Indicate whether "Restricted Data" is included. Marking is to be in accordance with appropriate security regulations.

2*b*. GROUP: Automatic downgrading is specified in DoD Directive 5200.10 and Armed Forces Industrial Manual. Enter the group number. Also, when applicable, show that optional markings have been used for Group 3 and Group 4 as authorized.

3. REPORT TITLE: Enter the complete report title in all capital letters. Titles in all cases should be unclassified. If a meaningful title cannot be selected without classification, show title classification in all capitals in parenthesis immediately following the title.

4. DESCRIPTIVE NOTES: If appropriate, enter the type of report, e.g., interim, progress, summary, annual, or final. Give the inclusive dates when a specific reporting period is covered.

5. AUTHOR(S): Enter the name(s) of author(s) as shown on or in the report. Enter last name, first name, middle initial. If military, show rank and branch of service. The name of the principal author is an absolute minimum requirement.

6. REPORT DATE: Enter the date of the report as day, month, year; or month, year. If more than one date appears on the report, use date of publication.

7*a*. TOTAL NUMBER OF PAGES: The total page count should follow normal pagination procedures, i.e., enter the number of pages containing information.

7*b*. NUMBER OF REFERENCES: Enter the total number of references cited in the report.

8*a*. CONTRACT OR GRANT NUMBER: If appropriate, enter the applicable number of the contract or grant under which the report was written.

8*b*, 8*c*, & 8*d*. PROJECT NUMBER: Enter the appropriate military department identification, such as project number, subproject number, system numbers, task number, etc.

9*a*. ORIGINATOR'S REPORT NUMBER(S): Enter the official report number by which the document will be identified and controlled by the originating activity. This number must be unique to this report.

9*b*. OTHER REPORT NUMBER(S): If the report has been assigned any other report numbers *(either by the originator or by the sponsor)*, also enter this number(s).

10. AVAILABILITY/LIMITATION NOTICES: Enter any limitations on further dissemination of the report, other than those imposed by security classification, using standard statements such as:

(1) "Qualified requesters may obtain copies of this report from DDC."

(2) "Foreign announcement and dissemination of this report by DDC is not authorized."

(3) "U. S. Government agencies may obtain copies of this report directly from DDC. Other qualified DDC users shall request through _____."

(4) "U. S. military agencies may obtain copies of this report directly from DDC. Other qualified users shall request through _____."

(5) "All distribution of this report is controlled. Qualified DDC users shall request through _____."

If the report has been furnished to the Office of Technical Services, Department of Commerce, for sale to the public, indicate this fact and enter the price, if known.

11. SUPPLEMENTARY NOTES: Use for additional explanatory notes.

12. SPONSORING MILITARY ACTIVITY: Enter the name of the departmental project office or laboratory sponsoring *(paying for)* the research and development. Include address.

13. ABSTRACT: Enter an abstract giving a brief and factual summary of the document indicative of the report, even though it may also appear elsewhere in the body of the technical report. If additional space is required, a continuation sheet shall be attached.

It is highly desirable that the abstract of classified reports be unclassified. Each paragraph of the abstract shall end with an indication of the military security classification of the information in the paragraph, represented as *(TS)*, *(S)*, *(C)*, or *(U)*.

There is no limitation on the length of the abstract. However, the suggested length is from 150 to 225 words.

14. KEY WORDS: Key words are technically meaningful terms or short phrases that characterize a report and may be used as index entries for cataloging the report. Key words must be selected so that no security classification is required. Identifiers, such as equipment model designation, trade name, military project code name, geographic location, may be used as key words but will be followed by an indication of technical context. The assignment of links, rules, and weights is optional.